8-26-2014 12:00 AM

Surface Modification of Aluminum Alloys by Plasma Electrolytic Oxidation

Vahid Dehnavi
The University of Western Ontario

Supervisor
Prof. Sohrab Rohani
The University of Western Ontario Joint Supervisor
Prof. David W. Shoesmith
The University of Western Ontario

Graduate Program in Chemical and Biochemical Engineering
A thesis submitted in partial fulfillment of the requirements for the degree in Doctor of Philosophy

SURFACE MODIFICATION OF ALUMINUM ALLOYS BY PLASMA ELECTROLYTIC OXIDATION

by

Vahid Dehnavi

Graduate Program in Chemical and Biochemical Engineering

A thesis submitted in partial fulfillment
of the requirements for the degree of
Doctor of Philosophy

The School of Graduate and Postdoctoral Studies
The University of Western Ontario
London, Ontario, Canada

Abstract

Plasma electrolytic oxidation (PEO) is a surface treatment for the production of ceramic oxide coatings with great properties, such as high wear and corrosion resistance, on metal substrates, particularly aluminum and magnesium alloys. Formation of PEO coatings involves complex processes and mechanisms that are difficult to study. Currently, the PEO process is in a transition phase from research to commercial application, with a primary focus on the corrosion and wear protection of light alloys, and has recently generated interest as a promising surface treatment for biomedical applications.

To justify the industrial application of PEO, a more systematic and in-depth study of the influence of various parameters on the process is required. The control of the PEO process to yield the desired morphology and microstructure for specific applications is a key requirement if the process is to be industrially applied. The aim of the research in this thesis is to study the influence of electrical parameters, so they can be optimized to produce coatings with enhanced properties mainly for tribological applications.

Alumina coatings were deposited on 6061 aluminum alloy substrates in an alkaline silicate electrolyte using a unipolar pulsed DC current mode. The influence of processing conditions, mainly electrical parameters (applied frequency, duty cycle, and current density), on the formation, growth behaviour and properties of PEO coatings were investigated. Different characterization methods including scanning electron microscopy, energy dispersive X-ray spectroscopy, X-ray diffractometry, microhardness testing, electrochemical impedance spectroscopy, and linear polarization resistance measurements were used to study the microstructure, morphology and properties of the coatings.

The correlation between the stage of the PEO process and the properties of the coating has been shown. The voltage-time response was found to be important since it provided readily measurable and useful information about these stages. It was found that the microstructure, morphology, growth rate, phase distribution and composition of coatings

could be changed by varying the electrical parameters. To some degree corrosion performance could be tailored by adjusting processing parameters.

Keywords: Plasma electrolytic oxidation; Ceramic coatings; Voltage-time response; Aluminum; Electrical parameters; Microstructure; Morphology; Phase transformation; Alpha alumina; Gamma alumina; Corrosion performance

Co-Authorship Statement

Chapter 3: This chapter is a combination of the following two published articles:

(1) V. Dehnavi, B. L. Luan, D. W. Shoesmith, X. Y. Liu, S. Rohani, "Effect of duty cycle and applied current frequency on plasma electrolytic oxidation (PEO) coating growth behavior", Surface & Coatings Technology 226 (2013) 100–107.

(2) V. Dehnavi, B. L. Luan, X. Y. Liu, S. Rohani, D. W. Shoesmith, "Effect of Electrical parameters on plasma electrolytic oxidation of 6061 al alloy", in: New and Advanced Material International Congress (NAMIC 2012), Isfahan, Iran, May 2012.

The experimental works were conducted by Vahid Dehnavi under the guidance of Dr. Ben Li Luan and Dr. Xing Yang Liu from National Research Council Canada (NRC), London, ON, Canada, and the supervision of my advisors, Prof. D. W. Shoesmith and Prof. S. Rohani. Writing and data analysis of these publications were conducted by Vahid Dehnavi. It was reviewed and revised by Dr. Luan, Dr. Liu, Prof. Shoesmith, and Prof. Rohani.

Chapter 4: A version of this chapter was published as: V. Dehnavi, B. L. Luan, X. Y. Liu, D. W. Shoesmith, S. Rohani, "Production of ceramic coatings on AA6061 aluminium alloy using plasma electrolytic oxidation" , in: Materials Science and Technology (MS&T 2013) Conference, Montreal, Canada, 2013,: pp. 2247-2254. The experimental works, data analysis and writing of the article manuscript were done by Vahid Dehnavi under the guidance of Dr. Luan, Dr. Liu, Prof. Shoesmith, and Prof. Rohani who also revised the article and made recommendations.

Chapter 5: This chapter is a version of the combination of two published articles:

(1) V. Dehnavi, X. Y. Liu, B. L. Luan, D. W. Shoesmith, S. Rohani, "Phase transformation in plasma electrolytic oxidation coatings on 6061 aluminum alloy", Surface & Coatings Technology 251 (2014) 106-114.

(2) V. Dehnavi, X. Y. Liu, B. L. Luan, S. Rohani, D. W. Shoesmith, "Effect of heating cycles on phase transformation in ceramic coatings produced by plasma electrolytic oxidation of Al6061 alloy", in: International Conference on Materials Heat Treatment (ICMH 2012), Isfahan, Iran, May 2012.

The experiments, data collections and analysis, and writing of the articles were performed by Vahid Dehnavi under the guidance of Dr. Liu, Dr. Luan, and the supervision of my advisors, Prof. D. W. Shoesmith and Prof. S. Rohani who also revised the publications and made recommendations.

Chapter 6: An article based on this chapter has been submitted to Surface & Coatings Technology journal as: V. Dehnavi, B. L. Luan, X. Y. Liu, D. W. Shoesmith, S. Rohani, "Correlation between plasma electrolytic oxidation treatment stages and coatings microstructure on aluminum". The experiments, data analysis, and preparation of the manuscript were done by Vahid Dehnavi under the guidance of Dr. Luan, Dr. Liu, Prof. Shoesmith, and Prof. Rohani who also proof read and revised the manuscript.

Chapter 7: A version of this chapter has been prepared and will be submitted to a journal as: V. Dehnavi, D. W. Shoesmith, B. L. Luan, M. Yari, X. Y. Liu, S. Rohani, "Electrochemical corrosion behavior of plasma electrolytic oxidation coated aluminum alloy, the effect of PEO process stage". The experimental work was conducted by Vahid Dehnavi under the guidance and supervision of Prof. D. W. Shoesmith, Dr. Luan, Dr. Liu, and Prof. S. Rohani. Dr. Mehdi Yari contributed greatly during the electrochemical tests, analyzing the corresponding data and discussions. The draft of the manuscript was written by Vahid Dehnavi and revised by Prof. Shoesmith, Dr. Luan, Dr. Liu, and Prof. Rohani.

Dedication

To the most important people in my life:

my parents

my wife Malihe

and

my son Parham

Acknowledgments

I would like to express my deepest gratitude to my supervisors at the University of Western Ontario, Prof David W. Shoesmith and Prof Sohrab Rohani, and my joint supervisors at National Research Council (NRC) Canada, Dr Ben Luan and Dr Mark Liu for their invaluable support, encouragement, advice and help throughout my PhD study. The good advice, support and guidance of Prof Shoesmith and Dr Luan have been invaluable on both an academic and a personal level, for which I am extremely thankful.

I would also like to acknowledge with much appreciation the crucial role of the people whose help and support was a great asset; the technical staff at NRC, namely, Dave Arnold, Marco Zeman, and Mike Meinert who provided great help with the experiments and sample characterization; Dr Jamie Noel and Dr Dmitrij Zagidulin for their help and useful comments on the electrochemical tests; Dr Hossein Kazemian for his constructive advice and encouragement; and Dr Mehdi Yari for providing help with electrochemical tests and data analysis.

I also gratefully acknowledge the financial assistance provided by the University of Western Ontario Graduate Studies, the Department of Chemical and Biochemical Engineering at the University of Western Ontario (Teaching Assistantship, Graduate Research Scholarship), and the Province of Ontario Graduate Scholarship fund.

My deepest appreciation and sincere gratitude are extended to my family, without whom I would have never been able to reach this point. Words cannot express how grateful I am to my parents for their love and support. At the end I would like to gratefully thank my beloved wife, Malihe, for her patience, care, unconditional love, encouragement and support during all these years.

Table of Contents

List of Tables

List of Figures

List of Appendices

List of Abbreviations and Symbols

Abbreviation	Meaning
PEO	Plasma Electrolytic Oxidation
DC	Direct Current
AC	Alternating Current
EDX	Energy Dispersive X-ray spectroscopy
SEM	Scanning Electron Microscopy
TEM	Transmission Electron Microscopy
EIS	Electrochemical Impedance Spectroscopy
LPR	Linear Polarization Resistance
XRD	X-ray Diffraction
CPE	Constant Phase Element

Symbol	Meaning
V	Voltage
J	Current density
R	Resistance
t	Time
t_{on}	Pulse on time
t_{off}	Pulse off time
D_t	Duty cycle
α-Al_2O_3	Alpha alumina phase

γ- Al_2O_3	Gamma alumina phase
Hv	Vickers hardness
θ	Half the angle of diffraction
C_α	Fraction of the α-Al_2O_3 formed
I_α	Integrated peak intensity of alpha alumina phase
I_γ	Integrated peak intensity of gamma alumina phase
R_p	Polarization resistance
E_{corr}	Corrosion potential

Chapter 1

General Introduction

1.1 Introduction

In the last decades, the increased consumption of materials and energy by industries has created widespread concerns about the need to use them in a more efficient manner. The need for sustainable development has substantially increased environmental pressures to improve the efficiency of resources utilization and to reduce waste generation and polluting emissions. To meet the requirements for environmental sustainability, different approaches are adopted in various industries and manufacturing practices [1,2]. For example in the transport sector, which contributes 19% to the worldwide greenhouse gas emissions, improving the fuel economy of, and reducing the emissions caused by, vehicles are fundamental factors the automotive industry is focusing on.

Many factors can influence vehicle energy consumption and emissions, among which the weight of vehicle is a key one. For these reasons, there is a growing effort to substitute conventional steel and cast irons with light metals and alloys [1,3,4]. Light metals, particularly aluminum and magnesium , have low densities (Al 2.7 g/cm^3, Mg 1.74 g/cm^3, Ti 4.5 g/cm^3) compared to iron (7.86 g/cm^3), good strength to weight ratios, are easy to fabricate, and are finding an ever-increasing importance in aerospace and automobile products. However, in general, they exhibit poor corrosion and wear properties and their widespread use in tribological applications demands suitable functional surface coatings capable of providing adequate protection against wear and corrosion [5,6]. A wide range of surface modification methods are available for aluminum products, such as conversion coating (with chromates, phosphates), anodizing, electrolytic and electroless plating, chemical and physical vapor deposition, plasma spray coating, etc. Anodising provides an important range of coating technologies for aluminum alloy substrates capable of producing coatings up to several microns thick. However, conventional anodized coatings do not provide effective protection against corrosion, and specifically wear, and require the use of acid-based solutions and environmentally hazardous substances [5,7,8].

Plasma electrolytic oxidation (PEO) is a relatively novel surface modification technique to create ceramic coatings on the surface of metals such as aluminum, magnesium, titanium, zirconium and their alloys. Other terminologies used for this process in the

literature include micro-arc oxidation (MAO), anodic oxidation by spark discharge, and spark anodizing [9–11]. In this thesis the term plasma electrolytic oxidation is used because it has become the dominant term over the past decade.

PEO is similar to conventional anodizing, but in contrast to anodizing, which is performed at voltages in the range of 10-50 V, PEO is applied above the breakdown voltages of the original oxide films, typically 400-800 V. Applying high potentials results in the formation of plasma micro-discharge events which appear as numerous sparks on the surface of the sample. Due to the local thermal action of the sparks, ceramic coatings composed of both oxides of the substrate and more complex oxides containing elements from the electrolyte are formed [8,12]. PEO coatings have excellent adhesion to the substrate, high hardness and wear resistance, and good electrical and corrosion resistances. Additionally, the process can produce coatings with a wide range of functional properties with little effect on the mechanical properties of the substrate material because of the negligible heating of the substrate [13–15].

PEO is gaining increased attention as a cost-effective, environmentally friendly surface engineering technique for depositing thick, dense and ultra-hard ceramic coatings on light metals and alloys. Currently, the PEO process is in a transition phase from research to commercial application, with a primary focus on the corrosion and wear protection of light alloys, and has recently gained great attention as a promising surface treatment for biomedical applications. Despite extensive research, the coating formation and growth mechanisms involved are not yet fully understood [8,16,17]. To extend their industrial applications, understanding and controlling the PEO process to yield the desired morphology and microstructure for specific applications are key requirements.

1.2 Research Objectives

The research in this thesis is primarily focused on the PEO treatment of 6061 aluminum alloy. Aluminum is the second most abundant metallic element on earth and because of its appearance, light weight, fabricability, physical and mechanical properties, and corrosion resistance is one of the most widely used materials in industry and consumer products [18]. The aim of this research is to improve the current understanding of PEO,

so it can be controlled to produce coatings with enhanced properties mainly for tribological applications. There are multiple processing parameters with a wide range of values that can affect the formation and microstructure of PEO coatings. The main theme of this work is a study of the effect of electrical parameters including applied frequency, duty cycle, and current density on the formation, growth behaviour and properties of PEO coatings on 6061 aluminum alloy substrates.

1.3 Approach and Methodology

Based on the literature [5,8,15], multiple parameters affect the formation and microstructure of PEO coatings, as indicated in Figure 1.1.

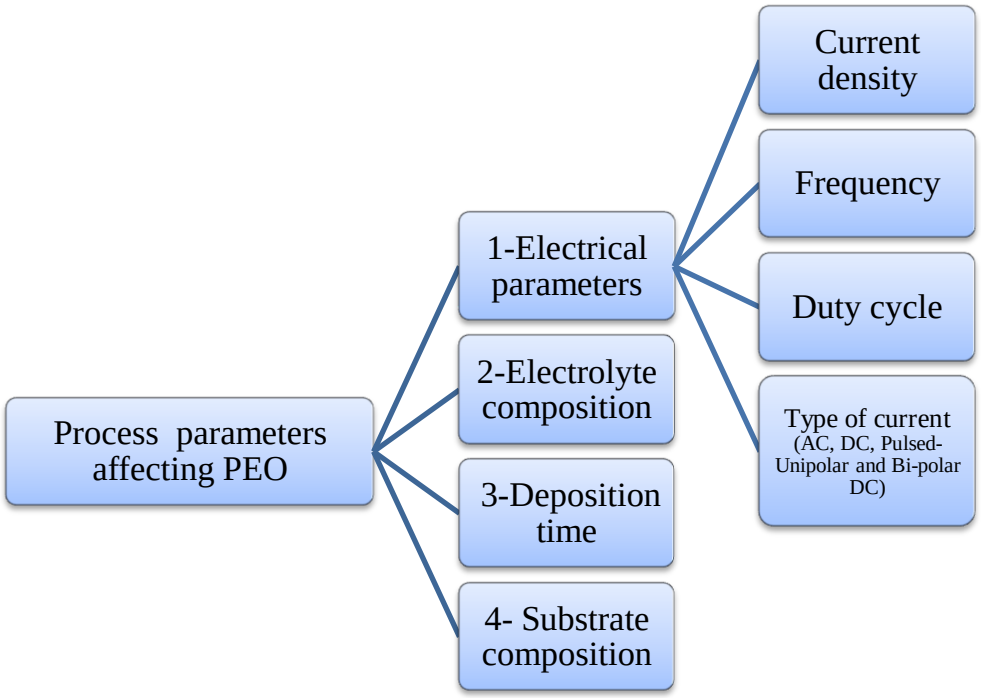

Figure 1.1- Process parameters affecting the PEO coating process.

An extremely wide range of electrolyte compositions has been used and there is a lot of data available. Electrical parameters also play an important role in the formation of PEO coatings, although the available literature is limited. In this study almost all coatings (except the coatings discussed in Chapter 4) were produced on 6061 aluminum alloy using one chemical formula for the aqueous electrolyte. All the coatings studied were

produced using a unipolar pulsed DC power supply with a square waveform. The wave form and corresponding parameters of the unipolar pulsed power source are given in Figure 1.2. During a single pulse, t_{on} and t_{off} are the periods during which the current is on and off, respectively. It is the pulse on time (t_{on}) that plays a crucial role in the formation of the coating microstructure. During the pulse off time (t_{off}), the micro-discharges are interrupted allowing the surface to cool.

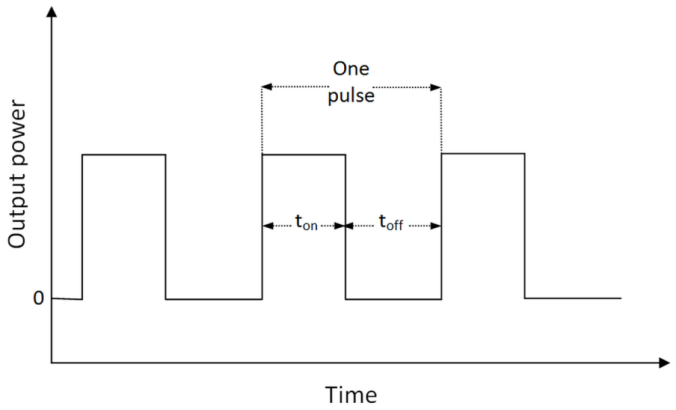

Figure 1.2- Schematic of the pulsed unipolar output of a PEO power source (t_{on}: pulse on time; t_{off}: pulse off time).

A PEO unit custom-built by the National Research Council Canada (NRC, Vancouver, Canada), equipped with a DC power supply was used to produce the coatings. The arrangement of the equipment used is illustrated in Figure 1.4 and the coating compartment is enlarged in Figure 1.5. The positive output of the power supply was connected to the sample (Figure 1.5-a) immersed in the electrolyte as the working electrode (anode), and the negative output was connected to the stainless steel electrolyte container (Figure 1.5-b), which acted as the counter electrode (cathode). To ensure a good connection between the power supply and the samples, a threaded hole was drilled on one side of each sample. Then the sample was bolted to a steel rod (insulated by a ceramic jacket from the electrolyte) connected to the power supply. The samples were coated under galvanostatic conditions, i.e. the current was kept constant during the process and the anode potential was allowed to vary. To determine the required applied current to achieve a specific current density (J) during each pulse on time (t_{on}), the area of the sample was measured and multiplied by the desired current density. 1.3 shows the

variation in current amplitude during pulse on-times as a function of time for a current set to 4.57 A in order to achieve a current density of 20 A/dm^2.

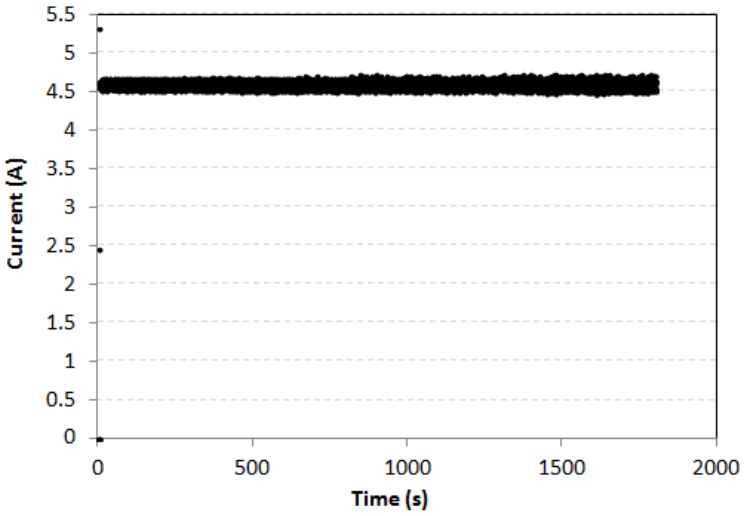

1.3- Variation of current with time for a current set to 4.57 A to achieve a current density of 20 A/dm^2.

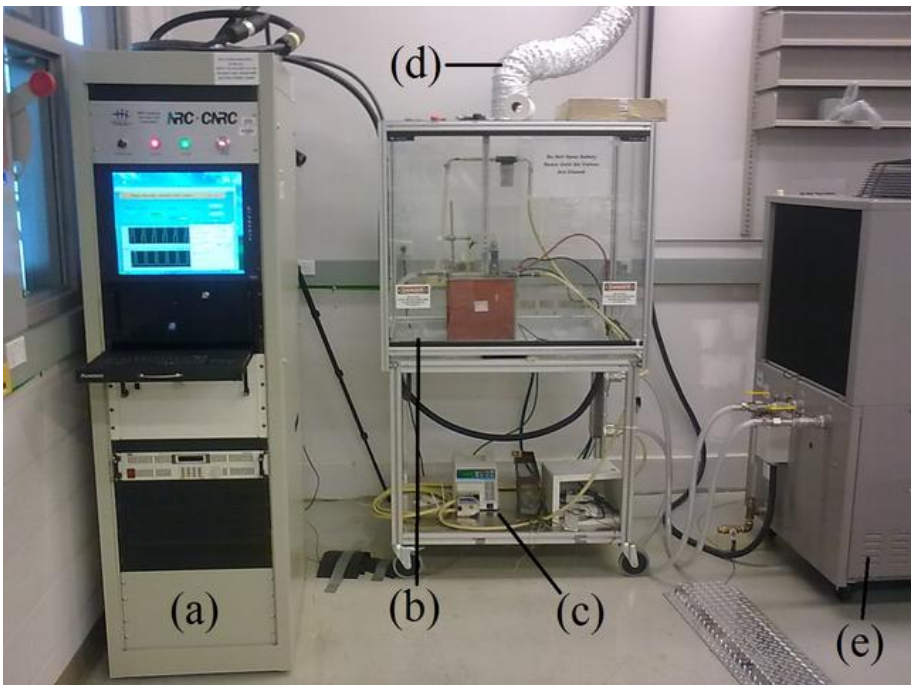

Figure 1.4- Arrangement of the equipment used for PEO coating: (a) power supply and control unit; (b) insulated enclosure; (c) mixing pump; (d) exhaust/ventilation system; (e) cooling system.

PEO coatings were prepared using different processing conditions and different characterization methods were employed to study the correlation between coating parameters and characteristics of the coatings including growth microstructure and morphology, thickness, phase composition, mechanical properties and corrosion performance.

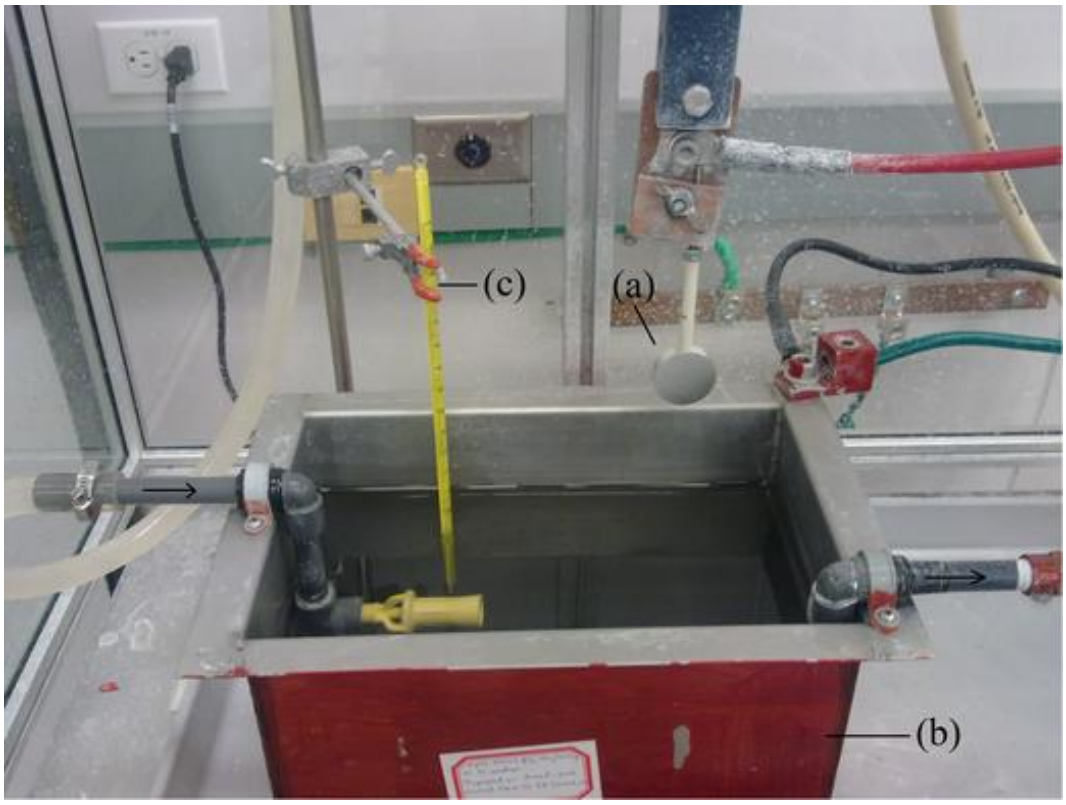

Figure 1.5- An enlarged view of the insulated enclosure of the PEO setup: (a) workpiece; (b) electrolyte holding tank and counter electrode; (c) thermometer.

1.4 Main Contributions

The main contributions of this research to the science and technology of plasma electrolytic oxidation can be summarized as follows:

- The results of this research show that the voltage-time response of the PEO process can provide readily measurable and useful information about different stages of PEO and is an important tool in the study of PEO coatings.

- Based on the findings of this study, it is possible to control the properties of PEO coatings including surface morphology, microstructure, thickness, phase distribution and composition by adjusting the electrical parameters and coating deposition time.

- The outcomes of this research can help produce coatings with desired properties for different applications such as wear resistance, corrosion resistance and heat resistance.

1.5 Thesis Organization

The thesis consists of eight chapters organized in the following sequence:

Chapter 1 provides a general introduction to the importance of PEO as a coating method with a great industrial and environmental potential. The research objectives, approach and methodology and thesis structure are outlined.

Chapter 2 presents a brief overview of the available literature on the PEO process and discusses the PEO equipment setup and existing theories on the coating growth mechanisms. Important process parameters and their effects on the characteristics of PEO coatings and application of these coatings are also described.

Chapter 3 describes the effect of duty cycle and applied current frequency on micro-discharge behaviour during PEO, the coating growth process and surface morphology, and, the distribution of elements in the coatings. Based on these results, a new conceptual model is proposed to explain the concentration distribution of Si on the surface of coatings prepared using different duty cycles.

Chapter 4 investigates the effect of deposition time in a relatively concentrated sodium silicate electrolyte on the characteristics of PEO coatings. A correlation is reported between the deposition time, voltage-time response of the process, and characteristics of the coatings produced. It is proposed that the PEO stage during which a coating is formed could have a very important role in determining its properties and controlling the processing conditions so that coatings are produced in the proper stage is essential.

Chapter 5 presents results of a study on phase transformations in PEO coatings using x-ray diffractometry. A detailed discussion on the effect of electrical parameters including frequency, duty cycle and current density on phase composition, transformation and distribution is presented. Control of the phase transformation reactions to maximize the amount of alpha-alumina, the hardest alumina phase, and the distribution of various phases in the film are discussed.

Chapter 6 provides an investigation of the correlation between PEO treatment stages and coating microstructure and discusses how electrical parameters can affect the duration of the PEO stages which, in turn, control the growth rate, surface morphology, microstructure and microhardness of the coatings. It also includes a discussion of the importance of the voltage-response curve which can provide readily measurable and useful information concerning the different PEO stages.

Chapter 7 describes an electrochemical corrosion study of PEO coatings grown using different processing parameters. Electrochemical impedance spectroscopy (EIS) and the linear polarization resistance (LPR) technique were employed to investigate the electrochemical properties of the coatings. The correlation between the PEO process stage, the microstructure of the coatings, and corrosion performance is discussed.

Chapter 8 summarises the main conclusions derived from this research and provides suggestions for further studies.

1.6 References

[1] G. Ingarao, R. Di Lorenzo, F. Micari, Sustainability issues in sheet metal forming processes: an overview, J. Clean. Prod. 19 (2011) 337–347.

[2] T.E. Norgate, S. Jahanshahi, W.J. Rankin, Assessing the environmental impact of metal production processes, J. Clean. Prod. 15 (2007) 838–848.

[3] J.W. McAuley, Global sustainability and key needs in future automotive design., Environ. Sci. Technol. 37 (2003) 5414–6.

[4] G.S. Cole, A.M. Sherman, Lightweight Materials for Automotive Applications, Mater. Charact. 35 (1995) 3–9.

[5] F.C. Walsh, C.T.J. Low, R.J.K. Wood, K.T. Stevens, J. Archer, A.R. Poeton, et al., Plasma electrolytic oxidation (PEO) for production of anodised coatings on lightweight metal (Al, Mg, Ti) alloys, Trans. Inst. Met. Finish. 87 (2009) 122–135.

[6] R. Gadow, D. Scherer, Composite coatings with dry lubrication ability on light metal substrates, Surf. Coatings Technol. 151-152 (2002) 471–477.

[7] K. Funatani, Emerging technology in surface modification of light metals, Surf. Coatings Technol. 133-134 (2000) 264–272.

[8] B.L. Jiang, Y.M. Wang, Plasma Electrolytic Oxidation Treatment of Aluminum and Titanium Alloys, in: H. Dong (Ed.), Surf. Eng. Light Alloy. Aluminum, Magnes. Titan. Alloy., Woodhead Publishing, 2010: pp. 110–153.

[9] L. Rama Krishna, K.R.C. Somaraju, G. Sundararajan, The tribological performance of ultra-hard ceramic composite coatings obtained through microarc oxidation, Surf. Coat. Technol. 163-164 (2003) 484–490.

[10] P. Kurze, W. Krsymann, H.G. Schneider, Application Fields of ANOF Layers and Composites, Cryst. Res. Technol. 21 (1986) 1603–1609.

[11] F. Monfort, A. Berkani, E. Matykina, P. Skeldon, G.E. Thompson, A Tracer Study of Oxide Growth during Spark Anodizing of Aluminum, J. Electrochem. Soc. 152 (2005) C382–C387.

[12] A.L. Yerokhin, V. V. Lyubimov, R. V. Ashitkov, Phase formation in ceramic coatings during plasma electrolytic oxidation of aluminium alloys, Ceram. Int. 24 (1998) 1–6.

[13] W. Xue, Z. Deng, Y. Lai, R. Chen, Analysis of Phase Distribution for Ceramic Coatings Formed by Microarc Oxidation on Aluminum Alloy, J. Am. Ceram. Soc. 81 (1998) 1365–1368.

[14] R.O. Hussein, D.O. Northwood, X. Nie, Coating growth behavior during the plasma electrolytic oxidation process, J. Vac. Sci. Technol. A Vacuum, Surfaces, Film. 28 (2010) 766–773.

[15] A.L. Yerokhin, X. Nie, A. Leyland, A. Matthews, S.J. Dowey, Plasma electrolysis for surface engineering, Surf. Coatings Technol. 122 (1999) 73–93.

[16] G. Sundararajan, L. Rama Krishna, Mechanisms underlying the formation of thick alumina coatings through the MAO coating technology, Surf. Coatings Technol. 167 (2003) 269–277.

[17] X. Lin, X. Wang, L. Tan, P. Wan, X. Yu, Q. Li, et al., Effect of preparation parameters on the properties of hydroxyapatite containing micro-arc oxidation coating on biodegradable ZK60 magnesium alloy, Ceram. Int. (2014).

[18] E.L. Rooy, Introduction to aluminum and its alloys, in: ASM Met. Handbook, Vol 2, Prop. Sel. Nonferrous Alloy. Spec. Mater., 10th ed., ASM international, 1990: pp. 3–215.

Chapter 2

Literature Review

In this chapter the available literature on PEO is reviewed. Most of the information relates to PEO on aluminum and its alloys, which are the main focus of this work. The results of some PEO processing studies on other metals and alloys have also been included in the discussion where relevant. Following a brief overview of the development of PEO, the equipment setup is discussed, followed by the published theories on the mechanism of coating growth, and the formation, chemical and electrochemical reactions involved. Then the important process parameters affecting the PEO process are briefly reviewed. Finally the properties and applications of these coatings are summarized.

2.1 Development of PEO Processing

The PEO process has a long history of development. Although the discharge phenomena in aqueous electrolytes were discovered more than a century ago, they were not studied in detail until the 1930s.The practical benefit of spark discharge was first employed in the 1960s to deposit cadmium niobate onto a cadmium anode. During the 1970s, the application of surface discharges in order to deposit oxide coatings on light metals and alloys, mainly aluminum, was extensively studied. However, due to the poor quality of the coatings and their low growth efficiency, development was delayed. From the 1980s onwards, developments in the PEO process such as replacing acidic electrolytes with newly developed alkaline electrolytes and the application of pulsed current instead of direct current, improved the efficiency of the process and the quality of the coatings making it possible to commercialize the process. Companies such as Keronite (UK), Magoxide-coat (Germany) and Microplasmic (USA) are currently active in the field of commercial exploitation of PEO coatings to improve the tribological properties of light alloys. [1–3]. In recent years increasing attention has been paid to the adoption of light alloys for weight reduction in transportation and aerospace applications, and PEO has proven effective in protecting light alloys against corrosion and wear, two main weaknesses of these materials. Currently, PEO processes are in a transition phase from research to commercial application [4–6].

2.2 PEO Equipment Setup

Plasma electrolytic oxidation uses a similar configuration to that applied in conventional anodizing but is operated at much higher voltages, usually in the range 400-700 V [7,8]. A typical arrangement of the equipment used in PEO is presented in Figure 2.1. The unit consists of a high power electrical source and an electrolyser. The electrolyser is usually made of stainless steel which also serves as the counter electrode (cathode) and is connected to a cooling system to maintain the electrolyte temperature at the desired level. The stainless steel container is placed on an insulating base and confined in a grounded case. The grounded case is connected to a ventilation system for safety. Various types of power sources including direct current (DC), pulsed DC, and alternating current (AC) sources can be used for PEO [1,9–14].

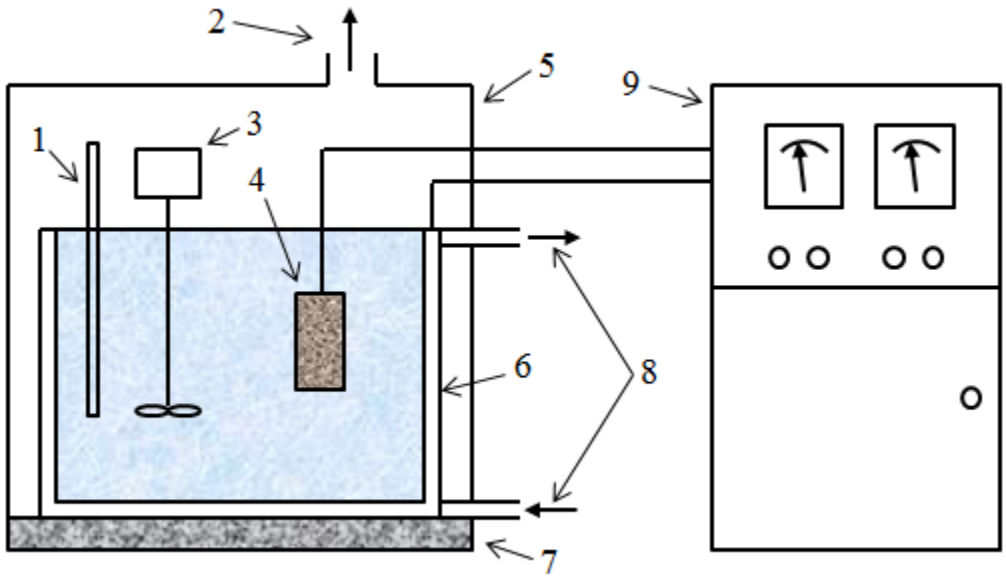

Figure 2.1-Typical arrangement of the equipment used for PEO coating: (1) thermocouple, (2) exhaust/ventilation system, (3) mixer, (4) workpiece, (5) grounded case, (6) bath, (7) insulating plate, (8) flow circulation via cooling system/filter, (9) power supply unit.

To deposit coatings, samples, which serve as the anode, are attached to the current supply and immersed in the electrolyte. A metal rod with a jacket is typically used to hold the sample. After the electrolyte mixing and cooling system and gas exhaust are activated, the current is applied to the workpiece based on the selected treatment regime [3].

2.3 Fundamentals and Mechanism of the PEO Process

PEO can be considered a technology intermediate between conventional anodising in aqueous solutions at low voltages and high energy plasma coating under dry conditions in a controlled gas pressure environment. During PEO, complex physical, chemical, electrochemical and plasma thermo-chemical reactions occur, and despite several investigations, the coating formation mechanisms in the PEO process are not fully understood, due primarily to the difficulty of catching the instantaneous discharge events occurring during PEO [2,3,12,15].

2.3.1 The Coating Growth Phenomenon

There are a few studies on the coating formation mechanisms. Based on the voltage-time response, shown in Figure 2.2, the PEO process can be divided into a number of stages in which different phenomena occur. At the beginning of the PEO process, stage 1, the cell voltage increases linearly and rapidly and a very thin insulating oxide film is formed on the surface of metals such as Al, Mg and Ti, when a suitable electrolyte is employed. In this stage, conventional anodization occurs and intensive gas evolution is observed. Eventually, the voltage reaches a critical value, the breakdown voltage, and dielectric breakdown occurs in weak sites across the oxide film accompanied by the formation of a large number of fine, uniform, white micro-discharges on the surface of the sample. Sparks are characteristic of the PEO process and play a crucial role in the formation of the coating. In stage 2, after breakdown has occurred, the voltage increases slowly and the oxide film growth rate decreases. This is thought to be caused by coating growth and dissolution happening simultaneously. In stage 3, the rate of voltage change increases slightly, the micro-discharges become more intense and last longer while their spatial density decreases, and their color changes from white to yellow and then gradually to orange. In stage 4, the rate of voltage increase becomes slightly slower than in stage 3,

and the sparks become stronger, but their population decreases while their colour remains orange.

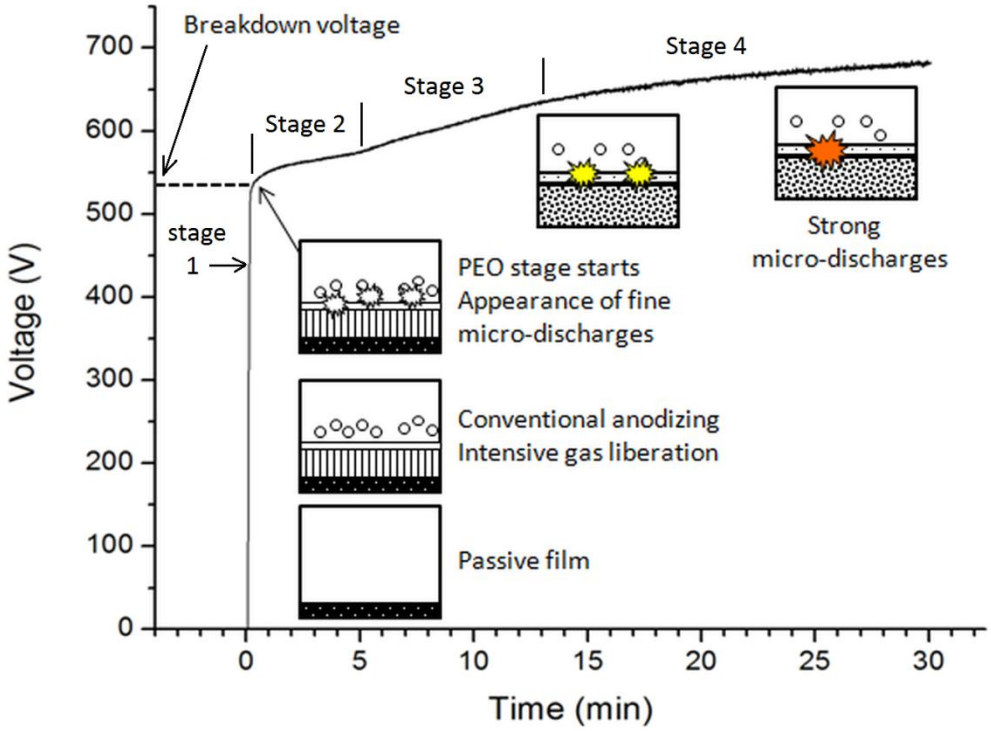

Figure 2.2- Schematic of the different stages and associated phenomena occurring during PEO coating.

Discharges play a very important role in the coating growth mechanism. Since discharge events are very short in PEO, it is very difficult to catch them instantaneously to analyze the physical and chemical processes occurring in the discharge channels. As a result, controversy exists over the growth mechanism of PEO coatings [3].

The PEO coating formation as the result of micro-discharges takes place through the following steps: (i) when the breakdown voltage is reached, many discharge channels are created as a result of micro-regional instability in the coating. The discharge temperature is estimated to be in the range of 4000-10000 K [1,16]. The low temperature range corresponds to small discharges happening in the early stages, i.e. immediately after the breakdown voltage is reached. The high temperature range corresponds to strong, long-lasting discharges happening in the final stages of the process, Figure 2.2. The local

plasma temperature is high enough to excite all the species that exist in the close vicinity of the discharge channels, and the induced electron collapse makes the coating materials move into these channels. Anionic species present in the electrolyte, such as SiO_3^{2-}, enter the channels electrophoretically under a strong electric field. The high temperature and pressure inside the discharge channels melt the substrate elements which diffuse into the channels. (ii) This molten material is ejected from the coating/substrate interface and solidifies when cooled by the surrounding electrolyte, whose temperature is controlled using an external heat exchanger. This solidified oxide increases the coating thickness in areas close to the discharge channels. (iii) The gases produced escape through the discharge channels resulting in the formation of circular areas with a hole in the centre, resembling the structure of a crater in a volcano. These volcano-like morphologies are often referred to as either a 'pancake structure' [17–19], or a 'crater' [20–23]. Throughout this thesis, the latter term is used. Figure 2.3 shows an SEM micrograph of the surface morphology of a PEO coating on aluminum with the craters marked with arrows. During PEO, melting, solidification, sintering and densification of the oxide layer occurs repeatedly in relatively weak regions of the coating surface leading to a uniform increase in overall coating thickness [3,16,24–29].

It is suggested that the PEO coating grows simultaneously above and below the original substrate surface by the combination of two growth mechanisms: (i) an outward growth, from the substrate towards the electrolyte, by the melting, oxidation and solidification of ejected species; and (ii) an inner growth into the substrate by an oxygen transport due to the high electric field. During the inner growth, oxygen anions transfer into the coating and react with metal cations from the metal substrate to form an oxide ceramic coating. Due to the high cooling rate enforced by the cold substrate, the molten oxide at the coating/substrate interface rapidly solidifies, creating a thin crystalline layer with small uniform nano-sized grains. TEM studies confirm the presence of this layer in PEO coatings on aluminum [12,30] and titanium [31]. The nano-crystalline layer is constantly formed during PEO and moves inwards by 'eating' the substrate and is considered as the main inner growth mechanism [3,28].

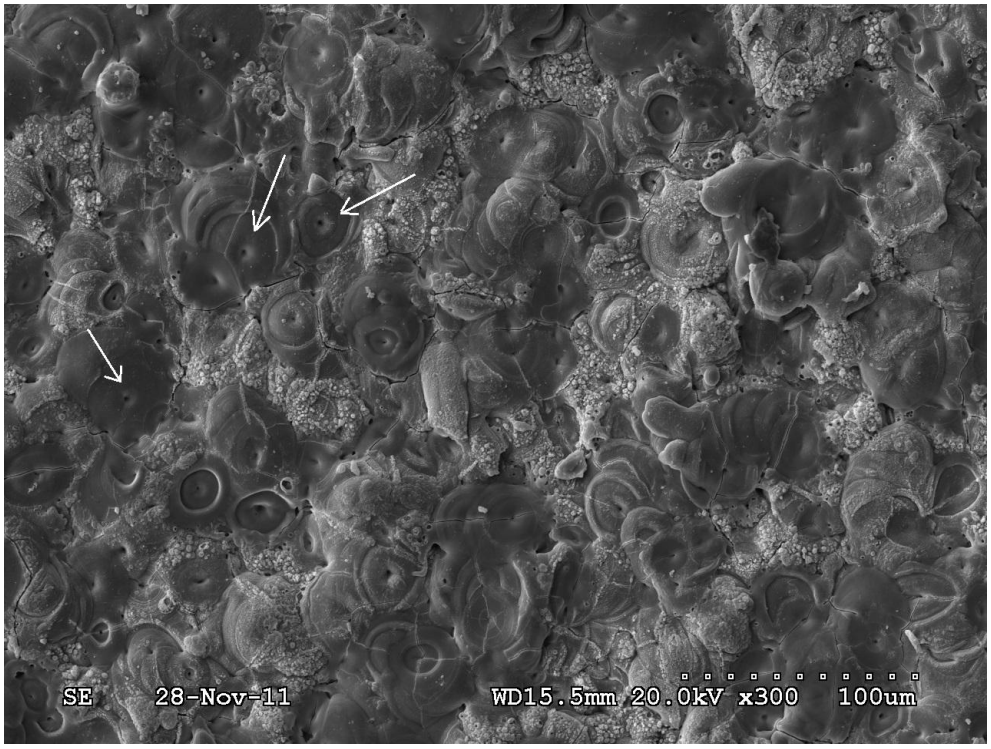

Figure 2.3- Scanning electron microscope (SEM) micrograph of the free surface of a PEO coating on an aluminum alloy. The arrows indicate the craters with discharge channels in the centre.

2.3.2 Micro-discharge Formation Models

During the PEO process different types of discharge are believed to occur. Previous researchers have proposed a variety of models to describe micro-discharge formation during PEO such as glow discharge electrolysis [32], electronic avalanche [33], electronic tunneling [34,35], and the model by Yerokhin et al. [27] which assumes the possibility of free electron generation and glow discharge ignition in the gaseous media at the oxide-electrolyte interface. However, there is still disagreement on the discharge and growth mechanisms because discharges are short-lived making it extremely difficult to study the complex reactions including plasma-chemical, thermal and anodic oxidation processes taking place in discharge regions [36]. The main problem is the fact that the proposed models do not explain all the characteristics of the coatings growth behaviour observed during PEO.

In a recent discharge model based on optical emission spectroscopy measurements, Hussein et al. [16,37] identified the elements present in the plasma and estimated the plasma temperature. They proposed a model in which three different types of discharge occurred (Figure 2.4). The B-type discharge was attributed to dielectric breakdown in a strong electric field occurring through the oxide layer. The A- and C-type discharges were related to gas discharges occurring in micro-pores in the oxide film: type A from the surface micro-pores, and type C from discharges in relatively deep micro-pores.

When the strength of the electric field reaches a critical value at the breakdown voltage, Figure 2.2, the coating breaks down and discharge channels are formed in which plasma reactions take place. It was suggested that type B discharges were the intense micro-discharges that typically occur in the later stages of the process creating large spikes on the discharge temperature profile. This implies they have a higher intensity than types A and C discharges. It was proposed that type B discharges, forming the strongest signal peaks, probably started from the substrate/coating interface.

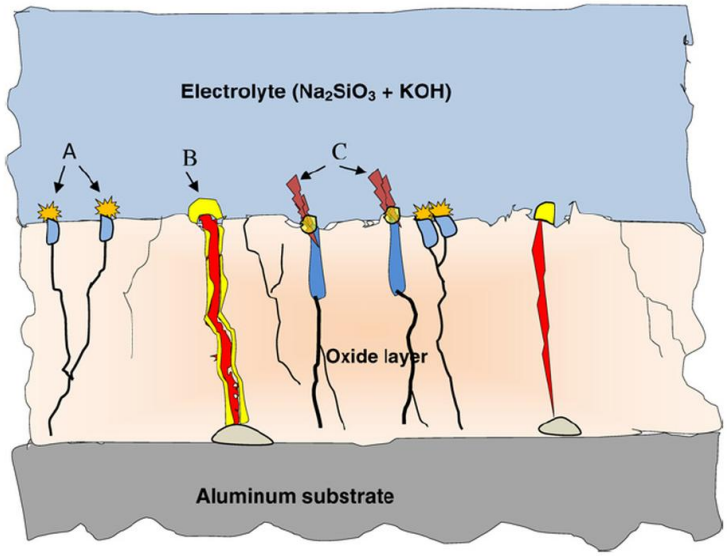

Figure 2.4- Schematic diagram of the discharge characteristics during the PEO of an aluminum substrate (Reprinted with permission from [37]).

Type A discharges involve surface discharges in relatively small holes near the surface and type C discharges occur in the micro-pores within the coating. During these discharges, the temperature increases significantly to a level sufficient to excite the species present in the system, such as aluminum. However, the results showed that their intensities were much less than those for type B discharges [16]. The plasma temperature was estimated to be in the range of 4000-10000 K. The low temperature range corresponded to the weak discharges and the high temperature to the strong ones [37].

The molten alumina generated by the three types of micro-discharge is abruptly ejected from the discharge channels to the outer surface, thus creating many craters. [19]

2.3.3 Possible Chemical and Electrochemical Reactions

Different processes of oxide formation, dissolution and gas evolution may occur for aluminum anodising in alkaline solutions [38]. PEO coatings have been produced using various types of current modes as illustrated in Figure 2.5. Depending on the applied current mode, three distinct periods in which different reactions may occur can be defined:

(1) The period when the current pulse is off (t_{off}). During t_{off}, Figure 2.5-c, when no current is applied, chemical reactions can etch the aluminum substrate and release the aluminate ion AlO_2^- and $Al(OH)_4^-$ into the electrolyte through the following reactions [39,40];

$$2Al + 2H_2O + 2OH^- = 2AlO_2^- (aq) + 3H_2 \quad (2.1)$$

$$Al + 4OH^- \rightarrow Al(OH)_4^- (gel) \quad (2.2)$$

The thickness of the alumina coating can decrease as a result of chemical dissolution [40];

$$Al_2O_3 + 2OH^- + 3H_2O \rightarrow 2Al(OH)_4^- (gel) \rightarrow 2Al(OH)_3\downarrow + 2OH^- \quad (2.3)$$

and boehmite may also be produced [39];

$$Al(OH)_4^- + H_2O \rightarrow AlO_2H \downarrow + 2\,H_2O + OH^- \quad (2.4)$$

Aluminum hydroxide could be redissolved by OH^- [41];

$$Al(OH)_3 + OH^- \rightarrow Al(OH)_4^- \quad (2.5)$$

and aluminum oxidation may also occur [41];

$$2Al + 3H_2O \rightarrow Al_2O_3 + 3H_2\uparrow \quad (2.6)$$

Based on this set of reactions, it can be concluded that the surface of the workpiece is only chemically dissolved by reactions with OH^- [41] and the dissolution rate will increase when the temperature of the electrolyte is elevated by the heat liberated during PEO [39].

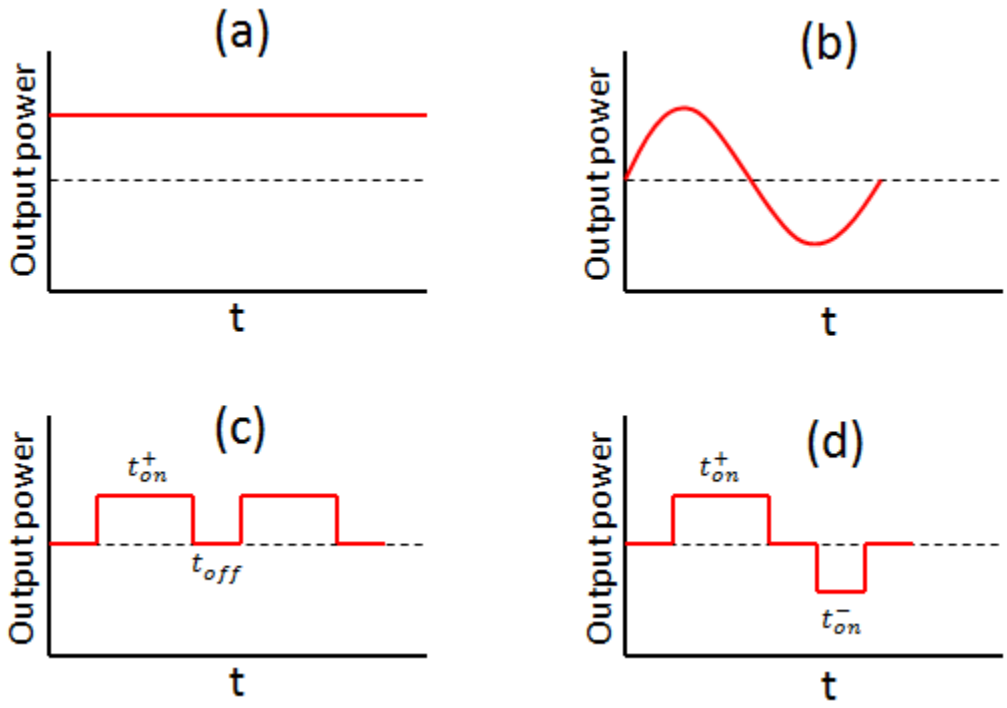

Figure 2.5- Various types of current modes used in PEO: (a) direct current (DC); (b) alternating current (AC); (c) unipolar pulsed current; (d) bipolar pulsed current.

(2) The anodic on time (t_{on}^{+}) period. During this period (Figure 2.5-c and d), the workpiece serves as the anode and discharge occurs under a high electric field above the breakdown voltage. Oxygen evolution occurs due to the oxidation of water [2]:

$$2H_2O \rightarrow O_2 + 4H^+ + 4e^- \quad (2.7)$$

and under the influence of the high electric field, oxygen is ionized and oxygen anions (O^{2-}), diffuse toward the substrate, and react with metal cations (Al^{3+}) migrating out toward the electrolyte to form aluminum oxide [42–44]:

$$2Al^{3+} + 3O^{2-} \rightarrow Al_2O_3 \quad (2.8)$$

Some of the aluminum cations may be ejected into the electrolyte and react with hydroxide or silicate [39,45]:

$$Al^{3+} + 3OH^- \rightarrow Al(OH)_3\downarrow \quad (2.9)$$

$$2Al^{3+} + 3SiO_2^{2-} \rightarrow Al_2(SiO_3)_3 \quad (2.10)$$

Anodic dissolution of metal will release cations to the electrolyte [2,45]:

$$Al \rightarrow Al^{3+} + 3e^- \quad (2.11)$$

Oxygen evolution also occurs due to the oxidation of water [2]:

(3) The cathodic on time (t_{on}^{-}) period. During this period (Figure 2.5-d), cations are attracted to the negatively charged substrate, anions are repelled, and metal deposition could occur [39]:

$$Al^{3+} + 3e^- \rightarrow Al \quad (2.12)$$

In neutral or alkaline electrolytes, hydrogen evolution can also occur [2]:

$$2H_2O + 2e^- \rightarrow H_2 + 2OH^- \quad (2.13)$$

During PEO coating of aluminum substrates in alkali electrolytes containing sodium silicate, a combination of mainly alumina and some aluminosilicate phases can be produced as a result of these reactions [39].

2.4 PEO Process Parameters

The PEO coating morphology and microstructure, which determine the characteristics of these coatings, are affected by many parameters such as electrolyte composition and temperature, substrate material, type of power source employed and the electrical parameters applied [3,46]. Here, a brief overview of the results of studies investigating the effect of process parameters on PEO coatings is given.

2.4.1 Current Mode

Power sources specially designed for PEO play a key role in the preparation of coatings. Various types of power sources capable of producing different current modes (AC, DC, and pulsed DC), as shown in Figure 2.5, have been employed to produce coatings on light alloys such as aluminum, magnesium and titanium [3]. A bipolar current mode is comprised of two components, i.e., a positive component and a negative component, while a unipolar current mode is only comprised of the positive component. Table 2.1 provides examples of published studies in which different current modes were employed.

Table 2.1- Examples of published studies using different current modes to produce PEO coatings.

Current mode	References
AC	[12], [36], [47], [48], [49]
DC	[10], [31], [50], [51], [52]
Unipolar pulsed DC	[53], [54], [55], [56]
Bipolar pulsed DC	[57], [58], [59], [60], [61]
Hybrid current (combination of pulsed unipolar and bipolar DC)	[62], [63]

The type of applied current mode can affect the surface discharge characteristics, namely the intensity and density of discharge events. These discharges play a key role in determining the coating microstructure, thickness, roughness, degree of porosity, hardness, and coating growth rate [64].

The direct current (DC) mode (Figure 2.5-a) is used only for simple-shape components and thin coatings because it offers limited control and flexibility due to the difficulty in adjusting discharge characteristics. The application of a DC current has been reported to result in a lower oxide growth rate with greater porosity than achieved with pulsed bipolar current (Figure 2.5-d) [1–3].

Use of the AC current mode eliminates the additional polarisation of the electrode and improves the ability to control the process by means of arc interruption. Furthermore, using an unbalanced AC mode in which the positive and negative segments have different amplitudes, allows improved control of the coating process. However, the limitation in power, which is typically less than 10 kW, and the current frequency (main frequency only) are disadvantages that restrict the commercial upscaling of this mode [1].

Application of the pulsed DC current mode allows control of the discharge duration and pulse form which makes it possible to use the available power more efficiently by reducing the energy consumption caused by interval discharge [3,65]. The application of bipolar pulsed mode has been reported to produce denser PEO coatings on aluminum and magnesium with fewer defects and a more uniform coating thickness compared to other types of current modes [57,66]. Recently, the pulsed bipolar current mode has attracted great interest due to the improved properties of the produced coatings.

Yerokhin et al. [57] compared the properties of PEO coatings formed on aluminum using either a 50Hz AC input or a pulsed bipolar DC current mode and observed that the coating produced by the pulsed bipolar mode had an improved morphology, with the thickness of the porous outer layer being reduced compared to that produced by the AC mode.

PEO coatings produced using the pulsed bipolar current mode on Al, Mg, and Ti alloys have been shown to be more corrosion resistant and to have a higher average thickness compared to coatings produced using the AC, DC, and pulsed unipolar modes [4,13,62,67].

The use of a hybrid current mode, a combination of pulsed unipolar and bipolar current modes, has been reported to result in improved coating properties. Recent studies [17,62] suggest that the application of the hybrid mode resulted in coatings with a denser inner layer and fewer defects on an Mg alloy. The order of the applied current modes was found to significantly influence the morphology and corrosion resistance. A unipolar followed by a bipolar current mode yielded the best results.

The improved properties of coatings produced using a pulsed bipolar mode could be attributed to the change in plasma discharge behavior caused by the bipolar mode which can significantly influence the microstructure and morphology of the oxide coatings. Using optical emission spectroscopy, it was concluded that applying the pulsed bipolar mode resulted in a reduction of the strong intensity B-type discharges (Figure 2.4) and a delay in their formation. The B-type discharge is the strongest among the different discharge types as described earlier in section 2.3.2.The reduction of B-type discharges in the pulsed bipolar mode due to the polarity change, reduces the detrimental effects associated with such discharge events [17,46,67].

2.4.2 Current Density

Current density is one of the most important parameters affecting the properties of PEO coatings and should be applied in a range high enough to provide the conditions required for PEO. Values within the range 1 to 30 A/dm^2 have been reported in the published literature. Changing the current density can affect the composition, phase content, microstructure, growth rate, and physical and chemical properties of coatings [1,68,69]. For aluminum alloys, increasing the current density enhanced the coating growth rate and increased the relative content of α-Al_2O_3. PEO coatings on aluminum alloys are typically composed of a mixture of α-Al_2O_3 (the thermodynamically stable alumina phase with the highest hardness) and γ- Al_2O_3 (a low temperature phase). These results suggest a thermal

effect of the applied current density on phase transformations in the coatings [10,15]. Studies on magnesium alloys showed that current density had a great effect on the corrosion resistance of coated samples [70,71].

2.4.3 Pulse Parameters

For pulsed current modes (Figure 2.5-c and d), the pulse parameters (voltage or current, positive and negative pulse on (t_{on}) and off (t_{off}) time durations and their ratios) can be adjusted providing great flexibility in controlling the process.

The sparking intensity depends on the energy of each pulse and the single pulse energy increases when using higher currents or voltages and longer t_{on} periods. The single pulse energy (E_p) is defined as:

$$E_p = \int_0^{t_{on}} U_p . I_p \, dt \tag{2.14}$$

where U_p is the pulse voltage, I_p is the pulse current and t_{on} is the pulse on time. Therefore, changing pulse parameters can adjust the characteristics of the discharge events, and influence the growth rate, microstructure, and phase composition of the coatings [3]. Increasing the pulse on time was found to enhance the $\gamma \rightarrow \alpha$-$Al_2O_3$ phase transformation resulting in a different distribution of elements and phases in the coatings [8,15].

2.4.4 PEO Treatment Time

Various treatment times from a few minutes up to a few hours have been used. Increasing the treatment time generally results in thicker coatings and creates more intense and larger micro-discharges that are more widely spaced and produce bigger discharge channels in the coating. It also results in coarsening of the coating surface due to the formation of relatively large pores. The results of a previous study [26] showed that the average size of discharge channels, as well as the diameters of the craters, increased gradually as the treatment time was extended from 1 to 30 min. Micro-discharges are created as the result of dielectric breakdown through weak spots in the PEO coating and the number of weak spots is reduced in thicker coatings. A higher energy is required for

the current to pass through the coating and, since the number of weak sites is limited, the current is highly localized and creates bigger discharge channels [72–74].

In a recent study, Bajat et al. [75] investigated the corrosion performance of coatings on aluminum produced at different treatment times from 2 to 60 min and observed that the corrosion behavior was a function of treatment time. Initially the corrosion resistance increased to a maximum before it decreased for longer treatment times.

2.4.5 Electrolyte Composition

The composition of the electrolyte plays a very important role in the PEO process. A suitable electrolyte promotes metal passivation and creates a thin insulating film which is required for dielectric breakdown to induce discharge events. It also acts as a medium to conduct current and transmit the necessary energy for the process and provides the oxygen needed for oxidation. Components present in the electrolyte can be incorporated into the coatings which affect their properties. A wide range of electrolyte compositions has been used, Table 2.2. The electrolyte is usually maintained at a temperature in the range 20 to 55 °C using an external heat exchanger.

To facilitate the conditions required for dielectric breakdown, electrolyte additives such as silicates and phosphates, which promote metal passivation, are widely used as the basic constituents of PEO electrolytes. These additives decrease the breakdown voltage and can increase the coating growth rate by incorporation of components in the electrolyte (e.g. SiO_3^{2-}) into the coatings [2,3].

It has been reported that electrolyte composition can affect a wide range of coating properties such as the morphology and microstructure, growth rate and composition, strength of adhesion to the substrate, micro-hardness, and tribological properties [76,79–81].

Table 2.2- Electrolyte compositions used to grow PEO coatings on aluminum alloys and coating phases formed.

Reference	Substrate	Electrolyte composition	Phase composition of coating
[76]	Al	30 g/l Na_2SiO_3; 10-40 g/l NaOH	α-Al_2O_3, γ- Al_2O_3, mullite, Al_2SiO_5
[77]	Al 2024	2-5 g/l Na_2SiO_3; 3-5 g/l NaOH; 1 g/l organic agent	α-Al_2O_3, γ- Al_2O_3
[78]	Al 2017A	0-8 g/l Na_2SiO_3; 2 g/l KOH	α-Al_2O_3, γ- Al_2O_3, mullite
[12]	Al 2024	20 g/ l Na_2SiO_3	γ- Al_2O_3 dominant, α-Al_2O_3, mullite, δ- Al_2O_3
[65]	Al 6082	1 g/l KOH	α-Al_2O_3, γ- Al_2O_3

Alkaline electrolytes containing sodium silicate are most commonly used. It has been observed that the use of an electrolyte containing 2-20 g/l Na_2SiO_3 and 2-4 g/l KOH thickens the inner dense layer in the coating which is mainly composed of γ- and α-Al_2O_3 with some complex Al-Si-O phases also present. Also, changing the concentrations of KOH and Na_2SiO_3 has been shown to affect the voltage-time response and influence the onset of the breakdown voltage. Increasing the concentration of sodium silicate generally leads to an increase in coating growth rate which could be related to the incorporation of silicon-rich species into the coating. Increasing the alkalinity has been reported to cause local dissolution of the oxide layer [2,78,82].

Organic or inorganic electrolyte additives could be used to improve the solution conductivity, the initial passivation of the substrate, to increase the stability of the electrolyte, and to enhance coating performance. Liu et al. [83,84] demonstrated that the addition of Na_2WO_4 reduced the breakdown voltage and energy consumption and increased the density, coating thickness and corrosion resistance of the coatings.

Using cataphoretic effects, i.e. the transfer of particles both to and away from the substrate in the strong electric fields during PEO, it is possible to incorporate additives such as hard, high melting point particles (SiC, ZrO_2), dry lubricants, and coloring agents into the coatings [1,83]. For example, titania sol was used to form blue coatings on a Mg-

Li alloy [85], black coatings were formed on the 2A70 aluminum alloy by adding K_2TiF_6 to the electrolyte [86], and NH_4VO_3 was used to create black coatings on the LY12 aluminum alloy [87]. The formation of black vanadium oxide (V_2O_3) was suggested to be the reason for the colour.

Composite ceramic coatings containing hard particles have been formed using PEO. Arrabel et al. [88] reported that zirconia particles could be incorporated into the coatings formed on aluminum, and coatings containing TiO_2, ZrO_2 and Al_2O_3 nanoparticles were produced on a Mg alloy by Mandelli et al. [89]. They observed that these coatings had both a higher adhesion to the substrate and an increased scratch hardness. Coatings on pure titanium treated in an electrolyte containing 6 g/l Al_2O_3 nanoparticles showed an improved wear resistance [90]. Adding carbon nanotubes to the electrolyte decreased the coating micro-pore size and produced a higher density coating on aluminum alloys. Electrochemical tests showed that samples treated in electrolytes with carbon nanotubes possessed superior corrosion resistance compared to those coated in conventional electrolytes [91,92].

The short service lifetime of the electrolyte affects the reproducibility of coatings and is a challenge for industrial applications. The primary focus of published studies on PEO electrolytes has been on the development and optimization of composition and concentration to achieve desirable coating properties, although the stability of the electrolyte is a major issue and an important research direction [3].

2.4.6 Composition of the Substrate

Substrate composition can influence the properties of PEO coatings. In a study where pure Mg and three different Mg alloys were treated under similar conditions, the results showed that surface morphologies, coating thickness and porosity level were affected by the substrate alloying elements [93].

2.5 Properties of PEO Coatings

The PEO coatings can typically contain up to three layers: adjacent to the substrate, there is a thin inner layer termed “the barrier layer” followed by an intermediate layer of variable thickness and relatively low porosity, termed the “functional layer”, which provides the main thermo-mechanical and tribological functionality of the coating. A third porous and loose layer, located on top of the functional layer has also been observed on some samples. The functional layer normally constitutes about 70-80% of the total coating thickness. The outer layer may be used as a base for sealants and primers for improved corrosion resistance [2,57,94].

Figure 2.6 shows the cross-section of an aluminum alloy sample coated by PEO. The coating which is mainly composed of the functional layer has a low level of porosity with some cracks that are the result of strong micro-discharges across the coating.

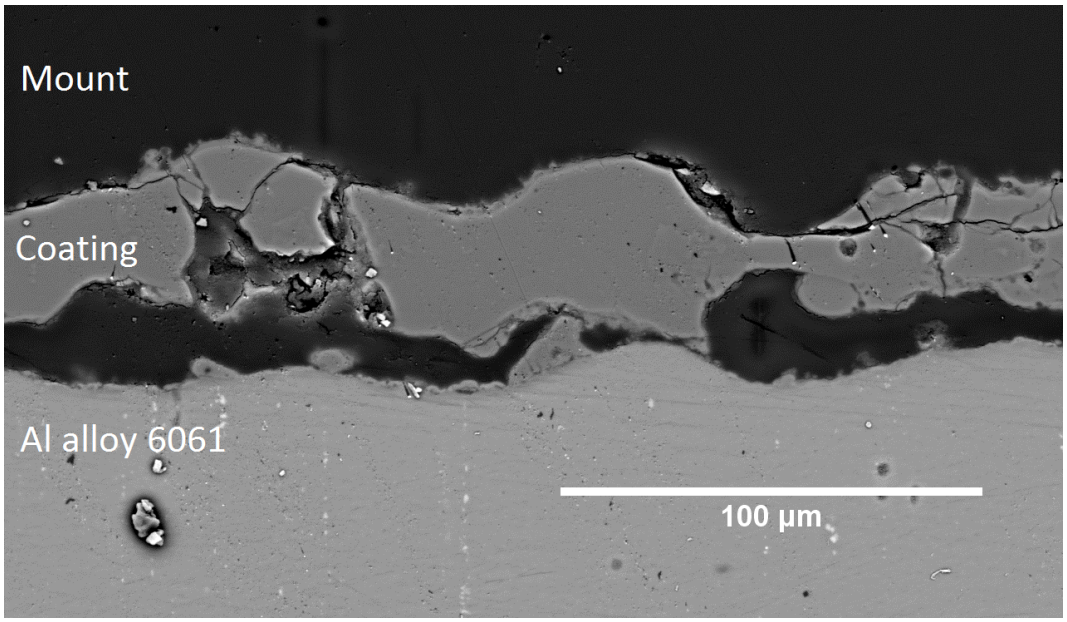

Figure 2.6- SEM micrograph of a cross-section of a PEO coating on the aluminum 6061 alloy.

Pore formation in PEO coatings is almost inevitable. In a detailed study of porosity, Curran and Clyne [95] provided evidence that the coatings contain sub-micrometer, surface-connected porosity that can reach ~20% on aluminum alloys. It is believed that the formation of pores arises from oxygen evolution that can become trapped later in the coating during the PEO process. The pressures and temperatures are likely to result in a significant concentration of dissolved oxygen in the molten oxides. Depending on the duration of the anodic coating cycle, discharge duration can be very short, less than a millisecond [36], leading to the trapping of oxygen in the molten material.

The relatively low stiffness of PEO coatings may be partly due to the presence of this porosity and the presence of micro-cracks. The hardness and corrosion resistance can also be negatively affected by porosity. However, one advantage of porosity is its contribution to the low thermal conductivity of coatings, which is beneficial for the thermal protection of the substrate [95,96].

The PEO technique provides better adhesive strength between coating and substrate compared to electrochemical plating and anodizing [97]. Terleeva et al. [98] reported that PEO coatings on titanium have sufficiently high adhesion strength and a suitable roughness for implant applications.

2.5.1 Mechanical Properties

Phase composition is one of the principal factors that determine the mechanical or tribological performance of PEO coatings. Previous studies on coated aluminum alloys in alkali electrolytes [10,25,68,99,100], suggest that the coatings mainly consist of α-Al_2O_3 and γ-Al_2O_3. For silicate based electrolytes, mullite ($3Al_2O_3.2SiO_2$) can also be present in the coating. Alpha alumina is a stable, rhombohedral phase with a melting point of 2050 °C and gamma alumina is a cubic metastable phase that can transform into α- Al_2O_3 if heated in the range of 800- 1200 °C [10,101,102]. The content of the harder α- Al_2O_3 phase can reach up to 60% for PEO coatings on aluminum substrates containing copper, whereas on aluminum substrates containing magnesium, the γ phase is dominant [1]. It has been suggested that contact of the molten oxide formed during sparking with the electrolyte results in the formation of γ-Al_2O_3 rather than α-Al_2O_3 because of the

extremely high cooling rate and the lower critical energy for nucleation of γ-Al_2O_3 [26,103]. Since γ-Al_2O_3 is a metastable phase, it can transform into α-Al_2O_3 upon heating. By controlling the electrical parameters such as current density, duty cycle and frequency it would be possible to control the $\gamma \rightarrow \alpha$-$Al_2O_3$ phase transformation.

The elastic modulus and hardness of PEO coatings were found to be appreciably higher than those of hard anodized coatings on the 6082 aluminum alloy [104]. The crystalline phases in the coatings result in a higher hardness compared to the amorphous oxides formed during conventional anodizing. It has been reported that the hardness of PEO coatings on different aluminum alloys can reach 900-2000 Hv [21,105].

2.5.2 Wear Resistance Properties

Wear resistance properties of coatings mainly depend on hardness. The hardness of the PEO coating is a function of the nature of the dominant phases present, as well as their ratio and distribution and the porosity and density of micro-cracks in the coatings. The hardness of alumina phases has been reported to be about 26 GPa for α-Al_2O_3, 17 GPa for γ-Al_2O_3, 10.5 GPa for mullite, and 7 GPa for the amorphous anodically formed alumina. However, the measured hardness of PEO coatings is lower than that of the dense bulk alumina due to the porosity [4,10,106]. Tribological studies indicate coatings composed of α-Al_2O_3 show a higher wear resistance [107].

PEO coatings produced on aluminum alloys have a superior wear resistance to hard anodized coatings. A comparative study of the tribilogical behavior of coatings on the 6061 aluminum alloy indicated that the hard-anodized coatings reduced the abrasive wear rate by a factor of two, while the PEO coatings reduced the wear rate by a factor of 12-30 [108]. Figure 2.7 illustrates the relative wear resistance of various materials and coatings. As can be seen, the abrasive wear resistance of PEO coatings is very high and comparable to that of tungsten carbide composites, boride diffusion coatings and corundum [1].

In recent years, the demand for the reduction of fuel consumption and exhaust emissions has increased the need for the weight reduction of automobiles. The high wear resistance

provided by PEO coatings makes it possible to replace steel and cast-iron parts with lighter alloys. The resulting weight savings from such replacements can provide large commercial efficiency by improving the performance and reducing the fuel consumption in the automotive, aircraft and aerospace industries [3,109].

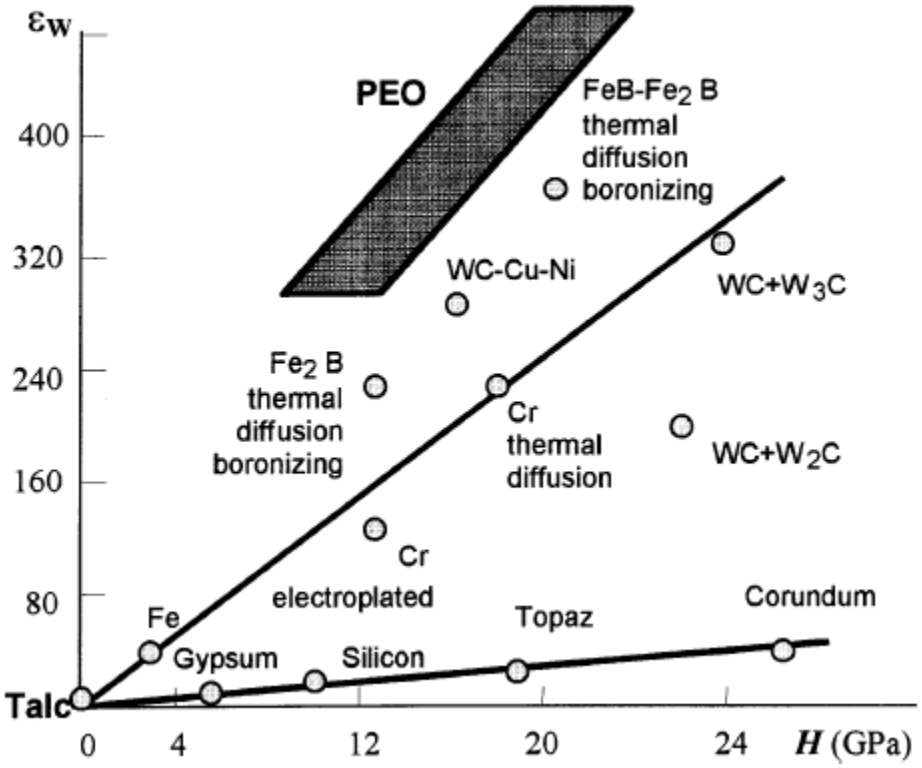

Figure 2.7- Relative wear resistance (ε_w) of various materials with different hardness (H) values with respect to talc (Reprinted with permission from [1]).

2.5.3 Corrosion Resistance Properties

Light alloys, namely Mg alloys followed by aluminum, are susceptible to corrosion, which limits their practical application, especially in aggressive environments. PEO can significantly improve the corrosion resistance properties of these alloys [110]. Electrochemical impedance spectroscopy studies on Mg, Al, and Ti alloys show that the barrier layer contributes most to the overall coating corrosion resistance of PEO coatings.

This is mainly because the corrosive medium can penetrate the pores and micro-cracks of the functional layer leaving the compact barrier layer as the main barrier to prevent the substrate from corrosion [75,93,111,112].

The surface morphology and coating microstructure have been found to play a significant role in determining corrosion resistance by influencing the number and size of coating defects such as porosity and microcracks. Preventing the formation of defective coatings containing large pores and micro-cracks to improve the corrosion protection is the present focus of many studies [93].

In order to effectively improve the corrosion resistance, surface porosity and micro-cracks in PEO coatings can be used for surface impregnation by sealants. Chen et al. [113], applied a thin layer of polypropylene to seal the PEO-coated surface on the 2519 aluminum alloy and observed that the corrosion current density was reduced by about two orders of magnitude.

Galvanic corrosion is a big problem when light alloys are coupled with other metals. Light alloys (especially Mg and Al) are more active in the galvanic series and are corroded when put in contact with other metals. PEO coatings have been shown to help eliminate galvanic corrosion by providing a layer that prevents direct contact between light alloys and other metals [3,114,115].

2.5.4 Thermal Protection Properties

To be suitable as thermal barrier coatings, a combination of properties including low thermal conductivity, good oxidation and thermal shock resistance, and good adhesion to the substrate is required. The conductivity of PEO coatings has been found to be at least one order of magnitude lower than typical values for corresponding bulk materials, making them potentially attractive for thermal barrier applications. Measured conductivity values of ~1.6 $W.m^{-1}.K^{-1}$ and ~0.8 $W.m^{-1}.K^{-1}$ were reported for PEO coatings on Al and Mg, respectively, which can be compared with the corresponding expected values of ~30 $W.m^{-1}.K^{-1}$ for Al and ~20 $W.m^{-1}.K^{-1}$ for Mg. Oxide ceramic coatings produced by PEO, especially mullite-rich coatings on aluminum alloys prepared

in silicate-rich electrolytes which can reach a thickness of up to 200 µm, offer considerable promise as thermal barriers [96,116].

2.5.5 Dielectric Properties

The high electrical resistance and breakdown strength of ceramic coatings such as Al_2O_3, SiO_2, and ZrO_2 provide strong dielectric properties in PEO coatings [1].

2.6 Applications of PEO Coatings

Existing and potential applications of PEO coatings span a wide range of industries including the automotive, aerospace, construction, electrical, biomedical, oil and gas processing, textile, and sports and leisure industries. This wide range of applications can be mainly related to the following properties:

a) high hardness;
b) good tribological properties (corrosion and wear resistance);
c) adhesion for top coats such as paints and polymers;
d) high heat resistance which makes them suitable as thermal barrier coatings;
e) biocompatibility for cell growth and implant integration;
f) dielectric properties as electrical insulation, capacitors and many more.

PEO coatings have been successfully applied to aluminum [101,117], magnesium [36,63], titanium [31,118] and their alloys. Recently, the PEO process has also been applied to zirconium [119,120] and tantalum [121,122].

2.7 References

[1] A.L. Yerokhin, X. Nie, A. Leyland, A. Matthews, S.J. Dowey, Plasma electrolysis for surface engineering, Surf. Coatings Technol. 122 (1999) 73–93.

[2] F.C. Walsh, C.T.J. Low, R.J.K. Wood, K.T. Stevens, J. Archer, A.R. Poeton, et al., Plasma electrolytic oxidation (PEO) for production of anodised coatings on lightweight metal (Al, Mg, Ti) alloys, Trans. Inst. Met. Finish. 87 (2009) 122–135.

[3] B.L. Jiang, Y.M. Wang, Plasma Electrolytic Oxidation Treatment of Aluminum and Titanium Alloys, in: H. Dong (Ed.), Surf. Eng. Light Alloy. Aluminum, Magnes. Titan. Alloy., Woodhead Publishing, 2010: pp. 110–153.

[4] Y. Cheng, Z. Xue, Q. Wang, X.-Q. Wu, E. Matykina, P. Skeldon, et al., New findings on properties of plasma electrolytic oxidation coatings from study of an Al–Cu–Li alloy, Electrochim. Acta. 107 (2013) 358–378.

[5] Y. Cheng, F. Wu, E. Matykina, P. Skeldon, G.E.E. Thompson, The influences of microdischarge types and silicate on the morphologies and phase compositions of plasma electrolytic oxidation coatings on Zircaloy-2, Corros. Sci. 59 (2012) 307–315.

[6] P. Gupta, G. Tenhundfeld, E.O. Daigle, D. Ryabkov, Electrolytic plasma technology: Science and engineering—An overview, Surf. Coatings Technol. 201 (2007) 8746–8760.

[7] F. Xu, Y. Xia, G. Li, The mechanism of PEO process on Al–Si alloys with the bulk primary silicon, Appl. Surf. Sci. 255 (2009) 9531–9538.

[8] V. Dehnavi, B.L. Luan, D.W. Shoesmith, X.Y. Liu, S. Rohani, Effect of duty cycle and applied current frequency on plasma electrolytic oxidation (PEO) coating growth behavior, Surf. Coatings Technol. 226 (2013) 100–107.

[9] Y. Gao, A. Yerokhin, A. Matthews, DC plasma electrolytic oxidation of biodegradable cp-Mg: In-vitro corrosion studies, Surf. Coatings Technol. 234 (2013) 132–142.

[10] R.H.U. Khan, A. Yerokhin, X. Li, H. Dong, A. Matthews, Surface characterisation of DC plasma electrolytic oxidation treated 6082 aluminium alloy: Effect of current density and electrolyte concentration, Surf. Coatings Technol. 205 (2010) 1679–1688.

[11] Y. Gu, C. Chen, S. Bandopadhyay, C. Ning, Y. Zhang, Y. Guo, Corrosion mechanism and model of pulsed DC microarc oxidation treated AZ31 alloy in simulated body fluid, Appl. Surf. Sci. 258 (2012) 6116–6126.

[12] Y. Guan, Y. Xia, G. Li, Growth mechanism and corrosion behavior of ceramic coatings on aluminum produced by autocontrol AC pulse PEO, Surf. Coatings Technol. 202 (2008) 4602–4612.

[13] S. Wang, Y. Xia, L. Liu, N. Si, Preparation and performance of MAO coatings obtained on AZ91D Mg alloy under unipolar and bipolar modes in a novel dual electrolyte, Ceram. Int. 40 (2014) 93–99.

[14] X. Guo, K. Du, Y. Wang, Y. Shao, F. Wang, A new nanoparticle penetrant used for plasma electrolytic oxidation film coated on AZ31 Mg alloy in service environment, Surf. Coatings Technol. 206 (2012) 4833–4839.

[15] V. Dehnavi, X.Y. Liu, B.L. Luan, D.W. Shoesmith, S. Rohani, Phase Transformation in Plasma Electrolytic Oxidation Coatings on 6061 Aluminum Alloy, Surf. Coatings Technol. 251 (2014) 160-114.

[16] R.O. Hussein, X. Nie, D.O. Northwood, A. Yerokhin, A. Matthews, Spectroscopic study of electrolytic plasma and discharging behaviour during the plasma electrolytic oxidation (PEO) process, J. Phys. D. Appl. Phys. 43 (2010) 105203–105216.

[17] R.O. Hussein, X. Nie, D.O. Northwood, The influence of pulse timing and current mode on the microstructure and corrosion behaviour of a plasma electrolytic oxidation (PEO) coated AM60B magnesium alloy, J. Alloys Compd. 541 (2012) 41–48.

[18] Y. Cheng, E. Matykina, R. Arrabal, P. Skeldon, G.E. Thompson, Plasma electrolytic oxidation and corrosion protection of Zircaloy-4, Surf. Coatings Technol. 206 (2012) 3230–3239.

[19] X. Shen, X. Nie, H. Hu, J. Tjong, Effects of coating thickness on thermal conductivities of alumina coatings and alumina/aluminum hybrid materials prepared using plasma electrolytic oxidation, Surf. Coatings Technol. 207 (2012) 96–101.

[20] W. Zhu, Y.-J. Fang, H. Zheng, G. Tan, H. Cheng, C. Ning, Effect of applied voltage on phase components of composite coatings prepared by micro-arc oxidation, Thin Solid Films. 544 (2013) 79–82.

[21] J.M. Wheeler, J. A. Curran, S. Shrestha, Microstructure and multi-scale mechanical behavior of hard anodized and plasma electrolytic oxidation (PEO) coatings on aluminum alloy 5052, Surf. Coatings Technol. 207 (2012) 480–488.

[22] B. Kasalica, M. Petkovic, I. Belca, S. Stojadinovic, L. Zekovic, Electronic transitions during plasma electrolytic oxidation of aluminum, Surf. Coatings Technol. 203 (2009) 3000–3004.

[23] Y. Chen, T. Cheng, X. Nie, Wear failure behaviour of titanium-based oxide coatings on a titanium alloy under impact and sliding forces, J. Alloys Compd. 578 (2013) 336–344.

[24] H. Guo, M. An, S. Xu, H. Huo, Formation of oxygen bubbles and its influence on current efficiency in micro-arc oxidation process of AZ91D magnesium alloy, Thin Solid Films. 485 (2005) 53–58.

[25] W. Xue, Z. Deng, Y. Lai, R. Chen, Analysis of Phase Distribution for Ceramic Coatings Formed by Microarc Oxidation on Aluminum Alloy, J. Am. Ceram. Soc. 81 (1998) 1365–1368.

[26] G. Sundararajan, L. Rama Krishna, Mechanisms underlying the formation of thick alumina coatings through the MAO coating technology, Surf. Coatings Technol. 167 (2003) 269–277.

[27] A.L. Yerokhin, L.O. Snizhko, N.L. Gurevina, A. Leyland, A. Pilkington, A. Matthews, Discharge characterization in plasma electrolytic oxidation of aluminium, J. Phys. D. Appl. Phys. 36 (2003) 2110–2120.

[28] R.O. Hussein, X. Nie, D.O. Northwood, An investigation of ceramic coating growth mechanisms in plasma electrolytic oxidation (PEO) processing, Electrochim. Acta. 112 (2013) 111–119.

[29] M. Treviño, R.D. Mercado-Solis, R. Colás, A. Pérez, J. Talamantes, A. Velasco, Erosive wear of plasma electrolytic oxidation layers on aluminium alloy 6061, Wear. 301 (2012) 434–441.

[30] X. Nie, E.I. Meletis, J.C. Jiang, A. Leyland, A.L. Yerokhin, A. Matthews, Abrasive wear/corrosion properties and TEM analysis of Al_2O_3 coatings fabricated using plasma electrolysis, Surf. Coat. Technol. 149 (2002) 245–251.

[31] E. Matykina, R. Arrabal, P. Skeldon, G.E. Thompson, Transmission electron microscopy of coatings formed by plasma electrolytic oxidation of titanium., Acta Biomater. 5 (2009) 1356–66.

[32] A. Hickling, M.D. Ingram, Glow-discharge electrolysis, J. Electroanal. Chem. 8 (1964) 65–81.

[33] A.K. Vijh, Sparking voltages and side reactions during anodization of valve metals in terms of electron tunnelling, Corros. Sci. 11 (1971) 411–417.

[34] S. Ikonopisov, A. Girginov, M. Machkova, Post-breakdown anodization of aluminium, Electrochim. Acta. 22 (1977) 1283–1286.

[35] S. Ikonopisov, Theory of electrical breakdown during formation of barrier anodic films, Electrochim. Acta. 22 (1977) 1077–1082.

[36] R. Arrabal, E. Matykina, T. Hashimoto, P. Skeldon, G.E. Thompson, Characterization of AC PEO coatings on magnesium alloys, Surf. Coatings Technol. 203 (2009) 2207–2220.

[37] R.O. Hussein, D.O. Northwood, X. Nie, Coating growth behavior during the plasma electrolytic oxidation process, J. Vac. Sci. Technol. A Vacuum, Surfaces, Film. 28 (2010) 766–773.

[38] L. Snizhko, A. Yerokhin, A. Pilkington, N. Gurevina, D. Misnyankin, A. Leyland, et al., Anodic processes in plasma electrolytic oxidation of aluminium in alkaline solutions, Electrochim. Acta. 49 (2004) 2085–2095.

[39] M.M.S. Al Bosta, K. Ma, H. Chien, M.M.S. Al Bosta, The effect of MAO processing time on surface properties and low temperature infrared emissivity of ceramic coating on aluminium 6061 alloy, Infrared Phys. Technol. 60 (2013) 323–334.

[40] E. V. Koroleva, G.E. Thompson, G. Hollrigl, M. Bloeck, Surface morphological changes of aluminium alloys in alkaline solution: effect of second phase material, Corros. Sci. 41 (1999) 1475–1495.

[41] S.M. Moon, S.-I. Pyun, The corrosion of pure aluminium uring cathodic ploarization in aqeous solutions, Corros. Sci. 39 (1997) 399–408.

[42] Y.K. Pan, C.Z. Chen, D.G. Wang, X. Yu, Z.Q. Lin, Influence of additives on microstructure and property of microarc oxidized Mg–Si–O coatings, Ceram. Int. 38 (2012) 5527–5533.

[43] K. Wang, B.H. Koo, C.G. Lee, Y.J. Kim, S. Lee, E. Byon, Effects of Hybrid Voltages on Oxide Formation on 6061 Al-alloys During Plasma Electrolytic Oxidation, Chinese J. Aeronaut. 22 (2009) 564–568.

[44] V.S. Rudnev, T.P. Yarovaya, D.L. Boguta, L.M. Tyrina, P.M. Nedozorov, P.S. Gordienko, Anodic spark deposition of P , Me (II) or Me (III) containing coatings on aluminium and titanium alloys in electrolytes with polyphosphate complexes, J. Electroanal. Chem. 497 (2001) 150–158.

[45] H. Li, R. Song, Z. Ji, Effects of nano-additive TiO2 on performance of micro-arc oxidation coatings formed on 6063 aluminum alloy, Trans. Nonferrous Met. Soc. China. 23 (2013) 406–411.

[46] R.O. Hussein, X. Nie, D.O. Northwood, Influence of process parameters on electrolytic plasma discharging behaviour and aluminum oxide coating microstructure, Surf. Coatings Technol. 205 (2010) 1659–1667.

[47] E. Matykina, R. Arrabal, P. Skeldon, G.E. Thompson, P. Belenguer, AC PEO of aluminium with porous alumina precursor films, Surf. Coat. Technol. 205 (2010) 1668–1678.

[48] C.S. Dunleavy, J. A. Curran, T.W. Clyne, Time dependent statistics of plasma discharge parameters during bulk AC plasma electrolytic oxidation of aluminium, Appl. Surf. Sci. 268 (2012) 397–409.

[49] X. Nie, L. Wang, E. Konca, A. T. Alpas, Tribological behaviour of oxide/graphite composite coatings deposited using electrolytic plasma process, Surf. Coatings Technol. 188-189 (2004) 207–213.

[50] Y. Gao, A. Yerokhin, A. Matthews, DC plasma electrolytic oxidation of biodegradable cp-Mg : In-vitro corrosion studies, Surf. Coat. Technol. 234 (2013) 132–142.

[51] S. Verdier, M. Boinet, S. Maximovitch, F. Dalard, Formation, structure and composition of anodic films on AM60 magnesium alloy obtained by DC plasma anodising, Corros. Sci. 47 (2005) 1429–1444.

[52] D.K. Ivanou, M. Starykevich, A. D. Lisenkov, M.L. Zheludkevich, H.B. Xue, S.V. Lamaka, et al., Plasma anodized ZE41 magnesium alloy sealed with hybrid epoxy-silane coating, Corros. Sci. 73 (2013) 300–308.

[53] I. Han, J.H. Choi, B.H. Zhao, H.K. Baik, I.-S. Lee, Changes in anodized titanium surface morphology by virtue of different unipolar DC pulse waveform, Surf. Coatings Technol. 201 (2007) 5533–5536.

[54] S.F. Zhang, R.F. Zhang, W.K. Li, M.S. Li, G.L. Yang, Effects of tannic acid on properties of anodic coatings obtained by micro arc oxidation on AZ91 magnesium alloy, Surf. Coatings Technol. 207 (2012) 170–176.

[55] I. V. Lukiyanchuk, V.S. Rudnev, Tungsten oxide films on aluminum and titanium, Inorg. Mater. 43 (2007) 264–267.

[56] V.S. Rudnev, V.P. Morozova, I. V. Lukiyanchuk, M. V. Adigamova, I. A. Tkachenko, A. Y. Ustinov, et al., Oxide layers with ferro- and ferrimagnetic characteristics formed on aluminum via plasma electrolytic oxidation, Russ. J. Phys. Chem. A. 87 (2013) 1052–1056.

[57] A.L. Yerokhin, A. Shatrov, V. Samsonov, P. Shashkov, A. Pilkington, A. Leyland, et al., Oxide ceramic coatings on aluminium alloys produced by a pulsed bipolar

plasma electrolytic oxidation process, Surf. Coatings Technol. 199 (2005) 150–157.

[58] F. Jaspard-Mécuson, T. Czerwiec, G. Henrion, T. Belmonte, L. Dujardin, A. Viola, et al., Tailored aluminium oxide layers by bipolar current adjustment in the Plasma Electrolytic Oxidation (PEO) process, Surf. Coatings Technol. 201 (2007) 8677–8682.

[59] H. Tang, D. Yu, Y. Luo, F. Wang, Preparation and characterization of HA microflowers coating on AZ31 magnesium alloy by micro-arc oxidation and a solution treatment, Appl. Surf. Sci. 264 (2013) 816–822.

[60] J. Martin, A. Melhem, I. Shchedrina, T. Duchanoy, A. Nominé, G. Henrion, et al., Effects of electrical parameters on plasma electrolytic oxidation of aluminium, Surf. Coatings Technol. 221 (2013) 70–76.

[61] Q. Li, J. Liang, B. Liu, Z. Peng, Q. Wang, Effects of cathodic voltages on structure and wear resistance of plasma electrolytic oxidation coatings formed on aluminium alloy, Appl. Surf. Sci. 297 (2014) 176–181.

[62] R.O. Hussein, D.O. Northwood, J.F. Su, X. Nie, A study of the interactive effects of hybrid current modes on the tribological properties of a PEO (plasma electrolytic oxidation) coated AM60B Mg-alloy, Surf. Coatings Technol. 215 (2013) 421–430.

[63] R.O. Hussein, D.O. Northwood, X. Nie, The influence of pulse timing and current mode on the microstructure and corrosion behaviour of a plasma electrolytic oxidation (PEO) coated AM60B magnesium alloy, J. Alloys Compd. 541 (2012) 41–48.

[64] R.O. Hussein, D.O. Northwood, J.F. Su, X. Nie, A study of the interactive effects of hybrid current modes on the tribological properties of a PEO (plasma electrolytic oxidation) coated AM60B Mg-alloy, Surf. Coatings Technol. 215 (2013) 421–430.

[65] R.H.U. Khan, A.L. Yerokhin, T. Pilkington, A. Leyland, A. Matthews, Residual stresses in plasma electrolytic oxidation coatings on Al alloy produced by pulsed unipolar current, Surf. Coatings Technol. 200 (2005) 1580–1586.

[66] R.O. Hussein, P. Zhang, X. Nie, Y. Xia, D.O. Northwood, The effect of current mode and discharge type on the corrosion resistance of plasma electrolytic oxidation (PEO) coated magnesium alloy AJ62, Surf. Coatings Technol. 206 (2011) 1990–1997.

[67] R.O. Hussein, X. Nie, D.O. Northwood, A spectroscopic and microstructural study of oxide coatings produced on a Ti–6Al–4V alloy by plasma electrolytic oxidation, Mater. Chem. Phys. 134 (2012) 484–492.

[68] Y. Guangliang, L. Xianyi, B. Yizhen, C. Haifeng, J. Zengsun, The effects of current density on the phase composition and microstructure properties of micro-arc oxidation coating, J. Alloys Compd. 345 (2002) 196–200.

[69] Y. Yangi, H. Wu, Effects of Current Density on Microstructure of Titania Coatings by Micro-arc Oxidation, J. Mater. Sci. Technol. 28 (2012) 321–324.

[70] Z. Qiu, R. Wang, X. Wu, Y. Zhang, Influences of Current Density on the Structure and Corrosion Resistance of Ceramic Coatings on ZK60 Mg Alloy by Plasma Electrolytic Oxidation, Int. J. Electrochem. Sci. 8 (2013) 1957–1965.

[71] Y. Yang, H. Wu, Effect of current density on corrosion resistance of micro-arc oxide coatings on magnesium alloy, Trans. Nonferrous Met. Soc. China. 20 (2010) s688–s692.

[72] E. Matykina, A. Berkani, P. Skeldon, G.E. Thompson, Real-time imaging of coating growth during plasma electrolytic oxidation of titanium, Electrochim. Acta. 53 (2007) 1987–1994.

[73] S. Stojadinovic, R. Vasilic, I. Belca, M. Petkovic, B. Kasalica, Z. Nedic, et al., Characterization of the plasma electrolytic oxidation of aluminium in sodium tungstate, Corros. Sci. 52 (2010) 3258–3265.

[74] S. Moon, Y. Jeong, Generation mechanism of microdischarges during plasma electrolytic oxidation of Al in aqueous solutions, Corros. Sci. 51 (2009) 1506–1512.

[75] J.B. Bajat, R. Vasilić, S. Stojadinović, V. Mišković-Stanković, Corrosion Stability of Oxide Coatings Formed by Plasma Electrolytic Oxidation of Aluminum : Optimization of Process Time, Corrosion. 69 (2013) 693–702.

[76] D.S. Doolabi, M. Ehteshamzadeh, S.M.M. Mirhosseini, Effect of NaOH on the Structure and Corrosion Performance of Alumina and Silica PEO Coatings on Aluminum, J. Mater. Eng. Perform. 21 (2012) 2195–2202.

[77] K. Du, X. Guo, Q. Guo, F. Wang, Y. Tian, A monolayer PEO coating on 2024 Al alloy by transient self-feedback control mode, Mater. Lett. 91 (2013) 45–49.

[78] A. Polat, M. Makaraci, M. Usta, Influence of sodium silicate concentration on structural and tribological properties of microarc oxidation coatings on 2017A aluminum alloy substrate, J. Alloys Compd. 504 (2010) 519–526.

[79] S. Durdu, M. Usta, Characterization and mechanical properties of coatings on magnesium by micro arc oxidation, Appl. Surf. Sci. 261 (2012) 774–782.

[80] S. Abbasi, F. Golestani-Fard, S.M.M. Mirhosseini, A. Ziaee, M. Mehrjoo, Effect of electrolyte concentration on microstructure and properties of micro arc oxidized hydroxyapatite/titania nanostructured composite., Mater. Sci. Eng. C. Mater. Biol. Appl. 33 (2013) 2555–2561.

[81] H.Y. Zheng, Y.K. Wang, B.S. Li, G.R. Han, The effects of Na_2WO_4 concentration on the properties of microarc oxidation coatings on aluminum alloy, Mater. Lett. 59 (2005) 139–142.

[82] F. Monfort, A. Berkani, E. Matykina, P. Skeldon, G.E. Thompson, H. Habazaki, et al., Development of anodic coatings on aluminium under sparking conditions in silicate electrolyte, Corros. Sci. 49 (2007) 672–693.

[83] Y. Liu, J. Xu, Y. Gao, Y. Yuan, C. Gao, Influences of additive on the formation and corrosion resistance of micro-arc oxidation ceramic coatings on aluminum alloy, Phys. Procedia. 32 (2012) 107–112.

[84] X. Liu, G. Liu, J. Xie, Preliminary Study on Preparation of Black Ceramic Coating Formed on Magnesium Alloy by Micro-arc Oxidation in Carbon Black Pigment-contained Electrolyte, Procedia Eng. 36 (2012) 261–269.

[85] C. Ma, Y. Lu, P. Sun, Y. Yuan, X. Jing, M. Zhang, Characterization of plasma electrolytic oxidation coatings formed on Mg–Li alloy in an alkaline polyphosphate electrolyte, Surf. Coatings Technol. 206 (2011) 287–294.

[86] M. Tang, W. Li, H. Liu, L. Zhu, Influence of K_2TiF_6 in electrolyte on characteristics of the microarc oxidation coating on aluminum alloy, Curr. Appl. Phys. 12 (2012) 1259–1265.

[87] J. Li, H. Cai, B. Jiang, Growth mechanism of black ceramic layers formed by microarc oxidation, Surf. Coatings Technol. 201 (2007) 8702–8708.

[88] E. Matykina, R. Arrabal, P. Skeldon, G.E. Thompson, Incorporation of zirconia nanoparticles into coatings formed on aluminium by AC plasma electrolytic oxidation, J. Appl. Electrochem. 38 (2008) 1375–1383.

[89] A. Mandelli, M. Bestetti, A. Da Forno, N. Lecis, S.P. Trasatti, M. Trueba, A composite coating for corrosion protection of AM60B magnesium alloy, Surf. Coatings Technol. 205 (2011) 4459–4465.

[90] M. Aliofkhazraei, A. S. Rouhaghdam, Wear and coating removal mechanism of alumina/titania nanocomposite layer fabricated by plasma electrolysis, Surf. Coatings Technol. 205 (2011) S57–S62.

[91] K.M. Lee, Y.G. Ko, D.H. Shin, Incorporation of multi-walled carbon nanotubes into the oxide layer on a 7075 Al alloy coated by plasma electrolytic oxidation: Coating structure and corrosion properties, Curr. Appl. Phys. 11 (2011) S55–S59.

[92] K.M. Lee, Y.G. Ko, D.H. Shin, Incorporation of carbon nanotubes into micro-coatings film formed on aluminum alloy via plasma electrolytic oxidation, Mater. Lett. 65 (2011) 2269–2273.

[93] R.O. Hussein, D.O. Northwood, X. Nie, The effect of processing parameters and substrate composition on the corrosion resistance of plasma electrolytic oxidation (PEO) coated magnesium alloys, Surf. Coatings Technol. 237 (2013) 357–368.

[94] E. Matykina, R. Arrabal, A. Mohamed, P. Skeldon, G.E. Thompson, Plasma electrolytic oxidation of pre-anodized aluminium, Corros. Sci. 51 (2009) 2897–2905.

[95] J.A. Curran, T.W. Clyne, Porosity in plasma electrolytic oxide coatings, Acta Mater. 54 (2006) 1985–1993.

[96] J.A. Curran, T.W.W.T. Clyne, Thermo-physical properties of plasma electrolytic oxide coatings on aluminium, Surf. Coatings Technol. 199 (2005) 168–176.

[97] Y.G. Ko, K.M. Lee, B.U. Lee, D.H. Shin, An electrochemical analysis of AZ91 Mg alloy processed by plasma electrolytic oxidation followed by static annealing, J. Alloys Compd. 509 (2011) S468–S472.

[98] O.P. Terleeva, Y.P. Sharkeev, A. I. Slonova, I.V. Mironov, E.V. Legostaeva, I. A. Khlusov, et al., Effect of microplasma modes and electrolyte composition on micro-arc oxidation coatings on titanium for medical applications, Surf. Coatings Technol. 205 (2010) 1723–1729.

[99] C.-H. Hsu, H.-P. Teng, F.-H. Lu, Effects of addition of $Al(NO_3)_3$ to electrolytes on alumina coatings by plasma electrolytic oxidation, Surf. Coatings Technol. 205 (2011) 3677–3682.

[100] H. Wu, J. Wang, B.B. Long, Z. Jin, W. Naidan, F. Yu, et al., Ultra-hard ceramic coatings fabricated through microarc oxidation on aluminium alloy, Appl. Surf. Sci. 252 (2005) 1545–1552.

[101] G. Lv, W. Gu, H. Chen, W. Feng, M.L. Khosa, L. Li, et al., Characteristic of ceramic coatings on aluminum by plasma electrolytic oxidation in silicate and phosphate electrolyte, Appl. Surf. Sci. 253 (2006) 2947–2952.

[102] C.J.-P. Steiner, D.P.H. Hasselman, R.M. Spriggs, Kinetics of the Gamma-to-Alpha Alumina Phase Transformation, J. Am. Ceram. Soc. 54 (1971) 412–413.

[103] R. McPherson, Formation of metastable phases in flame- and plasma-prepared alumina, J. Mater. Sci. 8 (1973) 851–858.

[104] U. Malayoglu, K.C. Tekin, U. Malayoglu, S. Shrestha, An investigation into the mechanical and tribological properties of plasma electrolytic oxidation and hard-anodized coatings on 6082 aluminum alloy, Mater. Sci. Eng. A. 528 (2011) 7451–7460.

[105] E. Matykina, R. Arrabal, P. Skeldon, G.E. Thompson, Investigation of the growth processes of coatings formed by AC plasma electrolytic oxidation of aluminium, Electrochim. Acta. 54 (2009) 6767–6778.

[106] H. Kalkancı, S.C. Kurnaz, The effect of process parameters on mullite-based plasma electrolytic oxide coatings, Surf. Coatings Technol. 203 (2008) 15–22.

[107] J. Tian, Z. Luo, S. Qi, X. Sun, Structure and antiwear behavior of micro-arc oxidized coatings on aluminum alloy, Surf. Coatings Technol. 154 (2002) 1–7.

[108] L.R. Krishna, A.S. Purnima, G. Sundararajan, A comparative study of tribological behavior of microarc oxidation and hard-anodized coatings, Wear. 261 (2006) 1095–1101.

[109] X. Shen, X. Nie, H. Hu, Numerical Analysis of Thermal Distributions in Aluminum Engine Cylinders Influenced by Alumina Ceramic Coatings, Numer. Heat Transf. Part A Appl. 62 (2012) 463–478.

[110] H. Guo, Y. Ma, J. Wang, Y. Wang, H. Dong, Y. Hao, Corrosion behavior of micro-arc oxidation coating on AZ91D magnesium alloy in NaCl solutions with different concentrations, Trans. Nonferrous Met. Soc. China. 22 (2012) 1786–1793.

[111] A. Venugopal, R. Panda, S. Manwatkar, K. Sreekumar, L.R. Krishna, G. Sundararajan, Effect of micro arc oxidation treatment on localized corrosion behaviour of AA7075 aluminum alloy in 3.5% NaCl solution, Trans. Nonferrous Met. Soc. China. 22 (2012) 700–710.

[112] D. Krupa, J. Baszkiewicz, J. Zdunek, J.W. Sobczak, W. Lisowski, J. Smolik, et al., Effect of plasma electrolytic oxidation in the solutions containing Ca, P, Si, Na on the properties of titanium., J. Biomed. Mater. Res. B. Appl. Biomater. 100 (2012) 2156–2166.

[113] M. Chen, S. Liu, J. Li, N. Cheng, X. Zhang, Improvement to corrosion resistance of MAO coated 2519 aluminum alloy by formation of polypropylene film on its surface, Surf. Coatings Technol. 232 (2013) 674–679.

[114] C.-E. Barchiche, E. Rocca, J. Hazan, Corrosion behaviour of Sn-containing oxide layer on AZ91D alloy formed by plasma electrolytic oxidation, Surf. Coatings Technol. 202 (2008) 4145–4152.

[115] W. Xue, C. Wang, H. Tian, Y. Lai, Corrosion behaviors and galvanic studies of microarc oxidation films on Al–Zn–Mg–Cu alloy, Surf. Coatings Technol. 201 (2007) 8695–8701.

[116] J.A. Curran, H. Kalkancı, Y. Magurova, T.W. Clyne, Mullite-rich plasma electrolytic oxide coatings for thermal barrier applications, Surf. Coatings Technol. 201 (2007) 8683–8687.

[117] V.S. Rudnev, A. E. Lysenko, P.M. Nedozorov, T.P. Yarovaya, a. N. Minaev, Thermal behavior of an oxide layer on aluminum, Prot. Met. 43 (2007) 465–469.

[118] H. Jiang, Z. Shao, B. Jing, Effect of Electrolyte Composition on Photocatalytic Activity and Corrosion Resistance of Micro-Arc Oxidation Coating on Pure Titanium, Procedia Earth Planet. Sci. 2 (2011) 156–161.

[119] Y. Cheng, F. Wu, J. Dong, X. Wu, Z. Xue, E. Matykina, et al., Comparison of plasma electrolytic oxidation of zirconium alloy in silicate- and aluminate-based electrolytes and wear properties of the resulting coatings, Electrochim. Acta. 85 (2012) 25–32.

[120] S. Stojadinović, R. Vasilić, M. Petković, I. Belča, B. Kasalica, M. Perić, et al., Luminescence during the anodization of zirconium, Electrochim. Acta. 79 (2012) 133–140.

[121] M. Sowa, A. Kazek-Kęsik, R.P. Socha, G. Dercz, J. Michalska, W. Simka, Modification of tantalum surface via plasma electrolytic oxidation in silicate solutions, Electrochim. Acta. 114 (2013) 627–636.

[122] M. Petković, S. Stojadinović, R. Vasilić, L. Zeković, Characterization of oxide coatings formed on tantalum by plasma electrolytic oxidation in 12-tungstosilicic acid, Appl. Surf. Sci. 257 (2011) 10590–10594.

Chapter 3

Effect of Duty Cycle and Applied Current Frequency on Plasma Electrolytic Oxidation (PEO) Coating Growth Behaviour

Abstract

Plasma Electrolytic Oxidation (PEO) is a novel technique to create ceramic coatings on light weight metals particularly aluminum and magnesium alloys. PEO is a simple, high efficiency and eco-friendly technology. The wear and corrosion resistance of components manufactured from Al-based alloys can be drastically increased by the application of ceramic coatings produced by PEO. Ceramic coatings were created on the surface of 6061 aluminum alloy using a plasma electrolytic oxidation (PEO) process employing a pulsed direct current (DC) power mode in an alkaline electrolyte. The effect of electrical parameters including frequency and duty cycle on the micro-discharge behavior and coating growth was investigated at constant current. Surface features of the coatings were studied using scanning electron microscopy. Energy dispersive X-ray spectroscopy was employed to investigate elemental distribution on the coating surfaces and cross-sections. Applying lower duty cycles resulted in increased breakdown voltages and micro-discharges with higher spatial density and lower intensity. Further, applying a lower duty cycle was also found to promote the uniformity of silicon distribution in the coating. Based on these findings, a new conceptual model is proposed to explain the concentration distribution of Si on the surface of coatings prepared at different duty cycles.

3.1 Introduction

Light metals, especially aluminum and magnesium alloys, are finding increasing applications in different industries such as automotive and aerospace because of their strength to weight ratio, low density compared to steel, ease of fabrication and recycling potential. In the automotive industry, for instance, the total of about 110 kg of aluminum used per vehicle in 1996 is predicted to rise to 250-340 kg by 2015. These metals require careful finishing to produce surface coatings with adequate resistance to both wear and corrosion because they are reactive and have low hardness [1,2].

A relatively novel technique to create functional oxide layers on light metals, which has generated growing interest recently, is plasma electrolytic oxidation (PEO), also called micro-arc oxidation (MAO) [3], anodic oxidation by spark discharge [4] or spark anodizing [5–8]. The PEO process uses the same configuration as conventional anodizing but is operated at much higher voltages , usually in the range 400-700 V, and involves many short-lived micro-discharges as a result of localized dielectric breakdown of the growing coating [8,9].

Prior to application of the duty cycle, the surface of the substrate is partially protected by a very thin, naturally formed passive film. As the applied voltage increases on starting the duty cycle, a large number of gas bubbles are produced, which is the traditional anodizing stage with the formation of a porous insulation film with a columnar structure perpendicular to the substrate. When the voltage exceeds a certain threshold (i.e. breakdown voltage), dielectric breakdown occurs in some scattered weak regions across the insulating film, accompanied by the phenomenon of micro-arc discharge. As a result, a large number of fine, uniform, white sparks are generated on the sample surface which results in the formation of a large number of small uniform micro-pores [10].

PEO provides coatings with better characteristics compared to conventional and hard anodizing procedures. The coatings produced by conventional anodizing are not thick enough to provide effective protection against wear and corrosion and therefore are used mainly for decoration. The PEO method is capable of producing thicker coatings with higher hardness, better wear and corrosion resistance and great bonding strength with the

substrate as compared to the conventional anodizing method. The electrolyte used in PEO is typically a low concentration alkaline solution which is more environmentally friendly than hard anodizing processes employing strong acids [10,11].

Since the discharge events are very short in PEO, it is difficult to catch instantaneously the discharge event to analyze the physical and chemical processes occurring in the discharge channels. As a result, controversy exists over the growth mechanism of PEO coatings [10]. In an earlier work [12], three models were proposed to explain micro-discharge formation: (1) dielectric film breakdown in a strong electric field; (2) gas discharges in micro pores in the oxide film; (3) free electron generation and contact glow discharge. In a recent work [13], using optical emission spectroscopy (OES), a discharge model based on the locations of discharge initiation was proposed. This model assumes three types of discharge, types A, B and C. Type B discharges originate from the metal-oxide interface and are strong as a result of dielectric breakdown through the oxide layer creating cratered structures. Types A and C, originating from the oxide-electrolyte interface, are weaker than type B discharges, and occur as a result of gas discharges in micro pores in the oxide layer.

Discharges play an important role in the coating growth mechanism. Several investigations have been conducted to characterize discharge behavior during PEO using different methods. Digital imaging [9,12,14] revealed that, as the PEO process proceeds, micro-discharge intensity increases while their spatial density decreases. Yerokhin et al. [12] estimated the mean value of current density passing through a discharge to be between 18 and 50 KA/m^2. Mécuson et al. [15] used a pulse bipolar current mode with different ratios of positive to negative charge density. Using a video camera, they observed that when a higher negative than positive current was applied, the intensity of micro-discharges decreased in the later stages of the PEO process and a “softer” sparking resulted.

Hussein et al. [7,13] applied optical emission spectroscopy using different current modes. They found that electrical parameters (current density, frequency and duty cycle) and process time affect the plasma temperature as a result of different types of discharges

such as dielectric breakdown and gas discharges. They estimated the average temperature of discharges to be in the 4900-5400 K range, while strong discharges can produce temperatures in the range 6000-10000 K.

To justify industrial application of PEO, a more systematic and in-depth study of the influence of various parameters on the process is required. Many previous studies have investigated the effects of electrolyte composition [16–19] and current mode [20–22] on the characteristics of the coatings. However, information on the role of electrical parameters such as frequency and duty cycle is limited in the literature. The present study investigates the effect of frequency and duty cycle on the coating growth behavior during PEO.

3.2 Experimental Procedure

Disk samples with a diameter of about 3 cm and a thickness of 7-9 mm were cut from a 6061-T651 aluminum alloy bar supplied by Kaiser Aluminum, USA. To ensure a reproducible initial surface condition, samples were polished with 600 grit emery polishing paper followed by degreasing in propanol and rinsing with distilled water. A PEO unit custom-built by the National Research Council Canada (NRC, Vancouver, Canada) equipped with a DC power supply was used to produce the coatings. The positive output of the power supply was connected to the sample immersed in the electrolyte serving as the working electrode (anode) and the negative output was connected to the stainless steel electrolyte container acting as the counter electrode (cathode). To ensure a good connection between the power supply and the samples, a threaded hole was drilled in one side of each sample. Then the sample was bolted to a steel rod (insulated by a ceramic jacket from the electrolyte) connected to the power supply. PEO coatings were produced using the uni-polar pulsed DC mode with a square waveform applied at different power frequencies of 50, 500, 1000 and 2000 Hz. Two duty cycles (D_t), 80% and 20%, were used. At the frequency of 1000 Hz two additional duty cycles of 10% and 50% were also used. The duty cycle is defined as:

$$D_t = [\ t_{on} / (t_{on} + t_{off})] \times 100 \qquad (3.1)$$

where t_{on} is the 'on' duration and t_{off} is the 'off' duration during a single cycle.

The PEO process was carried out at a constant current density of 15 A/dm^2 for 30 minutes for all samples. Table 3.1 lists the sample codes and the processing conditions.

Table 3.1- PEO process parameters and sample codes for coating deposition on 6061 Al alloy.

Sample code	Frequency (Hz)	Duty cycle (%)	t_{on} (ms)	t_{off} (ms)
A2	50	20	4	16
A8	50	80	16	4
B2	500	20	0.4	1.6
B8	500	80	1.6	0.4
C1	1000	10	0.1	0.9
C2	1000	20	0.2	0.8
C5	1000	50	0.5	0.5
C8	1000	80	0.8	0.2
D2	2000	20	0.1	0.4
D8	2000	80	0.4	0.1

The electrolyte was a solution of 2 g/l Na_2SiO_3 and 2 g/l KOH in deionized water with a pH of 12.5. The electrolyte temperature was maintained in the range of 33-38 °C during treatment using an external DCA 500 Durachill heat exchanger manufactured by Polyscience.

Coating thickness was evaluated using an Eddy current gauge. Twenty measurements were taken on the coated surface of each sample. Statistical treatments were applied to extract the mean data values and scatter.

Coating surfaces and cross sections were examined using a LEO 440 scanning electron microscope (SEM) equipped with a Quartz EDX system and a Hitachi S-3500N SEM

equipped with an Oxford Instruments 7490 X-ray detector. The samples were sputter-coated with gold prior to SEM imaging to minimize surface charging.

A Philips X'Pert_MRD diffractometer with Cu K_α (40 kV and 40 mA) radiation was used to study the phase composition of the coatings. The samples were scanned in the 2θ range from 15° to 90° with a 0.02 ° step size. In order to minimize interference from the substrate to the diffraction, glancing angle XRD was used with an angle of incidence (α) set to 3.5°.

3.3 Results and Discussion

3.3.1 Voltage-time Response

Voltage-time responses for PEO coatings formed using the various duty cycles and frequencies are shown in Figure 3.1. As previously reported [16,19,23,24], an initial linear, abrupt voltage increase occurs within a short period of time (about 15 seconds) followed by a sudden reduction in slope of the voltage-time curve. The point at which the slope of the voltage-time curve changes is designated the sparking, or breakdown, voltage.

The PEO process is accompanied by sparking micro-discharges as a result of dielectric breakdown [13,25], gas discharge [13], contact glow discharge [12] or any of their combinations which is a unique feature of PEO as compared to conventional anodization [25].

Throughout the PEO process the color, intensity and density of micro discharges constantly change. The color of the micro-discharges changes from bluish white to yellow and eventually to orange while the intensity increases and density decreases [3,11,26].

The sparking or breakdown voltage as well as the maximum voltage eventually achieved (Figure 3.1) were higher in samples treated at a duty cycle of 20% compared to those treated at a duty cycle of 80%. Figure 3.2 demonstrates the effect of duty cycle on the voltage-time response of coatings grown at a frequency of 1000 Hz. Decreasing the duty

cycle from 80% to 10% was found to result in higher breakdown and maximum voltages. At a duty cycle of 80%, the sparking and maximum voltages were 424 and 532 V respectively, while for a duty cycle of 10% the corresponding numbers rose to 594 and 759 V, respectively.

A comparison of the curves in Figure 3.1 showed no considerable difference in sparking and maximum voltage reached during PEO of samples treated at the same duty cycle but different frequencies.

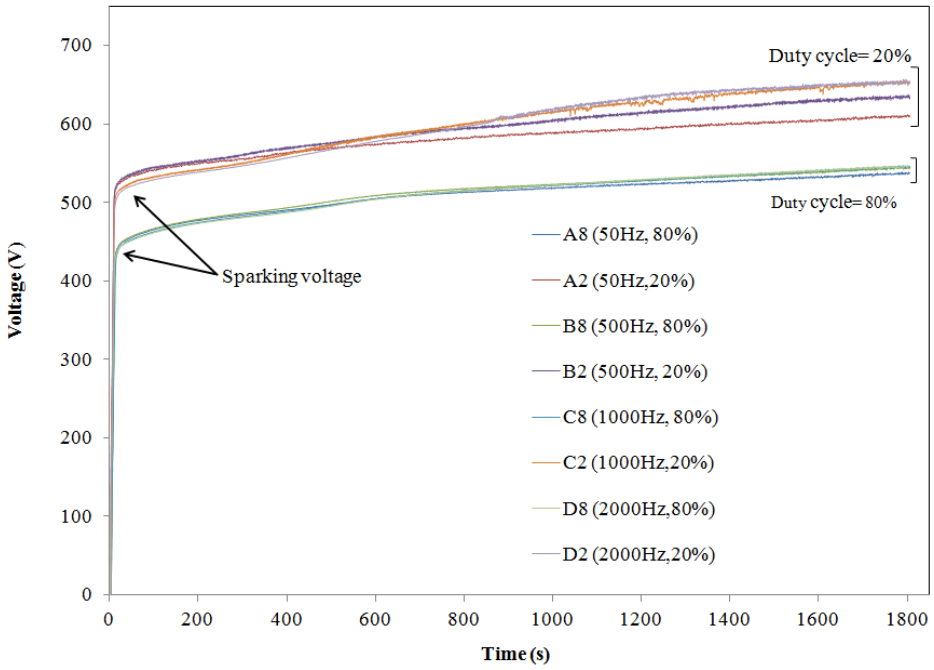

Figure 3.1- Voltage-time response at duty cycles of 20% and 80%.

Increasing the duty cycle results in an increased overall power input to the system. At higher duty cycles, the total duration of pulse on time in 30 min is more compared to lower duty cycles, and although the voltages are generally higher at lower duty cycles, the product of the average voltage and total pulse on time duration at a constant current density is greater at higher duty cycles indicating a higher overall power input to the system.

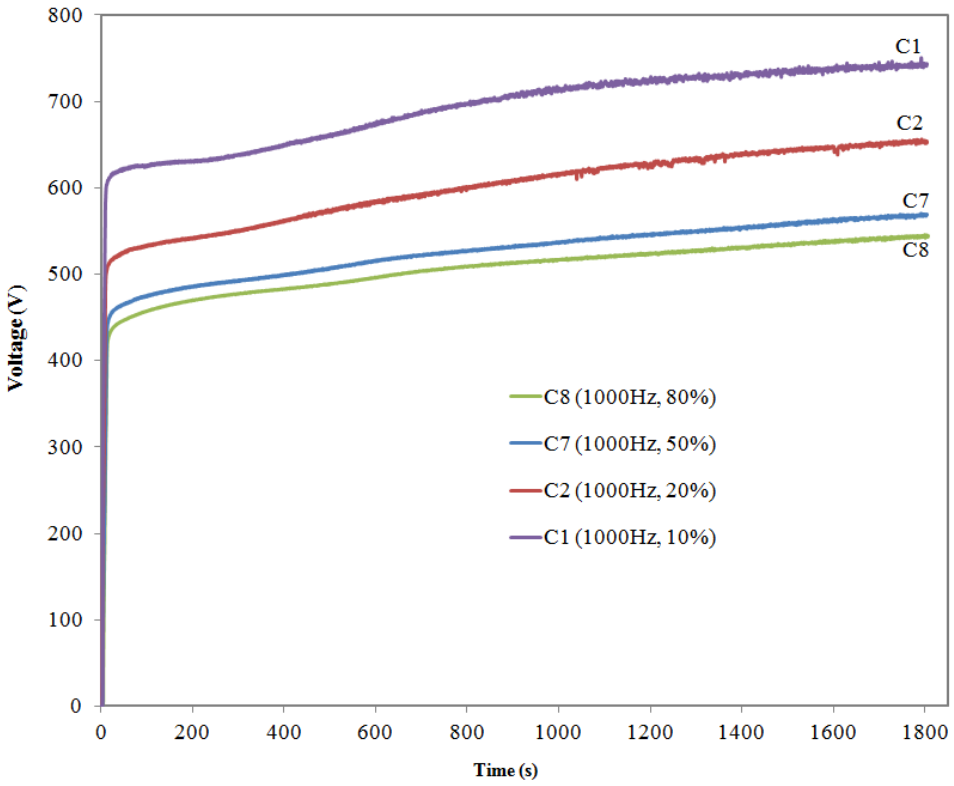

Figure 3.2- Effect of duty cycle on voltage-time response at a frequency of 1000 Hz.

3.3.2 Coating Surface Morphology and Composition

A typical SEM micrograph of a coated surface is shown in Figure 3.3-a. Two distinct regions can be observed on the surface of all samples: a cratered structure with a central hole (Area “b”) and a lighter area with a nodular structure (Area “c”). The central hole in the cratered region is a discharge channel through which molten material was ejected from the coating/substrate interface due to the high temperature and strong electric field. After ejection this material rapidly solidified upon contact with the electrolyte.

EDX spectra measured at these two characteristic regions are presented in Figure 3.3-b and c. The cratered region is rich in aluminum, consistent with its ejection through the film from the substrate/coating interface. The nodular structure is rich in Si suggesting it formed by the codeposition of aluminum and silicon in the solution.

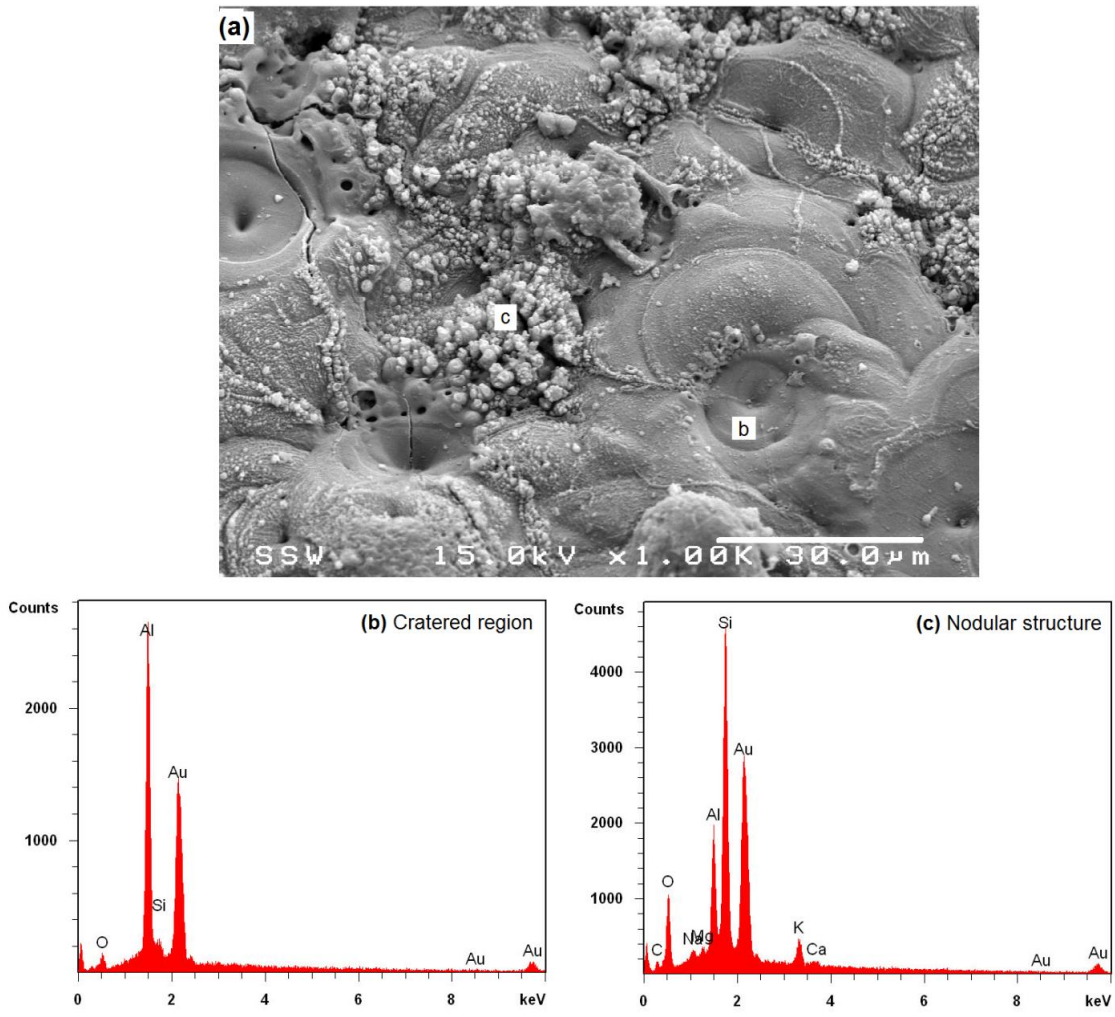

Figure 3.3- (a) SEM image (secondary electron mode) of free surface of PEO coating on sample C8; (b) and (c) EDX analysis from regions “b” and “c” respectively.

It is generally believed [3,15,27] that coating growth is the result of the flow of oxidized molten aluminum through discharge channels. The discharges created during PEO play a key role in the coating growth [8]. The size and surface features of the craters could be a reflection of the density and intensity of the discharges [7,13]; i.e., the stronger the discharges, the bigger the craters. Figure 3.4 illustrates the effect of the duty cycle on the size of craters (the average standard deviation of measured crater sizes was 2.8 µm). Image analysis software (MIP from Metsofts) was employed to measure the size of craters in the SEM micrographs and the measured values were statistically treated and reported. Since the intensity of the micro-discharges varies significantly during the PEO

process, the values of the crater radii reported here show a general trend and should not be treated as quantitatively certain. It is observed (Figure 3.4) that the crater size tends to increase with increasing duty cycle, which could indicate enhanced or intensified micro-discharges as the duty cycle increases.

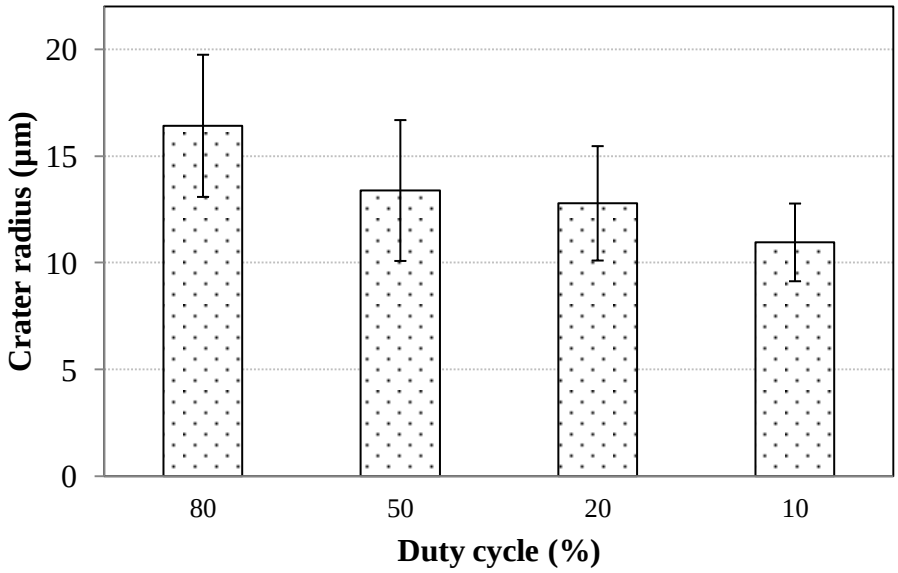

Figure 3.4- Effect of duty cycle on the size of craters on the surface of PEO coated samples at a frequency of 1000 Hz.

The effect of duty cycle on the surface morphologies of coatings formed at a frequency of 1000 Hz is presented in Figure 3.5. Comparison of sample C8 (Figure 3.5-a, 80% duty cycle) with sample C2 (Figure 3.5-b, 20% duty cycle) shows that fewer craters are formed on C8 and the surface is more densely covered with nodular structures shown to be rich in Si by EDX analyses.

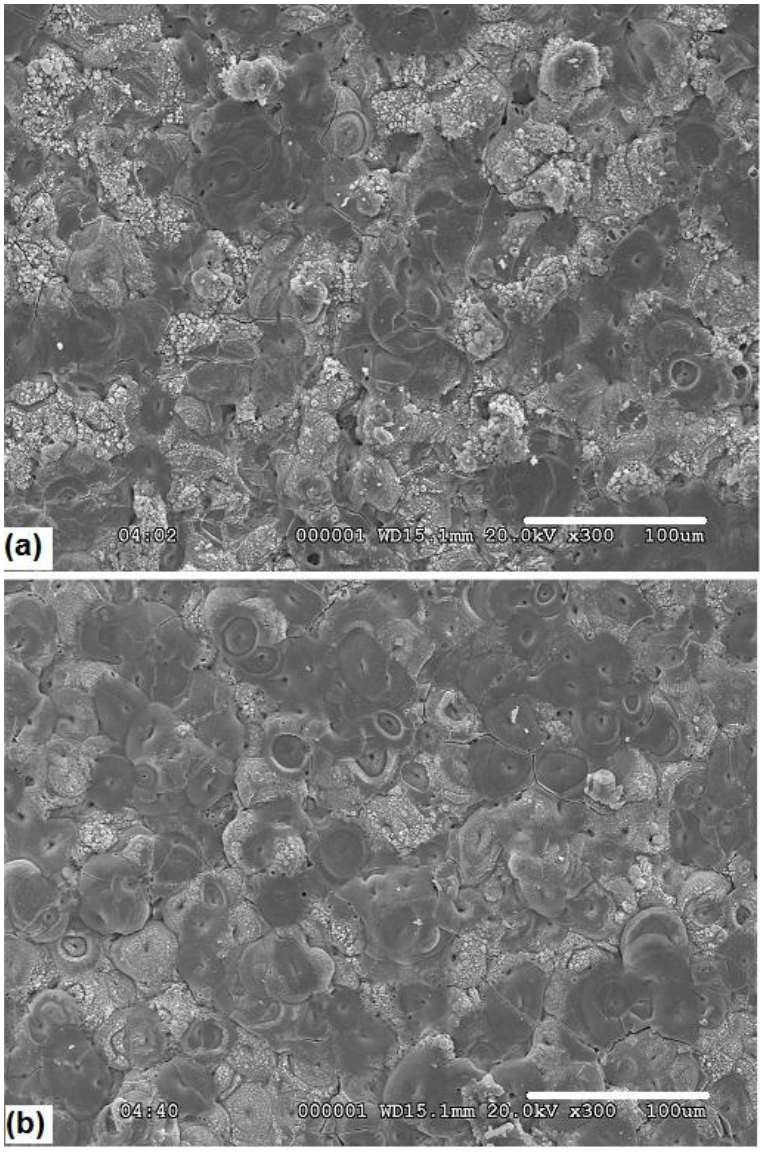

Figure 3.5- SEM micrographs (BS mode) of PEO coating surfaces, (a) C8, D_t=80%; and (b) C2, D_t=20% (Table 3.1).

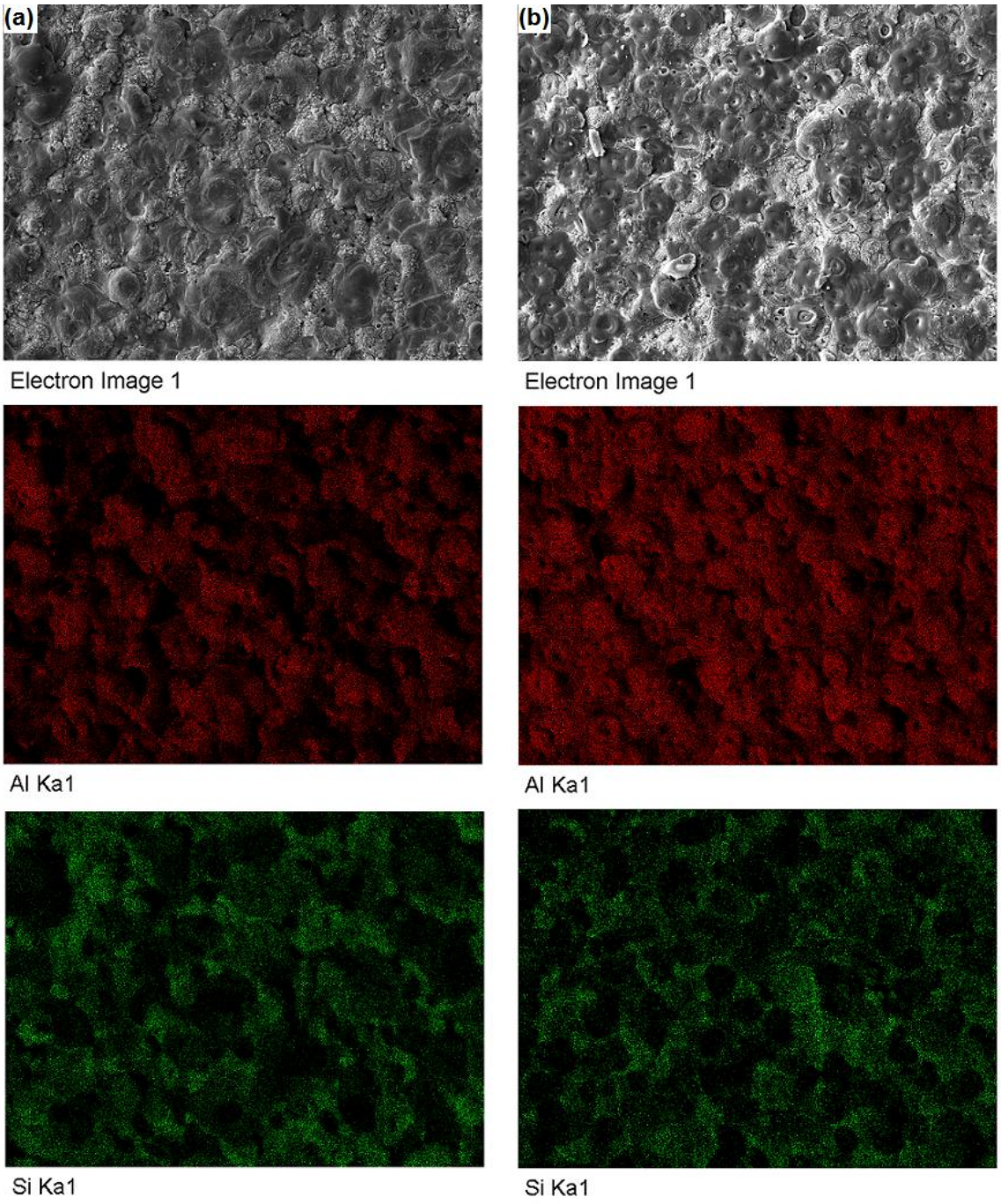

Figure 3.6- Surface EDX elemental maps for (a) sample D8 (80% duty cycle); and (b) sample D2 (20% duty cycle) (Table 3.1).

The EDX elemental surface maps of samples D2 (20% duty cycle) and D8 (80% duty cycle) are compared in Figure 3.6. The accuracy of the elemental concentration measurements may vary between 2% and 7% [13]. It could be observed that a higher surface concentration of Al is obtained at a low, compared to a high, duty cycle (sample D2 and D8, respectively). On the contrary, the Si presence appears to be higher at a higher duty cycle, though this is not as obvious as in the case of Al. The Al/Si intensity ratios for different frequencies obtained from EDX elemental surface mapping (Figure 3.7) reveal that this ratio increases with decreasing duty cycle, consistent with the observations from Figure 3.6. This suggests that at a lower duty cycle more discharges occurred resulting in more Al participating in the discharge process.

Visual observation of the sample surfaces at various stages of the coating process (Figure 3.8) revealed that the population, size and color of micro-discharge events vary throughout the oxidation process. At the beginning (Figure 3.8-a and 3.8-b) micro-discharges are smaller with a bluish white color but grow in size and turn orange at later stages (Figure 3.8-c and 3.8-d). It was also observed that, at lower duty cycles (Figure 3.8-b and 3.8-d) micro-discharges are less intense and have a higher spatial density at all stages of the process. The difference between the high and low duty cycles becomes more apparent at longer times (Figure 3.8-c and 3.8-d).

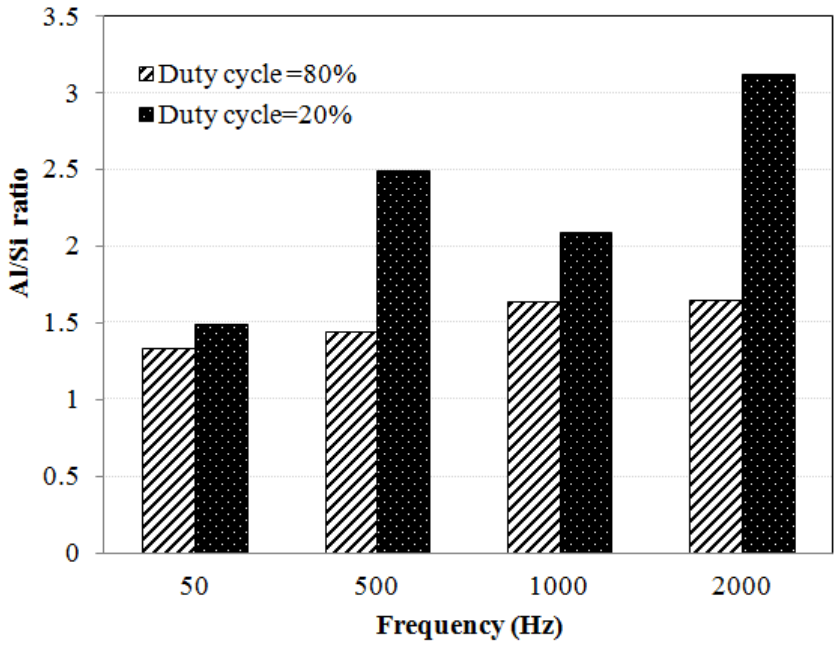

Figure 3.7- Al/Si ratio calculated from surface EDX elemental maps.

Yerokhin et al. [12] suggest the most likely cause of the micro-discharge color change as the process continues could be due to ionic emission from the molten oxide film. As the coating thickens, less heat is transferred to the aluminum substrate since more is absorbed by the coating. The high heating rates developed in the anode make it possible for the oxide film to be partially melted, resulting in an ionic emission.

The results presented in Figure 3.3 to Figure 3.8 confirm that the intensity of the micro-discharges decreases while their spatial density increases when a lower duty cycle is applied. As previously mentioned in section 3.1, craters are the result of strong micro-discharges caused by dielectric breakdowns of the coating that penetrate through its entire thickness. As such, the larger number of smaller craters at low duty cycles (Figure 3.4 and Figure 3.5) suggests a higher number of sparks with lower intensity. One possible explanation for the lower intensity of micro-discharges at low duty cycles could be the higher number of sparks on the surface. As the number of micro-discharges increases, the current passing through each individual micro-discharge channel decreases because the overall current is kept constant, resulting in smaller crater sizes (Figure 3.5).

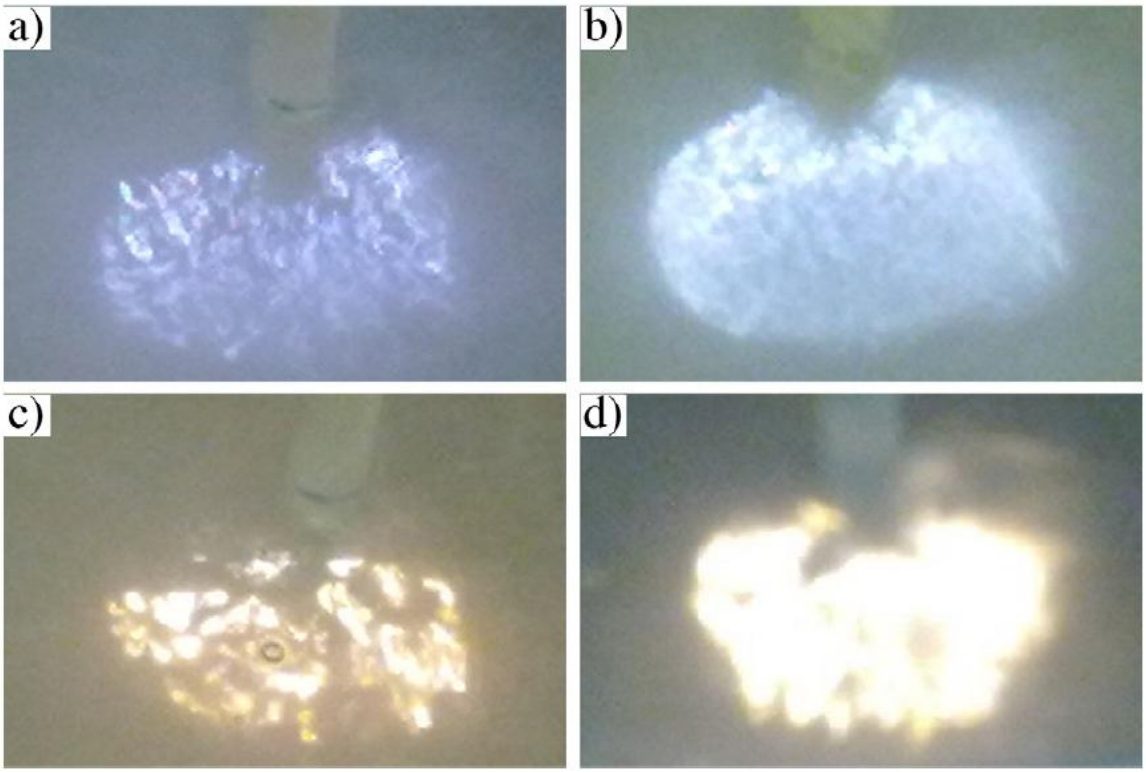

Figure 3.8- Appearance of micro-discharges during PEO; (a) C8 after 4 min , (b) C2 after 4 min , (c) C8 after 28 min, (d) C2 after 28 min

3.3.3 Coating Thickness

Thickness measurements (Figure 3.9) show that the coating growth rate increases gradually with decreasing duty cycle at constant frequency. This increased growth rate at lower duty cycles could be linked to the fact that coating growth is the result of oxidized molten aluminum as it flows out through discharge channels and more discharges are involved at lower duty cycles. The cross sections of PEO coatings examined by SEM (Figure 3.10-a and Figure 3.10-e) for samples treated at a frequency of 1000 Hz and duty cycles of 80% and 20% reveal some porosity and discharge channels within the coating. The porosity is assumed to be the result of dissolved oxygen being trapped in the molten oxides [28]. It should be noted that the defects adjacent to the coating/substrate interface are the result of polishing during sample preparation and the coatings are not separated from the substrates.

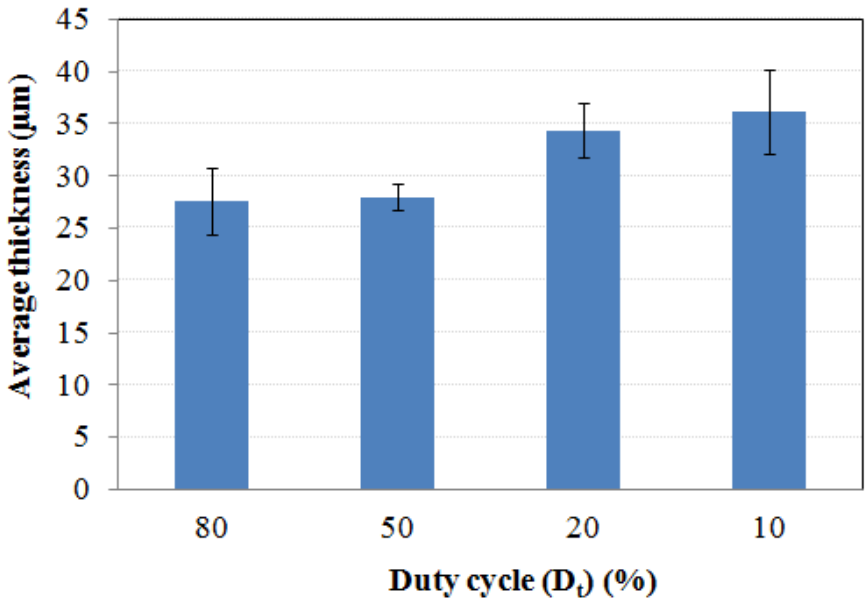

Figure 3.9- Effect of duty cycle on coating thickness on samples coated at a frequency of 1000 Hz.

3.3.4 Distribution of Elements

SEM micrographs and EDX analyses of the coating cross sections for samples C8 and C2 are presented in Figure 3.10. Comparison of the elemental maps does not detect any significant differences in the distribution of Al in the oxide coating but shows that the distribution of Si differs considerably in these two samples. When using a high duty cycle (C8), the Si is concentrated on the outer surface of the coating (Figure 3.10-b), whereas at low duty cycles (C2, Figure 3.10-f) Si is distributed more evenly within the coating.

The high concentration of Si at the coating surface in samples coated at high duty cycles could be linked to the micro-discharge behavior during PEO. It was previously reported [5,14,24] that in electrolytes containing silicate, silicon species are concentrated closest to the coating surface. It has been proposed [10,16] that Si forms insoluble gels which reduce Si ionic mobility and as a result a silicon rich outer part is formed by deposition of this gel at the coating interface.

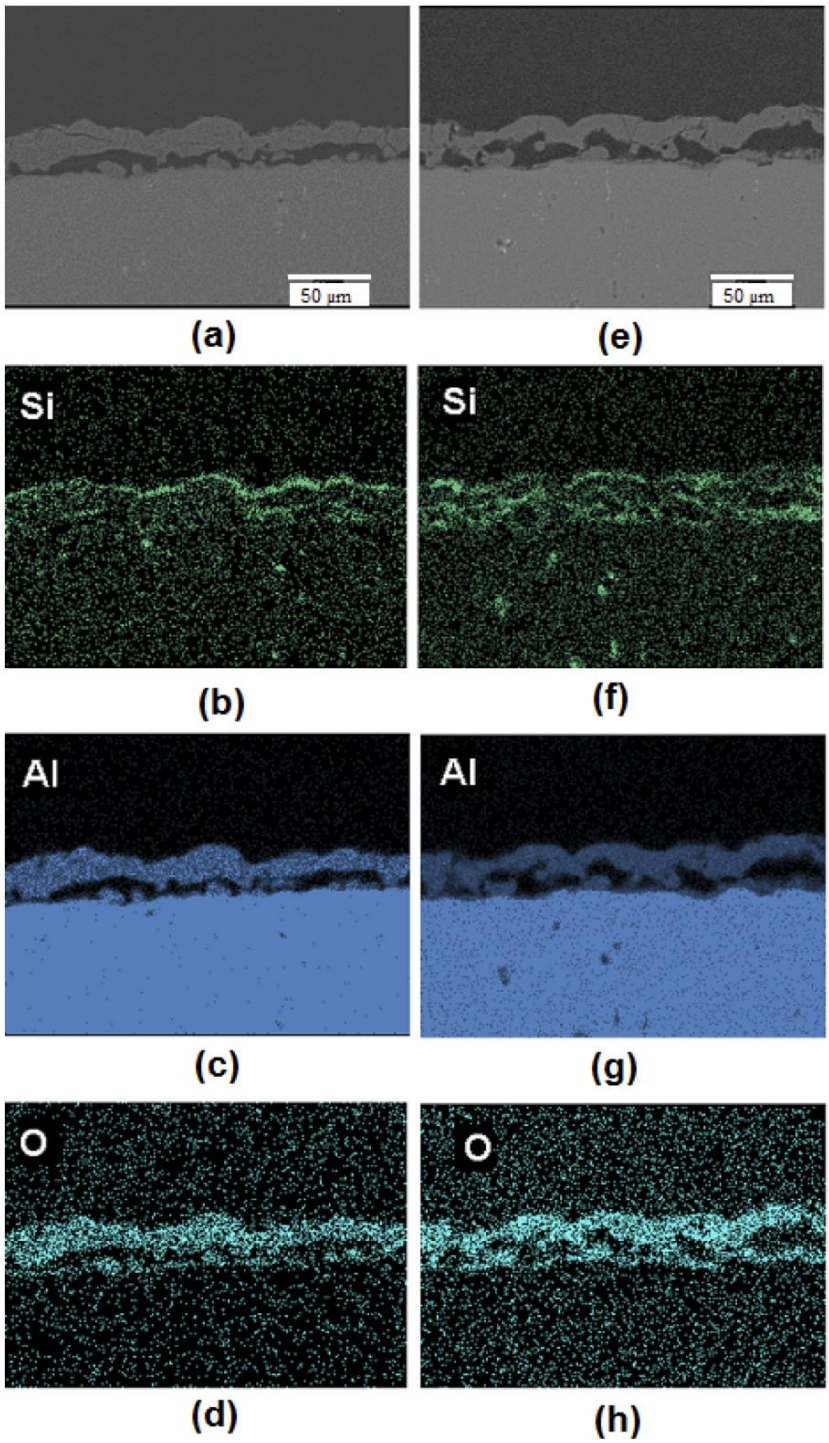

Figure 3.10- Results of EDX analyses on the cross sections of coatings. Sample C8 (a) Scanning electron micrograph (b) Silicon (c) Aluminum and (d) Oxygen elemental maps; Sample C2 (e) Scanning electron micrograph (f) Silicon (g) Aluminum and (h) Oxygen elemental maps.

At low duty cycles the micro-discharges are less intense and their spatial density is higher (Figure 3.8-b and Figure 3.8-d) whereas at high duty cycles micro-discharges are stronger with lower spatial density (Figure 3.8-a and Figure 3.8-c). Each micro-discharge ejects oxidized molten aluminum onto the surface. As a result of the force of theses ejections, adsorbed negative ions on the surface, for instance SiO_3^{2-} , or Si containing gels, as proposed by some researchers [10,16], would be detached from the surface. We propose a new schematic diagram in Figure 3.11 showing how micro-discharge spatial density could affect Si distribution on the surface. In Figure 3.11-a, where sparks are further apart, Si containing species can be adsorbed on the surface of the anode (substrate) while in Figure 3.11-b most of the Si containing species are detached from the surface due to the larger number of sparks on the surface.

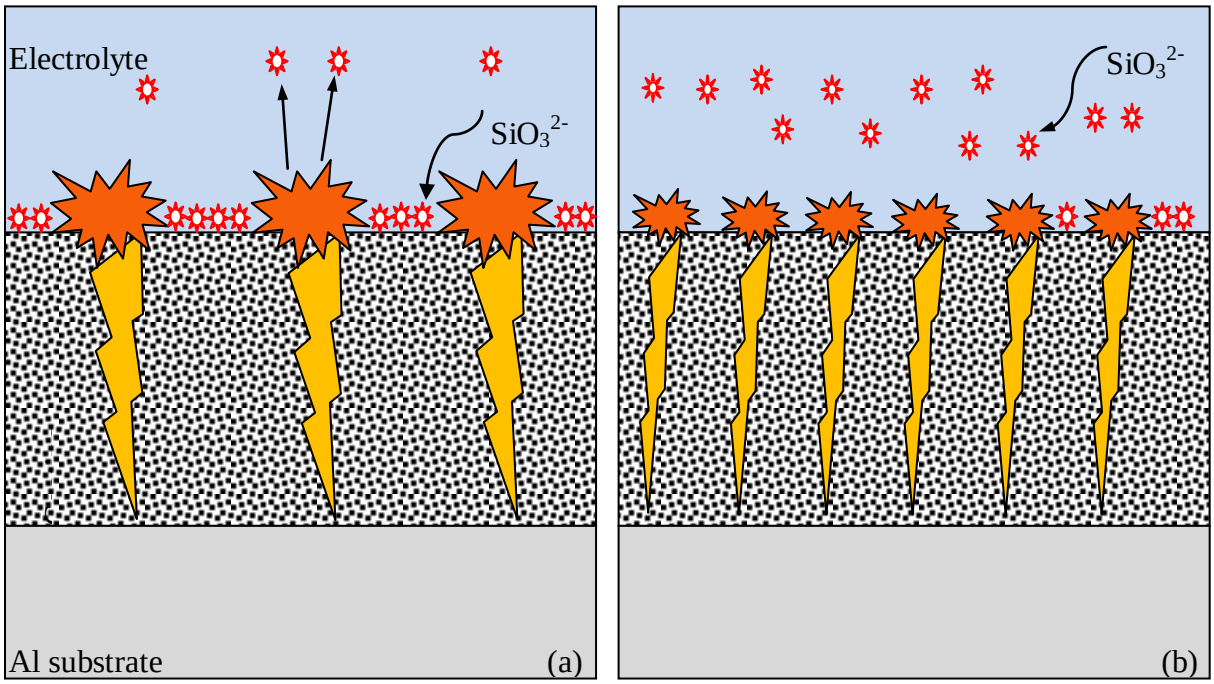

Figure 3.11- Schematic diagrams showing the effect of micro-discharge characteristics on the distribution of silicon on the surface of PEO coated samples for (a) high duty cycle and (b) low duty cycle conditions.

The more uniform distribution of silicon across the ceramic coating could be ascribed to the higher electric fields produced in samples coated at lower duty cycles. Anions present in the electrolyte, SiO_3^{-2} for instance, enter the discharge channels under a strong electric field through electrophoresis [10]. Since a decrease in duty cycle results in higher electric fields (Figure 3.1 and Figure 3.2) and more sparks, the possibility of silicon entering discharge channels increases and results in a more uniform distribution.

3.3.5 X-ray Diffraction Analysis

The XRD patterns of the coatings after PEO are displayed in Figure 3.12. The γ-Al_2O_3, α-Al_2O_3 and Al diffraction peaks were observed in the samples. The results suggest that the ceramic coating formed contains mainly α-Al_2O_3 and γ-Al_2O_3 phases. The presence of Al could be from the substrate interference even though a relatively low angle (3.5°) of incidence X-ray beam was used.

For example in B2, C2 and D2 samples only γ-Al_2O_3 peaks were observed in the coating; however in other samples, α-Al_2O_3 peaks were observed in addition to γ-Al_2O_3 peaks.

Alpha alumina is a stable, rhombohedral phase with a melting point of 2050°C and gamma alumina is a cubic metastable phase that can transform into α-Al_2O_3 if heated in the range of 800- 1200 °C. [19,21,29]

From the XRD results it can be found that for short t_{on} times (C2 and D2 samples) the coating is mainly composed of γ-Al_2O_3. As the t_{on} time increases more γ to α alumina transformation occurs and the amount of α alumina increases.

When the oxide is ejected out of the channel, it immediately comes in contact with the electrolyte which results in a high cooling rate. It is suggested that homogeneous nucleation of the solidification of liquid droplets at considerable under-cooling results in the formation of γ-Al_2O_3 rather than α-Al_2O_3 because of its lower critical free energy for nucleation. However, due to the low thermal conductivity of alumina coating, the temperature rises in the coating as the process continues, causing transformation of γ-Al_2O_3 to α-Al_2O_3. [3,30]

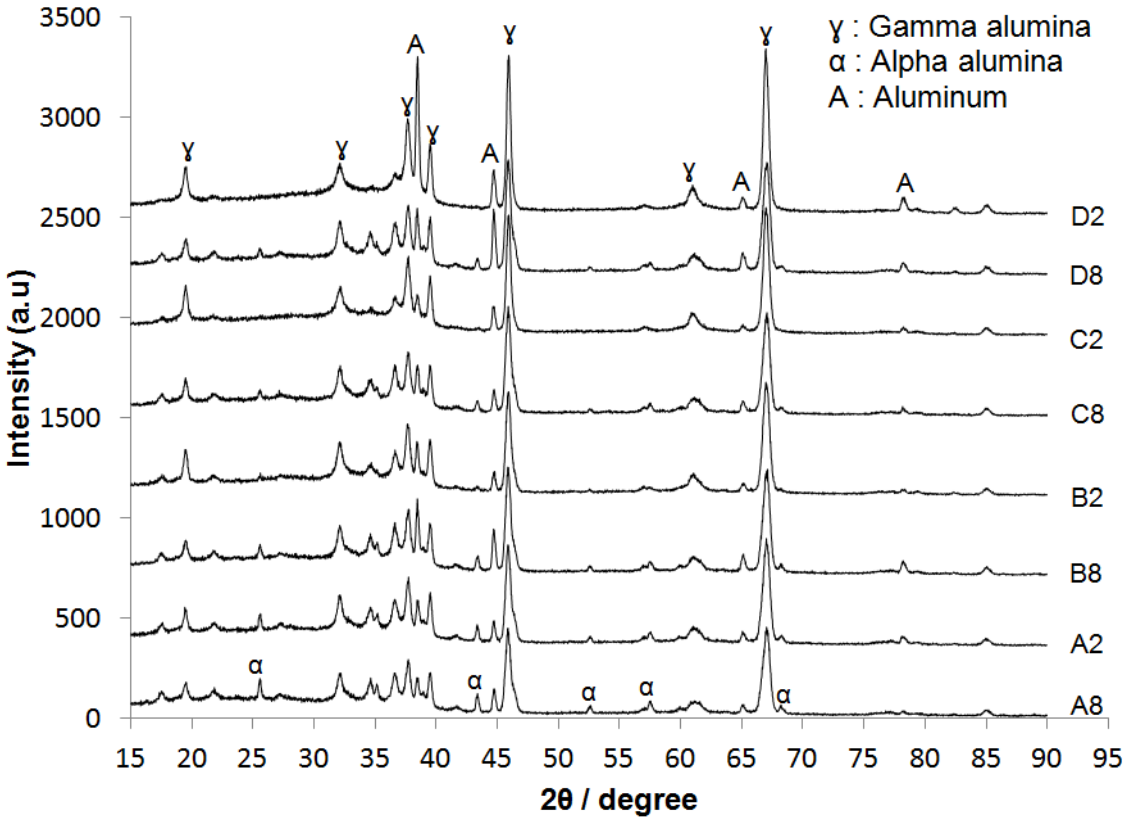

Figure 3.12- X-ray diffraction (glancing angle of 3.5 degrees) spectra of ceramic coatings formed by PEO on 6061 Al alloy using different frequencies and duty cycles (Table 3.1).

Higher γ-Al_2O_3 phase content in samples with shorter t_{on} times suggests that the temperature rise in these samples is lower and as a result the $\gamma \rightarrow \alpha$-$Al_2O_3$ transformation which requires heat is inhibited.

3.3.6 Effect of Electrolyte Stability on the Coating Growth

The service lifetime of the electrolytes used in the PEO coating process is an important issue for industrial applications both for the quality of the produced coatings and also the cost of replacing the electrolyte. The stability of the electrolyte could directly affect the reproducibility and quality of the PEO coatings. Almost all the published literature involves optimizing the composition and concentration of electrolytes for desired applications and information on the stability of the electrolyte, and the impact it might have on the PEO coating process, is very scarce [10].

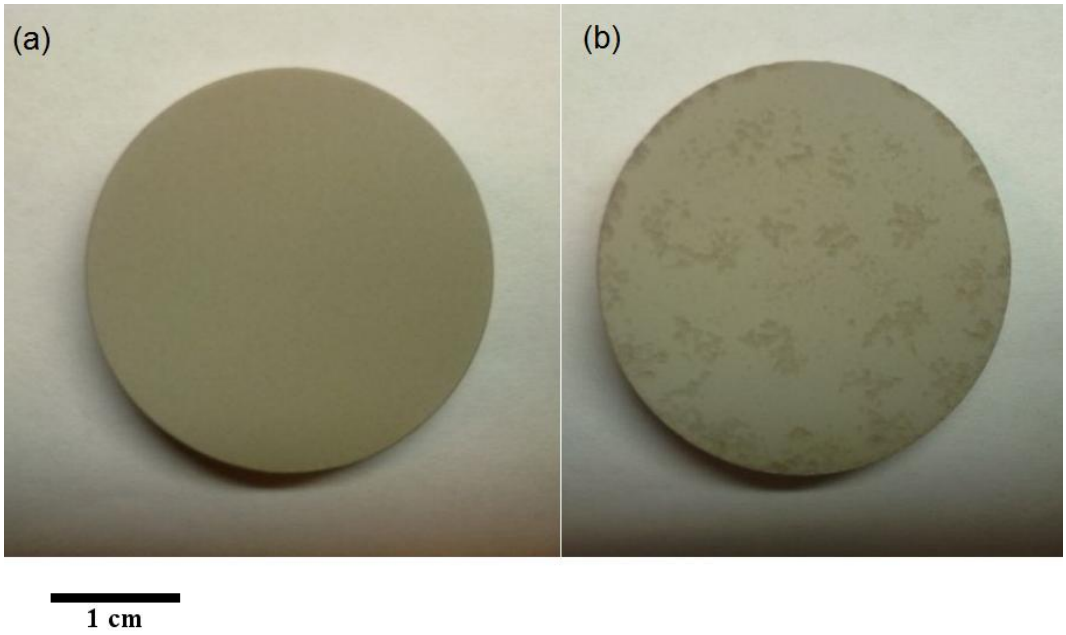

Figure 3.13- The effect of electrolyte stability on the appearance of PEO coatings on sample C5 (PEO coated for 30 min at a frequency of 1000 Hz and duty cycle of 50% on 6061 aluminum alloy); (a) sample C5-a (4^{th} sample coated in the electrolyte); (b) sample C5-b (18^{th} sample coated in the same electrolyte).

During the PEO process it was observed that after using an electrolyte to coat a number of samples, the surface of the coated samples started to show some defects. The surfaces of samples C5-a and C5-b both coated at a frequency of 1000 Hz and duty cycle of 50%, are shown in Figure 3.13. Sample C5-a (Figure 3.13-a) was the fourth sample coated in the electrolyte, while C5-b was the eighteenth sample coated with the same electrolyte. The surface of the C5-a coating is uniform while that of the C5-b coating exhibits defects in the form of darker areas.

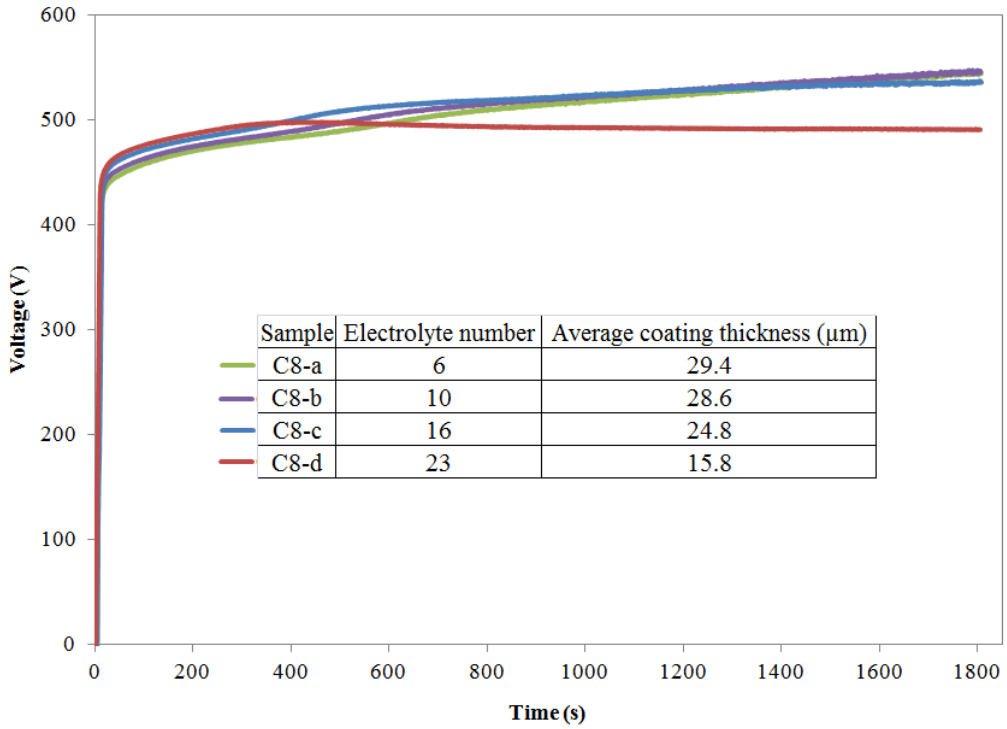

Figure 3.14- The effect of electrolyte stability on the voltage-time response of sample C8 (coated at a frequency of 1000Hz and duty cycle of 80% for 30 min). The 'electrolyte number' is the number of times the electrolyte was used to coat samples.

Further investigations revealed that the voltage-time curves, coating thickness, and surface morphology of the samples are also influenced by the electrolyte stability. Figure 3.14 shows how the number of runs, indicated by the 'electrolyte number', could affect the voltage-time response and coating thickness of the samples coated at a frequency of 1000 Hz and duty cycle of 80% (sample C8, Table 3.1). The voltage-time curves of samples C8-a, C8-b, and C8-c with electrolyte numbers of 6, 10, and 16, respectively, are relatively similar. The voltage increases with time in these samples throughout the coating process. The average coating thickness values of samples C8-a and C8-b are very close, 29.4 and 28.6 µm, respectively, and sample C8-c has a slightly lower thickness, 24.8 µm, on the other hand, and sample C8-d, the twenty third sample coated in the same electrolyte, has a totally different voltage-time response compared to the other three samples. For the first 400 seconds, the voltage-time response of C8-d is

similar to those of the other three samples, but after 400 seconds no further increase in the voltage is observed at extended deposition times. The average thickness of the coating on C8-d is 15.8 μm, which is considerably lower than the other samples.

Surface SEM micrographs also confirm that prolonged use of the electrolyte can change the morphology of the coatings. The SEM image of the surface of sample D8-a, the eighth sample coated in the electrolyte at 2000 Hz and a duty cycle of 80% for 30 min (Figure 3.15-a), shows the regular PEO coating morphology consisting of craters and nodular structure, discussed previously. The surface of sample D8-b (Figure 3.15-b), the twenty first sample coated in the same electrolyte, contains open micropores which would be expected to degrade the properties of the coating.

These results, the lack of a voltage increase with time, the decreased coating thickness in the electrolytes used for a long time (Figure 3.14), and coating porosity (Figure 3.15) all indicate that the PEO electrolyte has a limited service life. The EDX results, Figure 3.10, suggest that Si is incorporated into the coatings during PEO. It has been reported previously that the species in the electrolyte, such as silicon [24], graphite additives [31], carbon nanotubes [32] and non-soluble particles (e.g., ZrO_2) [33], can be incorporated into the coating during PEO. The incorporation of these species can result in a variation in chemical composition of the electrolyte during the PEO process, which in turn could affect the coating process. Although the study of the electrolyte stability is beyond the scope of this research, our observations clearly demonstrate the importance of the service life of the electrolyte. Optimizing the electrolyte composition for long-term stability is an important research direction.

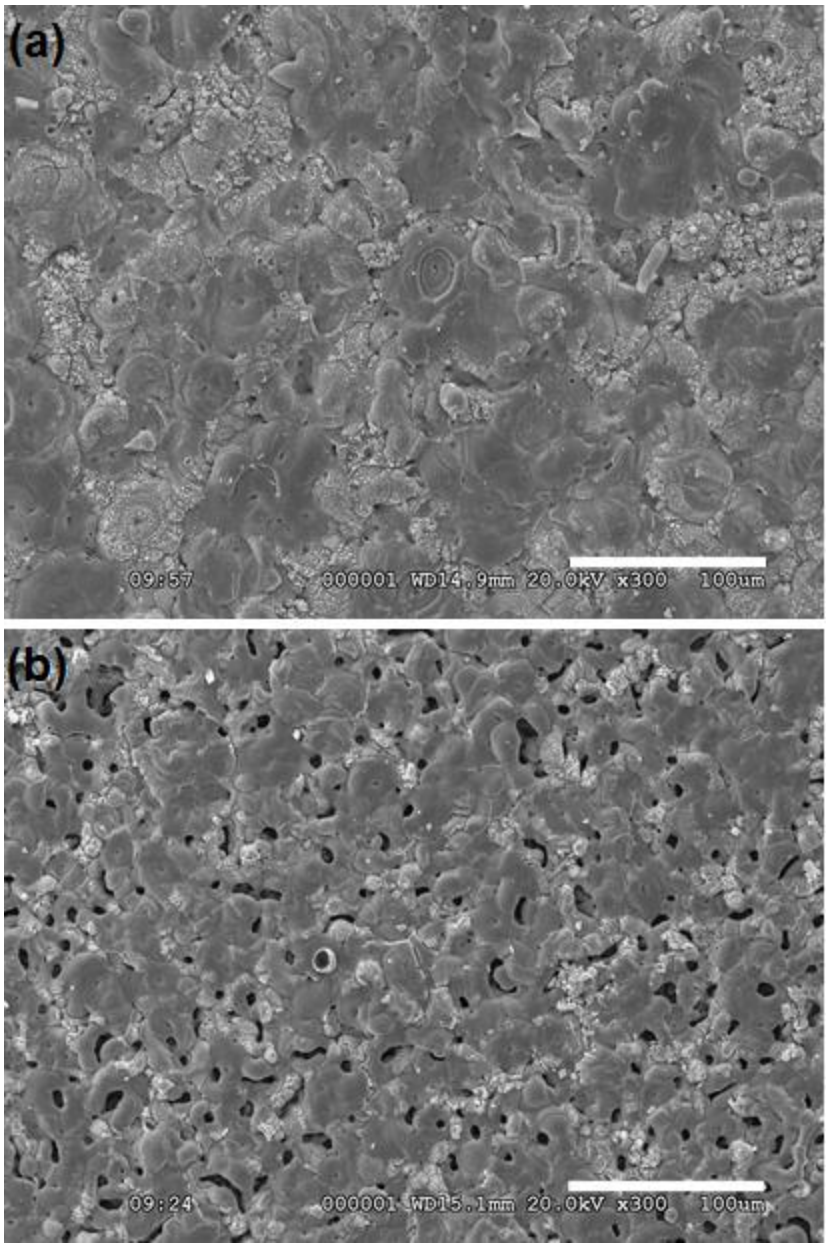

Figure 3.15- SEM micrographs showing the effect of electrolyte stability on the surface morphology of samples D8 (coated at a frequency of 2000 Hz and duty cycle of 80% for 30 min); (a) D8-a, the 8th sample coated in the electrolyte, (b) D8-b, the 21st sample coated in the same electrolyte.

3.4 Conclusions

The PEO processing of the 6061 aluminum alloy using different frequencies and duty cycles was investigated. At low duty cycles the sparking and maximum voltages were both higher. Two regions were observed on the surface of all samples: (i) cratered regions, rich in aluminum, with discharge channels in the center, implying they were the result of dielectric breakdown across the coating, and (ii) a nodular structure, rich in silicon. Applying lower duty cycles produced micro-discharges with higher spatial density and lower intensity. These softer micro-discharges created smaller craters.

During the PEO process at high duty cycles, micro-discharges became stronger but their number decreased, especially at longer times. However, at lower duty cycles the surface of the sample was totally covered by sparks even during the final stages.

The sparking behavior caused by the application of different electrical parameters affected the silicon distribution. Low duty cycles resulted in a lower concentration of Si on the surface and its more uniform distribution across the coating. This phenomenon could be ascribed to the higher density of sparks at low duty cycles which detaches adsorbed silicon containing species from the surface of the sample and also stronger electric fields which increase the possibility of incorporation of Si rich anions into the coating.

XRD patterns revealed that electrical parameters affect the $\gamma \rightarrow \alpha$-$Al_2O_3$ phase transformation. For B2, C2 and D2 samples in which t_{on} times were very short, 0.4, 0.2 and 0.1 milliseconds respectively, only γ-Al_2O_3 peaks were observed. However, for other samples with longer t_{on} times, α- and γ-Al_2O_3 coexist.

The stability of the electrolyte was found to directly affect the reproducibility and quality of the PEO coatings. The prolonged use of an electrolyte resulted in defective PEO coatings with reduced coating thickness and many open micro-pores, not suitable for many applications.

It is expected the results presented here could be utilised to better control the PEO process in order to produce coatings with desired properties.

3.5 References

[1] F.C. Walsh, C.T.J. Low, R.J.K. Wood, K.T. Stevens, J. Archer, A.R. Poeton, et al., Plasma electrolytic oxidation (PEO) for production of anodised coatings on lightweight metal (Al, Mg, Ti) alloys, Trans. Inst. Met. Finish. 87 (2009) 122–135.

[2] W. Miller, L. Zhuang, J. Bottema, A. Wittebrood, P. De Smet, A. Haszler, et al., Recent development in aluminium alloys for the automotive industry, Mater. Sci. Eng. A. 280 (2000) 37–49.

[3] G. Sundararajan, L. Rama Krishna, Mechanisms underlying the formation of thick alumina coatings through the MAO coating technology, Surf. Coatings Technol. 167 (2003) 269–277.

[4] P. Kurze, W. Krsymann, H.G. Schneider, Application Fields of ANOF Layers and Composites, Cryst. Res. Technol. 21 (1986) 1603–1609.

[5] F. Monfort, A. Berkani, E. Matykina, P. Skeldon, G.E. Thompson, A Tracer Study of Oxide Growth during Spark Anodizing of Aluminum, J. Electrochem. Soc. 152 (2005) C382–C387.

[6] V.S. Rudnev, M. a. Medkov, T.P. Yarovaya, N.I. Steblevskaya, P.M. Nedovzorov, M. V. Belobeletskaya, Combination of plasma-electrolytic oxidation and extraction-pyrolytic method for formation of metal oxide layers, Russ. J. Appl. Chem. 85 (2012) 621–628.

[7] R.O. Hussein, D.O. Northwood, X. Nie, Coating growth behavior during the plasma electrolytic oxidation process, J. Vac. Sci. Technol. A Vacuum, Surfaces, Film. 28 (2010) 766–773.

[8] C.S. Dunleavy, I.O. Golosnoy, J. A. Curran, T.W. Clyne, Characterisation of discharge events during plasma electrolytic oxidation, Surf. Coatings Technol. 203 (2009) 3410–3419.

[9] F. Mécuson, T. Czerwiec, T. Belmonte, L. Dujardin, A. Viola, G. Henrion, Diagnostics of an electrolytic microarc process for aluminium alloy oxidation, Surf. Coatings Technol. 200 (2005) 804–808.

[10] B.L. Jiang, Y.M. Wang, Plasma Electrolytic Oxidation Treatment of Aluminum and Titanium Alloys, in: H. Dong (Ed.), Surf. Eng. Light Alloy. Aluminum, Magnes. Titan. Alloy., Woodhead Publishing, 2010: pp. 110–153.

[11] J.M. Wheeler, J. A. Curran, S. Shrestha, Microstructure and multi-scale mechanical behavior of hard anodized and plasma electrolytic oxidation (PEO) coatings on aluminum alloy 5052, Surf. Coatings Technol. 207 (2012) 480–488.

[12] A.L. Yerokhin, L.O. Snizhko, N.L. Gurevina, A. Leyland, A. Pilkington, A. Matthews, Discharge characterization in plasma electrolytic oxidation of aluminium, J. Phys. D. Appl. Phys. 36 (2003) 2110–2120.

[13] R.O. Hussein, X. Nie, D.O. Northwood, A. Yerokhin, A. Matthews, Spectroscopic study of electrolytic plasma and discharging behaviour during the plasma electrolytic oxidation (PEO) process, J. Phys. D. Appl. Phys. 43 (2010) 105203–105216.

[14] S. Moon, Y. Jeong, Generation mechanism of microdischarges during plasma electrolytic oxidation of Al in aqueous solutions, Corros. Sci. 51 (2009) 1506–1512.

[15] F. Jaspard-mécuson, T. Czerwiec, G. Henrion, T. Belmonte, L. Dujardin, A. Viola, et al., Tailored aluminium oxide layers by bipolar current adjustment in the Plasma Electrolytic Oxidation (PEO) process, Surf. Coatings Technol. 201 (2007) 8677–8682.

[16] F. Monfort, A. Berkani, E. Matykina, P. Skeldon, G.E. Thompson, H. Habazaki, et al., Development of anodic coatings on aluminium under sparking conditions in silicate electrolyte, Corros. Sci. 49 (2007) 672–693.

[17] Z. Wang, L. Wu, W. Cai, Z. Jiang, Effects of fluoride on the structure and properties of microarc oxidation coating on aluminium alloy, J. Alloys Compd. 505 (2010) 188–193.

[18] A.A. Voevodin, A.L. Yerokhin, V. V. Lyubimov, M.S. Donley, J.S. Zabinski, Characterization of wear protective Al-Si-0 coatings forrned on Al-based alloys by micro-arc discharge treatment, Surf. Coat. Technol. 86-87 (1996) 516–521.

[19] G. Lv, W. Gu, H. Chen, W. Feng, M.L. Khosa, L. Li, et al., Characteristic of ceramic coatings on aluminum by plasma electrolytic oxidation in silicate and phosphate electrolyte, Appl. Surf. Sci. 253 (2006) 2947–2952.

[20] A.L. Yerokhin, A. Shatrov, V. Samsonov, P. Shashkov, A. Pilkington, A. Leyland, et al., Oxide ceramic coatings on aluminium alloys produced by a pulsed bipolar plasma electrolytic oxidation process, Surf. Coatings Technol. 199 (2005) 150–157.

[21] R.H.U. Khan, A. Yerokhin, X. Li, H. Dong, A. Matthews, Surface characterisation of DC plasma electrolytic oxidation treated 6082 aluminium alloy: Effect of current density and electrolyte concentration, Surf. Coatings Technol. 205 (2010) 1679–1688.

[22] Y. Guangliang, L. Xianyi, B. Yizhen, C. Haifeng, J. Zengsun, The effects of current density on the phase composition and microstructure properties of micro-arc oxidation coating, J. Alloys Compd. 345 (2002) 196–200.

[23] K.M. Lee, Y.G. Ko, D.H. Shin, Incorporation of multi-walled carbon nanotubes into the oxide layer on a 7075 Al alloy coated by plasma electrolytic oxidation: Coating structure and corrosion properties, Curr. Appl. Phys. 11 (2011) S55–S59.

[24] F. Monfort, E. Matykina, A. Berkani, P. Skeldon, G.E. Thompson, H. Habazaki, et al., Species separation during coating growth on aluminium by spark anodizing, Surf. Coatings Technol. 201 (2007) 8671–8676.

[25] H. Wu, J. Wang, B.B. Long, Z. Jin, W. Naidan, F. Yu, et al., Ultra-hard ceramic coatings fabricated through microarc oxidation on aluminium alloy, Appl. Surf. Sci. 252 (2005) 1545–1552.

[26] A.L. Yerokhin, X. Nie, A. Leyland, A. Matthews, S.J. Dowey, Plasma electrolysis for surface engineering, Surf. Coatings Technol. 122 (1999) 73–93.

[27] L. Rama Krishna, K.R.C. Somaraju, G. Sundararajan, The tribological performance of ultra-hard ceramic composite coatings obtained through microarc oxidation, Surf. Coat. Technol. 163-164 (2003) 484–490.

[28] J.A. Curran, T.W. Clyne, Porosity in plasma electrolytic oxide coatings, Acta Mater. 54 (2006) 1985–1993.

[29] C.J.-P. Steiner, D.P.H. Hasselman, R.M. Spriggs, Kinetics of the Gamma-to-Alpha Alumina Phase Transformation, J. Am. Ceram. Soc. 54 (1971) 412–413.

[30] R. McPherson, Formation of metastable phases in flame- and plasma-prepared alumina, J. Mater. Sci. 8 (1973) 851–858.

[31] G.-H. Lv, H. Chen, W.-C. Gu, W.-R. Feng, L. Li, E.-W. Niu, et al., Effects of graphite additives in electrolytes on the microstructure and corrosion resistance of Alumina PEO coatings, Curr. Appl. Phys. 9 (2009) 324–328.

[32] K.M. Lee, Y.G. Ko, D.H. Shin, Incorporation of carbon nanotubes into micro-coatings film formed on aluminum alloy via plasma electrolytic oxidation, Mater. Lett. 65 (2011) 2269–2273.

[33] K.R. Shin, Y.G. Ko, D.H. Shin, Surface characteristics of ZrO_2-containing oxide layer in titanium by plasma electrolytic oxidation in $K_4P_2O_7$ electrolyte, J. Alloys Compd. 536 (2012) S226–S230.

Chapter 4

Production of Ceramic Coatings on the AA6061 Aluminum Alloy in a Relatively High Concentration Sodium Silicate Electrolyte Using Plasma Electrolytic Oxidation

Abstract

Plasma electrolytic oxidation (PEO) is a relatively novel surface finishing technique that converts the surface of light metals and alloys into oxide layers. For Al alloys, the coatings produced by PEO consist mainly of oxides with high hardness and therefore are more suitable for tribological applications than the substrate material. The PEO coatings can also effectively protect the base metal against corrosion. In this study, ceramic coatings were deposited on 6061 Al alloy substrates using an alkaline electrolyte with a relatively high concentration of sodium silicate. The morphology, microstructure, composition, and growth behavior of the coatings were analyzed using scanning electron microscope (SEM), energy-dispersive X-ray spectroscopy (EDX), and X-ray diffraction (XRD). The results suggest that the coating growth behavior is influenced by the electrolyte composition and PEO process stages. Comparing the voltage-time response of these PEO coated samples with those of a different study in which similar electrical parameters with a different electrolyte were used, revealed that the electrolyte composition can alter the onset and duration of the PEO process stages, which in turn, will determine the properties of the resultant coatings. This information can be used to better understand the PEO coating growth behavior and to improve the quality of the coatings for required applications.

4.1 Introduction

Plasma electrolytic oxidation (PEO), which is a relatively novel surface modification technique, has attracted a lot of interest as an effective method to produce coatings with improved hardness, wear and corrosion resistance on the surface of aluminum alloys [1,2]. PEO is a plasma-assisted electrochemical surface treatment which operates at high electrical voltages, typically several hundred volts. At voltages greater than the breakdown voltage of the oxide film, a large number of short-lived micro-discharges are formed which create the oxide layer [3,4]. The structure of the coatings resembles sintered oxide ceramics and their formation is the result of the local thermal action of the sparks [5]. As the oxide layer grows and thickens, the micro-discharges developing on the sample surface become more intense which can result in detrimental defects in the oxide layer [6].

Aqueous solutions containing silicates can passivate the surface of the aluminum substrate and are considered as one of the most suitable electrolytes for the PEO process. These alkaline electrolytes are environmentally friendly and as a result PEO is attracting growing interest in many industries including transport, energy and medicine. PEO is a good substitute for conventional and hard anodizing methods in which acidic electrolytes containing chrome are used which create severe pollution and environmental issues [4,7,8].

Despite various investigations conducted by many researchers, the PEO coatings formation mechanism is still not fully understood [9,10]. Typically four stages are distinguished in the PEO process [8,11]. The phenomenon and mechanism happening in each stage and the resulting effects on the oxide layer growth behaviour are different. Applied process parameters can change the duration and ratio of these stages. Investigating the correlation between coating characteristics and different stages of PEO can improve the understanding of the process. In the present study, aluminum substrates were PEO coated in an electrolyte containing a relatively high concentration (10 g/l) of sodium silicate. Samples were coated at different treatment times and particular attention was paid to correlate the voltage-time responses of the PEO coating process and the oxide

layer characteristics so as to understand the coating growth behaviour during different stages of PEO.

4.2 Experimental Procedure

Disk samples with a diameter of about 3 cm and a thickness of 7-9 mm were cut from a 6061-T651 aluminum alloy bar supplied by Kaiser Aluminum, USA. To ensure a reproducible initial surface condition, samples were polished with 600 grit emery polishing paper followed by degreasing in propanol and rinsing with distilled water. A PEO unit custom-built by the National Research Council (Canada) equipped with a DC power supply was used to produce the coatings. The positive output of the power supply was connected to the sample immersed in the electrolyte serving as the working electrode (anode) and the negative output was connected to the stainless steel electrolyte container acting as the counter electrode (cathode). To ensure a good connection between the power supply and the samples, a threaded hole was drilled on one side of each sample. Then the sample was bolted to a steel rod (insulated by a ceramic jacket from the electrolyte) connected to the power supply. PEO coatings were produced using the uni-polar pulsed DC mode with a square waveform applied at a frequency of 900 Hz. Samples were coated at a duty cycle (D_t) of 20%. The duty cycle is defined as:

$$D_t = [\ t_{on} / (t_{on} + t_{off})] \times 100 \qquad (4.1)$$

where t_{on} is the positive pulse on time and t_{off} is the pulse off time during a single cycle. The schematic of the corresponding parameters and waveform of the uni-polar pulsed power source are given in Figure 4.1.

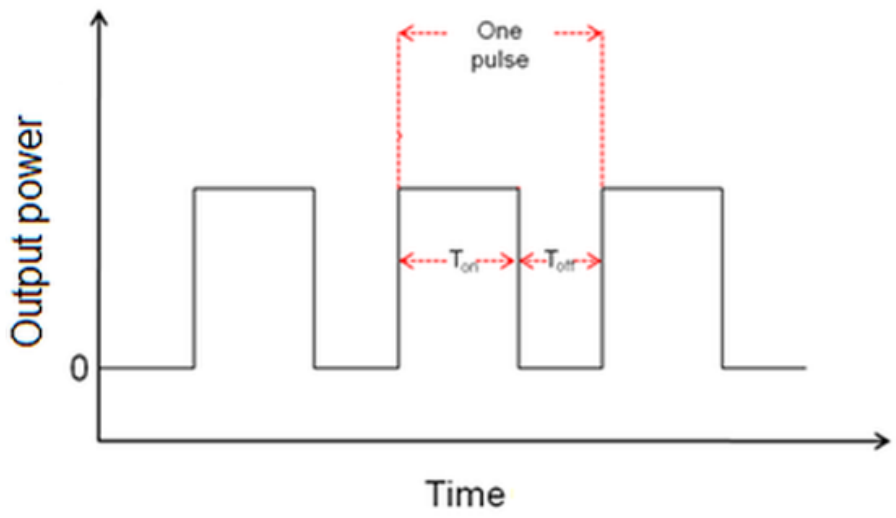

Figure 4.1- Schematic of uni-polar pulse output of a plasma electrolytic oxidation power supply unit: (t_{on}: positive pulse on time; t_{off}: pulse off time)

The PEO process was carried out at a constant current density of 10 A/dm^2. Table 4.1 lists the sample codes and corresponding deposition times.

Table 4.1- Sample codes and deposition times.

Sample code	Deposition time (min)
S1	10
S2	20
S4	40
S6	60

The electrolyte was a solution of 10 g/l Na_2SiO_3 and 0.5 g/l KOH in deionized water. The electrolyte temperature was maintained below 30 °C during treatment using an external DCA 500 Durachill heat exchanger manufactured by Polyscience.

Coating thickness was evaluated using an Eddy current gauge. Ten measurements were taken on the coated surface of each sample. Statistical treatments were applied to extract

the mean data values and scatter. Coating surfaces and cross sections were examined using a LEO 440 scanning electron microscope (SEM) equipped with a Quartz EDX system and a Hitachi S-3500N SEM equipped with an Oxford Instruments 7490 X-ray detector. The samples were sputter-coated with gold prior to SEM imaging to minimize surface charging. A Philips X'Pert_MRD diffractometer with Cu K_α (40 kV and 40 mA) radiation was used to study the phase composition of the coatings. The samples were scanned in the 2θ range from 20° to 100° with a 0.02 ° step size.

4.3 Results and Discussion

4.3.1 Voltage-time Response during PEO Treatment

The voltage-time curve of the PEO coating process of the sample treated for 60 min is presented in Figure 4.2. Since voltage-time curves for other samples coated at shorter times overlapped, only one curve is illustrated. Generally four different stages are believed to take place during PEO [8,11]. During the first stage, as the applied voltage increases, a large amount of bubbles is produced. This stage, which corresponds to the initial linear part of the voltage-time curve (Figure 4.2), is the traditional anodizing stage in which a thin porous film is formed.

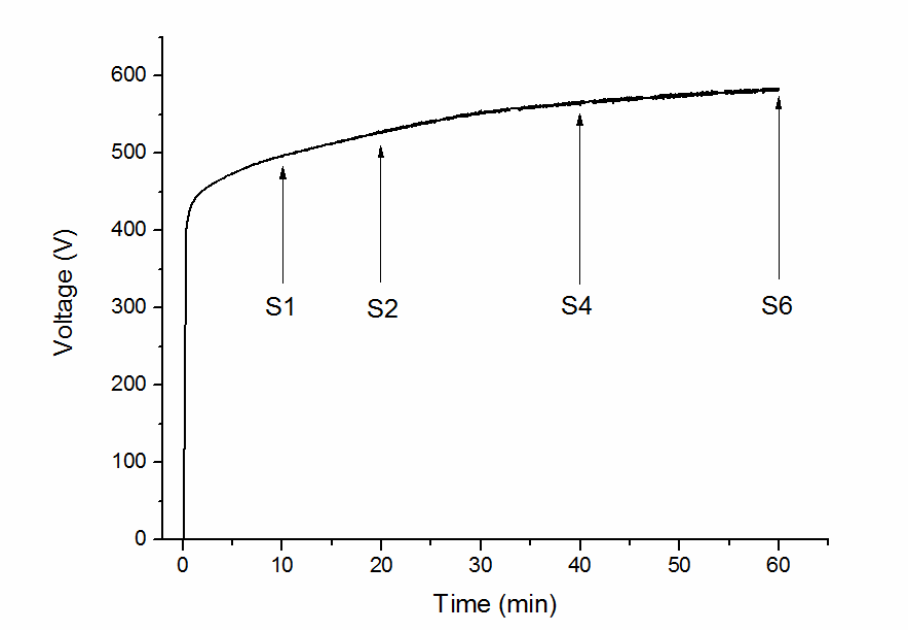

Figure 4.2- Voltage-time response for the PEO coated sample S6 coated for 60 min.

When the voltage reaches a certain threshold, which is termed the 'breakdown voltage', dielectric breakdown occurs in some regions of the coating and the surface of the sample becomes covered by many fine and uniform sparks with a bluish white color. This creates many small uniform micro-pores [8]. In stage two, three, and four, which occur after the breakdown voltage is reached, the rate of voltage changes varies based on the process conditions applied. In a study [12] in which an electrolyte containing 2 g/l Na_2SiO_3 and 2 g/l KOH was used with almost similar electrical conditions to the current study, the voltage-time response of the process showed a different behaviour with the four stages having different slopes, onset times, and durations. Stage II in the present study is more than twice as long as stage II in the abovementioned study. This shows how the electrolyte composition can affect the coating growth behavior during PEO.

4.3.2 Coating Surface Morphology and Composition

The surface morphology of sample S2 is illustrated in Figure 4.3. Typically two different regions are observed on the surface of PEO coated samples: a round, circular area (Area "a"), and a nodular structure (Area "b"). The circular area, which typically has a hole in the middle, is a discharge channel through which molten material flows out to the surface from the substrate and coating interface [12]. At higher magnifications, the nodular structure (Figure 4.4) appears as clusters of bubbles formed. During the PEO process, gaseous oxygen and hydrogen can be liberated on the anodic and cathodic surfaces, respectively [13].

Under the high anodic currents in PEO, oxygen evolution occurs via the oxidation of water:

$$2H_2O\text{-}4e^- \rightarrow O_2 + 4H^+ \quad (4.2)$$

At an inert cathode in alkaline electrolytes, hydrogen evolution occurs through the following reaction [14]:

$$2H_2O + 2e^- \rightarrow H_2 + 2OH^- \quad (4.3)$$

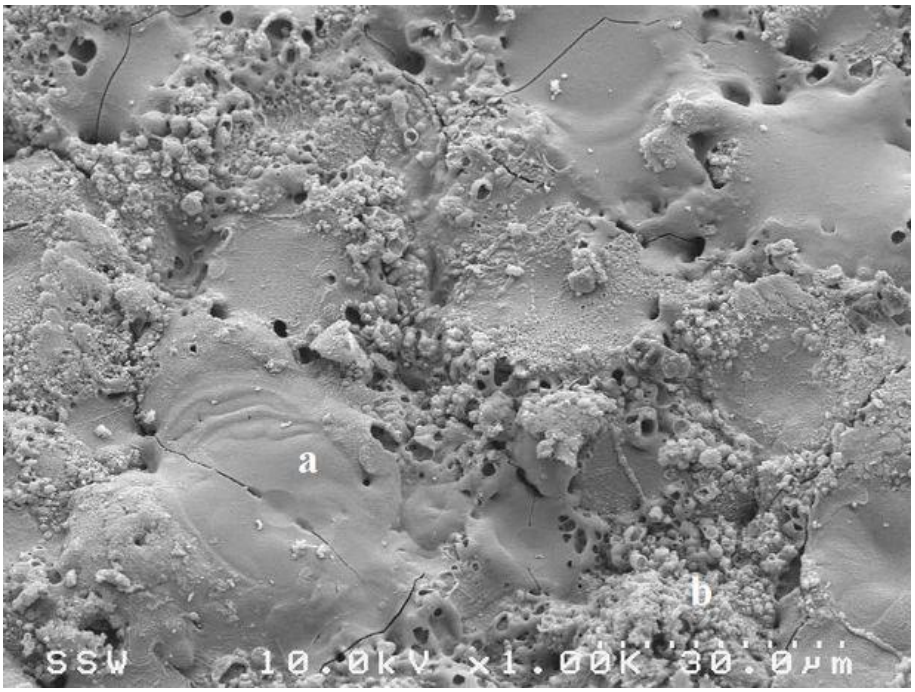

Figure 4.3- Scanning electron microscope image showing the surface morphology of sample S2 (coated for 20 min).

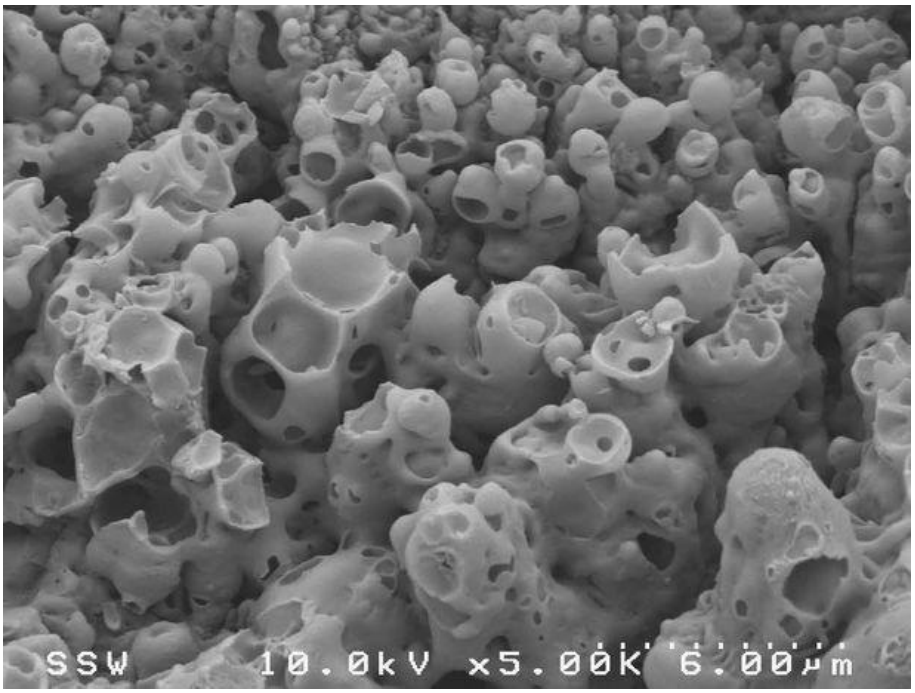

Figure 4.4- SEM micrograph of the nodular structure of sample S6.

The formation of the nodular structure with a bubble-like appearance on the surface of the PEO coatings could be linked to gas liberation on the surface of the anode during the coating process. The surface of the gas bubbles can provide a suitable site for the nucleation of the solids formed as the result of complex reactions taking place on the surface of the substrate material. However, this proposed formation mechanism requires further investigation.

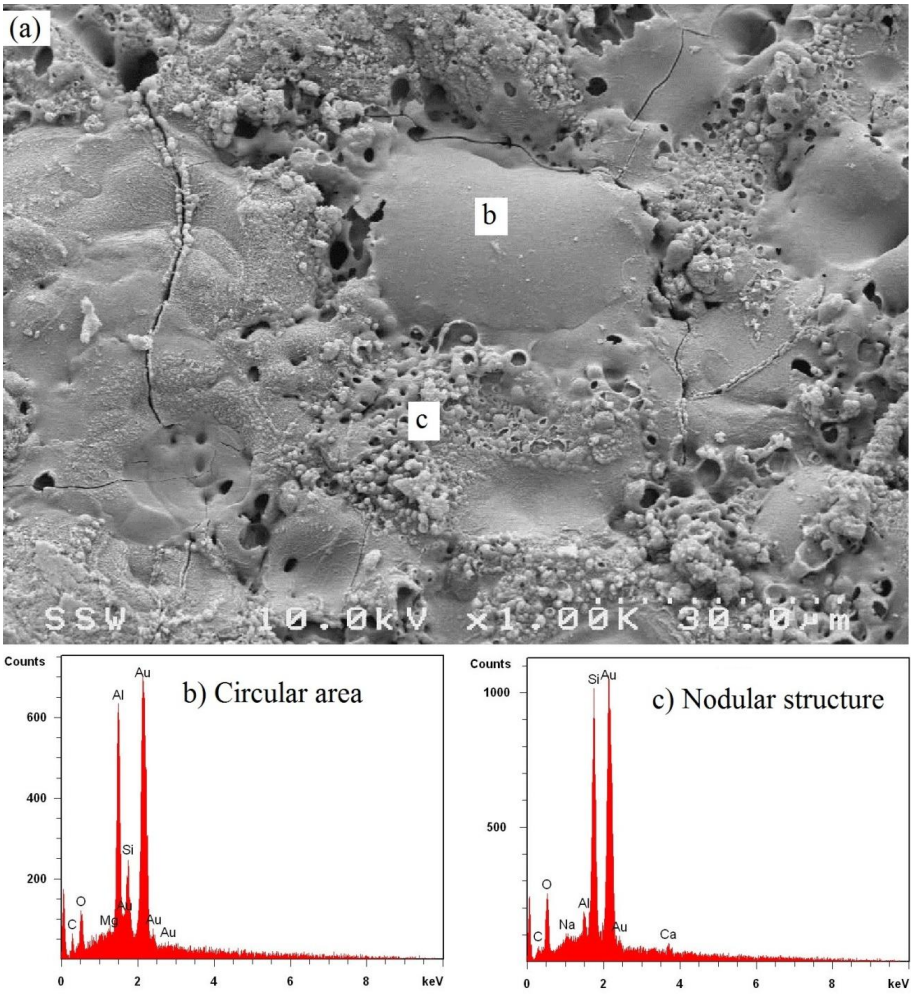

Figure 4.5- (a) SEM micrograph showing the coating surface morphology on sample S2; (b) and (c) EDX analysis from areas “b” and “c” respectively.

The SEM image and corresponding energy dispersive X-ray (EDX) spectra of the circular area and the nodular structure of sample S2 are presented in Figure 4.5. As can be seen, the craters are rich in aluminum while the nodular structure is rich in Si. The EDX

spectra of samples S1, S4, and S6 also show similar results for the two regions. Discharge channels are always surrounded by craters [6,15]. The oxide film growth is the result of the ejection and solidification of the molten aluminum oxide when it flows out through the discharge channels created due to the breakdown of the oxide layer [9].

Figure 4.6 illustrates the surface features of the PEO coated samples produced at different deposition times. In Figure 4.6-b to Figure 4.6-d, discharge channels can be observed as circular spots resembling craters.

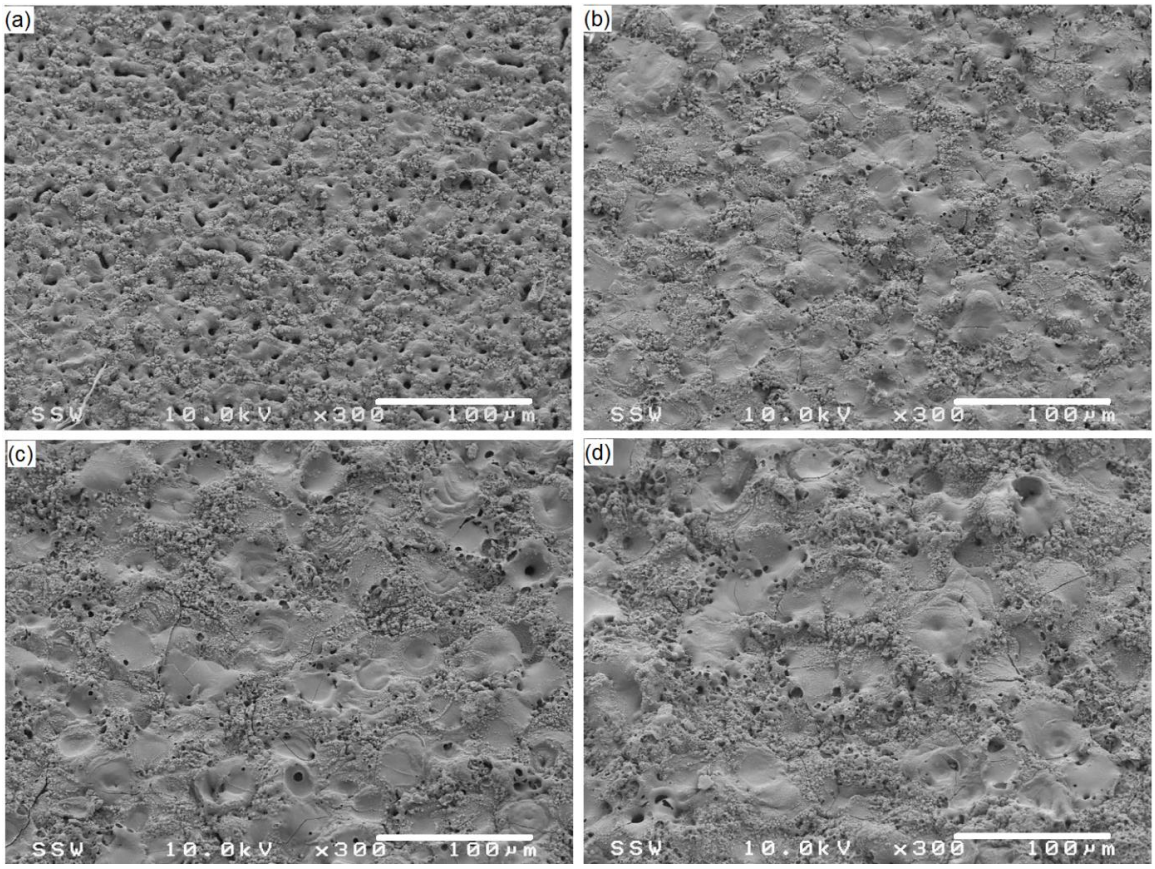

Figure 4.6- SEM micrographs of the free surfaces of samples, (a) S1, (b) S2, (c) S4, and (d) S6.

The surface features on sample S1 (Figure 4.6-a) are different from other samples. On sample S1, coated for 10 min, a nodular structure with many micro-pores is observed scattering across the surface area while samples coated for longer times (Figure 4.6-b, c, and d) exhibit nodular structures and craters with occasional micro-pores.

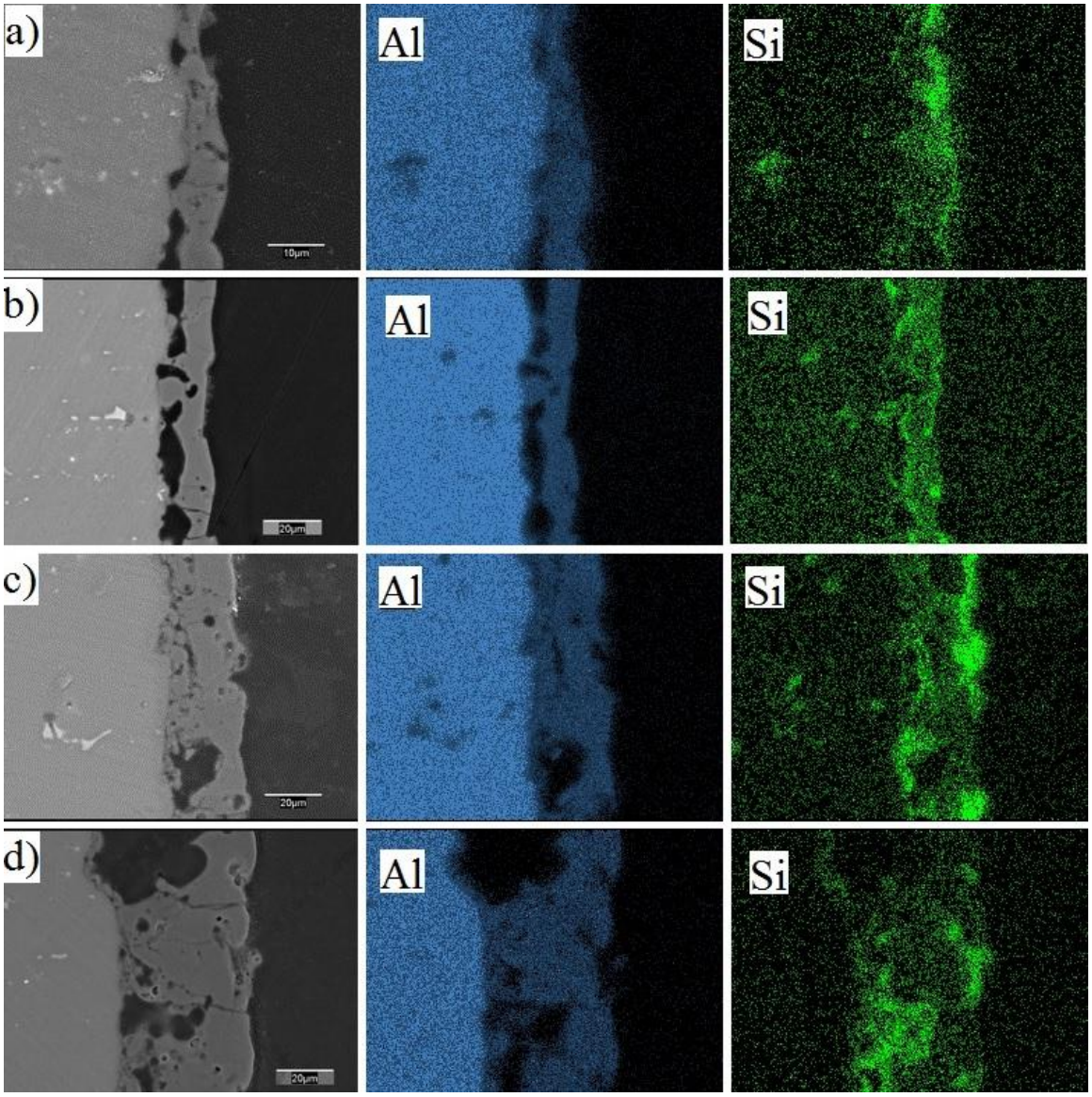

Figure 4.7- Cross sectional SEM micrographs and EDX elemental maps showing the distribution of Al and Si for samples (a) S1, (b) S2, (c) S4, and (d) S6.

As can be observed in Figure 4.2, the deposition time for sample S1 falls in stage II, while for other samples deposition times were long enough to enter stage III. Moreover, during the early stages of the coating process (first 10-12 min) the sparks appearing on the surface of the sample were small, bluish white in color and had a high spatial density. However, as the coating process proceeded, the color changed to yellow and then orange. From these observations it can be deduced that the coating growth behaviour and

sparking mechanisms change during different stages of the process. For the specific process conditions used in this study, a deposition time of 10 min produced many micro-pores on the surface of the coating which is not favourable.

EDX analysis revealed that Al and O were the main constituents of the PEO coatings. In addition to these two major elements, some Si was also observed. EDX elemental maps showing the distribution of chemical elements across the coating (Figure 4.7) suggest that Al and O were distributed uniformly throughout the coating thickness while Si concentration tends to increase in some areas. As can be seen in Figure 4.7, the Si-rich areas are located at the electrolyte-coating interface and also around the pores inside the coating. A similar distribution of Si has been reported elsewhere in the literature [16,17] for the PEO coating of aluminum alloys in electrolytes containing silicate species. A possible mechanism for the preferred distribution of the Si-rich areas on the surface of the PEO coatings has been proposed by Dehnavi et al. [12].

4.3.3 Coating Thickness

Coating thickness measurements (Figure 4.8) revealed an increase in the coating thickness with deposition time. The average coating growth rate was about 0.95 µm/min.

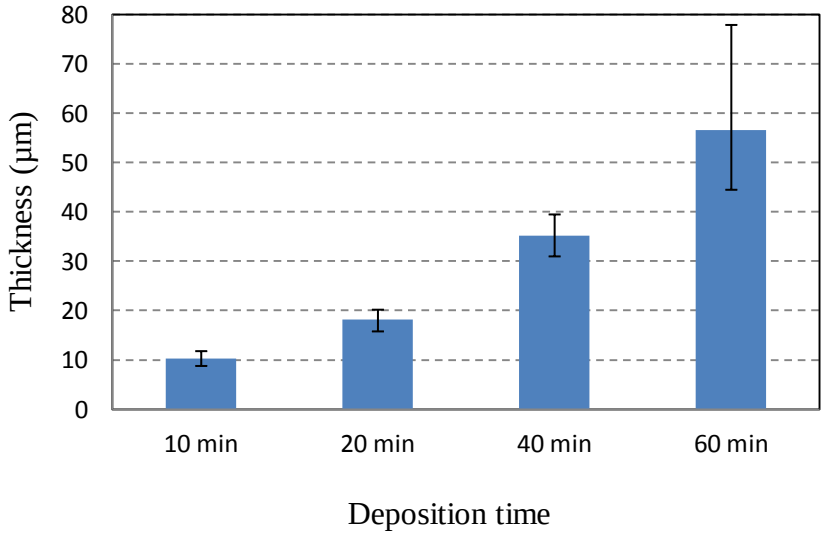

Figure 4.8- PEO coating thickness variations with deposition time.

Optical microscope images showing the cross sections of the coated samples are presented in Figure 4.9. There are pores present in the coating which could be the result of gas entrapment in the molten coating during formation.

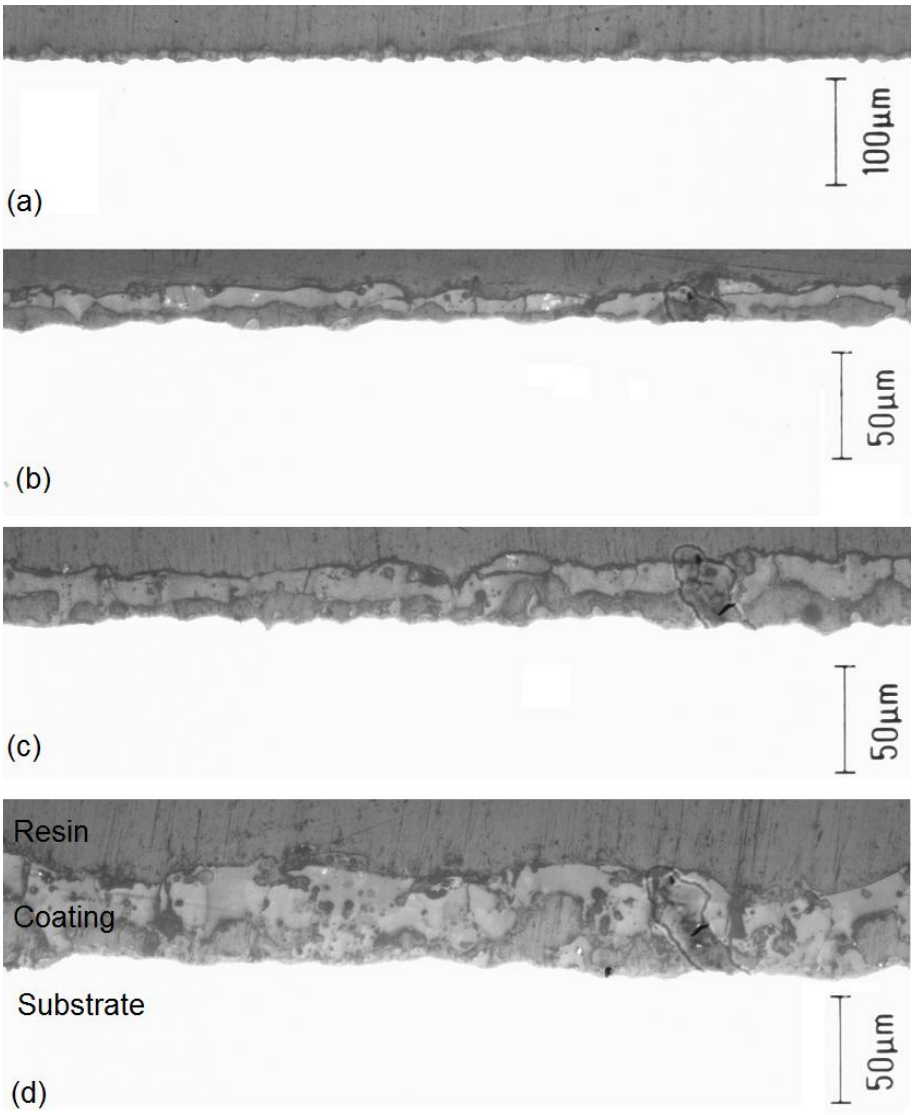

Figure 4.9- Optical microscope images of cross sections of coatings on samples (a) S1, (b) S2, (c) S4, and (d) S6.

4.3.4 Phase Analysis

Figure 4.10 illustrates the X-ray diffraction (XRD) spectra of the as deposited surface layers of PEO coatings processed for 10, 20, 40, and 60 min. To prevent the aluminum substrate peaks from masking the peaks belonging to phases present in the coating, glancing angle XRD was performed at an incident angle of 3.5°. It can be concluded from Figure 4.10 that PEO coatings are mainly comprised of γ-Al_2O_3 for treatment times of 10 and 20 min (samples S1 and S2, respectively). For samples S4 and S6, treated for longer times (40 and 60 min, respectively) some mullite is also observed in addition to γ-Al_2O_3.

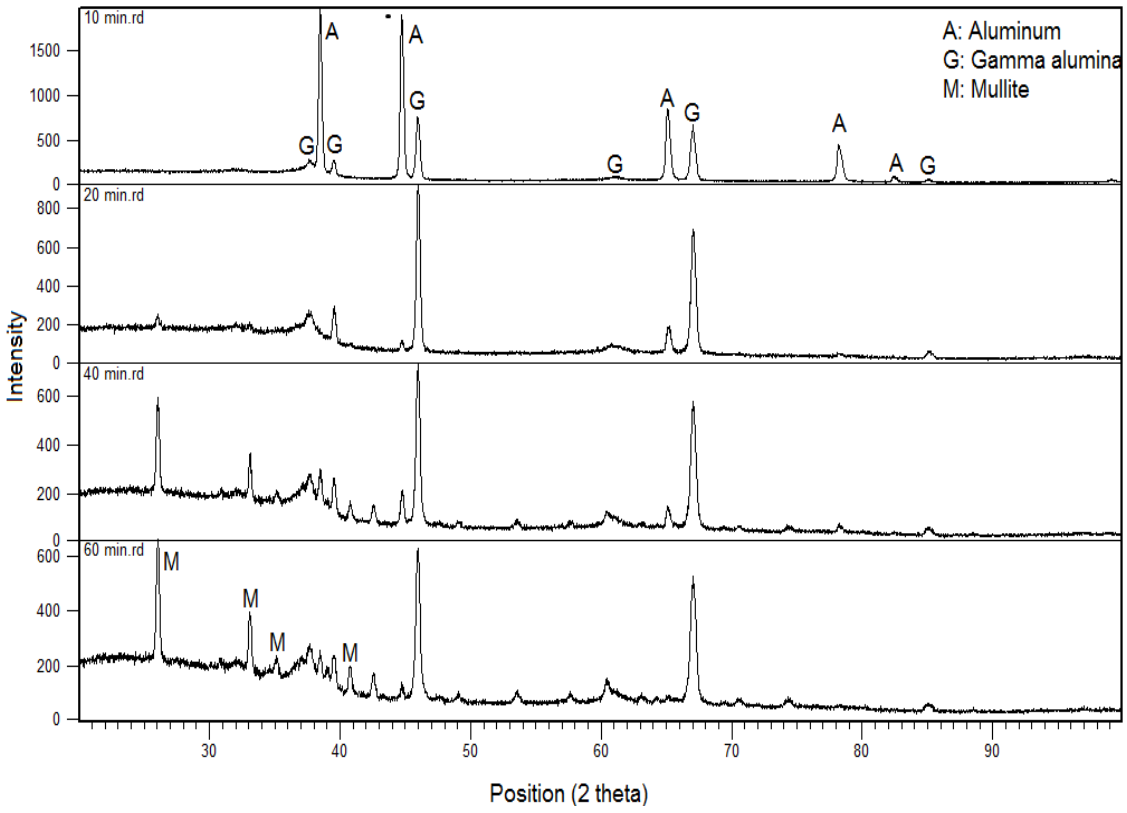

Figure 4.10- XRD spectra of PEO coatings processed for 10, 20, 40, and 60 min.

The extremely high cooling rates, when the molten alumina is ejected out and comes in contact with the electrolyte, favour the formation of γ-Al_2O_3 during solidification [9]. It was previously reported [10,18,19] that in Si containing electrolytes, the concentration of Si species is higher on the surface of the PEO coatings. It has been proposed [8,17] that Si forms insoluble gels on the surface of PEO coatings. A conceptual model proposed by Dehnavi et al. [12] explains Si distribution on the surface of samples coated in electrolytes containing Si species. It was suggested that the ejection force of the micro-discharges formed on the surface of the coating detaches the Si rich species adsorbed on the coating. As the deposition time increases, micro-discharges become more intense while their numbers decrease. The lower spatial density of micro-discharges leaves more areas with Si rich species and this could enhance the formation of mullite ($3Al_2O_3.SiO_2$) at treatment times of 40 and 60 min where the number of micro-discharges decreased compared to deposition times of 10 and 20 min.

4.4 Conclusions

6061 aluminum substrates were PEO treated at different times. The results obtained from the characterization techniques show a clear correlation of the coating microstructure with the voltage-time response of the process. The results suggest that the processing conditions affect the duration and ratio of the PEO stages. It was concluded that the coating growth behaviour and sparking mechanisms change during different stages of the process.

The sample coated merely in stage II showed many micro-pores scattered across the surface area. In samples coated for longer times, craters, which are characteristic of stages III and IV, were observed on the coating surface. The size of the craters increased while their spatial intensity decreased with deposition time.

X-ray diffraction results (XRD) revealed that the PEO coatings produced at deposition times of 10 and 20 min were comprised of γ-Al_2O_3. In samples coated for longer times (40 and 60 min) mullite peaks were observed in addition to γ-Al_2O_3.

4.5 References

[1] H. Li, R. Song, Z. Ji, Effects of nano-additive TiO_2 on performance of micro-arc oxidation coatings formed on 6063 aluminum alloy, Trans. Nonferrous Met. Soc. China. 23 (2013) 406–411.

[2] M.M. Student, V.M. Dovhunyk, M.D. Klapkiv, V.M. Posuvailo, V. V. Shmyrko, A.P. Kytsya, Tribological Properties of Combined Metal-Oxide–Ceramic Layers on Light Alloys, Mater. Sci. 48 (2012) 180–190.

[3] T. Abdulla, A. Yerokhin, R. Goodall, Effect of Plasma Electrolytic Oxidation coating on the specific strength of open-cell aluminium foams, Mater. Des. 32 (2011) 3742–3749.

[4] J. Martin, A. Melhem, I. Shchedrina, T. Duchanoy, A. Nominé, G. Henrion, et al., Effects of electrical parameters on plasma electrolytic oxidation of aluminium, Surf. Coatings Technol. 221 (2013) 70–76.

[5] A.L. Yerokhin, V. V. Lyubimov, R. V. Ashitkov, Phase formation in ceramic coatings during plasma electrolytic oxidation of aluminium alloys, Ceram. Int. 24 (1998) 1–6.

[6] F. Jaspard-mécuson, T. Czerwiec, G. Henrion, T. Belmonte, Tailored aluminium oxide layers by bipolar current adjustment in the Plasma Electrolytic Oxidation (PEO) process, Surf. Coat. Technol. 201 (2007) 8677–8682.

[7] A.L. Yerokhin, A.A. Voevodin, V. V. Lyubimov, J. Zabinski, M. Donley, Plasma electrolytic fabrication of oxide ceramic surface layers for tribotechnical purposes on aluminium alloys, Surf. Coat. Technol. 110 (1998) 140–146.

[8] B.L. Jiang, Y.M. Wang, Plasma Electrolytic Oxidation Treatment of Aluminum and Titanium Alloys, in: H. Dong (Ed.), Surf. Eng. Light Alloy. Aluminum, Magnes. Titan. Alloy., Woodhead Publishing, 2010: pp. 110–153.

[9] G. Sundararajan, L. Rama Krishna, Mechanisms underlying the formation of thick alumina coatings through the MAO coating technology, Surf. Coatings Technol. 167 (2003) 269–277.

[10] S. Moon, Y. Jeong, Generation mechanism of microdischarges during plasma electrolytic oxidation of Al in aqueous solutions, Corros. Sci. 51 (2009) 1506–1512.

[11] R.O. Hussein, X. Nie, D.O. Northwood, A. Yerokhin, A. Matthews, Spectroscopic study of electrolytic plasma and discharging behaviour during the plasma electrolytic oxidation (PEO) process, J. Phys. D. Appl. Phys. 43 (2010) 105203.

[12] V. Dehnavi, B.L. Luan, D.W. Shoesmith, X.Y. Liu, S. Rohani, Effect of duty cycle and applied current frequency on plasma electrolytic oxidation (PEO) coating growth behavior, Surf. Coatings Technol. 226 (2013) 100–107.

[13] A.L. Yerokhin, X. Nie, A. Leyland, A. Matthews, S.J. Dowey, Plasma electrolysis for surface engineering, Surf. Coatings Technol. 122 (1999) 73–93.

[14] F.C. Walsh, C.T.J. Low, R.J.K. Wood, K.T. Stevens, J. Archer, A.R. Poeton, et al., Plasma electrolytic oxidation (PEO) for production of anodised coatings on lightweight metal (Al, Mg, Ti) alloys, Trans. Inst. Met. Finish. 87 (2009) 122–135.

[15] L.R. Krishna, K.R.C. Somaraju, G. Sundararajan, The tribological performance of ultra-hard ceramic composite coatings obtained through microarc oxidation, Surf. Coatings Technol. 163-164 (2003) 484–490.

[16] A. L. Yerokhin, a. Shatrov, V. Samsonov, P. Shashkov, A. Pilkington, A. Leyland, et al., Oxide ceramic coatings on aluminium alloys produced by a pulsed bipolar plasma electrolytic oxidation process, Surf. Coatings Technol. 199 (2005) 150–157.

[17] F. Monfort, A. Berkani, E. Matykina, P. Skeldon, G.E. Thompson, H. Habazaki, et al., Development of anodic coatings on aluminium under sparking conditions in silicate electrolyte, Corros. Sci. 49 (2007) 672–693.

[18] F. Monfort, A. Berkani, E. Matykina, P. Skeldon, G.E. Thompson, A Tracer Study of Oxide Growth during Spark Anodizing of Aluminum, (2005) 382–387.

[19] F. Monfort, E. Matykina, A. Berkani, P. Skeldon, G.E. Thompson, H. Habazaki, et al., Species separation during coating growth on aluminium by spark anodizing, Surf. Coatings Technol. 201 (2007) 8671–8676.

Chapter 5

Phase Transformation in Plasma Electrolytic Oxidation Coatings on 6061 Aluminum Alloy

Abstract

Oxide coatings were produced on a 6061 aluminum alloy using a pulsed unipolar plasma electrolytic oxidation (PEO) process. The effect of electrical parameters including pulse frequency, duty cycle and current density on phase formation in the coatings was revealed using conventional and glancing angle X-ray diffraction. The results show that PEO coatings are mainly composed of γ-Al_2O_3. Depending on the electrical parameters employed, the coatings can also contain α-Al_2O_3 and mullite with varying concentrations. Higher current densities and higher duty cycle were found to favour the formation of mullite. Under the experimental conditions used, the ratio of the integrated XRD peaks for α- and γ-Al_2O_3 varied from 0 to about 0.6, indicating the relative content of α-Al_2O_3 in the PEO coatings varied over a wide range. Longer pulse on-times and higher current densities promoted the gamma to alpha-alumina phase transformation. Depth profiling of PEO ceramic coatings using glancing angle XRD with different incident beam angles revealed that mullite was more concentrated in the top surface of the coatings. No significant variation in α-Al_2O_3 concentration across the coatings could be concluded in this study, unlike the results of some other studies.

5.1 Introduction

Alumina ceramic coatings have great potential as hard, wear and corrosion resistant coatings on aluminum and its alloys. Various techniques including chemical vapour deposition (CVD), ionization-assisted magnetron sputtering PVD, and thermal spray, are available to deposit alumina coatings, most of which involve high temperatures, but are not suitable for aluminum which has a relatively low melting point. As an alternative, coatings prepared by plasma electrolytic oxidation (PEO) are less expensive and easier to apply to components with complex geometries and large dimensions than the CVD, PVD or thermal spray processes [1,2]. PEO is a relatively new surface modification technique which can convert the surface of valve metals and alloys such as aluminum, magnesium, zirconium, and titanium into oxide ceramic coatings [3–6]. The PEO process involves complex chemical, electrochemical and plasma thermo-chemical reactions.

Despite extensive research, the mechanism of the PEO process is not comprehensively understood [7–9]. Hussein et al. [10] proposed a discharge model involving three distinct types of discharges, A, B, and C, for PEO on aluminum alloy substrates. Types A and C were thought to result from gas discharges occurring in micro-pores in the ceramic coating, and type B was attributed to dielectric breakdown through the oxide layer. More recently, an additional type of discharge has been proposed, type D, which occurs in large pores near the interface between the inner and outer layers [7]. These discharges play an essential role in the formation and properties of the resulting coatings, by influencing phase transformation, crystallization, annealing and sintering of the coating [11].

The PEO process involves multiple features. The characteristics of PEO coatings are affected by the compositions of the substrate material and the electrolyte, process parameters such as the current regime (AC, DC, and pulsed DC), current density, duty cycle, frequency and treatment time [12–14]. In addition to the type of current regime, the current polarity and application sequence could also affect the properties of the coatings. It is suggested that the pulsed bipolar current mode generally improves the properties of the PEO coatings and results in coatings with higher density [15]. In a study on a magnesium alloy substrate, it was found that applying a hybrid current mode, in

which a unipolar current was applied first followed by a bipolar current, improved the coating properties in terms of microstructure and corrosion resistance [16].

PEO coatings produced on aluminum alloy substrates in dilute silicate electrolytes are mainly composed of α- and γ-Al_2O_3 with some amorphous alumina. In electrolytes with a high concentration of silicate, mullite is also observed [1,7,17–19]. Thick coatings with high mullite content, possess good thermal and chemical stability, and are good candidates for thermal barrier applications [2,20].

PEO coatings have also been reported to have superior wear and corrosion resistance compared to untreated aluminum alloy substrates [1,14]. The hardness of the PEO coating is a function of the nature of the dominant phases present, as well as their ratio and distribution and the porosity and density of micro-cracks in the coatings. The hardness of alumina phases have been reported to be around 26 GPa for α-Al_2O_3, 17 GPa for γ-Al_2O_3, 10.5 GPa for mullite, and 7 GPa for the amorphous anodically formed alumina. However, the measured hardness in PEO coatings is lower than in dense bulk alumina due to porosity in PEO coatings [7,11,20]. Tribological studies indicate coatings composed of α-Al_2O_3 show a higher wear resistance [21].

It is believed that increasing the α-Al_2O_3 content will enhance the wear performance of PEO coatings [22,23]. This improved hardness compared to conventional coatings formed by anodization is attributed to the presence of a large proportion of crystalline material, namely α- and γ-Al_2O_3, and to a reduced porosity [24]. Controlling the α-Al_2O_3 content of the coating, which is the hardest phase among alumina phases, may prove advantageous in producing coatings with higher hardness. There are a few studies in which some aspects of the phase transformation of coatings during PEO treatment on aluminum alloy substrates have been investigated, but the phenomenon is far from being well understood. Khan et al. [25] found a decreased duty cycle caused a corresponding decrease in the ratio of α- to γ-Al_2O_3 in PEO coatings on 6082 aluminum alloy produced by pulsed unipolar current, although large data scatter was observed. Xue et al. [17] investigated the phase distribution of ceramic coatings on 2024 aluminum alloy and concluded that the surface layer of coatings mainly contained γ-Al_2O_3 and the percentage

of α-Al_2O_3 gradually increased from the external surface towards the inner layers of the coatings. Applying higher current densities [11,12,26] and increasing the deposition time which resulted in thicker coatings [21,27], was reported to increase the α-Al_2O_3 content in the coatings.

Hard PEO coatings mainly composed of α-Al_2O_3 could be a promising candidate to protect Al alloy substrates against wear. Here, we report possible procedures to control the α-Al_2O_3 content in alumina oxide coatings by varying the electrical parameters in the PEO process. The results of the current study provide a reference for the possible industrial applications of PEO coatings where a high hardness is required.

5.2 Material and Methods

5.2.1 Sample Preparation

Disk specimens were cut from a 6061 aluminum alloy bar with an average diameter of 30 mm and an average thickness of 8 mm. The specimens were then ground with 600 grit SiC paper, degreased in propanol and rinsed with distilled water. Electrical contact to specimens was made using a steel rod bolted to a threaded hole drilled in the side of each specimen.

5.2.2 Coating Process

PEO coatings were produced using a custom built, unipolar pulsed DC source in an electrolyte containing 2 g/l Na_2SiO_3 + 2 g/l KOH in deionized water. Samples served as the anode and were submerged in the electrolyte in a stainless steel tank which also served as the counter cathode. During the PEO process, the electrolyte temperature was maintained below 40 °C by circulating the electrolyte through an external heat exchanger. To investigate the effect of electrical parameters on phase transformations in the coatings, two frequencies, 50 and 1000 Hz, at duty cycles of 20% and 80% with current densities (J) of 5, 10, 15, 20, and 25 A/dm^2 were used. The samples were coated under galvanostatic conditions, i.e. the current was kept constant during the entire process and the anode potential was allowed to vary. All samples were coated for 30 min. Table 5.1 lists the sample codes with the corresponding electrical conditions used.

Table 5.1-Electrical parameters and sample codes for PEO treatment on 6061 Al alloy.

Sample code	Frequency (Hz)	Duty cycle, D_t (%)	t_{on} (ms)	t_{off} (ms)	* : J (A/dm^2)
S12-*	1000	20	0.2	0.8	5, 10, 15, 20, 25
S18-*	1000	80	0.8	0.2	
S52-*	50	20	4	16	
S58-*	50	80	16	4	

During a single pulse, t_{on} and t_{off} are the periods during which the current is on and off, respectively, and the duty cycle (D_t) is defined by equation 5.1,

$$D_t = [\ t_{on} / (t_{on} + t_{off})] \times 100 \quad (5.1)$$

The waveform and corresponding parameters of the unipolar pulsed power source are given in Figure 5.1.

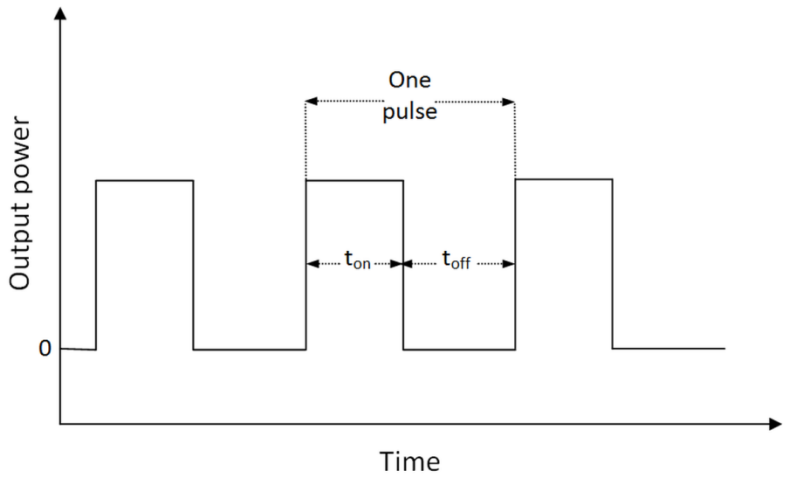

Figure 5.1- Schematic of the pulsed unipolar output of a plasma electrolytic oxidation power supply (t_{on}: pulse on time; t_{off}: pulse off time)

5.2.3 Coating Characterization

The surface morphologies of the PEO coatings were examined using a Hitachi S-3500N scanning electron microscope (SEM). The samples were sputter-coated with gold prior to SEM examination to minimize surface charging. A Philips X'Pert_MRD diffractometer with Cu Kα (40 kV and 40 mA) radiation was used to study the composition of the coatings. The samples were scanned over the 2θ range from 15° to 90° with a 0.02 ° step size. To determine the distribution of different crystalline phases throughout the coating, and to minimize interference from the aluminum substrate, glancing angle XRD at incidence angles of 1, 2.5 and 5 degrees was performed to supplement conventional (Bragg-Brentano configuration) X-ray diffraction measurements. Coating thickness was measured using an Eddy current gauge.

5.3 Results and Discussion

5.3.1 Coatings Surface Morphology and Thickness

SEM micrographs of four samples showing the typical surface morphology of PEO coatings are presented in Figure 5.2. Almost all samples contain two different kinds of regions: cratered regions with a central hole and lighter areas with a nodular structure. Craters are formed when molten material is ejected from the coating/substrate interface through central holes due to the high temperatures and strong electric field present during the PEO process. On contact with the electrolyte, the molten material solidifies rapidly [28].

Previously [13] the cratered regions were shown to be rich in aluminum while the nodular structures exhibited a higher concentration of Si compared to Al. Changing the electrical parameters, namely the duty cycle and frequency, was found to alter the size of the craters and also the ratio of the craters to the nodular structures on the sample surface.

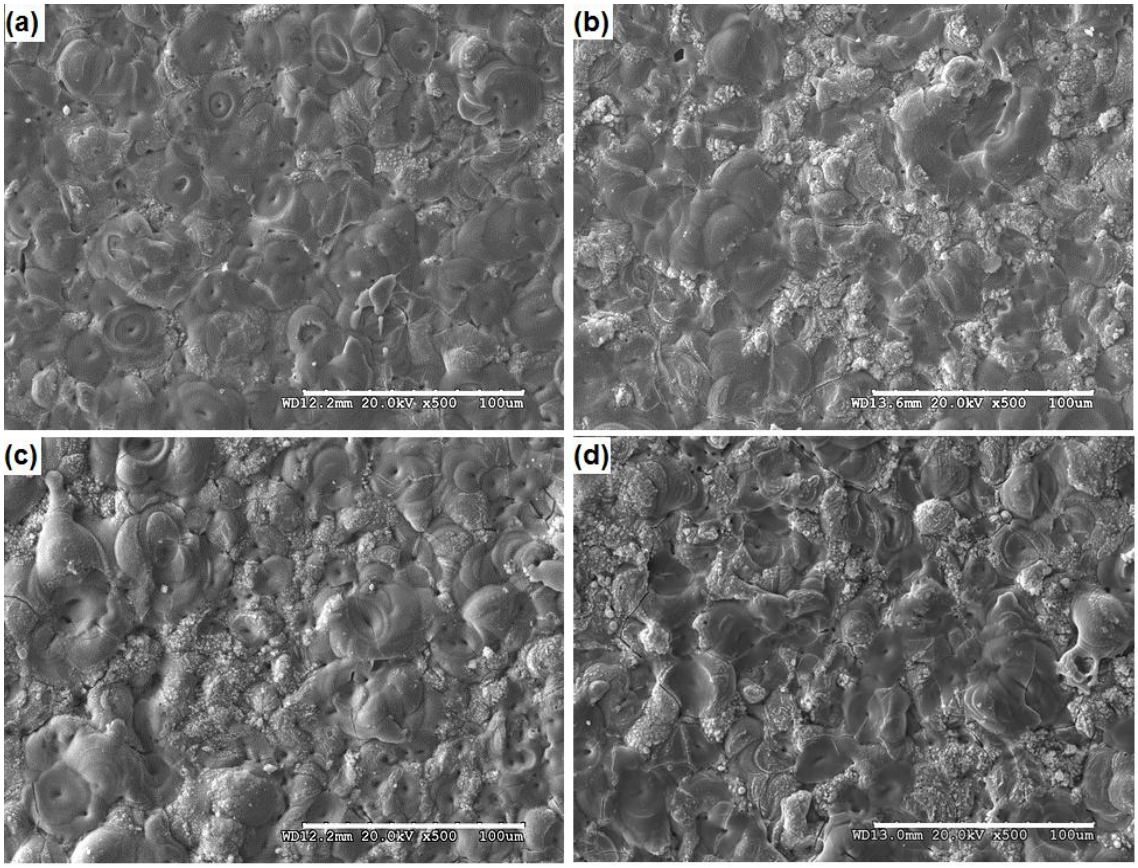

Figure 5.2- SEM images (secondary electron mode) of free surface of PEO coatings on samples (a) S12-10, (b) S18-10, (c) S52-10 and (d) S58-10.

The thicknesses of coatings prepared by PEO using different electrical parameters are presented in Figure 5.3. For each set, the thickness of the PEO coating increases with increasing current density as a result of the increased energy input. For samples PEO coated at 1000 Hz, the difference in the thickness of the samples processed at the same current density but different duty cycles is insignificant; however, the average thickness of each sample coated at a duty cycle of 20% is slightly greater than the sample coated at the same current density but a duty cycle of 80%.

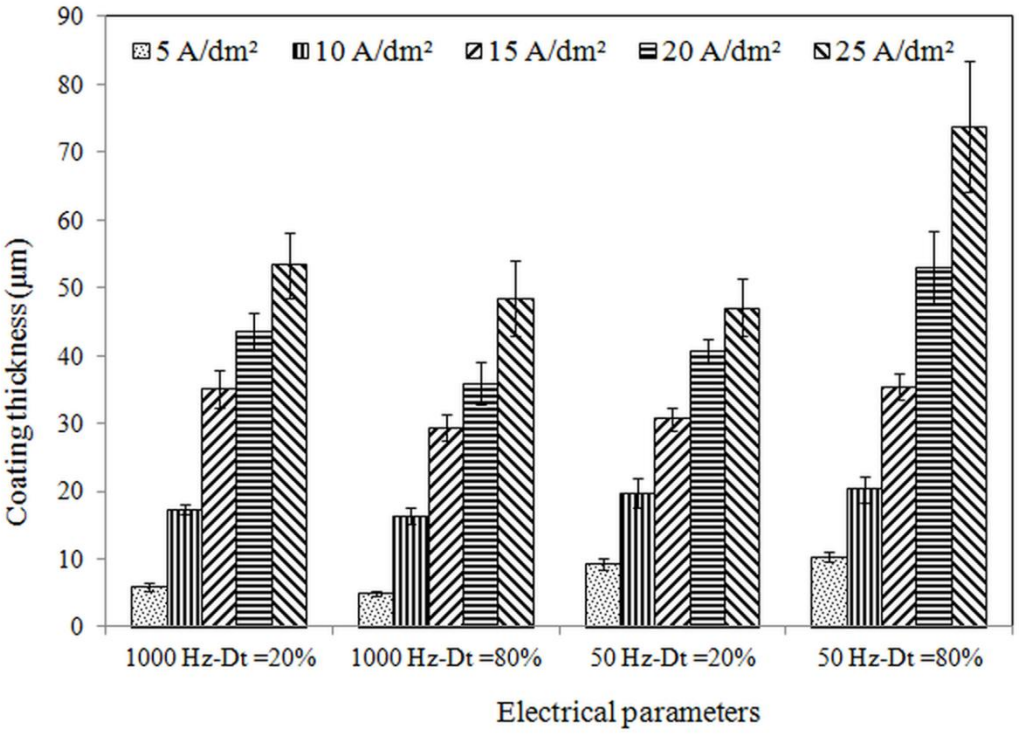

Figure 5.3- Effect of electrical parameters on coating thickness of PEO treated 6061 aluminum alloy substrates.

It should be pointed out that the coating measurements performed do not consider the porosity of the coatings. Studies [29] show that PEO coatings contain fine networks of channels, formed by localised electrical discharges, and pores due to the entrapment of gases formed during the process in the molten alumina. The shorter the t_{on} time, the greater the possibility of gases trapped inside the coating, resulting in coatings possibly of higher porosity. The slightly higher thickness readings of samples S12-* compared to samples S18-* is due to the higher porosity level in these samples, Figure 6.5 and Figure 6.6 .

For samples coated at 50 Hz and current densities of 5, 10, and 15 A/dm^2, variation of the duty cycle did not cause a significant change in the coating thickness. Samples S58-20 and S58-25, however, showed considerably higher thicknesses compared to all other samples. The reason for this is linked to the increased concentration of Si-rich species on the outer surface of the coatings on these samples and is discussed later in sections 5.3.3

and 5.3.4. The results suggest that frequency does not have a significant effect on the coating thickness variation of samples produced at the same current density.

5.3.2 Coatings Phase Analysis

Examples of the XRD patterns obtained using conventional X-ray diffraction for coatings produced at a current density of 20 A/dm^2 are presented in Figure 5.4. Studying the XRD patterns of all samples revealed the coatings were mainly composed of γ-Al_2O_3. In addition, in some samples, α-Al_2O_3 (S18-20, S52-20, and S58-20) and mullite (S58-20) were also observed.

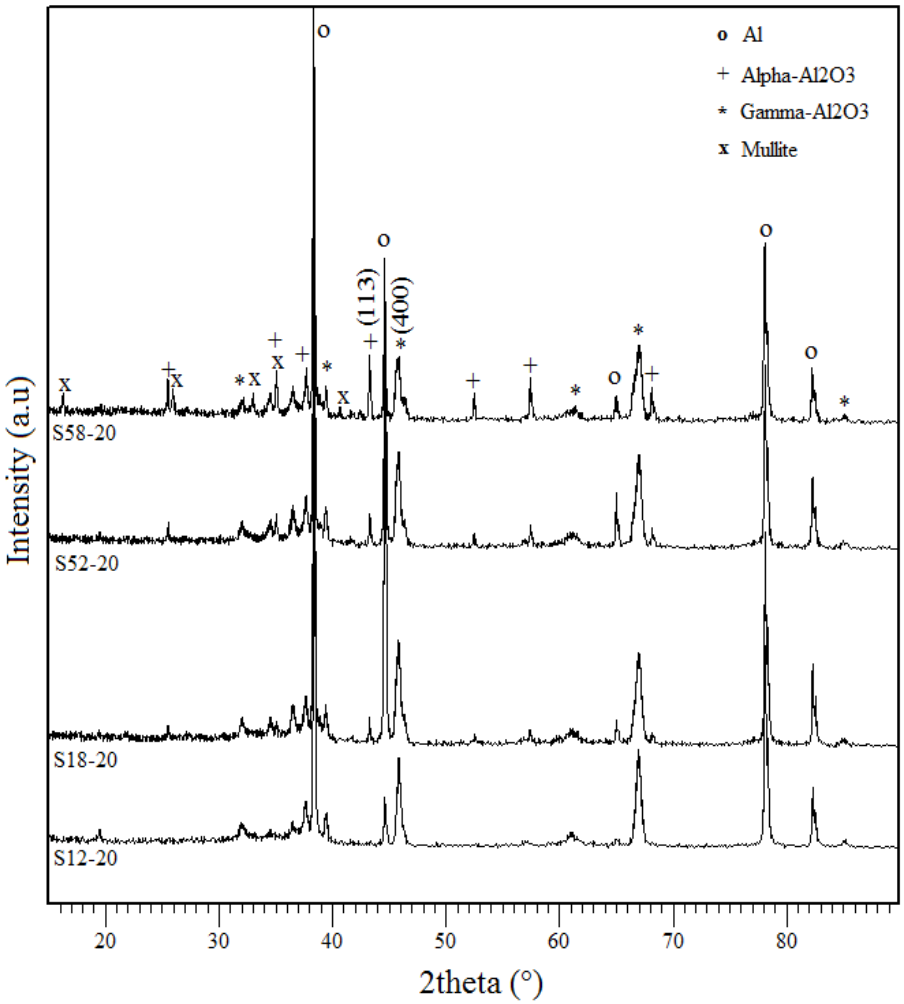

Figure 5.4- X-ray diffraction patterns (Bragg-Brentano configuration) of PEO ceramic coatings on samples S12-20, S18-20, S52-20, and S58-20 formed at J=20 A/dm^2.

Alpha alumina is a stable alumina phase with a high melting point (2050^{o}C) and possesses the corundum structure consisting of oxygen anions in hexagonal close-packed layers with cations occupying octahedral sites. Gamma alumina is a metastable phase which consists of layers of cubic close-packed oxygen anions with cations in the octahedral and tetrahedral sites [24,30]. It can transform to α-Al_2O_3 upon heating in the temperature range 800 to 1200 °C [22,31,32]. The phase transformation temperature can be affected by factors such as atmospheric conditions, the processing method used, and the presence of impurities in the alumina [33,34]. Schaper et al. [24] studied the phase transformation of gamma to alpha alumina quantitatively using high temperature differential thermal analysis (DTA) and observed an exothermic peak in all DTA curves in the temperature range 1100-1200 °C, which corresponds to the γ-$Al_2O_3 \rightarrow \alpha$-$Al_2O_3$ phase transformation. Cava et al. [35] investigated the phase transition in alumina nanopowders using XRD and micro-Raman spectroscopy and observed that it occurred in the temperature range 950-1050 °C.

5.3.3 Influence of Electrical Parameters on the Phase Content of Coatings

XRD patterns obtained using glancing angle XRD with an incident beam angle of 5 degrees are presented in Figure 5.5 and Figure 5.6. Glancing angle XRD greatly enhances the analysis of coatings by reducing interference from the sample substrate and increasing the path of the incident beam within the coating layer itself.

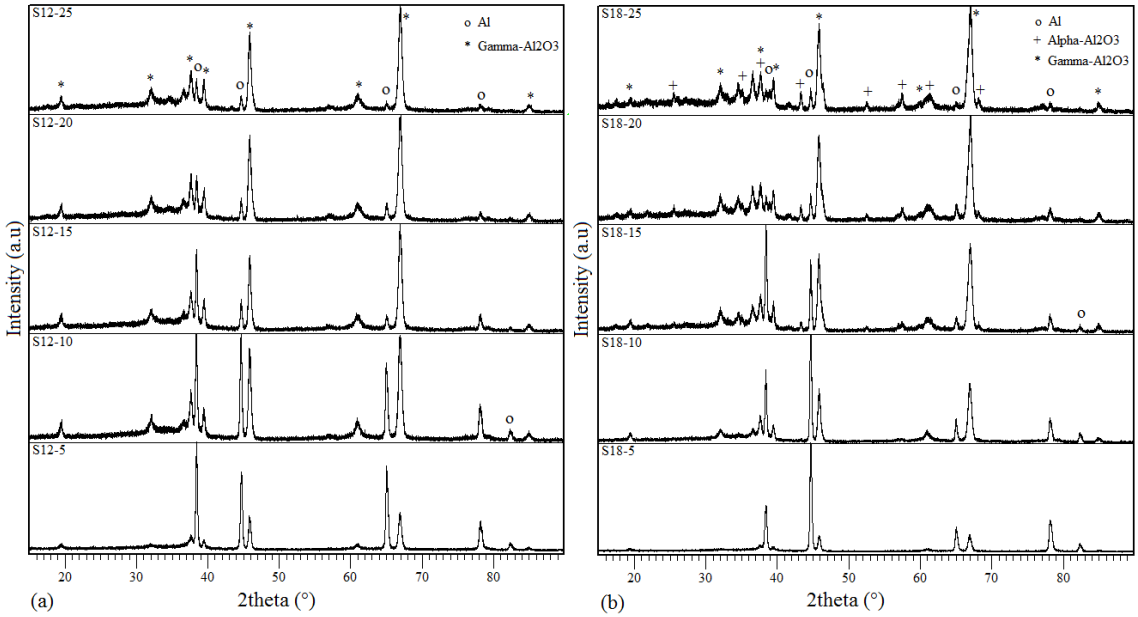

Figure 5.5- Glancing angle XRD (incident angle of 5 degrees) of samples PEO coated at a frequency of 1000 Hz and duty cycles of (a) 20% and (b) 80%.

Comparison of the four sets of XRD spectra in Figure 5.5 and Figure 5.6 shows that the intensities of Al diffraction peaks at each frequency and duty cycle decrease with increasing current density. Al diffraction peaks are from the substrate and increasing the current density results in a thicker coating. This was confirmed by coating thickness measurements, with the thickness of the coatings varying from a minimum of about 5 µm for sample S18-5 to above 70 µm for sample S58-25 (Figure 5.3). When glancing angle XRD is used, the path length of the incident beam through the coating is increased and the XRD patterns confirm the coating mainly consists of γ-Al_2O_3 with various contents of α-Al_2O_3.

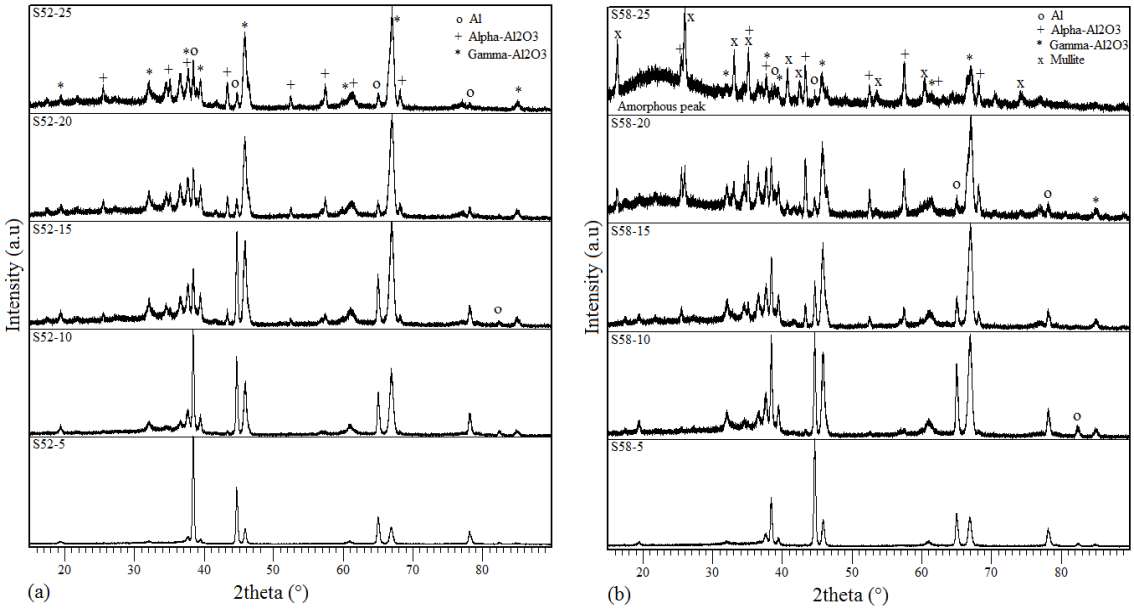

Figure 5.6- Glancing angle XRD (incident angle of 5 degrees) of samples PEO coated at a frequency of 50 Hz and duty cycles of (a) 20% and (b) 80%.

Coatings on samples treated at a frequency of 1000 Hz and a duty cycle of 20% with different current densities (Figure 5.5-a) contain mainly γ-Al_2O_3, while samples treated at the same frequency but a duty cycle of 80% (Figure 5.5-b), show the presence of α-Al_2O_3 peaks in addition to γ-Al_2O_3 at current densities of 15, 20 and 25 A/dm^2.

For samples treated at a lower frequency of 50 Hz and a duty cycle of 20% (Figure 5.6-a), the coating, at a current density of 5 A/dm^2 (S52-5), is mainly composed of γ-Al_2O_3 while for samples coated at higher current densities, α-Al_2O_3 peaks are also observed. A similar phase distribution was obtained on samples treated at the same frequency but a duty cycle of 80%. For both duty cycles the intensity of α-Al_2O_3 peaks increased when the current density was raised from 10 to 25 A/dm^2 indicating an increase in α-Al_2O_3 content in the coating.

Table 5.2 summarizes the identified phases in the PEO coatings formed using different electrical parameters. As can be seen in Table 5.2, samples treated at current densities of

20 and 25 A/dm^2 at 50 Hz and a duty cycle of 80%, contain mullite in addition to α- and γ-Al_2O_3, while samples treated at 1000 Hz contain no detectable mullite.

Table 5.2- Phase contents of the coatings on 6061 aluminum alloy samples PEO treated using different electrical parameters.

Frequency (Hz)	Duty cycle, D_t (%)	J (A/dm^2)	Main phases in the coating
1000	20	5	γ
		10	γ
		15	γ
		20	γ
		25	γ, little α
	80	5	γ
		10	γ, little α
		15	γ, α
		20	γ, α
		25	γ, α
50	20	5	γ
		10	γ, α
		15	γ, α
		20	γ, α
		25	γ, α
	80	5	γ
		10	γ, α
		15	γ, α
		20	γ, α, mullite, amorphous phase
		25	γ, α, mullite, amorphous phase

Mullite ($3Al_2O_3.2SiO_2$) is composed of aluminum, oxygen and silicon and is the only stable phase in the Al_2O_3-SiO_2 binary system at atmospheric pressure. Mullite formation occurs at temperatures above 1000 °C depending on the processing route employed, possibly by a nucleation and growth mechanism involving reaction between Al_2O_3 and SiO_2 [36–38]. It is generally assumed that increasing the concentration of sodium silicate in the electrolyte enhances the formation of mullite in the coatings [2,20]. A previous study [13] shows that the duty cycle and frequency affect the surface morphology, the micro-discharge characteristics, and the distribution of elements in the coatings. Lower duty cycles were found to result in micro-discharges with higher intensities but lower

spatial density. Al/Si ratios calculated from surface EDX elemental maps showed the concentration of Si increased on the surface of the coated samples when the current frequency was decreased and the duty cycle increased. For the same frequencies, samples treated at a duty cycle of 80% contained more Si on the surface than those treated at a duty cycle of 20%. Comparing the free surface SEM images (Figure 5.2) of the samples treated at the same frequency but different duty cycles confirms this fact. In sample S12-10 (Figure 5.2-a), treated at a frequency of 1000Hz and a duty cycle of 20%, the surface is mainly composed of craters which were previously shown to be rich in Al. However, sample S18-10 (Figure 5.2-b) treated at the same frequency but a duty cycle of 80% contains patches of lighter areas previously shown to be rich in Si [13].

Mullite was detected only in samples S58-20 and S58-25, which were treated at a frequency of 50 Hz and duty cycle of 80%. This could be linked to the increased concentration of Si on the surface of these samples. As mentioned earlier, mullite forms by reaction between Al_2O_3 and SiO_2 and in samples coated at 50 Hz and a high duty cycle of 80%, Si concentration is higher as compared to 1000 Hz.

The relative contents of α-Al_2O_3 and γ-Al_2O_3 phases were estimated on the basis of the integrated intensities of the $(113)_\alpha$ and $(400)_\gamma$ peaks (I_α and I_γ, respectively), Figure 5.7.

The integrated intensity ratio of the two peaks, I_α/I_γ, was used as an indicator of the approximate relative amounts of the two phases in the coatings. The possible effect of the involvement of the Al substrate peaks on the results will be discussed later in section 5.3.4.

The $(113)_\alpha$ and $(400)_\gamma$ peaks have strong intensities and can be used as the characteristic peaks for α-Al_2O_3 and γ-Al_2O_3, respectively. The interplanar distances of the $(113)_\alpha$ and $(400)_\gamma$ planes are similar (2.085Å and 1.977 Å, respectively). The diffraction angles of the two peaks are close but clearly separated and do not overlap with other peaks [17,27]. A similar approach was also used by Hsu et al. [39], Wu et al. [12], Guangliang et al. [26], Khan et al. [11] and Gu et al. [31].

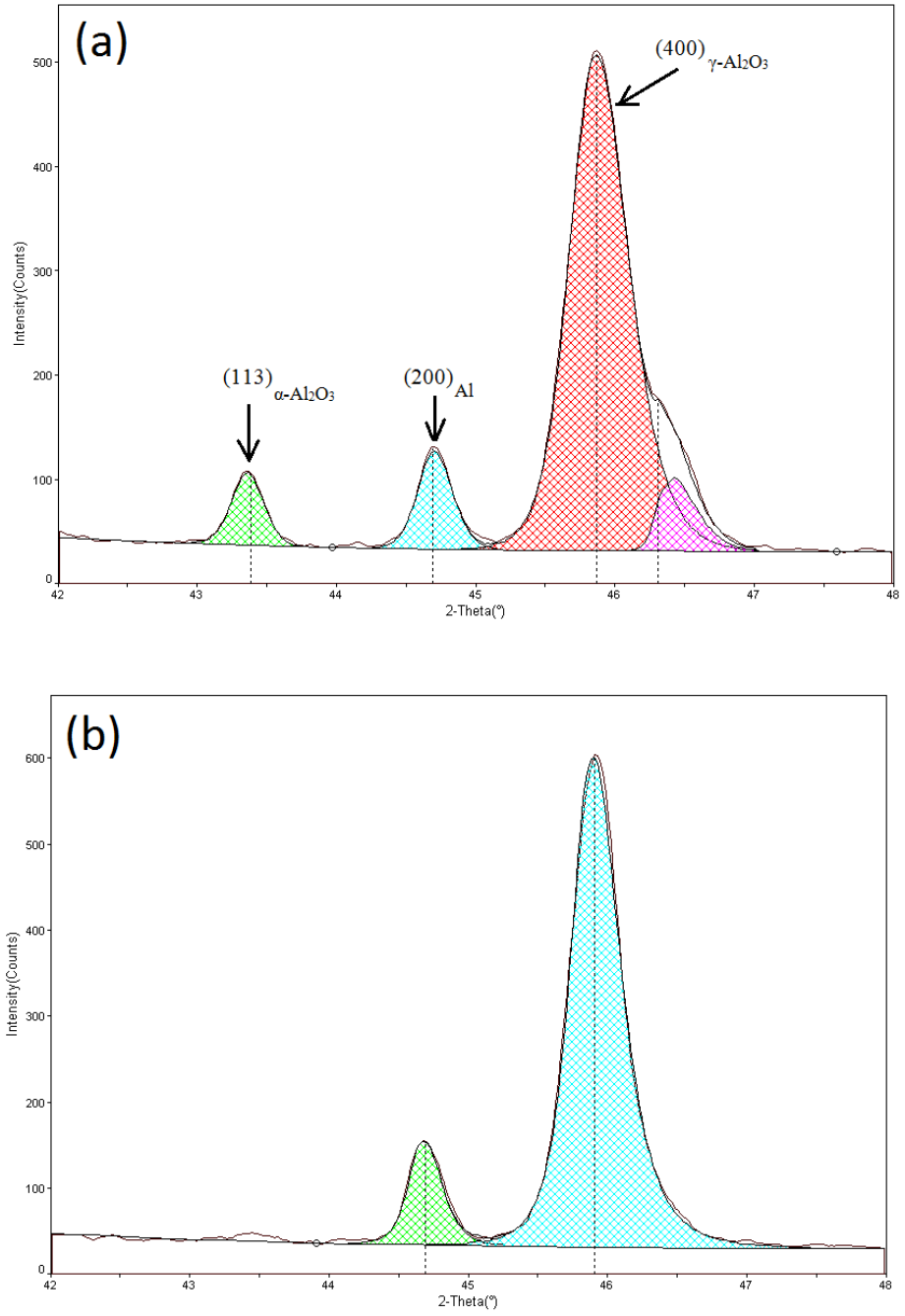

Figure 5.7- XRD peaks used to calculate the relative contents of α and γ-Al_2O_3; (a) S52-15 containing both α and γ-Al_2O_3 peaks; (b) S12-15 containing only γ-Al_2O_3 peak.

Figure 5.8 shows that I_α/I_γ varied in a range from 0 to about 0.6, indicating the relative contents of α-Al_2O_3 to γ-Al_2O_3 varied depending on the electrical parameters employed during the PEO treatment.

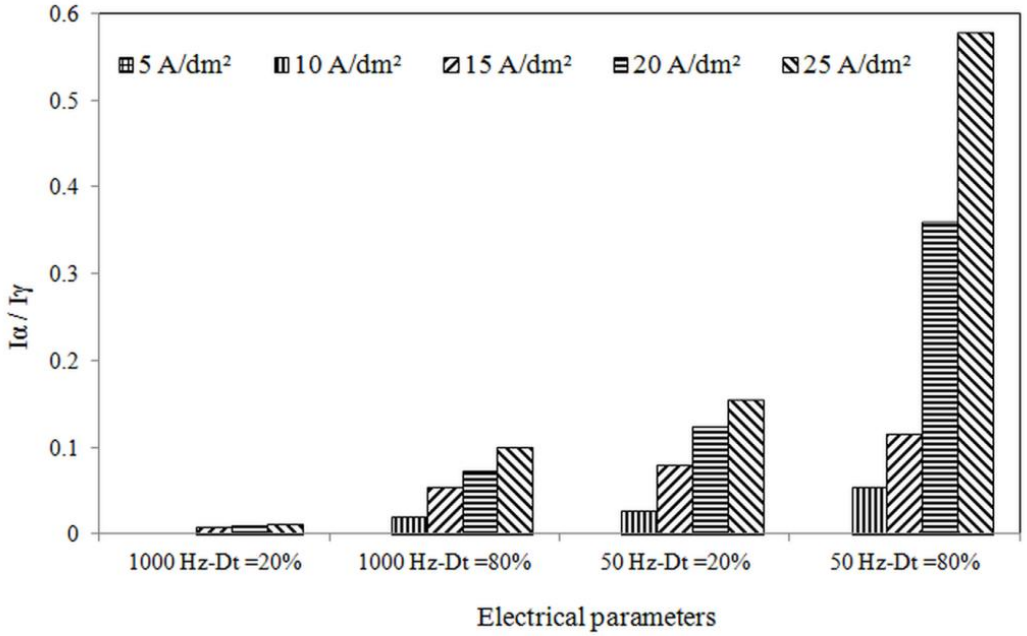

Figure 5.8- Influence of electrical parameters on the relative content of α-Al_2O_3 in PEO coatings on 6061 aluminum alloy.

It has been suggested that solidification of molten alumina at considerable undercoolings results in the formation of γ-Al_2O_3 rather than α-Al_2O_3 because the critical free energy of nucleation for γ-Al_2O_3 is lower [18,40]. For γ-Al_2O_3 to transform to α-Al_2O_3 both cation and anion rearrangement is required and this transformation occurs only at high temperatures. It is known that the γ-$Al_2O_3 \rightarrow \alpha$-$Al_2O_3$ transformation proceeds through a series of transition phases (δ- and θ-$A1_2O_3$) which leads to stable α-Al_2O_3 at room temperature. γ, δ and θ-$A1_2O_3$ are believed to be similar in structure with oxygen ions in a cubic close-packed arrangement and cations occupying different available octahedral and tetrahedral sites. Since these intermediate structures are similar to γ-$A1_2O_3$, the series of transitions can be conveniently represented as a single phase transformation of the γ-$Al_2O_3 \rightarrow \alpha$-$Al_2O_3$ [24,40–42].

Steiner et al. [41] studied the kinetics of the γ-Al_2O_3 → α-Al_2O_3 transformation in the temperature range of 1050 to 1200 °C and observed that the higher the temperature, the faster the transformation. It has been proposed that this transformation proceeds via a nucleation and growth mechanism with the kinetics obeying the Kolmogorov–Johnson–Mehl–Avrami (KJMA) equation (Eq. 5.2),

$$C_\alpha = 1 - \exp(-kt^n) \quad (5.2)$$

where C_α is the fraction of the α-Al_2O_3 formed, k is the temperature-dependent rate constant (s^{-1}), t is time (s), and n is the Avrami exponent [24,33,43].

By substituting properly estimated values for the parameters in the KJMA equation, it is possible to explain the variation in α-Al_2O_3 content with the different electrical parameters. According to equation 5.2, increasing the values of k and t will result in an increase in C_α providing n is positive. Fernando Macedo et al. [33] obtained a nearly constant value for the Avrami exponent (n = 2.1) for different isotherms, and values for the rate constant (k) for different constant temperatures in the range 700 to 1200 °C are available [33,43]. By substituting plausible values of k, n and t in equation 5.2, it is possible to estimate the kinetics of the γ-Al_2O_3 → α-Al_2O_3 phase transformation as a function of the electrical parameters.

Setting t equal to t_{on} (Table 5.1), i.e., the pulse on-time during PEO treatment, n equal to 2.1 and assuming the phase transition occurs isothermally at 1050 °C and with a value of k equal to 8.5×10^{-5} s^{-1} (the value at 1050 °C [43]) yields a value of the α-Al_2O_3 fraction formed in a single pulse. Figure 5.9 shows how this fraction varies for pulse on-times between the shortest and the longest pulse on-times of 0.2 and 16 ms corresponding to sample series S12 and S58, respectively.

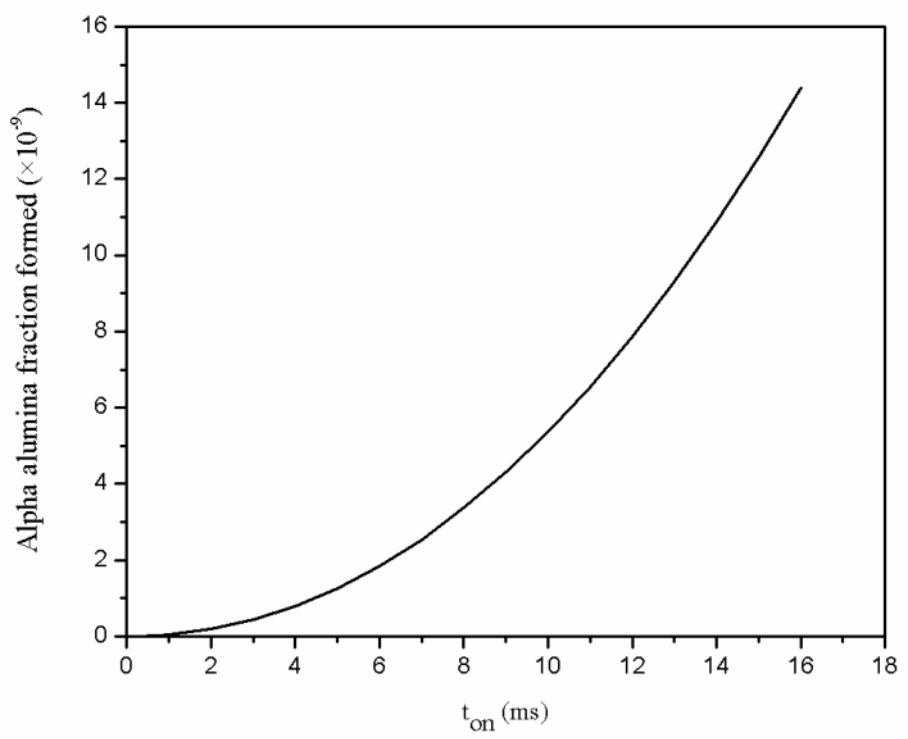

Figure 5.9- The calculated fraction of α-alumina formed in a single pulse as a function of t_{on} calculated using KJMA equation assuming an isothermal transformation temperature of 1050 °C.

Increasing the pulse on-time from 0.2 to 16 ms results in an exponential increase in the fraction of γ-Al_2O_3 transformed to α-Al_2O_3, Figure 5.9. The pulse on-time increases for each of the groups of data shown from left to right (0.2, 0.8, 4 and 16 ms) in Figure 5.8. For each specific current density, the integrated peak intensity ratio of $(113)_\alpha$ and $(400)_\gamma$, (I_α/I_γ), also increases from left to right, consistent with the trend observed in Figure 5.9. This explains why at a frequency of 1000 Hz and a duty cycle of 20% very little α-Al_2O_3 is formed only at high current densities of 20 and 25 A/dm^2. At short pulse on-times, there is insufficient time for the rearrangement of anions and cations required for the γ → α-Al_2O_3 phase transformation. It should be noted that, while this rationale is consistent with observations, the final fraction of α-Al_2O_3 formed depends on the interaction of a number of factors including the total duration of pulse on-time, the intensity and energy of micro-discharges, and the annealing effect of the subsequent micro-discharges on the already formed solid oxide layers. The γ-Al_2O_3 formed early in the PEO process could

transform to α-Al_2O_3 as a result of the heat generated in the coating by subsequent through-thickness discharges [20].

During PEO, the sparking intensity depends on the energy of each pulse and the single pulse energy increases when using higher current density. The single pulse energy (E_p) is defined as:

$$E_p = \int_0^{t_{on}} U_p . I_p \, dt \tag{5.3}$$

where U_p is the pulse voltage, I_p is the pulse current and t_{on} is the pulse on time [15]. This increase in pulse energy would explain why increasing the current density increases the α-Al_2O_3 fraction formed for each set of samples with the same frequency and duty cycle. Also, it can be deduced from Figure 5.8 that, regardless of the frequency and duty cycle employed, a current density of 5 A/dm^2 does not produce the conditions required for the $\gamma \rightarrow$ α-Al_2O_3 phase transformation. This could possibly be attributed to two factors: a current density of 5 A/dm^2 did not produce micro-discharges with sufficient energy to provide the heat necessary for the phase transformation, and the thinner coating thickness (<10 μm) created at low current densities (Figure 5.3) led to faster heat conduction into the aluminum substrate, and hence made it more difficult to achieve the temperature required for the $\gamma \rightarrow$ α-Al_2O_3 transformation.

5.3.4 Depth Profiling of Ceramic Coatings

The X-ray spectra of samples S52-20 and S58-20 obtained at glancing angles of 1, 2.5, and 5 degrees are compared with the conventional XRD (Bragg-Brentano configuration) spectra in Figure 5.10-a and Figure 5.10-b, respectively. It is observed that sample S58-20, treated at a higher duty cycle, contains mullite in addition to α- and γ-Al_2O_3. By varying the glancing angle it is possible to depth profile the surface layers. By comparing the mullite peak intensities to those of the other phases at different glancing angles in Figure 5.10-b, it can be inferred that mullite is more concentrated near the surface of the coatings since its peak intensities decrease relative to those of the other phases when the incident beam angle is increased from 1 to 5 degrees.

Changing the electrical parameters affects the micro-discharge characteristics. Increasing the duty cycle and lowering the frequency generates micro-discharges with lower spatial density but higher intensity which results in higher concentrations of Si rich species on the surface of the coatings [13,44]. This increased Si concentration facilitates the formation of mullite ($3Al_2O_3.2SiO_2$). Moreover, Glancing angle XRD patterns of samples S58-20 (Figure 5.10-b) and S58-25 (Figure 5.6-b) show the presence of an additional amorphous phase (2θ= 15-30). An amorphous peak at a similar 2θ position has been observed by others [2,20,45–47]. This amorphous phase cannot be easily distinguished in the conventional XRD patterns, Figure 5.4, due to the strong peak intensities for the other phases. The intensity of this peak decreases with an increase in glancing angle from 1 to 5 degrees, suggesting it is located at the outer surface of the coatings. In addition to the formation of mullite, deposition of Si rich species on the coatings surface could contribute to the coating thickness. Samples S58-20 and 58-25 have considerably thicker coatings compared to other samples prepared at the same current densities, Figure 5.3, which could be linked to the deposition of Si rich species on the surface of these samples. As discussed earlier, at later stages of the PEO coating process, micro-discharge behaviour changes and micro-discharges tend to become more intense with less spatial density. This change is more readily noticeable at lower frequencies and higher duty cycles. The results of the previous studies [15,46] suggest that silicon-rich species form a gel which deposits on the coating surface. For samples S58-20 and S58-25, the decreased spatial density of micro-discharges increases the chance of the Si-rich deposits to stay on the surface since the ejection of the Si-rich deposits by micro-discharges will act on a relatively smaller portion of the surface area.

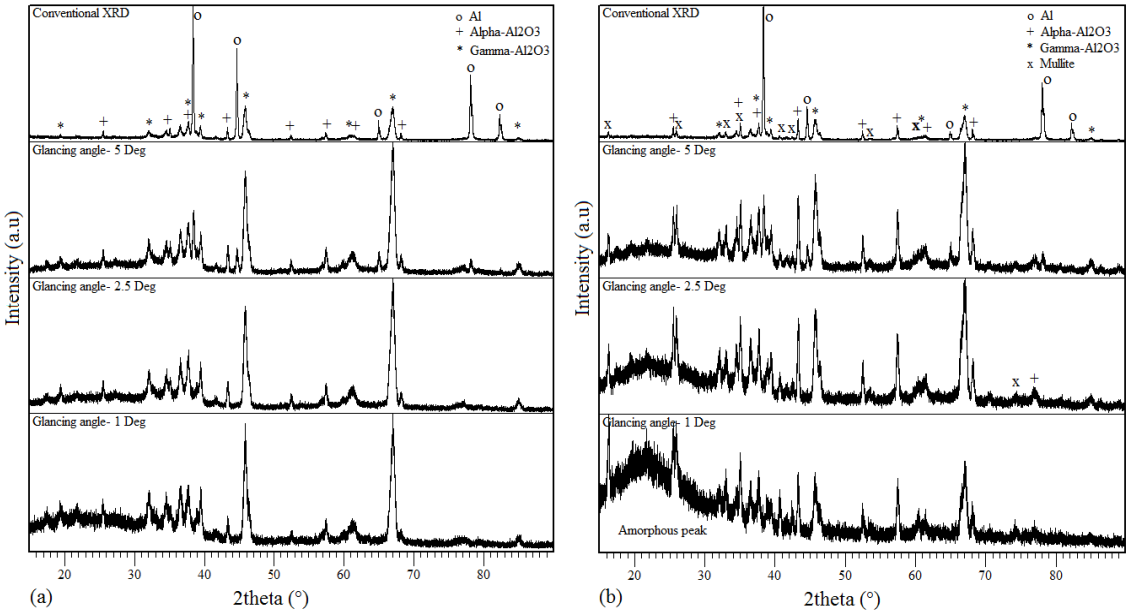

Figure 5.10- XRD patterns of samples (a) S52-20 and (b) S58-20 at glancing angles of 1, 2.5 and 5 degrees vs. the conventional XRD (Bragg-Brentano configuration) pattern.

The literature on the distribution of different phases across the PEO coatings is inconsistent. It has been reported [14,17] that the amount of α-Al_2O_3 gradually increases from the top surface towards the substrate-coating interface. Xue et al. [18] observed that the α-Al_2O_3 content gradually increases from the surface layer towards the interior of the coating but reached a maximum at ~50 µm from the coating/substrate interface before decreasing near the interface. Others [14,22] have reported that the α-Al_2O_3 content increased gradually with increasing coating thickness.

To investigate the distribution of the α-Al_2O_3 phase across the coatings, the integrated intensity ratio of $(113)_\alpha$ and $(400)_\gamma$ peaks (I_α/I_γ) was calculated for each sample using the XRD patterns obtained by conventional XRD (Bragg-Brentano configuration) and different glancing angles and the results were compared. The I_α/I_γ values for samples treated at a current density of 15 A/dm^2 are compared in Table 5.3. No significant differences were observed when comparing I_α/I_γ values of different samples calculated using the XRD spectra with different glancing angles. This implies that no α-Al_2O_3

concentration gradient occurs through the coatings. These results are at odds with studies [14,17] in which the α- and γ-Al_2O_3 phase distribution at different coating depths was determined by polishing the coating to a certain thickness and then performing XRD analysis.

Table 5.3- The integrated intensity ratios of $(113)_\alpha$ and $(400)_\gamma$ peaks (I_α/I_γ) calculated for different XRD conditions.

Sample / XRD condition	S12-15 I_α/I_γ	S18-15 I_α/I_γ	S52-15 I_α/I_γ	S58-15 I_α/I_γ
Glancing angle, 1 Deg	0	0.06	0.06	0.16
Glancing angle, 2.5 Deg	0	0.05	0.08	0.14
Glancing angle, 5 Deg	0.01	0.06	0.08	0.12
Conventional XRD	0	0.08	0.09	0.13

It has been suggested [14,22] that the α-Al_2O_3 content increases gradually as the PEO coating thickens. However, using short pulse t_{on} times, it was observed [44] that varying the coating thickness from 10 to ~80 μm by employing longer deposition times did not create any α-Al_2O_3, and only mullite was identified in addition to γ-Al_2O_3 at longer deposition times. The rearrangement of oxygen anions and aluminum cations, necessary during the γ-Al_2O_3 → α-Al_2O_3 phase transition, occurs via diffusion which is a function of time and temperature. However, alumina has a relatively low thermal conductivity [2], and the dominance of γ-Al_2O_3 in thinner coatings can be attributed to the higher cooling rates which favour the formation of γ-Al_2O_3. In thicker coatings, on the other hand, the thermal energy can accumulate in the coatings leading to the higher temperatures required to promote the γ → α-Al_2O_3 phase transition [14,22,40]. However, the effect of time should not be neglected since it plays an important role in diffusion processes. Previously [48], it was observed that in the PEO coatings prepared at a current density of 15 A/dm^2, decreasing the pulse t_{on} times below 0.2 ms resulted in no α-Al_2O_3 formation during coating growth.

In this study, the relative contents of α- and γ-Al_2O_3 phases in the PEO coatings were estimated using the relative peak intensity ratios of $(113)_\alpha$ and $(400)_\gamma$ and the Al substrate was not involved in the calculations. The reason for this is that the $(200)_{Al}$ peak, located at a 2θ angle of 44.72° (JCPDS 1-085-1327) is clearly separated and does not overlap with either $(113)_\alpha$ peak located at 2θ angle of 43.36° (JCPDS 10-0173), or $(400)_\gamma$ peak located at 2θ angle of 45.86° (JCPDS 10-0425), Figure 5.4. The integrated intensity ratios (I_α/I_γ) calculated using different XRD conditions, in which the contribution of the aluminum substrate might vary, suggested that excluding the Al substrate did not have a significant impact on the results. Table 5.3 lists I_α/I_γ values calculated for samples coated at a current density of 15 A/dm^2 as an example. Similar results were obtained for other samples as well. As can be observed in Table 5.3, although the X-ray beam penetration depth, and as a result, the contribution from the Al substrate in the total XRD pattern of the samples varied when different XRD conditions (conventional XRD, glancing XRD with incident beam angles of 1, 2.5 and 5 degrees) were applied, the obtained I_α/I_γ values for each sample at different XRD conditions were very similar.

5.4 Conclusions

Samples of 6061 aluminum alloy were PEO treated in an alkaline silicate electrolyte using a pulsed unipolar current regime. Two different frequencies of 50 and 1000 Hz and duty cycles of 20% and 80% were employed at a number of current densities of 5, 10, 15, 20, and 25 A/dm^2. The effect of electrical parameters on phase composition, transformation, and distribution was examined using conventional (Bragg-Brentano configuration) and glancing angle XRD. The following conclusions can be drawn from this study:

(1) Phase distribution and composition, including the α-Al_2O_3 to γ-Al_2O_3 ratio, in the PEO coatings can be controlled by using different electrical conditions.

(2) PEO coatings produced on 6061 Al alloys are mainly composed of γ-Al_2O_3. The relative content of α-Al_2O_3 in the coatings changed by varying the electrical parameters. Depending on the electrical parameters employed, various amounts of mullite and an

amorphous phase were identified. Alpha-Al_2O_3 represents the hardest form of alumina, and is believed to enhance the wear resistance of PEO coatings.

(3) Coatings on samples PEO treated at a frequency of 1000 Hz and a duty cycle of 20% with different current densities contained essentially only γ-Al_2O_3. Increasing the duty cycle to 80% at the same frequency resulted in the formation of α-Al_2O_3 in addition to γ-Al_2O_3. In samples treated at 50 Hz, α-Al_2O_3 was identified in all samples at a current density greater than 5 A/dm^2 in addition to γ-Al_2O_3. Some mullite was also detected in these samples plus an amorphous phase in samples treated at high current densities of 20 and 25 A/dm^2 and a duty cycle of 80%.

(4) It was found that increasing the pulse on-time by employing a lower frequency and higher duty cycle enhanced the γ → α-Al_2O_3 phase transformation. The results were consistent with the trend predicted by the Kolmogorov–Johnson–Mehl–Avrami (KJMA) equation which describes the kinetics of mechanisms involving nucleation and growth.

(5) Formation of mullite in samples treated at lower frequency was linked to the micro-discharge behavior. Increasing the duty cycle and lowering the frequency generates micro-discharges with lower spatial density but higher intensity which results in higher concentrations of Si rich species on the surface of the PEO coatings. Increased Si concentration facilitates the formation of mullite.

(6) Depth profiling of ceramic coatings using glancing angle XRD showed no significant variation in α-Al_2O_3 concentration across the coatings.

5.5 References

[1] X. Nie, E.I. Meletis, J.C. Jiang, A. Leyland, A.L. Yerokhin, A. Matthews, Abrasive wear/corrosion properties and TEM analysis of Al2O3 coatings fabricated using plasma electrolysis, Surf. Coat. Technol. 149 (2002) 245–251.

[2] J.A. Curran, H. Kalkancı, Y. Magurova, T.W. Clyne, Mullite-rich plasma electrolytic oxide coatings for thermal barrier applications, Surf. Coatings Technol. 201 (2007) 8683–8687.

[3] S. Dejiu, C. Jingrui, L. Guolong, H. Donglei, W. Lailei, M. Haojie, et al., Effect of ultrasonic on microstructure and growth characteristics of micro-arc oxidation ceramic coatings on 6061 aluminum alloy, Vacuum. 99 (2014) 143–148.

[4] E. Matykina, A. Berkani, P. Skeldon, G.E. Thompson, Real-time imaging of coating growth during plasma electrolytic oxidation of titanium, Electrochim. Acta. 53 (2007) 1987–1994.

[5] S. Wang, Y. Xia, L. Liu, N. Si, Preparation and performance of MAO coatings obtained on AZ91D Mg alloy under unipolar and bipolar modes in a novel dual electrolyte, Ceram. Int. 40 (2014) 93–99.

[6] Y. Cheng, F. Wu, E. Matykina, P. Skeldon, G.E.E. Thompson, The influences of microdischarge types and silicate on the morphologies and phase compositions of plasma electrolytic oxidation coatings on Zircaloy-2, Corros. Sci. 59 (2012) 307–315.

[7] Y. Cheng, Z. Xue, Q. Wang, X.-Q. Wu, E. Matykina, P. Skeldon, et al., New findings on properties of plasma electrolytic oxidation coatings from study of an Al–Cu–Li alloy, Electrochim. Acta. 107 (2013) 358–378.

[8] R.C. Barik, J.A. Wharton, R.J.K. Wood, K.R. Stokes, R.L. Jones, Corrosion, erosion and erosion–corrosion performance of plasma electrolytic oxidation (PEO) deposited Al_2O_3 coatings, Surf. Coatings Technol. 199 (2005) 158–167.

[9] L.O. Snizhko, A. Yerokhin, N.L. Gurevina, D.O. Misnyankin, A.V. Ciba, A. Matthews, Voltastatic studies of magnesium anodising in alkaline solutions, Surf. Coatings Technol. 205 (2010) 1527–1531.

[10] R.O. Hussein, D.O. Northwood, X. Nie, Coating growth behavior during the plasma electrolytic oxidation process, J. Vac. Sci. Technol. A Vacuum, Surfaces, Film. 28 (2010) 766–773.

[11] R.H.U. Khan, A. Yerokhin, X. Li, H. Dong, A. Matthews, Surface characterisation of DC plasma electrolytic oxidation treated 6082 aluminium alloy: Effect of current

density and electrolyte concentration, Surf. Coatings Technol. 205 (2010) 1679–1688.

[12] H. Wu, J. Wang, B.B. Long, Z. Jin, W. Naidan, F. Yu, et al., Ultra-hard ceramic coatings fabricated through microarc oxidation on aluminium alloy, Appl. Surf. Sci. 252 (2005) 1545–1552.

[13] V. Dehnavi, B.L. Luan, D.W. Shoesmith, X.Y. Liu, S. Rohani, Effect of duty cycle and applied current frequency on plasma electrolytic oxidation (PEO) coating growth behavior, Surf. Coatings Technol. 226 (2013) 100–107.

[14] T. Wei, F. Yan, J. Tian, Characterization and wear- and corrosion-resistance of microarc oxidation ceramic coatings on aluminum alloy, J. Alloys Compd. 389 (2005) 169–176.

[15] B.L. Jiang, Y.M. Wang, Plasma Electrolytic Oxidation Treatment of Aluminum and Titanium Alloys, in: H. Dong (Ed.), Surf. Eng. Light Alloy. Aluminum, Magnes. Titan. Alloy., Woodhead Publishing, 2010: pp. 110–153.

[16] R.O. Hussein, D.O. Northwood, X. Nie, The influence of pulse timing and current mode on the microstructure and corrosion behaviour of a plasma electrolytic oxidation (PEO) coated AM60B magnesium alloy, J. Alloys Compd. 541 (2012) 41–48.

[17] W. Xue, Z. Deng, Y. Lai, R. Chen, Analysis of Phase Distribution for Ceramic Coatings Formed by Microarc Oxidation on Aluminum Alloy, J. Am. Ceram. Soc. 81 (1998) 1365–1368.

[18] W. Xue, Z. Deng, R. Chen, T. Zhang, H. Ma, Microstructure and properties of ceramic coatings produced on 2024 aluminum alloy by microarc oxidation, J. Mater. Sci. 36 (2001) 2615–2619.

[19] L.R. Krishna, A.S. Purnima, G. Sundararajan, A comparative study of tribological behavior of microarc oxidation and hard-anodized coatings, Wear. 261 (2006) 1095–1101.

[20] H. Kalkancı, S.C. Kurnaz, The effect of process parameters on mullite-based plasma electrolytic oxide coatings, Surf. Coatings Technol. 203 (2008) 15–22.

[21] J. Tian, Z. Luo, S. Qi, X. Sun, Structure and antiwear behavior of micro-arc oxidized coatings on aluminum alloy, Surf. Coatings Technol. 154 (2002) 1–7.

[22] H.-H. Wu, Z.-S. Jin, B.-Y. Long, F.-R. Yu, X.-Y. Lu, Characterization of Microarc Oxidation Process on Aluminium Alloy, Chinese Phys. Lett. 20 (2003) 1815–1818.

[23] W. Xue, Z. Deng, R. Chen, T. Zhang, Growth regularity of ceramic coatings formed by microarc oxidation on Al-Cu-Mg alloy, Thin Solid Films. 372 (2000) 114–117.

[24] H. Schaper, L.L. Van Reijen, A quantitative investigation of the phase transformation of gamma to alpha alumina with high temperature DTA, Thermochim. Acta. 77 (1984) 383–393.

[25] R.H.U. Khan, A.L. Yerokhin, T. Pilkington, A. Leyland, A. Matthews, Residual stresses in plasma electrolytic oxidation coatings on Al alloy produced by pulsed unipolar current, Surf. Coatings Technol. 200 (2005) 1580–1586.

[26] Y. Guangliang, L. Xianyi, B. Yizhen, C. Haifeng, J. Zengsun, The effects of current density on the phase composition and microstructure properties of micro-arc oxidation coating, J. Alloys Compd. 345 (2002) 196–200.

[27] A.L. Yerokhin, L.O. Snizhko, N.L. Gurevina, A. Leyland, A. Pilkington, A. Matthews, Discharge characterization in plasma electrolytic oxidation of aluminium, J. Phys. D. Appl. Phys. 36 (2003) 2110–2120.

[28] G. Sundararajan, L. Rama Krishna, Mechanisms underlying the formation of thick alumina coatings through the MAO coating technology, Surf. Coatings Technol. 167 (2003) 269–277.

[29] J.A. Curran, T.W. Clyne, Porosity in plasma electrolytic oxide coatings, Acta Mater. 54 (2006) 1985–1993.

[30] G. Lv, W. Gu, H. Chen, W. Feng, M.L. Khosa, L. Li, et al., Characteristic of ceramic coatings on aluminum by plasma electrolytic oxidation in silicate and phosphate electrolyte, Appl. Surf. Sci. 253 (2006) 2947–2952.

[31] W.-C. Gu, G.-H. Lv, H. Chen, G.-L. Chen, W.-R. Feng, G.-L. Zhang, et al., Investigation of morphology and composition of plasma electrolytic oxidation coatings in systems of Na2SiO3–NaOH and (NaPO3)6–NaOH, J. Mater. Process. Technol. 182 (2007) 28–33.

[32] M. Bodaghi, A.R. Mirhabibi, H. Zolfonun, M. Tahriri, M. Karimi, Investigation of phase transition of γ- alumina to α-alumina via mechanical milling method, Phase Transitions. 81 (2008) 571–580.

[33] M.I.F. Macêdo, C.A. Bertran, C.C. Osawa, Kinetics of the γ → α-alumina phase transformation by quantitative X-ray diffraction, J. Mater. Sci. 42 (2007) 2830–2836.

[34] C.-K. Loong, J.W. Richardson Jr., M. Ozawa, Structural phase transformations of rare-earth modified transition alumina to corundum, J. Alloys Compd. 250 (1997) 356–359.

[35] S. Cava, S.M. Tebcherani, I.A. Souza, S.A. Pianaro, C.A. Paskocimas, E. Longo, et al., Structural characterization of phase transition of Al2O3 nanopowders obtained by polymeric precursor method, Mater. Chem. Phys. 103 (2007) 394–399.

[36] S. Sembiring, W. Simanjuntak, X-ray Diffraction Phase Analyses of Mullite Derived from Rice Husk Silica, Makara J. Sci. 16/2 (2012) 77–82.

[37] C. Gerardin, S. Sundaresan, J. Benziger, A. Navrotsky, Structural investigation and energetics of mullite formation from sol-gel precursors, Chem. Mater. 6 (1994) 160–170.

[38] M.A. Sainz, F.J. Serrano, J.M. Amigo, J. Bastida, A. Caballero, XRD microstructural analysis of mullites obtained from kaolinite–alumina mixtures, J. Eur. Ceram. Soc. 20 (2000) 403–412.

[39] C.-H. Hsu, H.-P. Teng, F.-H. Lu, Effects of addition of Al(NO3)3 to electrolytes on alumina coatings by plasma electrolytic oxidation, Surf. Coatings Technol. 205 (2011) 3677–3682.

[40] R. McPherson, Formation of metastable phases in flame- and plasma-prepared alumina, J. Mater. Sci. 8 (1973) 851–858.

[41] C.J.-P. Steiner, D.P.H. Hasselman, R.M. Spriggs, Kinetics of the gamma-to-alpha alumina phase transformation, J. Am. Ceram. Soc. 54 (1971) 412–413.

[42] R.. Damani, P. Makroczy, Heat treatment induced phase and microstructural development in bulk plasma sprayed alumina, J. Eur. Ceram. Soc. 20 (2000) 867–888.

[43] R.A. Shelleman, G.L. Messing, M. Kumagai, Alpha alumina transformation in seeded boehmite gels, J. Non. Cryst. Solids. 82 (1986) 277–285.

[44] V. Dehnavi, B. Luan, X.Y. Liu, D.W. Shoesmith, S. Rohani, Production of ceramic coatings on AA6061 aluminum alloy using plasma electrolytic oxidation, in: Mater. Sci. Technol., Montreal, Canada, 2013: pp. 2247–2254.

[45] M. Tarakci, Plasma electrolytic oxidation coating of synthetic Al–Mg binary alloys, Mater. Charact. 62 (2011) 1214–1221.

[46] F. Monfort, A. Berkani, E. Matykina, P. Skeldon, G.E. Thompson, H. Habazaki, et al., Development of anodic coatings on aluminium under sparking conditions in silicate electrolyte, Corros. Sci. 49 (2007) 672–693.

[47] T. Abdulla, A. Yerokhin, R. Goodall, Effect of Plasma Electrolytic Oxidation coating on the specific strength of open-cell aluminium foams, Mater. Des. 32 (2011) 3742–3749.

[48] V. Dehnavi, X.Y. Liu, B. Luan, S. Rohani, D.W. Shoesmith, Effect of heating cycles on phase transformation in ceramic coatings produced by Plasma Electrolytic Oxidation of Al6061 alloy, in: Int. Conf. Mater. Heat Treat. (ICMH 2012), Isfahan, Iran, 2012.

Chapter 6

Correlation between Plasma Electrolytic Oxidation Treatment Stages and Coating Microstructure on Aluminum

Abstract

Alumina coatings were deposited on 6061 aluminum alloy substrates using plasma electrolytic oxidation (PEO) in an alkaline silicate electrolyte. Different electrical parameters, including frequency, duty cycle, and current density were applied to obtain PEO coatings. Scanning electron microscopy (SEM) and microhardness tests were used to investigate the coating microstructure and properties. For each sample, the voltage-time response of the PEO process was obtained and compared with surface morphology, and coating cross sections and thicknesses. Special consideration was given to the connection between the electrical parameters, different stages of the PEO process, and the morphology and microstructure of the coatings. Applying different electrical parameters changed the duration and ratio of the PEO stages in the voltage-time response curve and affected the growth rate, surface morphology, microstructure and microhardness of the coatings. We report the new finding of a correlation between the stage of the PEO process and the microstructure and morphology of the coating.

6.1 Introduction

Plasma electrolytic oxidation (PEO) is a surface modification technique capable of producing oxide coatings with desirable properties on the surface of valve metals and alloys. PEO is an electrochemical process in which coatings are formed as a result of the oxidation of the substrate material via a series of localized electrical discharge events in an aqueous electrolyte [1–3].

Coatings prepared by PEO have been successfully produced on aluminum, magnesium and titanium substrates. Recently researchers have applied this technique to zirconium [4–6] and tantalum [7,8] as well. PEO coatings have existing and potential applications in a wide range of industry sectors. Examples of these applications include wear [9–12] and corrosion [13–15] resistant coatings, thermal barrier coatings [3,16,17], coatings for infrared concealment [18] and biocompatible coatings for implants [19–21].

Different techniques and methods have been employed by various researchers to study the PEO coating growth behavior and the phenomena occurring during the process. To study the micro-discharge behavior during PEO treatment of various substrate materials, researchers have used real-time imaging techniques. The results of the studies on different substrates such as aluminum [22,23], magnesium [24], titanium [25,26] and zirconium [5,27] revealed the spatial density, intensity, distribution and lifetime of the micro-discharges. Optical emission spectroscopy (OES) has been utilised to identify the elements present in the plasma and also to estimate the plasma temperature during PEO in aluminum [28–30], magnesium [31] and titanium [32].

Generally up to four stages are reported during PEO [28,33]. PEO typically starts with an abrupt linear increase in the voltage, which corresponds to the conventional anodic oxidation, followed by the appearance of micro-discharges on the surface of the sample as a result of dielectric breakdown after the breakdown voltage is reached. As the plasma coating process proceeds, the characteristics of the micro-discharges including their intensity, spatial density and color vary during subsequent stages of the process. The individual and collective characteristics of the micro-discharges, generated during the PEO process, determine the thermal and chemical conditions of the coating process and

as a result play a key role in the formation of the oxide coatings and affect the structure, morphology, phase formation and distribution in the coatings [5].

The phenomenon and mechanism happening in each stage during PEO and the resulting effects on the oxide layer growth behavior are different. Applied process parameters can change the duration and ratio of these stages which in turn could result in coatings with different morphology, microstructure and phase composition [34].

Different applications require PEO coatings with unique properties. A dense coating, free from pores and defects could be a good candidate for corrosion protection, and the porosity in the PEO layer could be used as a base for sealants and primers to improve corrosion protection [35]. Microporosity in the coatings on the surface of implants is beneficial and could have several functions including helping bone tissue in-growth and acting as a depot for bioactive constituents [36]. Controlling the PEO process to yield the desired morphology and microstructure for specific applications is a key requirement for the success of this method in industry.

The voltage-time response of the PEO process can provide readily measurable and useful information about the different stages occurring during PEO. Investigating the correlation between coating characteristics and different stages of PEO can improve understanding of, and provide more control over, the process. Despite the useful information that could be derived from the voltage-time response, studies addressing the correlation between voltage-time curves and coating properties are very scarce. This research investigates the effect of electrical parameters, including applied current density, frequency and duty cycle, on the voltage-time behavior during PEO and its correlation with the morphology and microstructure of the coatings.

6.2 Materials and Methods

A unipolar, pulsed DC PEO coating unit was used to coat 6061 aluminum alloy disk coupons with an average diameter of ~30 mm and a thickness of ~8 mm. The coupons were manually ground up to 600 grit using silicon carbide abrasive papers. After cleaning with isopropanol, they were rinsed and dried using compressed air. The coatings were

prepared in an aqueous alkaline electrolyte containing 2 g/l Na_2SiO_3 and 2 g/l KOH in deionized water. The temperature of the electrolyte was kept below 40 °C by an external heat exchanger/chiller. Samples were treated at two frequencies, 50 and 1000 Hz, at duty cycles (D_t) of 20% and 80% with current densities (J) of 5, 10, 15, 20, and 25 A/dm^2. The duty cycle (D_t) is the percentage of the on-time, t_{on}, during a single pulse. A schematic of the pulse wave form and the corresponding electrical parameters of the unipolar pulsed power source can be found elsewhere in the literature [37]. All samples were treated for 30 min under galvanostatic conditions, i.e. the current was kept constant during the entire process and the anode potential was allowed to vary. Sample codes and the corresponding electrical parameters used for each one are presented in Table 6.1.

Table 6.1- Electrical parameters and sample codes for PEO treatment on 6061 Al alloy.

Sample code	Frequency (Hz)	D_t (%)	t_{on} (ms)	* : J (A/dm^2)
S12-*	1000	20	0.2	5, 10, 15, 20, 25
S18-*	1000	80	0.8	
S52-*	50	20	4	
S58-*	50	80	16	

Scanning electron microscopy (Hitachi S-3500N operating at 20 kV) was used to study the coating surface morphology and cross sections. The samples were sputter-coated with a gold film before SEM analysis. Coating thickness measurements were performed using an Eddy current gauge. For each sample twenty measurements were taken on the coated surface. Statistical treatments were applied to extract the mean data values and the scatter.

Microhardness measurements were made on polished cross-sections of the PEO coatings using a Vickers diamond indenter mounted on a Buehler Micromet II microhardness tester under loads of 25 and 50 g, applied for 10 s. The average of ten measurements is reported for each microhardness value.

6.3 Results and Discussion

6.3.1 Voltage-time Behaviour and Coating Thickness

Typically, up to four stages are distinguished during the PEO process [28,33,38]. Figure 6.1 illustrates the voltage-time response of sample S12-25 containing all four stages.

During *stage I*, an abrupt linear increase in the voltage is observed within a short period of time. This stage is similar to conventional anodization which involves the rapid electrochemical formation of an initial thin oxide film [23,38]. At the end of stage I, the breakdown voltage is reached, which corresponds to the dielectric breakdown of the oxide film.

In *stage II*, after breakdown has occurred, a large number of small micro-discharges with a white color appear, covering the entire surface of the sample evenly. Sparks are characteristic of the PEO process and play a crucial role in the formation of the coatings. Seconds after the beginning of the PEO process, intense gas generation is observed on the surface of the sample. The slope of the voltage-time curve decreases during stage II.

In *stage III*, the rate of voltage change increases as compared to stage II. The micro-discharges become more intense and their color changes from white to yellow and then gradually to orange in subsequent stages of the process.

In *stage IV*, the rate of voltage increase becomes slightly slower than that in stage III. Sparks become even stronger while their population decreases and their color remains orange. It is believed [5,28] that the strong and long-lasting sparks could have a detrimental effect on the coatings in some cases. During stage IV, voltage fluctuations appear in the voltage-time curve, as can be seen in the inset in Figure 6.1, and has been reported by other researchers [39,40]. The onset of voltage fluctuations could be considered an indication of the beginning of stage IV.

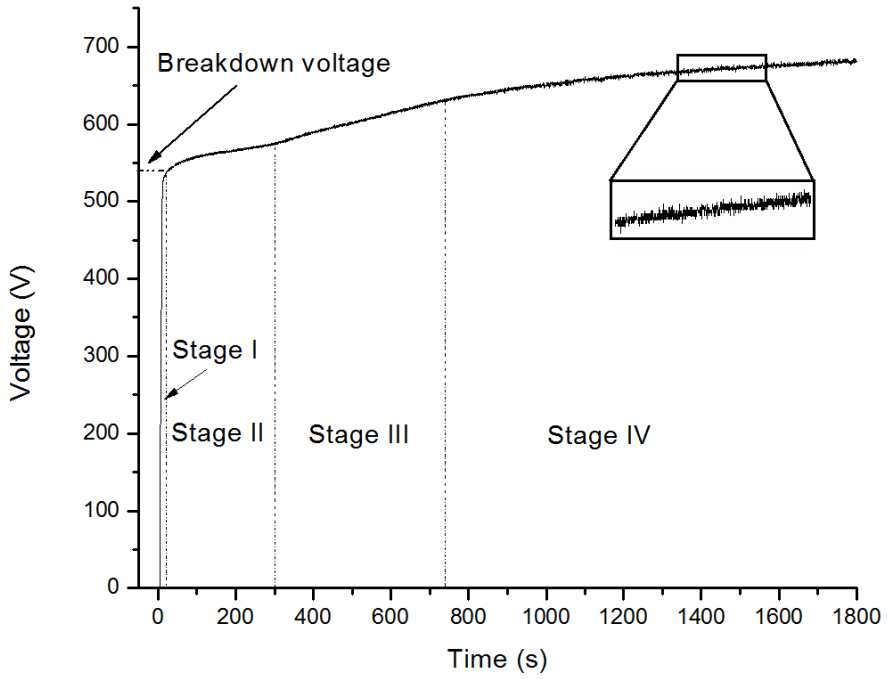

Figure 6.1- A typical voltage-time response of a PEO coated 6061 Al alloy sample (S12-25) showing the four different stages occurring during PEO.

The voltage-time response of coatings treated at different electrical parameters and the measured thicknesses are illustrated in Figure 6.2 and Figure 6.3. The oxide layers had average thicknesses ranging from 5 to 74 µm. Increasing the current density (*J*) at constant frequency and duty cycle resulted in thicker coatings.

Comparing the voltage-time response of samples coated at different electrical parameters (Figure 6.2 and Figure 6.3) revealed that increasing the current density from 5 to 25 A/dm^2 altered the duration and ratio of the different stages during PEO. This variation is more easily distinguished for samples coated at a frequency of 1000 Hz and the approximate onset of stage 3 and 4 have been marked on the voltage-time curves in Figure 6.2. As the current density decreased from 25 A/dm^2, the length of stage II increased and since the total deposition time was constant for all samples, i.e. 30 min, the last two stages became shorter.

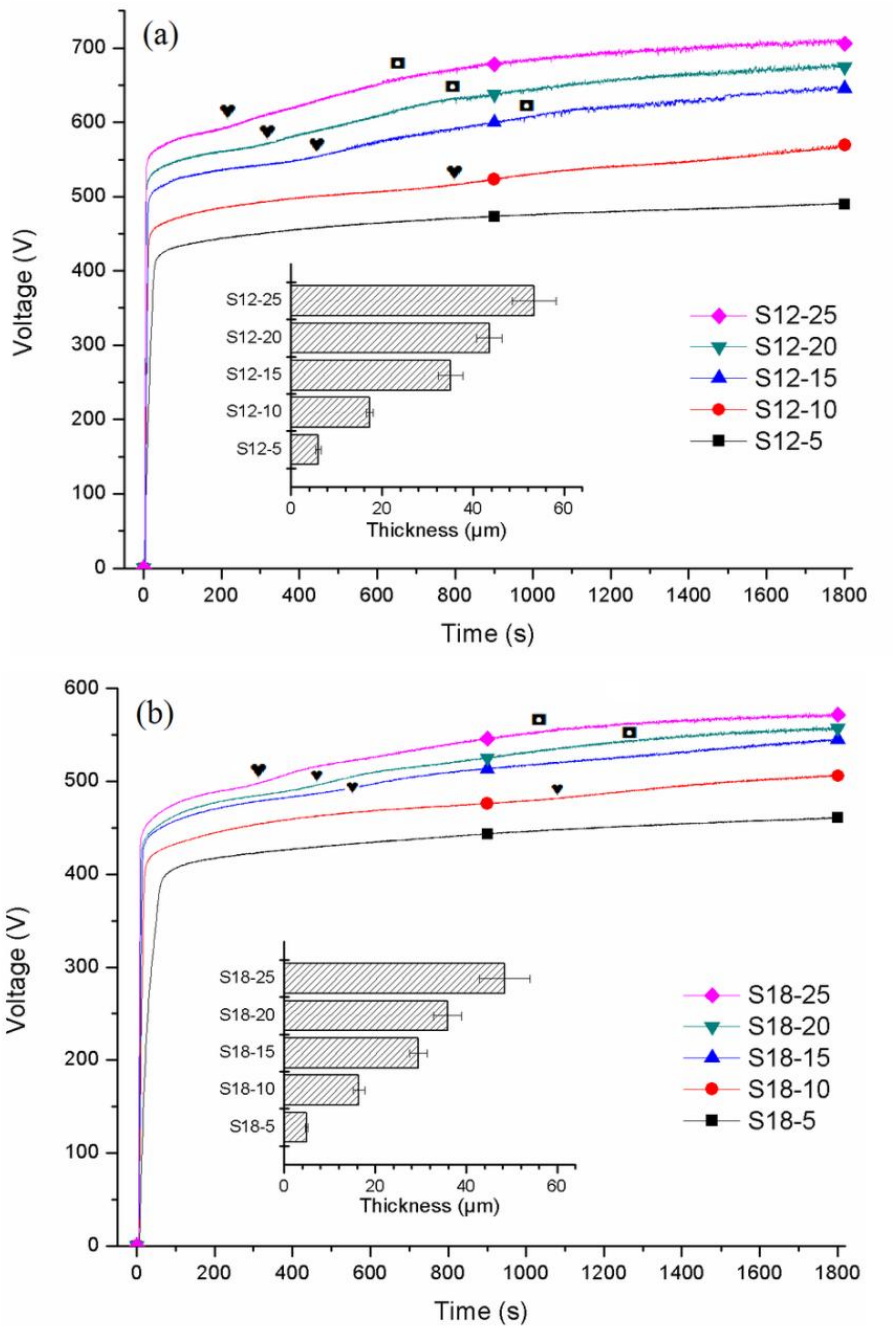

Figure 6.2- Voltage-time response and coating thicknesses of (a) samples coated at 1000 Hz and a duty cycle of 20% (S12-*), and (b) samples coated at 1000 Hz and a duty cycle of 80% (S18-*). The approximate onset of stage 3 and 4 are marked with ♥ and ◘, respectively.

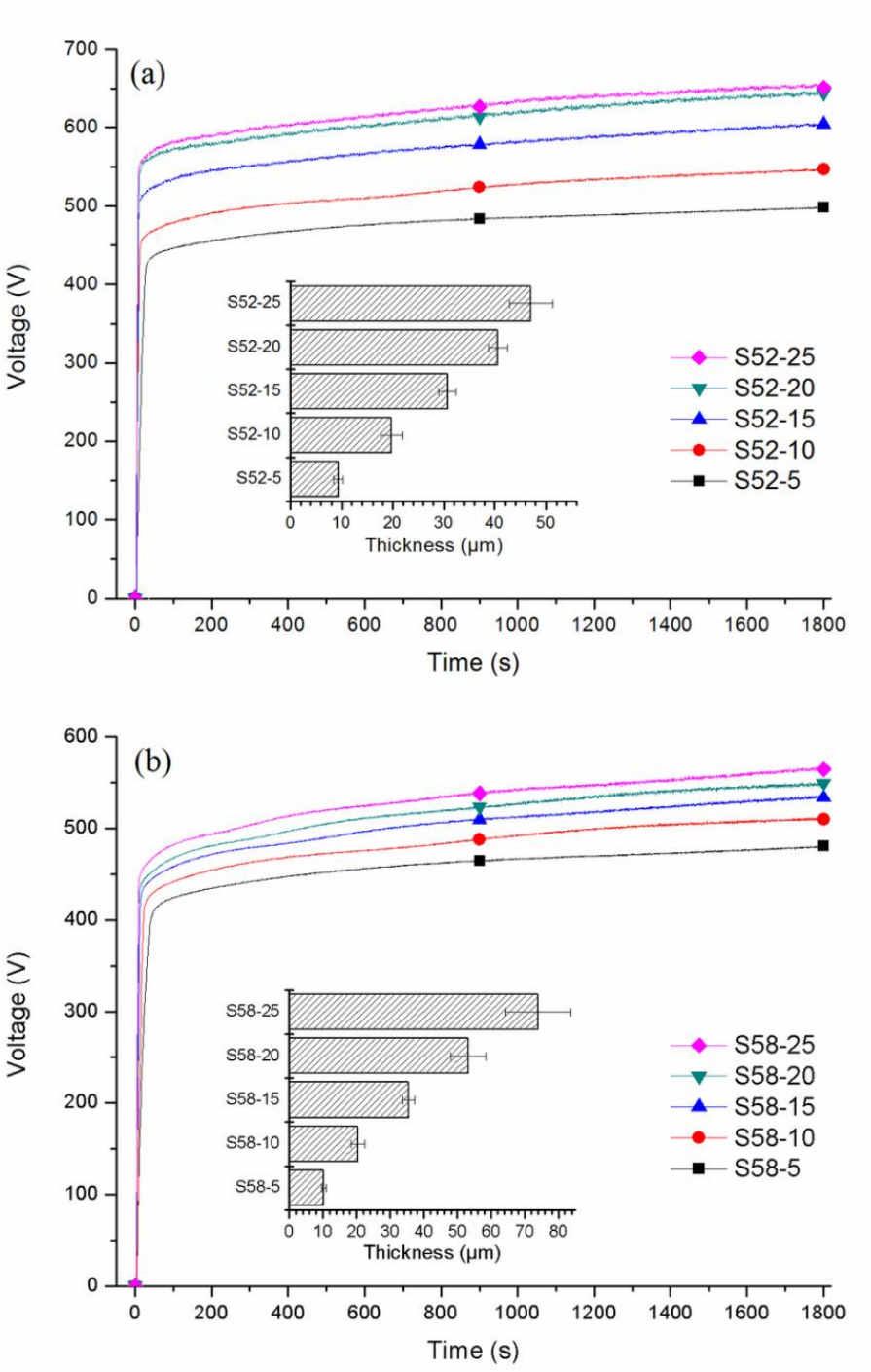

Figure 6.3- Voltage-time response and coating thicknesses of (a) samples coated at 50 Hz and a duty cycle of 20% (S52-*), and (b) samples coated at 50 Hz and a duty cycle of 80% (S58-*).

For sample S12-25, stage II finished after about 200 seconds from the beginning of the PEO process, while for samples S12-20, S12-15 and S12-10, stage II lasted longer and ended after about 300, 450 and 800 seconds, respectively. The voltage-time response of sample S12-5 had only stages I and II. Almost the same trend can be observed in the voltage-time response of sample sets S18-*, S52-* and S58-* as well. However, for samples S52-15, S52-20, and S52-25, Figure 6.3-a, the four stages are not distinguished and it seems that stage 4 has begun soon after the breakdown voltage was reached. Regardless of the frequency and duty cycles applied, samples coated at a current density of 5 A/dm^2 show only the first two stages in their voltage-time curves.

Figure 6.4 compares the maximum and breakdown voltages reached during PEO of each sample. For each column in the figure, the height represents the maximum voltage and the inner column the breakdown voltage for a given sample. Comparing the breakdown and maximum voltages achieved during the PEO of different samples (Figure 6.4) revealed that increasing the current density resulted in higher sparking and maximum voltages in each group of samples. Samples coated at a lower duty cycle of 20% had higher sparking and maximum voltages compared to samples coated at a higher duty cycle of 80% at constant frequency and current density.

In a previous study [34] where the effects of applied frequency and duty cycle were investigated at a constant deposition time of 30 min, it was observed that reducing the duty cycle from 80% to 10% decreased the duration of stage II and resulted in longer stage IV and higher breakdown and maximum voltages. Frequency was not found to influence the voltage-time response significantly at constant duty cycle and applied current density.

Altering the applied electrical process parameters changes the duration and ratio of different stages during PEO and as a result would influence the characteristics of the micro-discharges which have different spatial density and intensity during each stage. Micro-discharge characteristics and properties determine the thermal and chemical conditions during PEO and, as a result, play an important role in the morphology, phase formation and composition of the resulting oxide coatings [23].

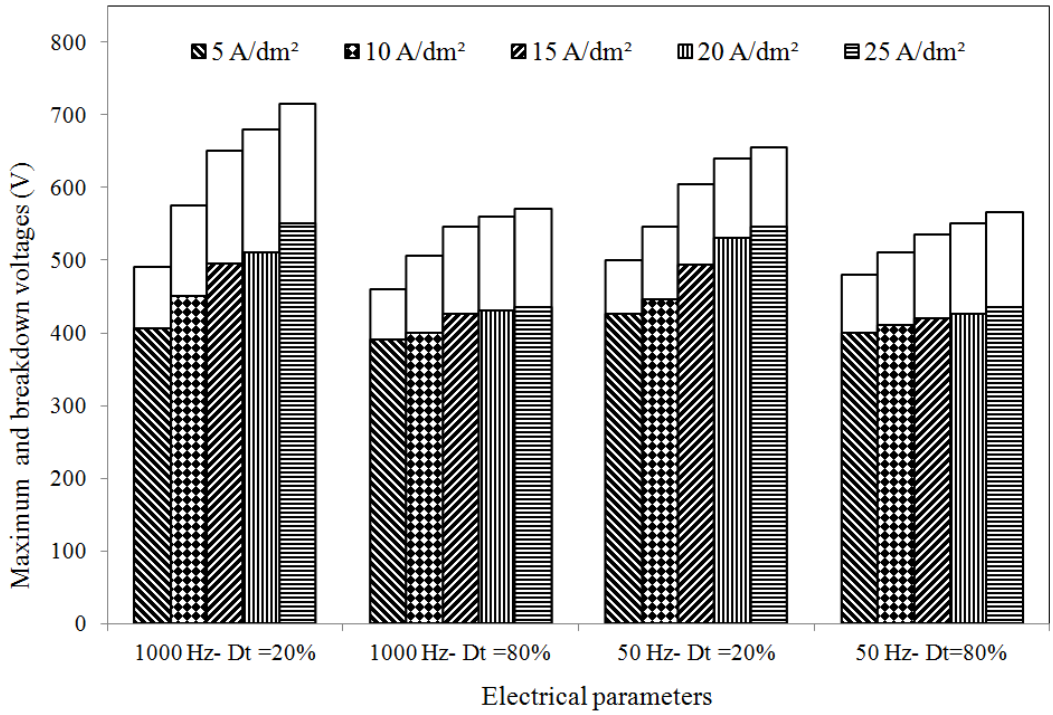

Figure 6.4- Maximum and breakdown voltages reached during PEO of 6061aluminum alloy samples using different electrical parameters (In each column, the height represents the maximum voltage and the inner column represents the breakdown voltage).

6.3.2 Coating Surface Morphology

The SEM images of the free surfaces and cross sections of the PEO coatings on samples prepared using different electrical conditions are compared in Figure 6.5-Figure 6.8. In each section of the figures, the lower part of the picture shows the free surface of the sample, and the upper part the corresponding cross section. The surfaces of the coatings in most samples exhibit two distinct regions, a cratered region and clusters of nodular structure, described in detail previously [34]. Craters are the circular areas with a hole in the middle, created by strong micro-discharges, and the nodular structure is composed of patches of lighter gray areas, as marked in Figure 6.6-e. The morphology and size of the

craters, as well as their ratio relative to the nodular structure, vary depending on the processing conditions applied.

Comparing the surface morphologies of samples coated at different conditions, Figure 6.5-Figure 6.8, it can be observed that samples coated at current densities above 5 A/dm^2 exhibit almost similar morphologies consisting of craters and nodular structures with varying ratios.

Samples coated at a current density of 5 A/dm^2, S12-5, S18-5, S52-5, and S58-5, contain elongated open pores on the surface of the coatings. This pore morphology was also observed by other researchers on aluminum [41,42] and magnesium [38,43] alloy substrates. Open pores are generally observed at short processing times when the PEO coating thickness is low. The voltage-time responses of samples treated at 5 A/dm^2 (Figure 6.2 and Figure 6.3) contain only the first two stages, I and II, and the thickness of these coatings is below 10 µm after 30 min of PEO coating which is considerably lower than for other samples. Formation of the open pores may be due to the low thickness of the coating and good thermal conductivity of the substrate which causes the molten material produced by the micro-discharges to be quickly quenched allowing formation of the open-pore structure [5]. These results indicate that the surface of samples whose voltage-time curve fell in stage II were composed of open micro-pores.

Comparing the surface morphology of samples coated at a frequency of 1000 Hz and a duty cycle of 20%, Figure 6.5, b-e, suggests that increasing the current density from 10 to 25 A/dm^2 affected the morphology of the PEO coatings in addition to their thickness, Figure 6.2-a. The surface of sample S12-10 is mainly composed of a large number of craters with very small areas of nodular structure. Each crater has a discharge channel in the centre through which the molten material flowed onto the surface of the coating. The results of EDX analyses on 6061aluminum alloy substrates coated by PEO in silicate containing electrolytes, suggested craters were rich in Al, while the nodular structure was rich in Si [34,44].

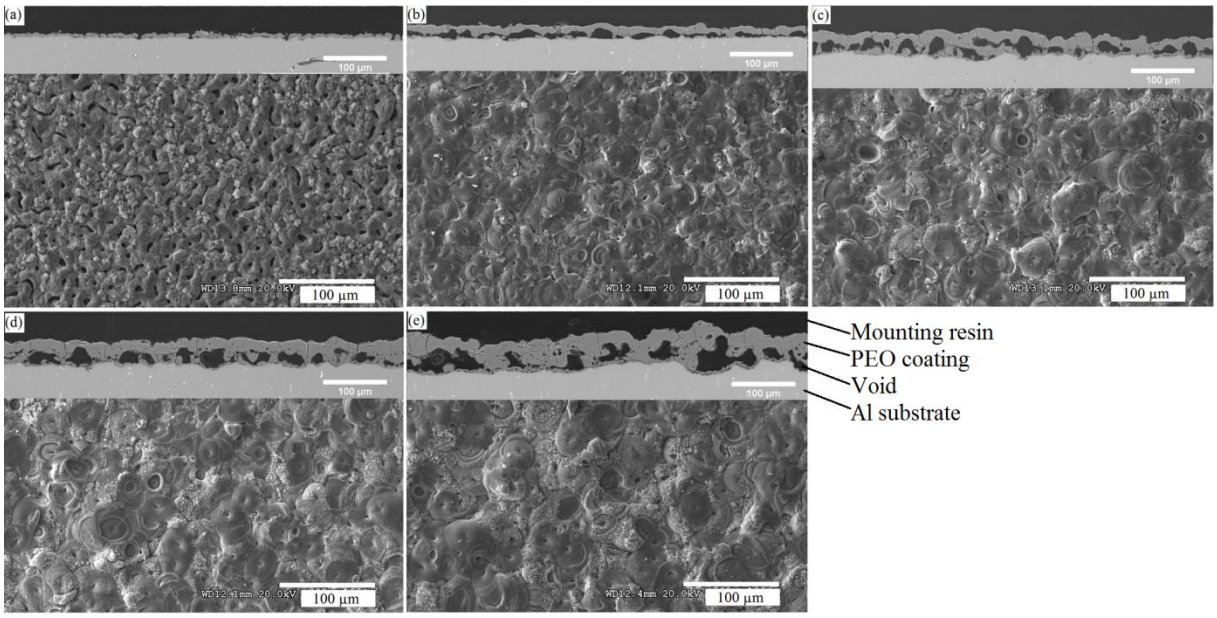

Figure 6.5- SEM images of the free surface (lower part) and cross sections (upper part) of coatings prepared at a frequency of 1000 Hz, duty cycle of 20% and different current densities on samples (a) S12-5, (b) S12-10, (c) S12-15, (d) S12-20, (e) S12-25.

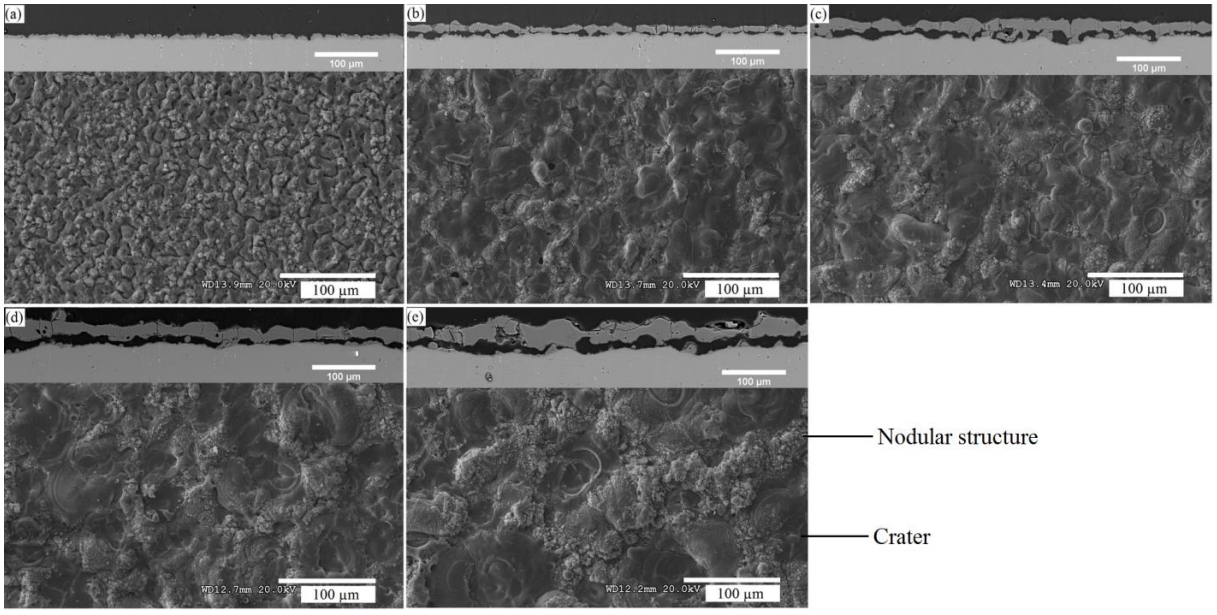

Figure 6.6- SEM images of the free surface (upper part) and cross sections (lower part) of coatings prepared at a frequency of 1000 Hz, duty cycle of 80% and different current densities on samples (a) S18-5, (b) S18-10, (c) S18-15, (d) S12-20, (e) S18-25.

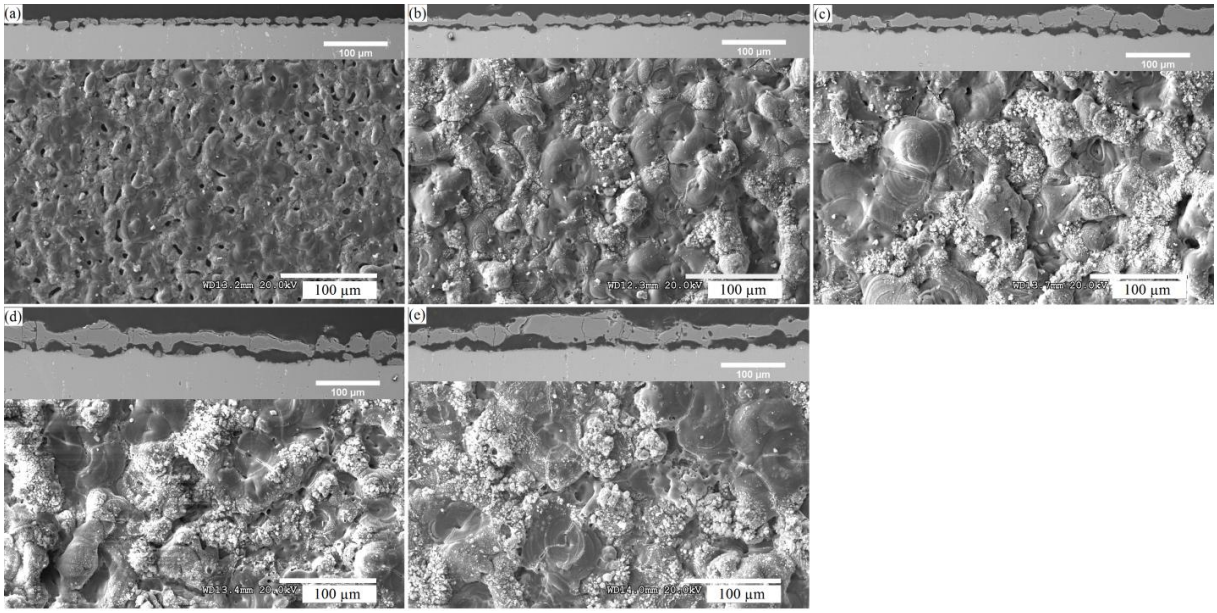

Figure 6.7- SEM images of the free surface (upper part) and cross sections (lower part) of coatings prepared at a frequency of 50 Hz, duty cycle of 20% and different current densities on samples (a) S52-5, (b) S52-10, (c) S52-15, (d) S52-20, (e) S52-25.

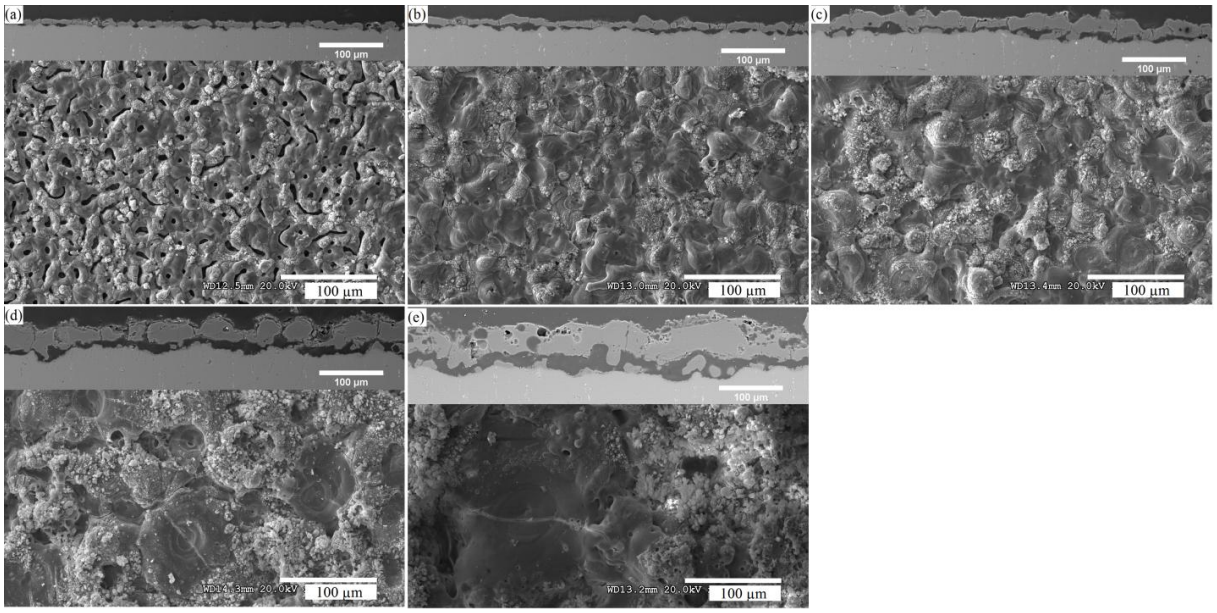

Figure 6.8- SEM images of the free surface (lower part) and cross sections (upper part) of coatings prepared at a frequency of 50 Hz, duty cycle of 80% and different current densities on samples (a) S58-5, (b) S58-10, (c) S58-15, (d) S58-20, (e) S58-25.

In samples S12-10 to S12-25, (Figure 6.5-b to e) as the current density increased, the size of the craters increased and the nodular structure covered a larger area fraction of the PEO coating surface. As discussed in section 3.1, increasing the current density shrank stage II and resulted in a longer stage IV. The surface of the coating on sample S12-10 which was in stage III after 30 min was mainly composed of craters, Figure 6.5-b. Samples S12-15, S12-20, and S12-25 were in stage IV after 30 min, Figure 6.2-a, and the length of stage IV was extended by increasing the current density. Examining the surface morphology of these samples in Figure 6.5, c-d, shows that the relative area fraction of the nodular structure covering the surface of the coating also grew with increasing the current density.

Samples S18-* (Figure 6.6), coated at the same frequency of 1000 Hz as S12-* but a higher duty cycle of 80%, exhibit the same trend. However, at an equal current density, the craters are bigger in size and the nodular structure covers a larger portion of the coating surface area as compared to samples S12-*.

Samples coated at the lower frequency of 50 Hz and duty cycles of 20% and 80%, Figure 6.7 and Figure 6.8 respectively, follow the same behavior as those coated at 1000 Hz. Again, for both duty cycles of 20% and 80%, higher current densities resulted in thicker coatings, bigger craters, and more nodular structures on the surface of the coatings.

It was observed that at both frequencies, 50 and 1000 Hz, higher duty cycle of 80% (Figure 6.6 and Figure 6.8) produced bigger craters and more nodular structure at a constant current density compared to the lower duty cycle of 20%. These observations are confirmed by a previous study [34] in which EDX elemental maps and measurements of crater radius were used to study the effect of duty cycle on Al/Si ratio and the size of craters on the surface of the samples. The larger crater size in samples coated at higher duty cycle and current densities at both frequencies could be attributed to the effect of the electrical parameters on the coating thickness and structure. Craters are the result of micro-discharges generated by dielectric breakdown at weak and defective spots in the oxide coating and increasing the thickness of the coatings, reduces the number of weak

sites. The increased size of craters, indicative of stronger micro-discharges, is ascribed to the reduced number of discharging sites through which higher current is able to pass [5,30,45]. The longer t_{on} at the higher duty cycle of 80% compared to lower duty cycle of 20% provides more time for the gases to leave the molten material, thus creating a coating with less porosity and fewer sites for micro-discharges to occur, as evident in cross-sectional SEM images in Figure 6.5-Figure 6.8. Increasing J in each set of samples resulted in thicker coatings (Figure 6.2 and Figure 6.3). In a thicker oxide coating, higher energy is required to pass through the coating and with reduced weak points the current is localized in fewer locations, resulting in stronger sparks creating bigger craters [30,34].

6.3.3 Cross-sectional Microstructures of the Coatings

The cross-sections of the PEO coatings examined by SEM are presented in Figure 6.5-Figure 6.8 for different processing conditions. A two-layered structure can be observed in the coating cross sections of nearly all samples. Adjacent to the substrate, there is a thin inner layer which is termed “the barrier layer” followed by a thicker layer of variable thickness or the “functional layer” which provides the main thermo-mechanical and tribological functionality of the coating [35,46].

In addition to the barrier and functional layer a third porous and loose layer, located on top of the functional layer (Figure 6.9-b), was also observed on some samples. The outer loose layer, also reported elsewhere in the literature [46,47], can be removed after PEO treatment to expose the dense functional layer [48]. However, it is suggested that the porosity in the outer loose layer could be used as a base for sealants and primers for corrosion protection [35].

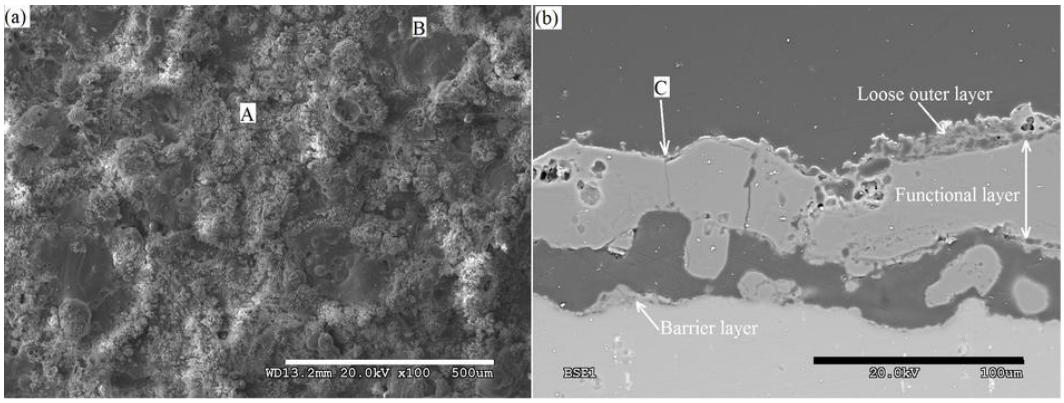

Figure 6.9- SEM images showing (a) the free surface, and (b) the cross-section of sample S58-25.

For all samples, the interface between the coatings and the substrate had a wavy appearance which might be the result of dissolution of the substrate in the early stages of the process [49] given the high pH (around 12) of the electrolyte. Large pores, which are connected in some areas and enlarged during polishing, are present between the inner and outer layers of the coatings (the dark area between the barrier layer and functional layer in Figure 6.9-b). Coatings with similar cross-sectional structure containing large pores between the inner and outer layers were also observed in studies using pulsed unipolar PEO on aluminum [29,50] and magnesium [51,52] alloy substrates. On the other hand, such a pore structure was not observed in coatings on titanium alloys after PEO [32]. A possible explanation for the formation of pores when pulsed unipolar current is used could be the corrosion of the substrate during the pulse off time due to the high pH (~12) of the electrolytes commonly used in PEO; however the mechanism of pore formation requires further investigation. Results of studies comparing the effect of current modes on the microstructure of PEO coatings on magnesium alloy substrates [52–54] suggest that the unipolar pulsed DC mode produces coatings with more porosity, larger defects and lower microhardness compared to the bipolar mode. Bipolar current mode was also found to improve the corrosion resistance of PEO coatings compared to the uinpolar mode which is indicative of the improved density of the coatings achieved using the bipolar mode.

Despite the fact that current mode, substrate composition, and electrolyte properties may play a role in the formation of large pores between the coating layers, the formation mechanism of these pores requires further investigation.

SEM images of the cross-sections of PEO coatings (Figure 6.5-Figure 6.8) show channels across the coatings created by individual discharge events and also scattered pores in the functional layer. Pores may form due to the entrapment of oxygen [55] or other types of gases that are formed during the strong discharges [29] in molten alumina.

The coatings produced with the shortest t_{on} time, Figure 6.5, contain more porosity and discharge channels in the coatings as compared to other samples coated at longer t_{on} times. This is more obvious when comparing the cross-sectional microstructure of S12-25 (Figure 6.5-e) produced at a t_{on} time of 0.2 ms with S18-25 (Figure 6.6-e), S52-25 (Figure 6.7-e), and S58-25 (Figure 6.8-e) with t_{on} times of 0.8, 4, and 16 ms, respectively. The longer t_{on} times can create longer strong discharges which would make it easier for the gases to escape the molten material and could result in a better sintering and thus denser coating.

The coating growth is the result of the molten materials flowing through discharge channels. The central hole in the cratered regions is the discharge channel through which the molten material was ejected and rapidly solidified upon contact with the electrolyte [56,57]. Area "C" in Figure 6.9-b shows a discharge channel in the coating cross section that created a crater (Area "B" in Figure 6.9-a) in sample S58-25. The coating growth rate is a function of the number and intensity of discharge channels. Thickness measurements (Figure 6.2 and Figure 6.3) show that the coating growth rate increased when higher current densities were applied in each set of samples. The average thickness of sample S58-25 (Figure 6.3-b), ~74 µm, was considerably higher than other samples. The SEM image of the free surface of S58-25 show that the nodular structure (as seen in Area "A" in Figure 6.9-a) covered a large portion of the area in this sample. The cross-sectional view of S58-25 in Figure 6.9-b revealed that the loose outer layer is actually the nodular structure with a thickness high enough to be observed in the cross section of the coating. The presence of the thicker nodular structure forming the loose outer layer in

S58-25 could be one of the reasons for the high thickness readings on this sample. A previous study of phase composition and distribution in PEO coatings prepared with conditions similar to the present work [37], showed the outer surface was composed of mullite and amorphous phases. The loose outer layer is an incomplete layer of nodular structure clusters on the surface and is therefore not suitable for applications where good mechanical properties are required: e.g., wear applications. Due to its poor bonding to the functional layer as a result of interfacial porosity, the outer loose layer can be easily removed when in contact with a sliding surface and should be removed prior to application to expose the inner functional layer with superior wear resistance [46,50].

The outer loose layer was also observed in some areas in the cross sectional views of other samples coated at high current densities, namely samples S18-25, S52-20, S52-25, and S58-20 in Figure 6.6-e, Figure 6.7-d, Figure 6.7-e, and Figure 6.8-d, respectively, but its thickness was lower than that of sample S58-25.

In a detailed study on the effect of electrical parameters on phase formation and distribution in PEO coatings on 6061 aluminum substrate [37] it was found that increasing the pulse on-time by employing a lower frequency and higher duty cycle resulted in coatings containing mullite and an amorphous phase in addition to α- and γ-Al_2O_3. Depth profiling of the coated samples suggested that mullite ($3Al_2O_3$-$2SiO_2$) and the amorphous phase were concentrated near the outer surface of the coatings. The formation of mullite and Si-rich amorphous phase was attributed to increased Si concentration as a result of longer pulse on-time. Our proposed mechanism [34] suggests that when t_{on} is long, the negative ions like SiO_3^{2-} have more time to get adsorbed on the surface of the anode. This, in addition to lower spatial density of sparks on the surface of samples coated at longer t_{on} times, would result in higher concentration of Si rich species on the surface of the coatings.

6.3.4 Coating Microhardness

Microhardness values determined from Vickers indentations on the cross sections of the coatings in the functional layer areas are given in Figure 6.10. Coatings on samples treated at current densities of 5 and 10 A/dm^2 were very thin compared to the size of the

indentation. To prevent error in the readings caused by low thickness, only hardness values of samples with enough thickness are reported.

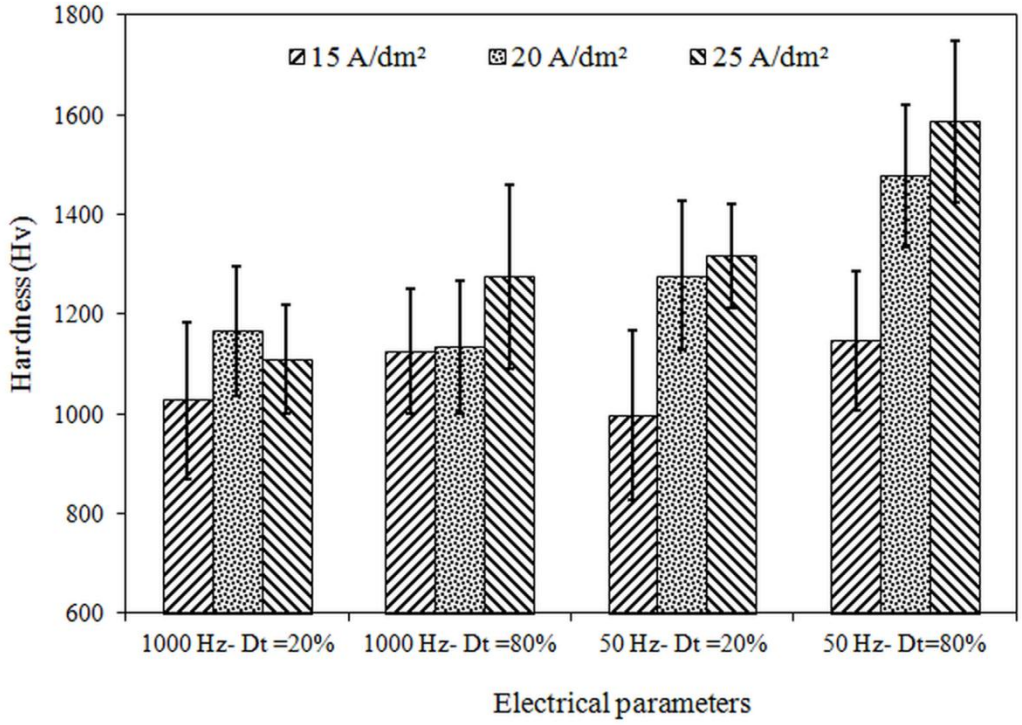

Figure 6.10- Cross sectional Vickers microhardness values in functional layer of PEO coatings on 6061 Al alloy as a function of electrical parameters.

The average coating hardness values ranged from 1000 Hv (9.8 GPa) to around 1600 Hv (15.7 GPa) in sample S58-25. These values are appreciably higher than the hardness of conventional anodising coatings (~ 4-6 GPa [58,59]). The improved hardness of PEO coatings compared to conventional anodic alumina is attributed to the reduced porosity and the existence of crystalline alumina phases, namely α-Al_2O_3. PEO coatings on aluminum alloys are normally a mixture of α-Al_2O_3 (~ 26 GPa), γ-Al_2O_3 (~17 GPa), mullite (~10.5 GPa), and amorphous alumina (~ 4-6 GPa) [50,56,60]. The measured hardness in PEO coatings is lower than in dense bulk alumina phases due to the presence of porosity caused by the entrapment of gases in the coating during the treatment process, and channels created by individual micro-discharges (demonstrated in Figure 6.9-b) in PEO coatings.

The microhardness test results (Figure 6.10) suggest that increasing t_{on} resulted in higher average hardness values. As given in Table 6.1, t_{on} duration for S12-*, S18-*, S52-*, and S58-* samples are 0.2, 0.8, 4, and 16 ms, respectively. It can also be deduced from Figure 6.10 that except for S12-* samples, coated at a frequency of 1000 Hz and a D_t of 20%, in all other samples increasing the current density from 15 to 25 A/dm^2 resulted in higher average hardness.

The hardness of the PEO coating is a function of the nature of the dominant phases present, as well as their ratio and distribution, and the porosity and density of micro-cracks in the coatings. As discussed in section 6.3.3, the coatings produced at 1000 Hz and a duty cycle of 20% had the shortest t_{on} time (0.2 ms) and contained more porosity and discharge channels in the coatings (Figure 6.5) as compared to other samples coated at longer t_{on} times. Longer t_{on} times can create longer discharges, making it easier for the gases to escape the molten material thus causing better sintering and a denser coating. It was previously reported [37] that increasing the pulse on-time and current density enhanced the $\gamma \rightarrow \alpha$-$Al_2O_3$ phase transformation resulting in more α-Al_2O_3, which is the hardest alumina phase, in the coatings. Coatings on samples PEO treated at a frequency of 1000 Hz and a duty cycle of 20% with different current densities contained essentially only γ-Al_2O_3. Increasing the duty cycle to 80% at the same frequency resulted in the formation of α-Al_2O_3 in addition to γ-Al_2O_3. In samples treated at 50 Hz, α-Al_2O_3 was identified in all samples at a current density greater than 5 A/dm^2 in addition to γ-Al_2O_3.

PEO coatings on samples treated at 1000 Hz contained a higher level of porosity and micro-cracks with respect to other samples (Figure 6.5). Variation in the coating microhardness values of S12-* samples is possibly more dependent on the amount of porosity and micro-cracks in these coatings since the phase composition of these coating were the same and composed only of γ-Al_2O_3. In other samples, however, the microhardness seems to be influenced by phase composition and content more than porosity because the cross sectional SEM micrographs (Figure 6.6-Figure 6.8) show relatively dense structures in the functional layer of the coatings. In samples S18-*, S52-*, and S58-*, the relative α-Al_2O_3 content in the coating increased by applying a longer

t_{on} and higher current density [37] which is indicative of the positive effect of increased relative content of α-Al_2O_3 on the coating hardness.

6.4 Conclusions

PEO was performed on the 6061 aluminum alloy in an alkaline silicate electrolyte using a pulsed unipolar current mode under galvanostatic conditions. Samples were coated at different frequencies, duty cycles, and current densities. For each sample the voltage-time response of the PEO process was obtained and compared with the surface morphology, cross-sectional view, and thickness of the coating. Vickers microhardness test was used to study the effect of the electrical parameters on the hardness of the coatings. Special consideration was given to the connection between the electrical parameters, different stages of the PEO process, and the morphology and microstructure of the coatings. The following conclusions can be drawn from this study:

- Voltage-time curves of samples coated with different electrical parameters showed up to four different stages. Applying different electrical parameters changed the duration and ratio of these stages during PEO and affected the surface morphologies of the coatings.
- The surfaces of the coatings in most samples exhibited two distinct regions, craters and clusters of nodular structure. The size of the craters, as well as the area fraction of the cratered region and the nodular structure changed when different electrical parameters were applied.
- For samples treated at a current density of 5 A/dm^2 the voltage-time curves exhibited only two stages, I and II. Elongated open micro-pores were observed on the surface of all these samples. The low thickness of the coating together with the good thermal conductivity of the substrate could suggest the formation of such pores is due to the rapid solidification of the molten material.
- Increasing the current density from 10 to 25 A/dm^2 decreased the duration of stage II and increased the extent of the last stage in the voltage-time response resulting in bigger craters and increased area fractions of the nodular structure on the PEO coating surfaces

- The application of higher current densities and longer pulse-on times, by employing higher duty cycles and a lower frequency, improved the microhardness of the coatings. This could be due to an enhanced $\gamma \rightarrow \alpha$-$Al_2O_3$ phase transformation resulting in more α-Al_2O_3 in the oxide layer and an increased density of the functional layer due to the reduction of porosity.

6.5 References

[1] D. Shen, G. Li, C. Guo, J. Zou, J. Cai, D. He, et al., Microstructure and corrosion behavior of micro-arc oxidation coating on 6061 aluminum alloy pre-treated by high-temperature oxidation, Appl. Surf. Sci. 287 (2013) 451–456.

[2] F. Monfort, A. Berkani, E. Matykina, P. Skeldon, G.E. Thompson, H. Habazaki, et al., Development of anodic coatings on aluminium under sparking conditions in silicate electrolyte, Corros. Sci. 49 (2007) 672–693.

[3] J.A. Curran, H. Kalkancı, Y. Magurova, T.W. Clyne, Mullite-rich plasma electrolytic oxide coatings for thermal barrier applications, Surf. Coatings Technol. 201 (2007) 8683–8687.

[4] Y. Cheng, E. Matykina, R. Arrabal, P. Skeldon, G.E. Thompson, Plasma electrolytic oxidation and corrosion protection of Zircaloy-4, Surf. Coatings Technol. 206 (2012) 3230–3239.

[5] Y. Cheng, F. Wu, E. Matykina, P. Skeldon, G.E.E. Thompson, The influences of microdischarge types and silicate on the morphologies and phase compositions of plasma electrolytic oxidation coatings on Zircaloy-2, Corros. Sci. 59 (2012) 307–315.

[6] W. Simka, M. Sowa, R.P. Socha, A. Maciej, J. Michalska, Anodic oxidation of zirconium in silicate solutions, Electrochim. Acta. 104 (2012) 518–525.

[7] M. Petković, S. Stojadinović, R. Vasilić, L. Zeković, Characterization of oxide coatings formed on tantalum by plasma electrolytic oxidation in 12-tungstosilicic acid, Appl. Surf. Sci. 257 (2011) 10590–10594.

[8] C. Wang, F. Wang, Y. Han, Structural characteristics and outward–inward growth behavior of tantalum oxide coatings on tantalum by micro-arc oxidation, Surf. Coatings Technol. 214 (2013) 110–116.

[9] Y. Cheng, F. Wu, J. Dong, X. Wu, Z. Xue, E. Matykina, et al., Comparison of plasma electrolytic oxidation of zirconium alloy in silicate- and aluminate-based electrolytes and wear properties of the resulting coatings, Electrochim. Acta. 85 (2012) 25–32.

[10] L.R. Krishna, A.S. Purnima, G. Sundararajan, A comparative study of tribological behavior of microarc oxidation and hard-anodized coatings, Wear. 261 (2006) 1095–1101.

[11] M. Treviño, R.D. Mercado-Solis, R. Colás, A. Pérez, J. Talamantes, A. Velasco, Erosive wear of plasma electrolytic oxidation layers on aluminium alloy 6061, Wear. 301 (2012) 434–441.

[12] G. Rapheal, S. Kumar, C. Blawert, N.B. Dahotre, Wear behavior of plasma electrolytic oxidation (PEO) and hybrid coatings of PEO and laser on MRI 230D magnesium alloy, Wear. 271 (2011) 1987–1997.

[13] X. Li, X. Liu, B.L. Luan, Corrosion and wear properties of PEO coatings formed on AM60B alloy in NaAlO2 electrolytes, Appl. Surf. Sci. 257 (2011) 9135–9141.

[14] S. Moon, Corrosion behavior of PEO-treated AZ31 Mg alloy in chloride solution, J. Solid State Electrochem. (2013) 3–8.

[15] W. Xue, C. Wang, H. Tian, Y. Lai, Corrosion behaviors and galvanic studies of microarc oxidation films on Al–Zn–Mg–Cu alloy, Surf. Coatings Technol. 201 (2007) 8695–8701.

[16] T. Akatsu, T. Kato, Y. Shinoda, F. Wakai, Thermal barrier coating made of porous zirconium oxide on a nickel-based single crystal superalloy formed by plasma electrolytic oxidation, Surf. Coatings Technol. 223 (2013) 47–51.

[17] J.A. Curran, T.W. Clyne, The thermal conductivity of plasma electrolytic oxide coatings on aluminium and magnesium, Surf. Coat. Technol. 199 (2005) 177–183.

[18] F.-Y. Jin, K. Wang, M. Zhu, L.-R. Shen, J. Li, H.-H. Hong, et al., Infrared reflection by alumina films produced on aluminum alloy by plasma electrolytic oxidation, Mater. Chem. Phys. 114 (2009) 398–401.

[19] Y. Yan, J. Sun, Y. Han, D. Li, K. Cui, Microstructure and bioactivity of Ca, P and Sr doped TiO2 coating formed on porous titanium by micro-arc oxidation, Surf. Coatings Technol. 205 (2010) 1702–1713.

[20] A. Krząkała, K. Służalska, M. Widziołek, J. Szade, A. Winiarski, G. Dercz, et al., Formation of bioactive coatings on a Ti–6Al–7Nb alloy by plasma electrolytic oxidation, Electrochim. Acta. 104 (2013) 407–424.

[21] S.A. Alves, R. Bayón, A. Igartua, V.S. De Viteri, L.A. Rocha, Tribocorrosion behaviour of anodic titanium oxide films produced by plasma electrolytic oxidation for dental implants, Lubrication Science (2013), doi: 10.1002/ls.1234.

[22] A.L. Yerokhin, L.O. Snizhko, N.L. Gurevina, A. Leyland, A. Pilkington, A. Matthews, Spatial characteristics of discharge phenomena in plasma electrolytic oxidation of aluminium alloy, Surf. Coatings Technol. 177-178 (2004) 779–783.

[23] J. Jovović, S. Stojadinović, N.M. Šišović, N. Konjević, Spectroscopic study of plasma during electrolytic oxidation of magnesium- and aluminium-alloy, J. Quant. Spectrosc. Radiat. Transf. 113 (2012) 1928–1937.

[24] S. Stojadinović, R. Vasilić, M. Petković, I. Belča, B. Kasalica, M. Perić, et al., Luminescence during anodization of magnesium alloy AZ31, Electrochim. Acta. 59 (2012) 354–359.

[25] E. Matykina, A. Berkani, P. Skeldon, G.E. Thompson, Real-time imaging of coating growth during plasma electrolytic oxidation of titanium, Electrochim. Acta. 53 (2007) 1987–1994.

[26] M. Göttlicher, M. Rohnke, A. Helth, T. Leichtweiß, T. Gemming, A. Gebert, et al., Controlled surface modification of Ti-40Nb implant alloy by electrochemically assisted inductively coupled RF plasma oxidation., Acta Biomater. 9 (2013) 9201–9210.

[27] S. Stojadinović, R. Vasilić, M. Petković, I. Belča, B. Kasalica, M. Perić, et al., Luminescence during the anodization of zirconium, Electrochim. Acta. 79 (2012) 133–140.

[28] R.O. Hussein, X. Nie, D.O. Northwood, A. Yerokhin, A. Matthews, Spectroscopic study of electrolytic plasma and discharging behaviour during the plasma electrolytic oxidation (PEO) process, J. Phys. D. Appl. Phys. 43 (2010) 105203–105216.

[29] R.O. Hussein, D.O. Northwood, X. Nie, Coating growth behavior during the plasma electrolytic oxidation process, J. Vac. Sci. Technol. A Vacuum, Surfaces, Film. 28 (2010) 766–773.

[30] S. Stojadinovic, R. Vasilic, I. Belca, M. Petkovic, B. Kasalica, Z. Nedic, et al., Characterization of the plasma electrolytic oxidation of aluminium in sodium tungstate, Corros. Sci. 52 (2010) 3258–3265.

[31] L. Wang, L. Chen, Z. Yan, W. Fu, Optical emission spectroscopy studies of discharge mechanism and plasma characteristics during plasma electrolytic oxidation of magnesium in different electrolytes, Surf. Coatings Technol. 205 (2010) 1651–1658.

[32] R.O. Hussein, X. Nie, D.O. Northwood, A spectroscopic and microstructural study of oxide coatings produced on a Ti–6Al–4V alloy by plasma electrolytic oxidation, Mater. Chem. Phys. 134 (2012) 484–492.

[33] L. Wang, X. Nie, Silicon effects on formation of EPO oxide coatings on aluminum alloys, Thin Solid Films. 494 (2006) 211–218.

[34] V. Dehnavi, B.L. Luan, D.W. Shoesmith, X.Y. Liu, S. Rohani, Effect of duty cycle and applied current frequency on plasma electrolytic oxidation (PEO) coating growth behavior, Surf. Coatings Technol. 226 (2013) 100–107.

[35] E. Matykina, R. Arrabal, a. Mohamed, P. Skeldon, G.E. Thompson, Plasma electrolytic oxidation of pre-anodized aluminium, Corros. Sci. 51 (2009) 2897–2905.

[36] Y.K. Pan, C.Z. Chen, D.G. Wang, X. Yu, Microstructure and biological properties of micro-arc oxidation coatings on ZK60 magnesium alloy., J. Biomed. Mater. Res. B. Appl. Biomater. 100 (2012) 1574–86.

[37] V. Dehnavi, X.Y. Liu, B.L. Luan, D.W. Shoesmith, S. Rohani, Phase Transformation in Plasma Electrolytic Oxidation Coatings on 6061 Aluminum Alloy, Surf. Coatings Technol. 251 (2014) 106-114.

[38] R.O. Hussein, X. Nie, D.O. Northwood, An investigation of ceramic coating growth mechanisms in plasma electrolytic oxidation (PEO) processing, Electrochim. Acta. 112 (2013) 111–119.

[39] F. Monfort, E. Matykina, a. Berkani, P. Skeldon, G.E. Thompson, H. Habazaki, et al., Species separation during coating growth on aluminium by spark anodizing, Surf. Coatings Technol. 201 (2007) 8671–8676.

[40] Y. Guan, Y. Xia, G. Li, Growth mechanism and corrosion behavior of ceramic coatings on aluminum produced by autocontrol AC pulse PEO, Surf. Coatings Technol. 202 (2008) 4602–4612.

[41] G. Sundararajan, L. Rama Krishna, Mechanisms underlying the formation of thick alumina coatings through the MAO coating technology, Surf. Coatings Technol. 167 (2003) 269–277.

[42] S. Moon, Y. Jeong, Generation mechanism of microdischarges during plasma electrolytic oxidation of Al in aqueous solutions, Corros. Sci. 51 (2009) 1506–1512.

[43] U. Malayoglu, K.C. Tekin, S. Shrestha, Influence of post-treatment on the corrosion resistance of PEO coated AM50B and AM60B Mg alloys, Surf. Coatings Technol. 205 (2010) 1793–1798.

[44] M.M.S. Al Bosta, K. Ma, H. Chien, M.M.S. Al Bosta, The effect of MAO processing time on surface properties and low temperature infrared emissivity of ceramic coating on aluminium 6061 alloy, Infrared Phys. Technol. 60 (2013) 323–334.

[45] W. Xue, Z. Deng, Y. Lai, R. Chen, Analysis of Phase Distribution for Ceramic Coatings Formed by Microarc Oxidation on Aluminum Alloy, J. Am. Ceram. Soc. 81 (1998) 1365–1368.

[46] F.C. Walsh, C.T.J. Low, R.J.K. Wood, K.T. Stevens, J. Archer, A.R. Poeton, et al., Plasma electrolytic oxidation (PEO) for production of anodised coatings on lightweight metal (Al, Mg, Ti) alloys, Trans. Inst. Met. Finish. 87 (2009) 122–135.

[47] A.L. Yerokhin, A. Shatrov, V. Samsonov, P. Shashkov, A. Pilkington, A. Leyland, et al., Oxide ceramic coatings on aluminium alloys produced by a pulsed bipolar plasma electrolytic oxidation process, Surf. Coatings Technol. 199 (2005) 150–157.

[48] E. Matykina, R. Arrabal, P. Skeldon, G.E. Thompson, Investigation of the growth processes of coatings formed by AC plasma electrolytic oxidation of aluminium, Electrochim. Acta. 54 (2009) 6767–6778.

[49] R.O. Hussein, X. Nie, D.O. Northwood, A spectroscopic and microstructural study of oxide coatings produced on a Ti–6Al–4V alloy by plasma electrolytic oxidation, Mater. Chem. Phys. 134 (2012) 484–492.

[50] Y. Cheng, Z. Xue, Q. Wang, X.-Q. Wu, E. Matykina, P. Skeldon, et al., New findings on properties of plasma electrolytic oxidation coatings from study of an Al–Cu–Li alloy, Electrochim. Acta. 107 (2013) 358–378.

[51] Y. Gao, A. Yerokhin, A. Matthews, DC plasma electrolytic oxidation of biodegradable cp-Mg: In-vitro corrosion studies, Surf. Coatings Technol. 234 (2012) 132–142.

[52] R.O. Hussein, D.O. Northwood, J.F. Su, X. Nie, A study of the interactive effects of hybrid current modes on the tribological properties of a PEO (plasma electrolytic oxidation) coated AM60B Mg-alloy, Surf. Coatings Technol. 215 (2013) 421–430.

[53] R.O. Hussein, P. Zhang, X. Nie, Y. Xia, D.O. Northwood, The effect of current mode and discharge type on the corrosion resistance of plasma electrolytic oxidation (PEO) coated magnesium alloy AJ62, Surf. Coatings Technol. 206 (2011) 1990–1997.

[54] M.V. Sidorova, S.L. Sinebrukhov, O. a. Khrisanfova, S.V. Gnedenkov, Effect of PEO-modes on the electrochemical and mechanical properties of coatings on MA8 magnesium alloy, Phys. Procedia. 23 (2012) 90–93.

[55] J.A. Curran, T.W. Clyne, Porosity in plasma electrolytic oxide coatings, Acta Mater. 54 (2006) 1985–1993.

[56] R.H.U. Khan, A. Yerokhin, X. Li, H. Dong, A. Matthews, Surface characterisation of DC plasma electrolytic oxidation treated 6082 aluminium alloy: Effect of current density and electrolyte concentration, Surf. Coatings Technol. 205 (2010) 1679–1688.

[57] F. Jaspard-mécuson, T. Czerwiec, G. Henrion, T. Belmonte, L. Dujardin, A. Viola, et al., Tailored aluminium oxide layers by bipolar current adjustment in the Plasma Electrolytic Oxidation (PEO) process, Surf. Coatings Technol. 201 (2007) 8677–8682.

[58] G. Alcala, P. Skeldon, G.E. Thompson, A.B. Mann, H. Habazaki, Mechanical properties of amorphous anodic alumina and tantala films using nanoindentation, Nanotechnology 13 (2002) 451–455.

[59] P.U. Skeldon, H.W. Wang, G.E. Thompson, Formation and characterization of self-lubricating MoS 2 precursor films on anodized aluminium, 206 (1997) 187–196.

[60] H. Kalkancı, S.C. Kurnaz, The effect of process parameters on mullite-based plasma electrolytic oxide coatings, Surf. Coatings Technol. 203 (2008) 15–22.

Chapter 7

Electrochemical Corrosion Behaviour of Plasma Electrolytic Oxidation Coated Aluminum Alloy, the Effect of PEO Process Stage

Abstract

The electrochemical properties of oxide coatings formed by plasma electrolytic oxidation (PEO) on an aluminum alloy (6061-T651) substrate were investigated using electrochemical impedance spectroscopy (EIS) and linear polarization resistance (LPR) measurements. PEO coatings were grown using different processing parameters which enabled samples to be coated to different stages of the PEO process, identified in the voltage-time response curves. Scanning electron microscopy was employed to relate the morphology of the coatings to their corrosion performance. A direct relationship was found between the stage of the PEO process, which affects the microstructure of the coatings, and the corrosion performance. Coating thickness and phase composition did not have any measurable influence on coating corrosion performance, which was mainly controlled by the morphology and microstructure of the coatings. To some degree corrosion performance could be tailored by the processing parameters.

7.1 Introduction

Plasma electrolytic oxidation (PEO) has attracted a lot of interest as a relatively novel surface engineering technology with great potential in different industrial applications. PEO is considered a cost-effective and environmentally friendly coating process mainly focused on the improvement of the wear and corrosion resistance of valve metals including aluminum, magnesium, titanium, zirconium and their alloys [1–5].

The configuration used in the PEO process is similar to conventional anodizing. The sample is immersed in an aqueous electrolyte but compared to anodizing, a much higher potential (400-700 V) is applied during PEO resulting in the formation of many electrical micro-discharges (plasma plum) caused by the localized dielectric breakdown of the growing oxide coating [6,7]. These micro-discharges are discrete and short-lived and play an important role in the formation of the coating phase composition, structure and morphology [8].

The characteristics of PEO coatings could be influenced by applying different processing parameters including the applied power mode, electrolyte composition, deposition time, and substrate chemical composition [9,10]. Prior studies have extensively investigated the effects of processing parameters on the properties of PEO coatings on aluminum alloy substrates. Current operating modes were found to significantly affect the aluminum oxide coating morphology and microstructure. A bipolar pulsed DC mode, as opposed to a unipolar current mode, was found to improve the coating quality and produce denser coatings with enhanced morphology and cross-sectional microstructure [11]. Changing the current mode from unipolar to bipolar was reported to improve the corrosion resistance of a magnesium alloy [12]. The enhanced properties of coatings prepared using the pulsed bipolar current mode were ascribed to the reduced number of strong plasma discharges during the PEO process.

The micro-discharge behaviour and coating growth process are also thought to be changed by the applied duty cycle, frequency and current density, which in turn would determine the composition, microstructure and morphology, as well as mechanical and tribological properties of the PEO coatings [6,8,10,13,14]. Lower duty cycles and higher

frequencies were reported to produce micro-discharges with higher spatial density and lower intensity resulting in a lower concentration of Si on the surface of the coatings, which were composed of mainly γ-Al_2O_3 on aluminum alloy substrates [6]. Application of higher current density and duty cycle generally increase the coating thickness and enhance the $\gamma \rightarrow \alpha$-$Al_2O_3$ phase transformation [8,10].

The electrolyte used in PEO is typically a low concentration alkaline solution free of heavy metals (Cr, Ni, V, etc.) and compared to hard anodizing, where strong acids are employed, is much more environmentally friendly [15]. The wastewater from PEO treatment can also be used to produce value added products, such as zeolite [16]. An extremely wide range of electrolyte compositions has been used for PEO coatings. Electrolytes used in the PEO of Al alloys are typically silicate and phosphate based aqueous solutions with organic and inorganic additives to further improve the properties of the coatings [17,18]. Increasing the sodium silicate content of the electrolyte enhances the growth rate, which may be attributed to the incorporation of more silicate into the coating structure, and promotes the formation of Si-rich species on the coating surface [19]. Increasing the alkali concentration is believed to lead to local dissolution of oxides thus decreasing the coating growth rate [20].

In recent years the effect of different processing parameters on the corrosion behavior of PEO coatings has been investigated. Bajat et al. [21] studied the influence of PEO treatment time on the corrosion stability of oxide coatings on aluminum in sodium tungstate and observed that neither the concentration of tungsten in the coating, nor the coating thickness was the governing factors in the corrosion stability of the coatings. Hussein et al [1] investigated the effect of PEO deposition time and substrate composition on the corrosion resistance of Mg alloys and concluded that surface morphologies, coating thickness and porosity level varied with both treatment time and substrate composition and influenced the corrosion behavior.

Given the multiple processing parameters that affect PEO and the wide range within which they can be varied, it is extremely difficult to find the optimum combination of parameters to achieve the best corrosion resistance. A more systematic approach is

required to determine the role of processing parameters on corrosion if these coatings are to be industrially applied.

The surface morphology and coating microstructure have been found to play a significant role in determining corrosion by influencing the amount and size of defects such as porosity and microcracks in the coatings [1]. The results of our studies discussed in chapter 6 suggested that applying different electrical parameters including frequency, duty cycle and current density affected the voltage-time behavior, and changed the duration and ratio of PEO treatment stages. A correlation was established between surface morphology, microstructure, and the stages within the voltage-time curve. This study presents an investigation of the corrosion behavior of an Al alloy coated in these different PEO stages and investigates the influence of different processing parameters including frequency, duty cycle, current density and time.

7.2 Materials and Methods

7.2.1 Materials

The substrate material used in the present investigation was the 6061-T651 aluminum alloy with a nominal chemical composition of (wt%): 0.40-0.80% Si, 0.70% Fe, 0.15-0.40% Cu, 0.15% Mn, 0.80-1.20% Mg, 0.04-0.35% Cr, 0.25% Zn, 0.15% Ti, and balance Al. Specimens in the shape of coupons with a thickness of 6-8 mm and a diameter of ~30 mm were ground with abrasive papers up to 600 grit, washed in propanol, rinsed with distilled water, and dried.

7.2.2 PEO Coating Process

An alkaline silicate solution (2 g/l KOH, 2 g/l Na_2SiO_3 in distilled water) held in a stainless steel container was used as the electrolyte. Aluminum coupons, connected to the positive output of the power supply, served as the working electrode (anode) and the stainless steel container as the counter electrode (cathode). The coating process was carried out at constant current densities (J) of 10, 15, and 20 A/dm^2 using a unipolar pulsed DC mode with a square waveform applied at different frequencies of 50 and 1000 Hz. Two duty cycles (D_t) of 20% and 80% were used. The temperature of the electrolyte

was maintained between 20 and 30 °C throughout the coating process using a heat exchanger. Samples were coated for 30 min. The PEO process parameters and sample codes used in this study are listed in Table 7.1.

Table 7.1- PEO process parameters and sample codes for coatings deposited on 6061 aluminum alloy substrates.

Sample code	Frequency (Hz)	D_t (%)	* : J (A/dm^2)
S12-*	1000	20	10, 15, 20
S18-*	1000	80	
S52-*	50	20	
S58-*	50	80	

7.2.3 Coating Characterization

Coating thickness was evaluated using an Eddy current gauge. Twenty measurements were taken on each coated sample and the average coating thickness and the statistical error calculated. Surface morphologies of the coatings were examined using a Hitachi S-3500N scanning electron microscope (SEM).

7.2.4 Electrochemical Experiments

Linear polarization resistance (LPR) and electrochemical impedance spectroscopy (EIS) measurements were carried out at room temperature in a 3.5 wt.% NaCl solution.

Measurements were made after allowing the sample to stabilize at the corrosion potential (E_{corr}) for 2 h. A standard three-electrode cell arrangement was used with the coated samples serving as the working electrode, with a platinum plate as the counter electrode, and a saturated calomel reference electrode (SCE). The cell was housed inside a Faraday cage to reduce electrical noise from external sources. Electrochemical measurements were made using a 1287 Solartron potentiostat and a Solartron 1255B frequency response analyzer connected to a computer equipped with Corrware software.

An electrode is polarized when its potential is forced away from its value at corrosion potential (E_{corr}). Polarization of an electrode causes current to flow due to electrochemical reactions it induces at the electrode surface. Many investigators have experimentally observed that the applied current density is a linear function of the electrode potential within a few millivolts of polarization from $E_{corr.}$ In the LPR measurement method, an overvoltage with respect to E_{corr} as a reference point is applied to the sample and the corrosion current is recorded. Polarization resistance (R_p) is then calculated from the overvoltage versus applied current plot.

Electrochemical impedance is measured by applying a sinusoidal AC potential to an electrochemical cell and then measuring the current through the cell. The EIS data is then analyzed by fitting it to an equivalent circuit model consisting of different common electrical elements such as resistors and capacitors and values for various elements of the equivalent circuit are obtained. To be useful, the elements in the model should have a basis in the physical electrochemistry of the sample under study.

Polarization resistance (R_p) values were determined by scanning the potential over a range of ±0.02 V with respect to E_{corr} at a sweep rate of 1.0 mV/s. EIS data were obtained using a sinusoidal input potential with an amplitude of ±10 mV with respect to E_{corr} over the frequency range of 10^{-1}-10^{3} Hz. EIS data were analyzed by fitting to an appropriate electrical equivalent circuit using ZView electrochemical analysis software. All electrochemical experiments were repeated three times to verify their reproducibility.

7.3 Results and Discussion

7.3.1 Voltage-time Response and Corrosion Properties

The electrochemical properties of PEO coatings prepared using different electrical parameters were investigated by EIS and LPR. EIS can provide useful information on the corrosion performance of the PEO coatings and on the resistance of the aluminum oxide coating to water and ionic transport [22].

PEO coatings may be comprised of up to three layers, depending on the processing conditions employed; a thin barrier layer close to the substrate, an intermediate or

functional layer with relatively low porosity, and a porous, loose outer layer [17,23]. The barrier layer is thought to be the major contributor to corrosion protection while the functional layer has high hardness, depending on the processing conditions and the substrate used, and can provide protection against wear [24]. PEO coatings produced under the conditions used in this study were previously (Chapter 6) verified to consist of two layers, the barrier and the functional layers with a patchy third outer loose layer on some samples coated at higher current densities.

Nyquist plots recorded on Al alloy substrates coated at 1000 Hz and 50 Hz are presented in Figure 7.1 and Figure 7.2, respectively. As commonly observed [21,25–27], the spectra exhibit two time constants, representative of the dual layer coatings [28]. The high frequency time constant (CPE1-R1) is attributed to the functional layer, and the second lower frequency time constant (CPE2-R2) to the inner barrier layer, Figure 7.1 and Figure 7.2.

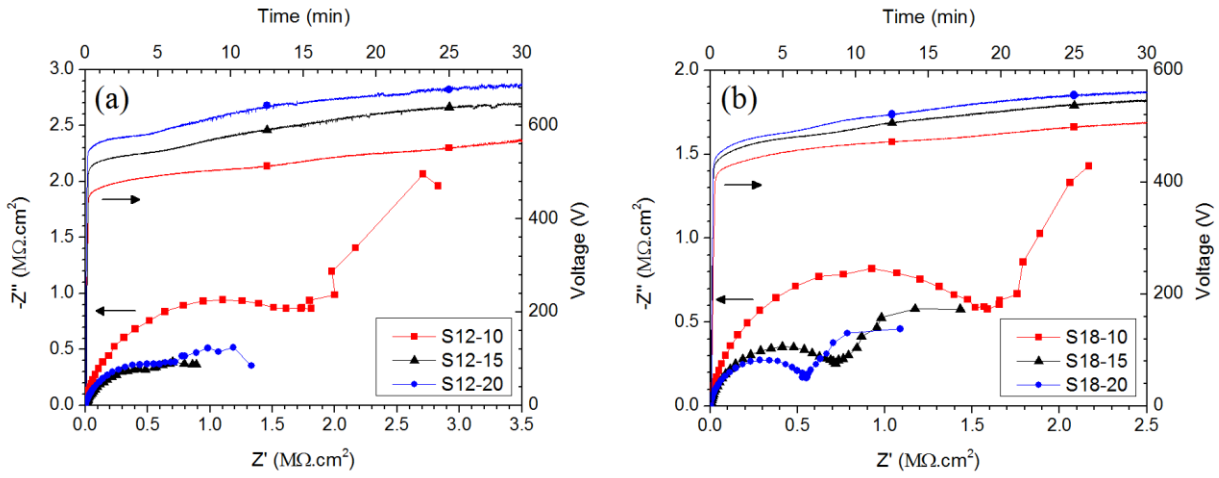

Figure 7.1-Voltage-time curves and Nyquist plots for PEO coatings on 6061 Al alloy substrates prepared using different electrical parameters; (a) S12-* samples, (b) S18-* samples (Table 7.1).

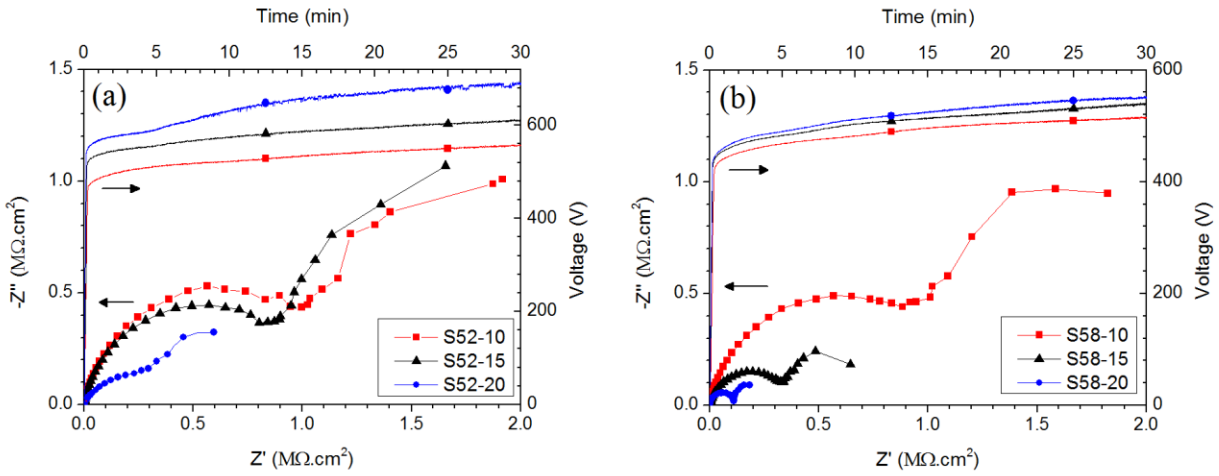

Figure 7.2-Voltage-time curves and Nyquist plots for PEO coatings on 6061 Al alloy substrates prepared using different electrical parameters; (a) S52-* samples, (b) S58-* samples (Table 7.1).

EIS data is commonly analyzed by fitting it to an equivalent electrical circuit model consisting of different common electrical elements. The impedance data in this study can be interpreted in terms of the demonstrated structure of PEO coatings on the 6061 Al alloy [6] and on previous studies on the corrosion resistance of PEO coatings using the equivalent circuit presented in Figure 7.3 [28–32].

The spectra were fitted to this circuit using non-linear least squares analysis software. In this circuit, R_s represents the solution resistance between the PEO-coated sample (working electrode) and the reference electrode. The value of R_s depends primarily on the geometry of the electrochemical cell and the conductivity of the test solution and the values obtained from the fitted spectra were consistently small (<100 $\Omega.cm^2$).

In the equivalent circuit in Figure 7.3, R1 represents the resistance of the pores and defects, such as the discharge channels in the outer functional layer of the PEO coating and is in parallel with a constant phase element, CPE1. The use of the more general constant phase element (CPE) to represent the capacitance of this functional layer yields a better fit of the experimental data [27,28].

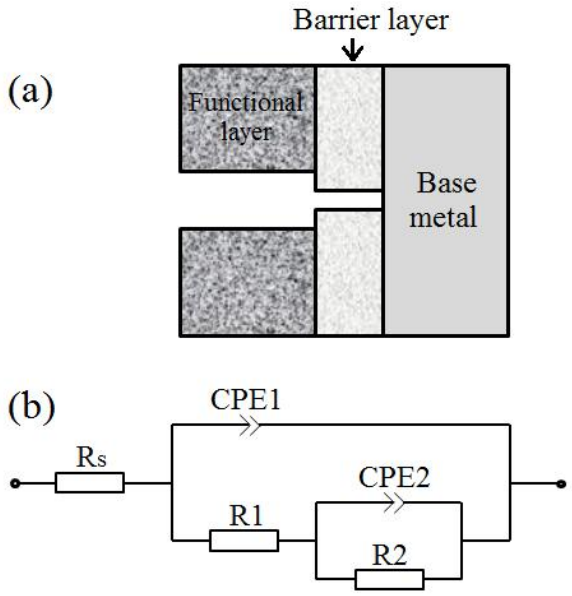

Figure 7.3- Schematic representation of PEO-coated 6061 Al alloy (a); and the equivalent circuit (b) used to model the EIS data recorded in 3.5 wt% NaCl solution.

The impedance of a CPE can be expressed by the following equation:

$$Z_{CPE} = 1/[Q(j\omega)^n] \quad (7.1)$$

in which Q is the CPE constant, j is the imaginary unit ($\sqrt{-1}$), ω is the angular frequency (rad/s) of the sine wave defined as $\omega=2\pi f$, f is the frequency in Hz, and n is an exponent representing the physical meaning of the CPE and ranges between 0 and 1. A value of zero for n implies pure resistance and a value of 1 (n=1) pure capacitance. Values of n in the range $0.25< n <0.5$ may indicate an impedance associated with mass transport, i.e., a Warburg impedance. Deviation of n from these values indicates the non-ideality of the system [1,28]. R2 and CPE2 represent the resistance and constant phase element for the barrier layer, respectively. Given the patchy loose nature of the porous outer layer, it is unlikely to influence the impedance of the coating and is not represented by elements in the electrical equivalent circuit.

The values of the circuit elements obtained from fits to the spectra are summarized in Table 7.2. The chi-squared (χ^2) values were in the range 3×10^{-4} to 1×10^{-3} indicating good agreement between the experimental data and equivalent circuit fits. The exponent

n for the two CPEs was generally > 0.85 for CPE1 and commonly close to 1 for CPE2 confirming the generally capacitative behaviour of the two layers.

The E_{corr} values obtained on the coated samples, measured prior to LPR (R_p) measurements, were in the range -773 to -732 mV compared to a value of -745 mV on an uncoated sample. For a coherent insulating PEO coating a much more positive E_{corr} would have been expected. The similarity in E_{corr} values between coated and uncoated samples indicates that E_{corr} is established at the aluminum substrate surface. The R_p values from the LPR measurements are in generally good agreement with R_P values obtained from EIS measurements (R_1 + R_2) confirming the validity of the latter values despite the limited amount of low frequency data. One of the reasons the R_p values obtained from the two methods are different is that in the Nyquist plots in EIS, R_2 is extrapolated by fitting the second semi circle in the low frequency range and since there are not many data points in this region, the approximation is not very accurate.

Table 7.2- Linear polarization resistance (R_P) values and the values of parameters obtained from fitted EIS plots for PEO coatings on the 6061 Al alloy treated for 30 min under different electrical conditions (Table 7.1).

Sample	CPE1-Q ($\mu F/cm^2\ s^{n-1}$)	CPE1 -n	R1 ($M\Omega.cm^2$)	CPE2-Q ($\mu F/cm^2\ s^{n-1}$)	CPE2 -n	R2 ($M\Omega.cm^2$)	* R_p ($M\Omega.cm^2$)
Bare Al	-	-	-	-	-	-	0.021
S12-10	0.046	0.90	2.181	0.622	~1	3.713	3.114
S12-15	0.347	0.79	0.882	3.241	~1	0.374	1.058
S12-20	0.174	0.83	0.989	1.729	~1	1.004	1.305
S18-10	0.036	0.93	1.788	0.953	0.99	3.836	4.281
S18-15	0.063	0.88	0.837	1.341	~1	0.885	1.288
S18-20	0.071	0.92	0.628	2.063	~1	0.631	0.841
S52-10	0.742	0.89	1.253	1.009	~1	1.374	1.536
S52-15	0.076	0.86	1.881	0.510	0.99	2.817	2.678
S52-20	0.374	0.72	0.360	2.330	0.84	0.774	0.615
S58-10	0.078	0.88	1.165	1.037	~1	1.545	1.615
S58-15	0.118	0.86	0.375	0.329	~1	0.348	0.791
S58-20	0.169	0.93	0.123	12.887	~1	0.132	0.354

* Extracted from linear polarization test results.

The R_p values are plotted in Figure 7.5 for the various conditions used in producing the coatings. The average R_p value for the untreated alloy was 0.021 MΩ.cm^2, while for the S18-10 sample the maximum average R_p value was 4.28 MΩ.cm^2 indicating a nearly 200-fold improvement in corrosion resistance. The parameter values obtained by fitting the EIS spectra show the resistance of the inner barrier layer, R_2, is generally higher than that of the outer functional layer, R_1, indicating that it contributes most to the overall coating corrosion resistance. The higher corrosion resistance properties of the barrier layer compared to the outer functional layer have been previously reported [21,29,33].

The voltage-time response curves and Nyquist plots for different groups of samples coated using different electrical parameters are presented together in Figure 7.1 and Figure 7.2. During the PEO process, up to four stages can be observed in the voltage-time curves. A schematic PEO voltage-time response curve is presented in Figure 7.4. During stage 1 which is similar to conventional anodic oxidation, the voltage increases rapidly within a short time as the result of electrochemical formation of aluminum oxide on the substrate. At the beginning of stage 2, the breakdown voltage is reached and white sparks, distributed uniformly on the metal surface, appear. The slope of the voltage –time curve decreases substantially and intensive gas liberation is observed on the surface of the sample. In stage 3, the rate of voltage change increases slightly compared to stage 2, and the micro-discharges become more intense. In the final stage (4) , the voltage becomes independent of time and the sparks become even stronger and slower moving but their population decreases and they become more widely spaced [34–37].

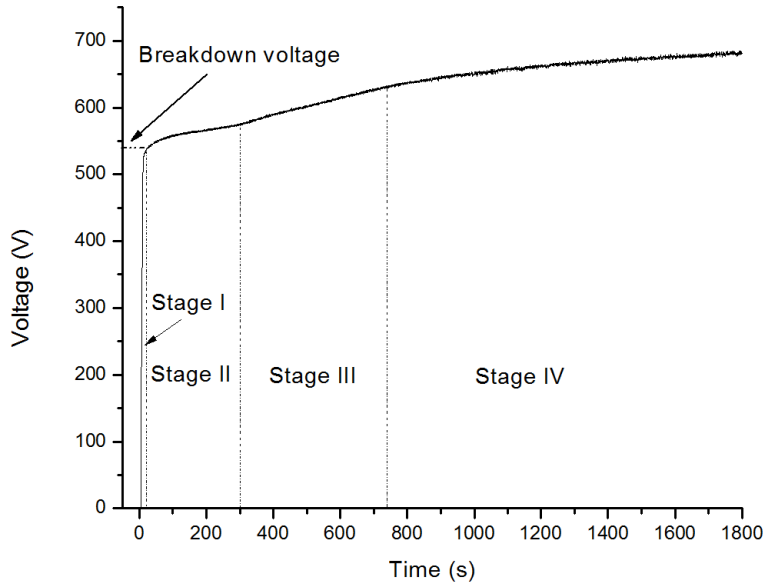

Figure 7.4- Schematic of a voltage-time response curve containing the four stages observed during the PEO process.

The characteristics of the electrical micro-discharges such as their population, size and color as well as the coating surface morphology, microstructure, density and phase content are all affected by the stage of the PEO process [6,10,38]. The results of our study (Chapter 6) on PEO coatings on the 6061 Al alloy, prepared under similar conditions to those employed here suggested a correlation existed between the stage of the PEO process and the microstructure and morphology of the coating. Applying different electrical parameters changed the duration of the PEO stages in the voltage-time response curve and affected the coating growth rate, surface morphology, microstructure and microhardness of the coatings.

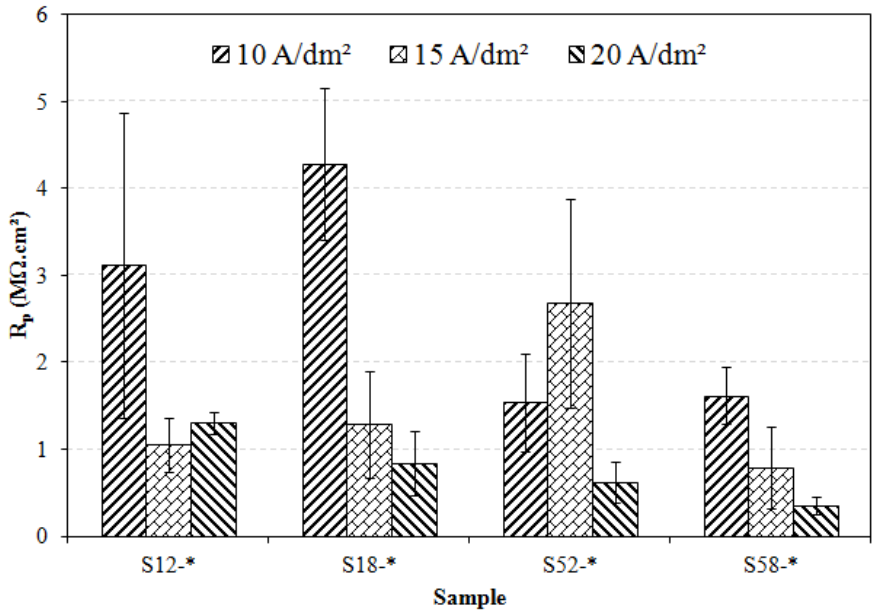

Figure 7.5- Polarization resistance (R_p) values calculated from LPR experiments on PEO coatings grown using different electrical parameters.

From Table 7.2 it can be appreciated that for the S12 series the coating formed at the lowest current density (10 A/dm^2) has the highest overall resistance (R_p) comprised of high barrier (R_1) and functional (R_2) layer resistances. Increasing the current density (S12-15 and S12-20) decreased the resistances by approximately similar values (Table 7.2, Figure 7.5). Inspection of the voltage-time curves in Figure 7.1-a shows that, after the 30 min coating period, S12-10 was at the beginning of stage 4 while S12-15 and S12-20 were both in stage 4. A similar trend with current density is observed for the S18 series, Table 7.2 and Figure 7.1-b, the layer resistances, R_1 and R_2, both being largest for the coating formed at the lowest current density.

Consistent with the S12 series, the voltage-time response, Figure 7.1-b, shows the high resistance S18-10 coating was in stage 3, while the lower resistance coatings, S18-15 and S18-20, were in stage 4. It is also worth noting that the S18-20 coating with the lowest resistances spent more time in stage 4 than the S18-15 with a slightly higher coating resistance. Again similar trends are observed for the S52-* and S58-* series. The influence of the time spent in stage 4 is apparent, as illustrated by a comparison of S58-

15 and S58-20, the latter exhibiting a less resistive coating having spent a longer period of time in stage 4.

7.3.2 Microstructure and Thickness of Coatings

The SEM micrographs of the free surfaces of the S12-* and S18-* samples, produced under different electrical conditions are presented in Figure 7.6. The coating surfaces generally exhibit two types of morphology: (i) a significant portion of the surface is occupied by craters; volcano-like microstructures formed by individual micro-discharge events, (ii) and a nodular structure consisting of hollow particles. The cratered areas are mainly composed of oxidized aluminum and contain discharge channels in the form of central holes through which the molten material flowed out of the channel to rapidly solidify and create distinctive boundaries of solidified pools [6,39,40]. The results of a previous study [40] showed that the average size of the discharge channels, as well as the diameters of the craters, increased gradually as the treatment time was extended from1 to 30 min.

The average thicknesses of the coatings produced using different electrical parameters are illustrated in Figure 7.7. In each group of samples, increasing the current density at constant frequency and duty cycle resulted in a thicker coating. A detailed discussion on the effect of electrical parameters on the coating thickness and cross-sections has been provided in Chapter 6.

The results indicate that increasing the thickness of the oxide coatings does not necessarily improve the corrosion performance of the samples. All samples coated at a current density of 20 A/dm^2 were thicker than samples coated at lower current densities (Figure 7.7) although, as shown above, their corrosion performance was generally worse.

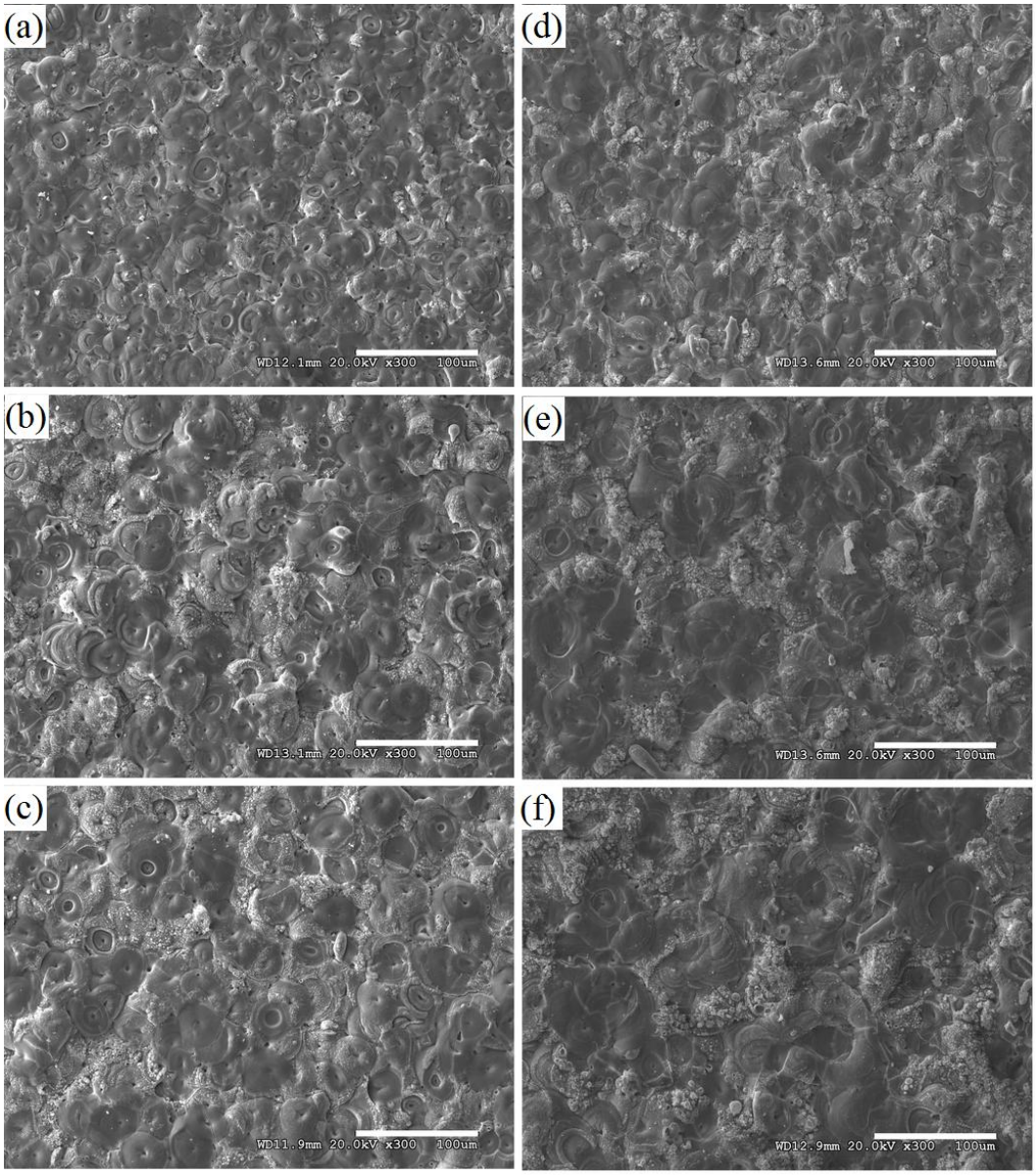

Figure 7.6- SEM micrographs of the free surfaces of PEO coatings on 6061 Al alloys formed using different process parameters: (a) S12-10; (b) S12-15; (c) S12-20; (d) S18-10; (e) S18-15; and (f) S18-20 (Table 7.1).

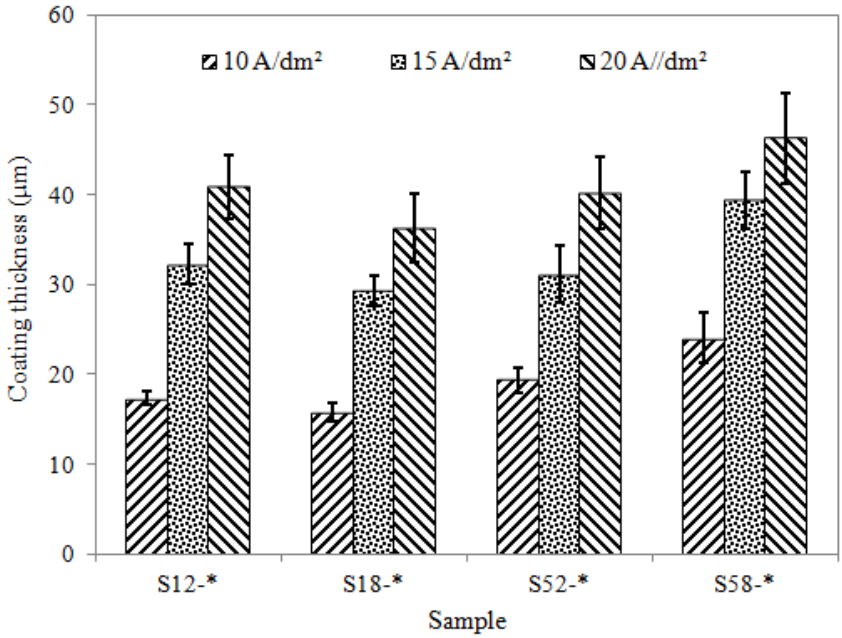

Figure 7.7- Thickness of PEO coatings on 6061 Al alloy samples coated using different electrical parameters.

However, examination of the surface morphologies of the samples, Figure 7.6, suggests a correlation between the microstructure of the coating and its corrosion performance. The coatings with the best corrosion resistance, S12-10 and S18-10, possess a large number of small craters, Figure 7.6 (a and d), while increasing the current density throughout these two series, S12-* (Figure 7.6, a and c) and S18-* (Figure 7.6, d and f), resulted in a decreased number of craters but an increase in their size. The size of the craters reflects the strength of the microarc discharge, and the holes in the center of these cratered regions suggest they were formed as a result of these strong discharges. A possibility is that the holes penetrate deep in to the coating allowing access of the corrosive solution to the alloy surface [1].

Micro-discharges are generated by dielectric breakdown through weak sites in the PEO coating with the number of weak sites being reduced as the coating is thickened by growth at a higher current density and/or for longer deposition times. The increased size of the craters in thicker coatings, which is a reflection of stronger micro-discharges, could

be ascribed to a reduced number of discharge sites through which current is able to pass. Under galvanostatic conditions this would lead to a higher current density at these locations. As the coating thickens, the diameter of the discharge channels increases because a higher energy is required for the current to pass through the thicker coating [41,42].

The characteristics of micro-discharges, which play a key role in the formation of the oxide coatings, vary during the different stages of the PEO process [43], and, as shown here, changes in electrical parameters can change the duration of the stages.

The coating resistance (corrosion) measurements showed that samples coated at the end of stage 3 and beginning of stage 4 generally demonstrated the highest corrosion resistance. This would be consistent with the surface morphology which consisted of small craters. Samples whose voltage-time curves had a longer stage 4 also had a lower corrosion resistance which can be related to the increased size of the discharge channels and access of the corrosive solution to deeper locations.

Re-examination of previous results on the influence of electrical growth parameters on the composition and transformation of phases within the coating [10] confirms that the phase composition does not play any significant role in coating corrosion performance. Despite the fact that the PEO coatings grown in this study contained different crystalline phases and had different thicknesses, coating microstructure and morphology seem to be the main factors in controlling the corrosion performance of the coatings.

7.3.3 Influence of PEO Deposition Time

To confirm the relationship between corrosion performance and the coating growth stage, a series of coatings were grown for different deposition times using the same electrical growth parameters. Based on the voltage-time response curve for the S12-15 set of conditions (Table 7.1), coatings were grown for 6 min (end of stage 2), 15 min (end of stage 3) as shown in Figure 7.8. The coating grown for the full 30 min was in stage 4. The Nyquist plots recorded on these three coatings are also shown in Figure 7.8 and the parameters determined from fits to the electrical equivalent circuit in Figure 7.3 are listed

in Table 7.3. Also shown in Table 7.3 are the R_p values obtained from LPR measurements.

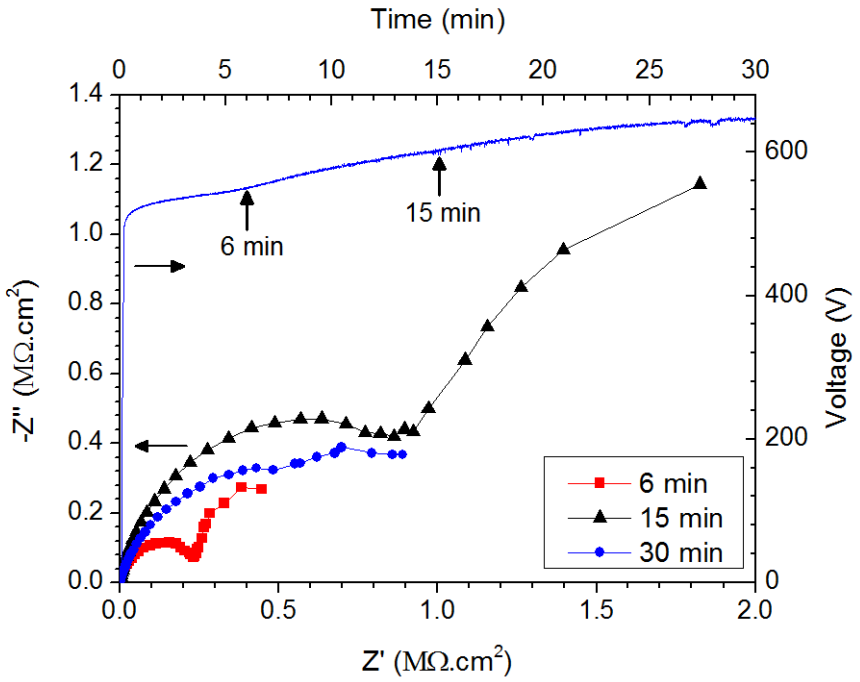

Figure 7.8- Nyquist plots recorded after 2 h exposure to 3.5% NaCl for various growth periods, two of which are indicated on the voltage-time response for the S12-15 set of electrical conditions (Table 7.1).

Table 7.3- Polarization resistance (R_p) values and electrical parameters from fits of EIS plots for coatings on 6061 Al alloys after 2 h of exposure to 3.5 wt% NaCl.

Sample	CPE1-Q ($\mu F/cm^2\ s^{n-1}$)	CPE1-n	R1 ($M\Omega.cm^2$)	CPE2-Q ($\mu F/cm^2\ s^{n-1}$)	CPE2-n	R2 ($M\Omega.cm^2$)	* R_p ($M\Omega.cm^2$)
S12-15-6min	0.202	0.84	0.297	4.260	~1	0.403	0.460
S12-15-15min	0.065	0.87	1.116	0.734	~1	1.915	1.859
S12-15-30min	0.347	0.79	0.882	3.241	~1	0.374	1.058

* Extracted from linear polarization test results.

These results show that the sample coated for 6 min (i.e., to the end of stage 2, Figure 7.8) exhibited the lowest resistances (R_1 and R_2) while that coated for 15 min (i.e., to the end of stage 3) had the highest resistances. The average coating thickness after 6, 15, and 30 min was measured to be 3.2, 12.1 and 32.2 µm, respectively, confirming that the coating thickness was not a key factor determining the corrosion resistance.

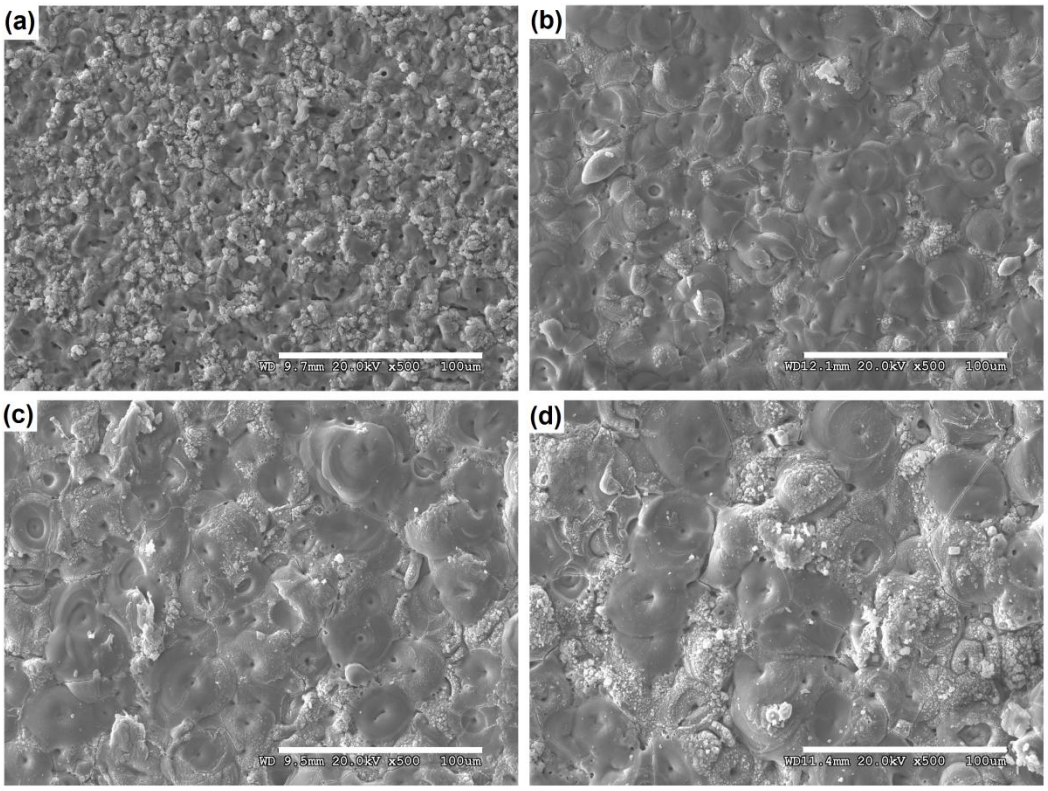

Figure 7.9- SEM micrographs of the free surface of S12-20 samples (Table 7.1) coated at different processing times and stages: (a) 4 min, stage 2; (b) 13 min, stage 3; (c) 20 min, beginning of stage 4; (d) 30 min, stage 4.

To confirm whether the surface morphology, and especially the properties of the craters formed, was the key feature controlling the corrosion resistance, coatings were grown for various times ranging from 4 to 30 min using the S12-20 set of electrical parameters (Table 7.1). The SEM micrographs for four of these coatings are shown in Figure 7.9. The voltage-time response curve and measured radii of the craters are plotted in

Figure 7.10. The size of the craters was determined from the SEM images using image analysis software.

The coating formed for 4 min contains many open micropores (Figure 7.9-a), and was in stage 2 when growth was stopped. After 13 min of growth, the coating was in stage 3. No open micropores appeared visible on the surface of the coating (Figure 7.9-b) and there were many small craters. When the growth time was extended to 20 min the sample was at the beginning of stage 4 with bigger craters and some areas of the surface were covered by the nodular structure. After 30 min, when the coating is in stage 4, the craters are significantly bigger and the nodular structure occupied a larger area of the surface.

The average radius of the craters on the PEO coatings for sample S12-20, coated for 6 min, was 7.3 µm which increased to 15.4 µm after 30 min, implying that micro-discharges became stronger with increasing coating process time.

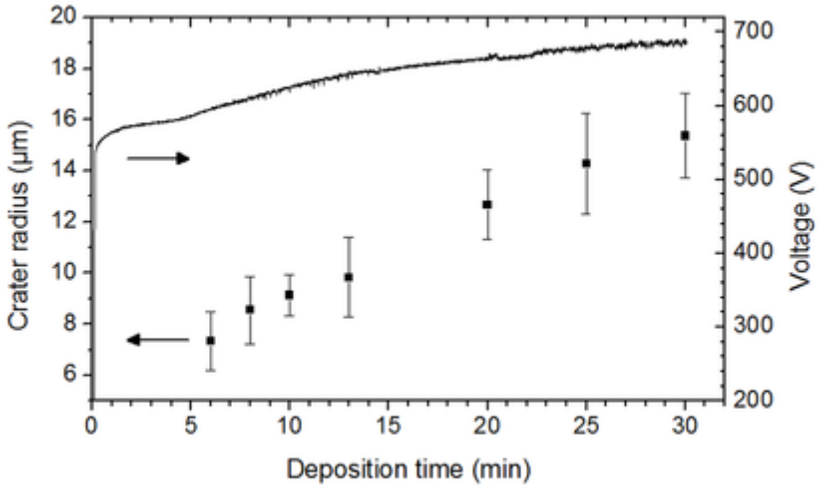

Figure 7.10-Variation in crater size of the PEO coatings on 6061 Al alloy substrate as a function of deposition time in sample S12-20 (Table 7.1). The voltage-time response for these conditions is also shown.

These results show that the poor corrosion resistance of coatings formed in Stage 2 can be attributed to the large number of open micropores present in the coating. The improved (corrosion) resistance observed when the coating enters Stage 3 can be

attributed to the presence of small craters with tight discharge channels. However, if the coating is completed in Stage 4 the presence of large craters with wider discharge channels accounts for the decreased corrosion resistance.

7.4 Summary and Conclusions

PEO coatings were produced on the 6061 aluminum alloy using different processing parameters under galvanostatic control. The corrosion performance of the coatings was evaluated using EIS and LPR.

The primary influence on corrosion performance was the stage within which the coatings were produced. This controlled the morphology of the coatings and was determined by the process parameters.

The coating thickness and phase composition were found not to have any significant influence on corrosion resistance.

The surface morphologies of samples coated in stage 2 contained many open micro-pores resulting in the very poor corrosion resistance.

In stage 3, the coating surface was composed of small craters with very small discharge channels and the corrosion resistance improved.

In stage 4 the size of the craters and discharge channels increased, thus negatively affecting the corrosion protection of coatings.

Samples coated at the end of stage 3 and the beginning of stage 4 generally demonstrated better corrosion properties.

7.5 References

[1] R.O. Hussein, D.O. Northwood, X. Nie, The effect of processing parameters and substrate composition on the corrosion resistance of plasma electrolytic oxidation (PEO) coated magnesium alloys, Surf. Coatings Technol. 237 (2013) 357–368.

[2] X. Nie, E.I. Meletis, J.C. Jiang, A. Leyland, A.L. Yerokhin, A. Matthews, Abrasive wear/corrosion properties and TEM analysis of Al2O3 coatings fabricated using plasma electrolysis, Surf. Coat. Technol. 149 (2002) 245–251.

[3] D. Sreekanth, N. Rameshbabu, K. Venkateswarlu, Effect of various additives on morphology and corrosion behavior of ceramic coatings developed on AZ31 magnesium alloy by plasma electrolytic oxidation, Ceram. Int. 38 (2012) 4607–4615.

[4] M. Shokouhfar, C. Dehghanian, M. Montazeri, A. Baradaran, Preparation of ceramic coating on Ti substrate by plasma electrolytic oxidation in different electrolytes and evaluation of its corrosion resistance: Part II, Appl. Surf. Sci. 258 (2012) 2416–2423.

[5] Y. Cheng, E. Matykina, R. Arrabal, P. Skeldon, G.E. Thompson, Plasma electrolytic oxidation and corrosion protection of Zircaloy-4, Surf. Coatings Technol. 206 (2012) 3230–3239.

[6] V. Dehnavi, B.L. Luan, D.W. Shoesmith, X.Y. Liu, S. Rohani, Effect of duty cycle and applied current frequency on plasma electrolytic oxidation (PEO) coating growth behavior, Surf. Coatings Technol. 226 (2013) 100–107.

[7] C.S. Dunleavy, I.O. Golosnoy, J. A. Curran, T.W. Clyne, Characterisation of discharge events during plasma electrolytic oxidation, Surf. Coatings Technol. 203 (2009) 3410–3419.

[8] R.H.U. Khan, A. Yerokhin, X. Li, H. Dong, A. Matthews, Surface characterisation of DC plasma electrolytic oxidation treated 6082 aluminium alloy: Effect of current density and electrolyte concentration, Surf. Coatings Technol. 205 (2010) 1679–1688.

[9] D.S. Doolabi, M. Ehteshamzadeh, S.M.M. Mirhosseini, Effect of NaOH on the Structure and Corrosion Performance of Alumina and Silica PEO Coatings on Aluminum, J. Mater. Eng. Perform. 21 (2012) 2195–2202.

[10] V. Dehnavi, X.Y. Liu, B.L. Luan, D.W. Shoesmith, S. Rohani, Phase Transformation in Plasma Electrolytic Oxidation Coatings on 6061 Aluminum Alloy, Surf. Coatings Technol. 251 (2014) 106-114.

[11] R.O. Hussein, X. Nie, D.O. Northwood, Influence of process parameters on electrolytic plasma discharging behaviour and aluminum oxide coating microstructure, Surf. Coatings Technol. 205 (2010) 1659–1667.

[12] R.O. Hussein, P. Zhang, X. Nie, Y. Xia, D.O. Northwood, The effect of current mode and discharge type on the corrosion resistance of plasma electrolytic oxidation (PEO) coated magnesium alloy AJ62, Surf. Coatings Technol. 206 (2011) 1990–1997.

[13] H. Wu, J. Wang, B.B. Long, Z. Jin, W. Naidan, F. Yu, et al., Ultra-hard ceramic coatings fabricated through microarc oxidation on aluminium alloy, Appl. Surf. Sci. 252 (2005) 1545–1552.

[14] R.O. Hussein, X. Nie, D.O. Northwood, A. Yerokhin, A. Matthews, Spectroscopic study of electrolytic plasma and discharging behaviour during the plasma electrolytic oxidation (PEO) process, J. Phys. D. Appl. Phys. 43 (2010) 105203–105216.

[15] J.M. Wheeler, J. a. Curran, S. Shrestha, Microstructure and multi-scale mechanical behavior of hard anodized and plasma electrolytic oxidation (PEO) coatings on aluminum alloy 5052, Surf. Coatings Technol. 207 (2012) 480–488.

[16] J. Behin, S.S. Bukhari, V. Dehnavi, H. Kazemian, S. Rohani, Using coal fly ash and wastewater for microwave synthesis of LTA zeolite, Chem. Eng. Technol. 37 (2014) 1-10.

[17] F.C. Walsh, C.T.J. Low, R.J.K. Wood, K.T. Stevens, J. Archer, A.R. Poeton, et al., Plasma electrolytic oxidation (PEO) for production of anodised coatings on lightweight metal (Al, Mg, Ti) alloys, Trans. Inst. Met. Finish. 87 (2009) 122–135.

[18] Y. Liu, J. Xu, Y. Gao, Y. Yuan, C. Gao, Influences of Additive on the Formation and Corrosion Resistance of Micro-arc Oxidation Ceramic Coatings on Aluminum Alloy, Phys. Procedia. 32 (2012) 107–112.

[19] A.A. Voevodin, A.L. Yerokhin, V. V. Lyubimov, M.S. Donley, J.S. Zabinski, Characterization of wear protective Al-Si-O coatings forrned on Al-based alloys by micro-arc discharge treatment, Surf. Coat. Technol. 86-87 (1996) 516–521.

[20] A.L. Yerokhin, A.A. Voevodin, V. V. Lyubimov, J. Zabinski, M. Donley, Plasma electrolytic fabrication of oxide ceramic surface layers for tribotechnical purposes on aluminium alloys, Surf. Coat. Technol. 110 (1998) 140–146.

[21] J.B. Bajat, R. Vasilić, S. Stojadinović, V. Mišković-Stanković, Corrosion Stability of Oxide Coatings Formed by Plasma Electrolytic Oxidation of Aluminum : Optimization of Process Time, Corrosion. 69 (2013) 693–702.

[22] R.C. Barik, J.A. Wharton, R.J.K. Wood, K.R. Stokes, R.L. Jones, Corrosion, erosion and erosion–corrosion performance of plasma electrolytic oxidation (PEO) deposited Al2O3 coatings, Surf. Coatings Technol. 199 (2005) 158–167.

[23] E. Matykina, R. Arrabal, D.J. Scurr, A. Baron, P. Skeldon, G.E. Thompson, Investigation of the mechanism of plasma electrolytic oxidation of aluminium using 18O tracer, Corros. Sci. 52 (2010) 1070–1076.

[24] E. Matykina, R. Arrabal, P. Skeldon, G.E. Thompson, Investigation of the growth processes of coatings formed by AC plasma electrolytic oxidation of aluminium, Electrochim. Acta. 54 (2009) 6767–6778.

[25] L. Wen, Y. Wang, Y. Zhou, L. Guo, J.-H. Ouyang, Microstructure and corrosion resistance of modified 2024 Al alloy using surface mechanical attrition treatment combined with microarc oxidation process, Corros. Sci. 53 (2011) 473–480.

[26] C.E. Barchiche, D. Veys-Renaux, E. Rocca, A better understanding of PEO on Mg alloys by using a simple galvanostatic electrical regime in a KOH–KF–Na3PO4 electrolyte, Surf. Coatings Technol. 205 (2011) 4243–4248.

[27] N.M. Alanazi, A. Leyland, A. L. Yerokhin, A. Matthews, Substitution of hexavalent chromate conversion treatment with a plasma electrolytic oxidation process to improve the corrosion properties of ion vapour deposited Al-Mg coatings, Surf. Coatings Technol. 205 (2010) 1750–1756.

[28] M. Shokouhfar, C. Dehghanian, A. Baradaran, Preparation of ceramic coating on Ti substrate by Plasma electrolytic oxidation in different electrolytes and evaluation of its corrosion resistance, Appl. Surf. Sci. 257 (2011) 2617–2624.

[29] A. Venugopal, R. Panda, S. Manwatkar, K. Sreekumar, L.R. Krishna, G. Sundararajan, Effect of micro arc oxidation treatment on localized corrosion behaviour of AA7075 aluminum alloy in 3.5% NaCl solution, Trans. Nonferrous Met. Soc. China. 22 (2012) 700–710.

[30] X. Zhang, Y. Zhang, L. Chang, Z. Jiang, Z. Yao, X. Liu, Effects of frequency on growth process of plasma electrolytic oxidation coating, Mater. Chem. Phys. 132 (2012) 909–915.

[31] H. Guo, Y. Ma, J. Wang, Y. Wang, H. Dong, Y. Hao, Corrosion behavior of micro-arc oxidation coating on AZ91D magnesium alloy in NaCl solutions with different concentrations, Trans. Nonferrous Met. Soc. China. 22 (2012) 1786–1793.

[32] J. Lee, Y. Kim, W. Chung, Effect of Ar bubbling during plasma electrolytic oxidation of AZ31B magnesium alloy in silicate electrolyte, Appl. Surf. Sci. 259 (2012) 454–459.

[33] M. Chen, S. Liu, J. Li, N. Cheng, X. Zhang, Improvement to corrosion resistance of MAO coated 2519 aluminum alloy by formation of polypropylene film on its surface, Surf. Coatings Technol. 232 (2013) 674–679.

[34] A.L. Yerokhin, L.O. Snizhko, N.L. Gurevina, A. Leyland, A. Pilkington, A. Matthews, Discharge characterization in plasma electrolytic oxidation of aluminium, J. Phys. D. Appl. Phys. 36 (2003) 2110–2120.

[35] F. Xu, Y. Xia, G. Li, The mechanism of PEO process on Al–Si alloys with the bulk primary silicon, Appl. Surf. Sci. 255 (2009) 9531–9538.

[36] Y. Guan, Y. Xia, G. Li, Growth mechanism and corrosion behavior of ceramic coatings on aluminum produced by autocontrol AC pulse PEO, Surf. Coatings Technol. 202 (2008) 4602–4612.

[37] H.M. Nykyforchyn, M.D. Klapkiv, V.M. Posuvailo, Properties of synthesised oxide-ceramic coatings in electrolyte plasma on aluminium alloys, Surf. Coatings Technol. 100-101 (1998) 219–221.

[38] L. Wang, X. Nie, Silicon effects on formation of EPO oxide coatings on aluminum alloys, Thin Solid Films. 494 (2006) 211–218.

[39] M.M.S. Al Bosta, K. Ma, H. Chien, M.M.S. Al Bosta, The effect of MAO processing time on surface properties and low temperature infrared emissivity of ceramic coating on aluminium 6061 alloy, Infrared Phys. Technol. 60 (2013) 323–334.

[40] G. Sundararajan, L. Rama Krishna, Mechanisms underlying the formation of thick alumina coatings through the MAO coating technology, Surf. Coatings Technol. 167 (2003) 269–277.

[41] S. Moon, Y. Jeong, Generation mechanism of microdischarges during plasma electrolytic oxidation of Al in aqueous solutions, Corros. Sci. 51 (2009) 1506–1512.

[42] S. Stojadinovic, R. Vasilic, I. Belca, M. Petkovic, B. Kasalica, Z. Nedic, et al., Characterization of the plasma electrolytic oxidation of aluminium in sodium tungstate, Corros. Sci. 52 (2010) 3258–3265.

[43] Y. Cheng, F. Wu, E. Matykina, P. Skeldon, G.E.E. Thompson, The influences of microdischarge types and silicate on the morphologies and phase compositions of plasma electrolytic oxidation coatings on Zircaloy-2, Corros. Sci. 59 (2012) 307–315.

Chapter 8

Conclusions and Future Work

8.1 Conclusions

The aim of this research was to improve the current understanding and control of the PEO process to produce coatings with enhanced properties mainly for tribological applications. The effect of process parameters, mainly electrical parameters including applied frequency, duty cycle, and current density, on the formation, growth behaviour and properties of PEO coatings on 6061 aluminum alloy substrates was investigated. Samples were coated in an alkaline silicate electrolyte using a unipolar pulsed current regime under galvanostatic conditions. The following conclusions could be drawn from this research:

- Samples coated with different electrical parameters show up to four different stages. During stage 1 the voltage increases rapidly within a short time. At the beginning of stage 2, the breakdown voltage is reached and the slope of the voltage–time curve decreases substantially and intensive gas liberation is observed on the surface of the sample. In stage 3, the rate of voltage change increases slightly compared to stage 2, and the micro-discharges become more intense. In the final stage (4), the sparks become even stronger and slower moving but their population decreases and they become more widely spaced. The voltage-time response of the PEO process can provide readily measurable and useful information about these stages and is an important tool in the study of PEO coatings.

- The surfaces of the coatings in most samples exhibited two distinct regions, cratered regions rich in aluminum, with discharge channels in the center, and some clusters with a nodular structure, rich in silicon. The amount of the nodular structure formed was a function of the process parameters.

- Samples coated in stage 2 showed many micro-pores scattered across the surface area. In samples coated in stage 3, the surface of the coatings was

mainly occupied by a large number of craters. In stage 4, the size of the craters increased while their spatial intensity decreased.

- The results obtained from the characterization techniques showed a clear correlation of the coating microstructure and properties with the voltage-time response of the process.

- It was found that the processing conditions affect the duration and ratio of the PEO stages. Sparking behaviour, coating growth rate, microstructure, and morphology, as well as its characteristics and performance were found to be dependent on the stage of the PEO process.

- The sparking behavior caused by the application of different electrical parameters affected the silicon distribution in the coating. Low duty cycles resulted in a lower concentration of Si on the surface but its more uniform distribution across the coating. This phenomenon could be ascribed to the higher density of sparks at low duty cycles which detaches adsorbed silicon containing species from the surface of the sample and also stronger electric fields which increase the possibility of incorporation of Si rich anions into the coating.

- PEO coatings produced on the 6061 aluminum alloy are mainly composed of γ-Al_2O_3. Depending on the electrical parameters employed, various amounts of α-Al_2O_3, mullite and an amorphous phase were also identified in addition to γ-Al_2O_3.

- Phase distribution and composition in the PEO coatings can be controlled by using different electrical conditions. It was found that increasing the pulse on-time by employing a lower frequency and a higher duty cycle enhanced the $\gamma \rightarrow \alpha$-$Al_2O_3$ phase transformation, resulting in a higher relative content of α-Al_2O_3 in the coatings.

- In samples coated at low frequencies, high current densities, and longer times, mullite was formed in the coatings and its formation was linked to the micro-discharge behaviour. Increasing the duty cycle and lowering the frequency results in longer t_{on} times and the generation of micro-discharges with a lower spatial density but a higher intensity. This lead to a higher concentration of Si rich species on the surface of the PEO coatings which facilitated the formation of mullite.

- Depth profiling of ceramic coatings using glancing angle XRD showed no significant variation in α-Al_2O_3 concentration across the coatings. When present, mullite and amorphous phases were found to be more concentrated near the surface of the coatings.

- The application of higher current densities and longer pulse-on times achieved by employing higher duty cycles and a lower frequency, improved the micro-hardness of the coatings. This was attributed to an enhanced $\gamma \rightarrow \alpha$-$Al_2O_3$ phase transformation resulting in more α-Al_2O_3 in the oxide layer and an increased density of the functional layer due to the reduction of porosity.

- The corrosion performance of the coatings was primarily influenced by the stage within which they were produced. This controlled the morphology of the coatings and was determined by the process parameters. The surface morphologies of samples coated in stage 2 contained many open micro-pores resulting in a very poor corrosion resistance. In stage 3, the coating surface was composed of small craters with very small discharge channels and the corrosion resistance improved. In stage 4 the size of the craters and discharge channels increased, which had a negative effect on the corrosion protection by the coating. Samples coated at the end of stage 3 and the beginning of stage 4 generally demonstrated the best corrosion performance.

- The stability of the electrolyte was found to directly affect the reproducibility and quality of the PEO coatings. The prolonged use of an electrolyte resulted in defective coatings with reduced coating thickness and many open micro-pores, not suitable for many applications.

8.2 Future Work

PEO is gaining increased attention as a promising surface treatment for light alloys in various applications and there remains a significant potential for further research to develop a better understanding and to improve control of the PEO process to yield the desired morphologies and microstructures for specific applications. The following studies would lead to further improvements in the current understanding of PEO.

- The results of this study confirm the correlation between the different PEO stages and the microstructure and properties of coatings on aluminum alloys coated under unipolar pulsed DC mode. Additional studies are required to support these results for coatings produced using alternative current modes, especially bipolar pulsed DC.

- Currently, a wide range of electrolyte compositions is being used in the production of PEO coatings, but there are no established criteria for the choice of electrolyte compositions for different applications. The primary focus of published studies on PEO electrolytes has been on the development and optimization of composition and concentration to achieve desirable coating properties. The results of this research suggest that there is a correlation between the coating microstructure and properties and the stage of the PEO process. Studying the effect of the electrolyte composition on the voltage-time response, mainly the duration and ratio of the various stages, would contribute to the current understanding of the PEO process, namely the choice of the appropriate electrolyte composition for a specific purpose.

- The presence of large pores between the inner and outer layers of coatings has been reported in studies on aluminum and magnesium alloy substrates formed using unipolar pulsed DC current mode. However, this issue has not been addressed in the published literature. Investigating the mechanism of pore formation when using unipolar pulsed DC current can provide useful information about the PEO process.

- Our observations clearly demonstrate the importance of the service life of the electrolyte. Stability of the electrolyte affects the reproducibility and quality of coatings. Optimizing the electrolyte composition for long-term stability is an important research direction.

Appendices

Appendix A: License Agreement with Elsevier Limited

ELSEVIER LICENSE TERMS AND CONDITIONS
Jul 08, 2014

This is a License Agreement between Vahid VD Dehnavi ("You") and Elsevier ("Elsevier") provided by Copyright Clearance Center ("CCC"). The license consists of your order details, the terms and conditions provided by Elsevier, and the payment terms and conditions.

All payments must be made in full to CCC. For payment instructions, please see information listed at the bottom of this form.

Supplier	Elsevier Limited The Boulevard,Langford Lane Kidlington,Oxford,OX5 1GB,UK
Registered Company Number	1982084
Customer name	Vahid VD Dehnavi
Customer address	TEB 472 London, ON N6A 5B9
License number	3424000627711
License date	Jul 08, 2014
Licensed content publisher	Elsevier
Licensed content publication	Surface and Coatings Technology
Licensed content title	Effect of duty cycle and applied current frequency on plasma electrolytic oxidation (PEO) coating growth behavior
Licensed content author	Vahid Dehnavi,Ben Li Luan,David W. Shoesmith,Xing Yang Liu,Sohrab Rohani
Licensed content date	15 July 2013
Licensed content volume number	226
Licensed content issue number	None
Number of pages	8
Start Page	100
End Page	107
Type of Use	reuse in a thesis/dissertation
Portion	full article
Format	electronic
Are you the author of this Elsevier article?	Yes

Will you be translating?	No
Title of your thesis/dissertation	Surface Modification of Aluminum Alloys by Plasma Electrolytic Oxidation
Expected completion date	Aug 2014
Estimated size (number of pages)	200
Elsevier VAT number	GB 494 6272 12
Permissions price	0.00 USD
VAT/Local Sales Tax	0.00 USD / 0.00 GBP
Total	0.00 USD

ELSEVIER LICENSE TERMS AND CONDITIONS

Jul 08, 2014

This is a License Agreement between Vahid VD Dehnavi ("You") and Elsevier ("Elsevier") provided by Copyright Clearance Center ("CCC"). The license consists of your order details, the terms and conditions provided by Elsevier, and the payment terms and conditions.

All payments must be made in full to CCC. For payment instructions, please see information listed at the bottom of this form.

Supplier	Elsevier Limited The Boulevard,Langford Lane Kidlington,Oxford,OX5 1GB,UK
Registered Company Number	1982084
Customer name	Vahid VD Dehnavi
Customer address	TEB 472 London, ON N6A 5B9
License number	3424001043375
License date	Jul 08, 2014
Licensed content publisher	Elsevier
Licensed content publication	Surface and Coatings Technology
Licensed content title	Phase transformation in plasma electrolytic oxidation coatings on 6061 aluminum alloy
Licensed content author	Vahid Dehnavi,Xing Yang Liu,Ben Li Luan,David W. Shoesmith,Sohrab Rohani
Licensed content date	25 July 2014

Licensed content volume number	251
Licensed content issue number	None
Number of pages	9
Start Page	106
End Page	114
Type of Use	reuse in a thesis/dissertation
Portion	full article
Format	electronic
Are you the author of this Elsevier article?	Yes
Will you be translating?	No
Title of your thesis/dissertation	Surface Modification of Aluminum Alloys by Plasma Electrolytic Oxidation
Expected completion date	Aug 2014
Estimated size (number of pages)	200
Elsevier VAT number	GB 494 6272 12
Permissions price	0.00 USD
VAT/Local Sales Tax	0.00 USD / 0.00 GBP
Total	0.00 USD

ELSEVIER LICENSE TERMS AND CONDITIONS

Jul 08, 2014

This is a License Agreement between Vahid VD Dehnavi ("You") and Elsevier ("Elsevier") provided by Copyright Clearance Center ("CCC"). The license consists of your order details, the terms and conditions provided by Elsevier, and the payment terms and conditions.

All payments must be made in full to CCC. For payment instructions, please see information listed at the bottom of this form.

Supplier	Elsevier Limited The Boulevard,Langford Lane Kidlington,Oxford,OX5 1GB,UK
Registered Company Number	1982084
Customer name	Vahid VD Dehnavi
Customer address	TEB 472 London, ON N6A 5B9
License number	3424010695542
License date	Jul 08, 2014
Licensed content publisher	Elsevier

Licensed content publication	Surface and Coatings Technology
Licensed content title	Plasma electrolysis for surface engineering
Licensed content author	A.L. Yerokhin,X. Nie,A. Leyland,A. Matthews,S.J. Dowey
Licensed content date	15 December 1999
Licensed content volume number	122
Licensed content issue number	2–3
Number of pages	21
Start Page	73
End Page	93
Type of Use	reuse in a thesis/dissertation
Intended publisher of new work	other
Portion	figures/tables/illustrations
Number of figures/tables/illustrations	1
Format	electronic
Are you the author of this Elsevier article?	No
Will you be translating?	No
Title of your thesis/dissertation	Surface Modification of Aluminum Alloys by Plasma Electrolytic Oxidation
Expected completion date	Aug 2014
Estimated size (number of pages)	200
Elsevier VAT number	GB 494 6272 12
Permissions price	0.00 USD
VAT/Local Sales Tax	0.00 USD / 0.00 GBP
Total	0.00 USD

Appendix B: License Agreement with AIP Publishing

AIP PUBLISHING LLC LICENSE TERMS AND CONDITIONS

Jul 08, 2014

All payments must be made in full to CCC. For payment instructions, please see information listed at the bottom of this form.

License Number	3424010398943
Order Date	Jul 08, 2014
Publisher	AIP Publishing LLC
Publication	Journal of Vacuum Science & Technology A
Article Title	Coating growth behavior during the plasma electrolytic oxidation process
Author	R. O. Hussein,D. O. Northwood,X. Nie
Online Publication Date	Jun 29, 2010
Volume number	28
Issue number	4
Type of Use	Thesis/Dissertation
Requestor type	Student
Format	Electronic
Portion	Figure/Table
Number of figures/tables	1
Title of your thesis / dissertation	Surface Modification of Aluminum Alloys by Plasma Electrolytic Oxidation
Expected completion date	Aug 2014
Estimated size (number of pages)	200
Total	0.00 USD

Curriculum Vitae

Name: Vahid Dehnavi

Education:

- Ph.D., Chemical and Biochemical Engineering, The University of Western Ontario, London, ON, Canada, 2010-2014.
- M.Sc., Materials Engineering, Shiraz University, Shiraz, Iran, 2001-2004.
- B.Sc., Materials Engineering, Ferdowsi University of Mashhad, Mashhad, Iran, 1996-2001.

Honours and Awards:

- Province of Ontario Graduate Scholarship, 2013-2014.
- First prize for oral presentation, Research Bridges Symposium, Sarnia, ON, Canada, 2013.
- Recipient of Department of Engineering Award for Research, Azad University of Neyshabur, Neyshabur, Khorasan Razavi, Iran, 2008.

Related Work Experience:

- Teaching assistant, The University of Western Ontario, London, ON, Canada, 2010-2014.
- Research assistant and visiting worker, National Research Council (NRC), Canada, London, ON, Canada, 2010-2014.
- Faculty member, Department of Materials Science and Engineering, Azad University of Neyshabur, Khorasan Razavi, Iran, 2005-2010.

Publications:

- **Books:**

  - *Metallurgy of Welding*, J. F. Lancaster, Translated to Persian by A. Haerian, M.H. Hemmati, A.R. Saba, **V. Dehnavi**, 2004.
  - *Materials and Processes in Manufacturing*, Vol. 4, E. Paul Degarmo, Translated to Persian by A. Haerian, **V. Dehnavi**, 2002.

- **Journal publications:**

  - **V. Dehnavi**, X.Y. Liu, B. Luan, D. W. Shoesmith, S. Rohani, "Phase transformation in plasma electrolytic oxidation coatings on 6061 aluminum alloys", Surface & Coatings Technology 251 (2014) 106-114.

- J. Behin, S. Bukhari, **V. Dehnavi**, H. Kazemian, S. Rohani, "Using coal fly ash and wastewater for microwave synthesis of LTA zeolite", Chemical and Engineering Technology 37 (2014) 1-10.
- **V. Dehnavi,** B. Luan, D. W. Shoesmith, X. Y. Liu, S. Rohani, "Effect of duty cycle and applied current frequency on plasma electrolytic oxidation (PEO) coating growth behavior ", Surface & Coatings Technology 226 (2013) 100–107.
- **V. Dehnavi**, K. Janghorban, A. Haerian, "An Investigation into the Effect of Warm Compaction on the Characteristics of PM Parts", Journal of Engineering, Ferdowsi University of Mashhad (In Persian), 20 (2008) 23-31.

▪ **Manuscript submitted for publication:**

- **V. Dehnavi**, B. Luan, X.Y. Liu, D. W. Shoesmith, S. Rohani, "Correlation between plasma electrolytic oxidation treatment stages and coating microstructure on aluminum". Submitted to Surface Coatings & Technology.

▪ **Manuscript to be submitted:**

- **V. Dehnavi**, D. W. Shoesmith, B. Luan, M. Yari, X.Y. Liu, S. Rohani, "Electrochemical corrosion behaviour of plasma electrolytic oxidation coated aluminum alloy, the effect of PEO process stage".

▪ **Conferences:**

- **V. Dehnavi**, B. Luan, X.Y. Liu, D. W. Shoesmith, S. Rohani, "Production of ceramic coatings on AA6061 aluminum alloy using plasma electrolytic oxidation", Materials Science & Technology (MS&T 2013), Montreal, QC, Canada, October 27-31, 2013.
- **V. Dehnavi**, B. Luan, X.Y. Liu, D. W. Shoesmith, S. Rohani, "Characterization of ceramic coatings on 6061 Al alloy produced by plasma electrolytic oxidation", Surface Canada Conference 2013 , London, Ontario, Canada, May 7-10, 2013.
- **V. Dehnavi**, X.Y. Liu, B. Luan, S. Rohani, D. W. Shoesmith, "Coating growth behavior during Plasma Electrolytic Oxidation of Al6061", 24th Canadian Materials Science Conference (CMSC 2012), London, Ontario, Canada, June 5-8, 2012.
- **V. Dehnavi**, B. Luan, X.Y. Liu, S. Rohani, D. W. Shoesmith, "Effect of electrical parameters on plasma electrolytic oxidation coatings of 6061 Al alloy", New and Advanced Materials International Conference (NAMIC 2012), Isfahan, Iran, May 30-31, 2012.
- **V. Dehnavi**, X.Y. Liu, B. Luan, S. Rohani, D. W. Shoesmith, "Effect of heating cycles on phase transformation in ceramic coatings produced by Plasma Electrolytic Oxidation of Al6061 alloy", International Conference on Materials Heat Treatment (ICMH 2012), Isfahan, Iran, May 30-31, 2012.

- **V. Dehnavi**, A. Babakhani, M. Makarem, "Studying the relation between microstructure and tensile properties of PM parts", 2nd Manufacturing Engineering Conference (NMEC 2009), Najafabad, Iran, (In Persian), 28-29 Oct 2009.
- **V. Dehnavi**, M. Makarem, E.Z.V Karimi, "A New Approach towards Characterization of Porosity in Sintered Steels ", Materials Science and Technology, Pittsburgh, PA, USA, October 25-29, 2009.
- **V. Dehnavi**, "Status of Powder Metallurgy in Automotive Industry", 1st Technical Conference on Automotive Industry, Mashhad, Iran, (In Persian), August 5-6 2009.
- **V. Dehnavi**, H. Amini, M. Golestanipour, M. H. Sadeghian, ""Influence of Al_2O_3 Particles on the Properties of Heat Treated Al Based Composites Produced by Evaporative Pattern Casting (EPC) Method" , The Canadian Society for Mechanical Engineering (CSME) Conference, Ottawa, ON, Canada, June 5-8, 2008.
- H. Amini, M. Golestanipour, M. H. Sadeghian, **V. Dehnavi**, "Production of Al/Al_2O_3p Composites Using Lost Foam Casting Method", The Canadian Society for Mechanical Engineering (CSME) Conference, Ottawa, Ontario, Canada, June 5-8, 2008.
- **V. Dehnavi**, M. Makarem, H. Amini, "Effect of Warm Compaction on Pore Geometry and Distribution", 5^{th} International Conference on Powder Metallurgy for Automotive Parts (PM Auto'08), Isfahan, Iran, April 6-8, 2008.
- A. Haerian, K. Janghorban, **V. Dehnavi** "An Investigation into the Effect of Die Temperature on the Characteristics of Warm Compacted Astaloy CrM Parts", International Conference on Powder Metallurgy for Automotive Parts (PM Auto 2005), Isfahan, Iran, April 17-21, 2005.